VIII INTERNATIONAL CONFERENCE

FRONTIERS OF NONLINEAR PHYSICS

PROCEEDINGS

Moscow — Kostroma — Moscow, Russia

September 1—6, 2024

2024

VIII INTERNATIONAL CONFERENCE

FRONTIERS OF NONLINEAR PHYSICS

The conference FNP-2024 is dedicated to the celebration of the 300th anniversary of the Russian Academy of Sciences

Organizers

Department of Physical Sciences of the Russian Academy of Sciences

Ministry of Science and Higher Education of the Russian Federation

Confenece operator: the International Center for Advanced Studies in Nizhny Novgorod (INCAS)

Conference Chairman

professor Alexander Litvak

Conference partners:

State Atomic Energy Corporation ROSATOM (general partner)

www.rosatom.ru

GYCOM Ltd.

www.gycom.ru

DIPAUL Company

dipaul.ru

Laser Components LLC

lasercomponents.ru

C O N T E N T S

PLENARY TALKS

SECTION 1

NONLINEAR DYNAMICS AND ITS APPLICATIONS IN GEOPHYSICS AND ASTROPHYSICS

SECTION 2

EXTREME-FIELD PHYSICS AND NONLINEAR PROCESSES IN LASER-MATTER INTERACTIONS

SECTION 3

SOURCES AND APPLICATIONS OF STRONG MICROWAVES, MODERN TRENDS IN NUCLEAR FUSION

PLENARY TALKS

Status of SEL-100PW laser facility Project

Jianda Shao

Shanghai Institute of Optics and Fine Mechanics, China

Development of ultra-intense and ultrafast lasers have promised scientists with unprecedented extreme physical conditions and new experimental techniques. In 2017, the Station of Extreme Light (SEL) project was approved and is under construction at Shanghai now. In parallel, the invention of X-ray free electron laser (XFEL) has broad applications in many disciplines including bio-science and material science. XFEL is a light source offering outstanding resolution in space, time, energy and momentum, providing an ideal probe for high energy density state. The SEL project is the product of the marriage of the most two powerful lasers 100 PW optical laser and hard XFEL, for quantum electrodynamics (QED) physics and other high energy density physics researches [1], powered by the unprecedented capability first in the world.

In this project, a 100 PW laser facility based on all optical parametric chirped pulse amplification (OPCPA) will be developed, which can provide the focused intensity of more than 10^{23} W/cm^2. Benefiting from small thermal effect, broad gain bandwidth and the availability of large aperture devices, OPCPA pushes forward the development of hundred-level PW laser systems (project or in plan), such as OPAL-75PW [2], XCELS-200PW [3], GEKKO-EXA [4] and ELI-200PW. And the SEL-100PW is also based on OPCPA, which will deliver 1.5 kJ energy in 15 fs pulse width. As we know, DKDP crystal is one of the few nonlinear crystals which can be grown to large size with over 400 mm and has been used in the inertial confinement fusion (ICF) laser facilities. So DKDP based OPCPA is a promising approach for the generation of the hundred-level PW femtosecond laser. Studies showed that non-collinear optical parametric amplifiers (NOPA) comprised of DKDP produce broadband gain for supporting pulses as short as 10 fs centered near 920 nm.

The SEL project has been approved by Chinese government in 2017 and is under construction since April, 2018. According to the schedule, the facility will be completed in 2027 and then open to users. At present, most of engineering designs have been finished, and the frontend of the facility is being developed which can be regarded as a small prototype of the SEL facility [5].

The repetition-rate OPCPA consists of three OPCPA stages: the first stage amplifiers the seed energy from 0.01 mJ to 10 mJ with pump energy of 100 mJ at 100 Hz, corresponding to an energy gain of 1000. The second stage further boosts the energy to 0.5 J with the pump energy of 2 J at 1Hz, corresponding to a gain of more than 50. And the third stage will increase the chirped pulse energy to 5 J with pump energy of 25 J. These OPCPAs are all based on LBO crystals. After three stage OPCPAs, the laser pulses are amplified to over 5 J with ~25 J pump energy, which can meet the design very well. And output full spectrum width keeps 200 nm, which can support a Fourier transform limited compressed pulse width of ~13 fs. And this prototype system will be installed as the frontend for SEL-100PW.

In addition, the optical components such as the coating, DKDP crystal and grating is under researching and development which will be also reported in this talk.

References

1. A. D. Piazza, C. Müller, K. Z. Hatsagortsyan, and C. H. Keitel. Rev. Mod. Phys. 84, 1177(2012).
2. J. Bromage, S. W. Bahk, I. A. Begishev, et al. High Power Laser Sci. Eng. 7, e4(2019).
3. A. V. Bashinov, A. A. Gonoskov, A. V. Kim, G. Mourou, and A. M. Sergeev. Eur. Phys. J. Spec. Top. 223, 1105(2014).
4. J. Kawanaka, K. Tsubakimoto, H. Yoshida, et al. Journal of Physics: 8th International Conference on Inertial Fusion Sciences and Applications Series 688, 2013 (IFSA, Nara-Japan, 2013)8–13.
5. X. Wang, X. Lu, Y. Xu, at al. Ultrafast Sci. 2022, 9894358 (2022).

Efficient solution of physical problems using modern methods: neural networks, tensors, hybrid approaches?

Ivan Oseledets

AIRI; Skoltech, Russia

Numerical modelling of complicated physical phenomena with computers has a very long story. If we know the governing equations, this typically leads to the numerical solution of systems of partial differential equations (PDEs) in two, three and more dimensions. This is also a very well-developed field: finite element, finite difference, finite volume methods. Many challenges are also present, especially for high-dimensional and non-stationary problems and modeling can take a lot of time. On the other hand, the models themselves can also be inaccurate, leading to bad predictions. A good example are climate models, where many terms in the equations are determined empirically.

The rise of machine learning / artificial intelligence techniques from 2012 make it very tempting to adapt those techniques for the numerical solution of PDEs. The use of neural networks to approximate the solution directly has a long story, and has been tried many times; now it has a new rise under then name 'physics-informed neural networks' or PINNs, which are just the idea of approximating the solution of a given PDE by a neural networks. If we want to learn not the solution of a PDE, but an inverse operator, which approximates the data → solution map, a pioneering work is the work on so-called Fourier Neural operators (FNO) which has been proposed recently, and has attracted numerous attention and follow-up approaches.

Finally, there are quite a few tasks, where one has to combine the solution of a PDE with learning part of the parameters; a recent DeepMind paper on climate modeling in Nature is a step in this direction.

The current state of the field is very interesting: from one hand, we have people from machine learning that claim that new methods are '100x – 100 000x' faster, than the classical ones; from the other side, people that work with real applications are not often impressed, because such models are difficult to learn, do not come with the same approximation, stability and convergence guarantees as the classical numerical methods and when compared with the numerical methods of the same quality, often loose. There is a movement of two communities towards one each other, which results in the development of hybrid approaches that combine the best of both words: advanced, nonlinear function approximation and classical physics and its properties. A lot of challenging problems results and achievement lie ahead. In this talk I will give:

a) overview of the basic concepts and definitions;
b) Outline current successful applications
c) Specify challenges.

Formation and stability of magnetic filaments in convective zone of the Sun

E. A. Kuznetsov[1,2,3] and **E. A. Mikhailov**[1,3,4]

[1] Lebedev Physical Institute of RAS, Moscow, Russia;
[2] Landau Institute for Theoretical Physics of RAS, Chernogolovka, Russia;
[3] Skolkovo Institute of Science and Technology, Moscow, Russia;
[4] Physics Department, Lomonosov Moscow State University, Moscow, Russia

As is well known, magnetic fields in space are distributed very inhomogeneously. Sometimes field distributions have forms of filaments with high magnetic field values. As many observations show, such a filamentation takes place in convective cells in the Sun and another astrophysical objects. This effect is associated with the frozenness of the magnetic field into a medium with high conductivity that leads to compression of magnetic field lines and forming magnetic filaments. Based on the general consideration of the convection top flows only, without knowledge of the cell structure, we demonstrate that the magnetic field intensifies in the regions of downward flows in both two-dimensional and three-dimensional convective cells. These regions of the hyperbolic type play a role of a specific attractor for the magnetic field. This theoretical analysis was confirmed by numerical simulations for 2D convective cells of the roll-type. Without dissipation the magnetic field grows exponentially in time and the growth rate does not depend on the aspect ratio between horizontal and vertical scales of a cell. An increase due to compression in the magnetic field in the high conductive plasma is saturated due to the natural limitation associated with dissipative effects when the maximum magnitude of the magnetic field is of the order of the root of the magnetic Reynolds number *Rem*. For the solar convective zone *Rem* is about 106−108, and the mean kinetic energy density exceeds mean magnetic energy density at least for two orders of magnitude that allows one to use the kinematic approximation for the MHD induction equation. On the basis of the stability analysis we explain why downward flows influence magnetic filaments by making them flatter with orientation along interfaces between convective cells [1].

Acknowledgements. The work was supported by the Russian Foundation for Basic Research (grant no. 19-72-30028).

References

1. E. A. Kuznetsov, E. A. Mikhailov. “Magnetic filaments: formation, stability, and feedback” Mathematics, **12**, 677 (1–14) (2024).

Extreme field physics and the 10/100 PW lasers at SIOM

Liangliang Ji

Shanghai Institute of Optics and Fine Mechanics, Chinese Academy of Sciences, Shanghai, China, jill@siom.ac.cn

The peak intensity of petawatt lasers on target has approached or even reached 10^{22} W/cm^2, bringing new opportunities for the development of laser particle acceleration. Currently, the Shanghai Ultra-intense and Ultra-short Laser Facility (SULF) is in normal operation, with its 10-petawatt laser experimental platform providing on-target peak power reaching several petawatts. By using new types of targets such as micro- and nanostructures, the cutoff energy of protons has been effectively increased to beyond 60 MeV [1]. The acceleration efficiencies over 8% have been achieved [2]. A comparison between experiments and simulations reveals that the large-charge electron beams generated by direct laser acceleration in micro- and nanostructures are the primary reason for achieving efficient proton acceleration. Additionally, through the interaction of the 10-petawatt laser with high-density gas targets, a hybrid acceleration mechanism has produced hundreds of MeV electron beams with charges of several tens of nC. These experimental results provide guidance for further improving the energy and efficiency of particle acceleration and lay a significant foundation for their application in fields such as laser nuclear physics and high-energy density physics.

A new 100PW laser station is also under construction by SIOM. The design, manufacturing and installation of the experimental vacuum chamber has been finished. Here the 100PW laser will collide with hard XFEL pulse to measure the “vacuum birefringence” effect [3], which relies on the materialization of quantum vacuum under extreme laser fields. Based on these ultra-intense lasers, we pointed out via strong-field QED theory and simulations that the efficient gamma-emission, electron-poistron pair production and high energy particles with quantum vortex states [4] can be achieved. For the latter, the wavefunction of relativistic electrons can be twisted using intense lasers, leading to vortex electrons carrying large orbital angular momentum, providing a novel source for particle and nuclear physics.

Acknowledgements. The work is supported by National Science Foundation of China and National Key R&D Program of China

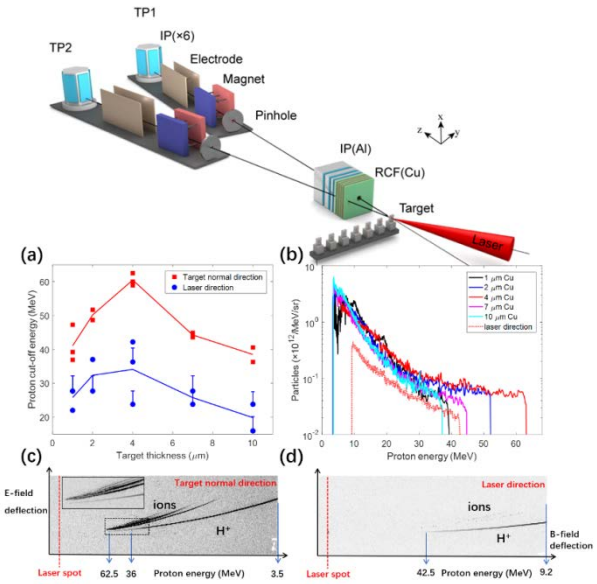

Fig. 1. Acceleration of protons beyond 60 MeV with SULF laser

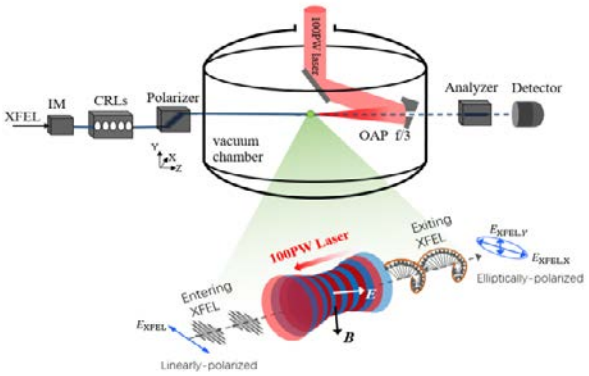

Fig. 2. Measuring vacuum birefringence using 100PW laser colliding with XFEL

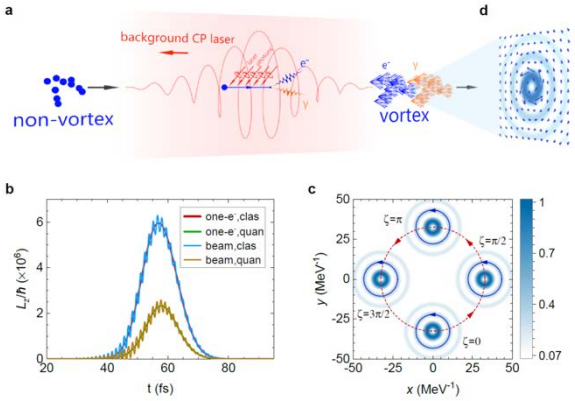

Fig. 3. The generation of relativistic quantum vortex electrons with circularly-polarized intense laser pulse

References

1. High Power Laser Science and Engineering 10, e26 (2022).
2. Communications Physics 5, 124 (2022).
3. Plasma Physics and Controlled Fusion 60, 044002(2018).
4. arXiv:2302.05065(2023).

Superheavy elements at JINR, Dubna

Alexander Karpov

Flerov Laboratory of Nuclear Reactions, JINR, Dubna

The journey to the borders of the world of atoms and nuclei began about 80 years ago and continues to this day. During this time, 24 artificial elements heavier than uranium were synthesized and they found their places in the Periodic Table of Chemical Elements. Over the past twenty years, outstanding success has been achieved in the synthesis and study of the properties of superheavy elements (SHE) of the Periodic table, as well as in understanding the laws governing nuclear reactions leading to their formation. These results obtained primarily at the Joint Institute for Nuclear Research (JINR) in Dubna, gave a powerful impetus to the development of this area of nuclear physics.

Until now, fusion reactions at energies near the Coulomb barrier have remained the only method for producing superheavy nuclei. In the reactions of the so-called "cold" fusion, based on the use of strongly bound lead and bismuth nuclei as a target, it was possible to synthesize SHE up to the atomic number Z = 113. The cross sections for "cold" fusion reactions fall extremely rapidly with an increase in the mass of the projectile nucleus. A record low cross section of about 0.08 pb was achieved in the synthesis of the element nihonium (Z = 113) by irradiation of the ^{209}Bi target with ^{70}Zn ions.

The cross sections for SHE formation are much higher when more asymmetric and “hotter” reactions of fusion of ^{48}Ca nuclei with actinides are applied. Using the hot synthesis method, JINR has succeeded to discover six new elements with Z = 113–118 and more than 50 new isotopes of heaviest elements from 104 to 118. Element 118 – oganesson completes the seventh period of the Periodic table and is currently the heaviest known. These experiments were performed at the Dubna gas-filled recoil separator (DGFRS-1) utilizing ^{48}Ca beams provided by the U400 cyclotron.

Despite the fact that the hypothesis of the existence of an island of stability of SHE can already be considered experimentally proven, a number of fundamental questions remain unclear. What are the boundaries of the SHE stability island? How long do the nuclei in its center live? What reactions should be used to synthesize the longest-lived nuclei of the island of stability? The synthesis and study of the properties of new SHE and their isotopes continues in the world's leading centers, which is associated with the development of an experimental base. At JINR, a record-breaking new-generation accelerator complex has been commissioned – the world's first Superheavy Element Factory, which should become the center of future SHE research [1, 2]. The basic facility of the SHE Factory is the high-current cyclotron DC-280 providing beams of ^{48}Ca up to 10 pμA (6×10^{13} s^{-1}). Today, earlier discovered superheavy elements have become available for a detailed study of their properties [3].

The synthesis of new even heavier elements and the related search for the limits of the existence of chemical elements remains an urgent task for the nuclear physics. Unfortunately, the heaviest available target is californium. It being fused with calcium leads to element 118. In order to synthesize heavier elements one needs to use heavier beams such as titanium or chromium.

References

1. Yu. Ts. Oganessian, V. K. Utyonkov, A. G. Popeko et al, NIMA **1033**, 166640 (2022).
2. D. I. Solovyev and N. D. Kovrizhnykh, J. Instrum., **17**, P07033 (2022).
3. Yu. Ts. Oganessian, V. K. Utyonkov et al., Phys. Rev. C **106**, L031301 (2022); **106**, 064306 (2022); **106**, 026412 (2022); **108**, 024611 (2023).

Gyro-devices. State-of-the-art and trends of development

G. G. Denisov

A.V. Gaponov-Grekhov Institute of Applied Physics of the Russian Academy of Sciences, Nizhny Novgorod, Russia, den@ipfran.ru

A gyrotron is an oscillator – a source of powerful coherent electromagnetic radiation in the range of millimeter and submillimeter waves, using the maser effect of stimulated electron emission in a constant magnetic field, associated with the bunching of electrons in rotation phases due to the relativistic dependence of the cyclotron frequency on particle energy. The electrodynamic system of the gyrotron can significantly exceed the radiation wavelength in transverse dimensions (for example, 30 times) while maintaining the single-mode single-frequency generation mode, which makes it possible to obtain a high level of power at very high frequencies up to the THz range. Priority in the development of the physical principles of gyrotron operation and the creation of the first operating devices belongs to A.V. Gaponov-Grekhov with his students and collaborators.

The first and, of course, the most important object of application of gyrotrons is electron cyclotron heating (ECH) of plasma in nuclear fusion installations. Such experiments were started at the Kurchatov Institute and the Ioffe Institute in the early 70 s. Following the publication of the results of the first ECRH experiments, similar work was followed by large industrial companies and fusion laboratories around the world, so that by the early 1990s, gyrotrons had become an established and sought-after tool in fusion research. At the same time, international competition among gyrotron manufacturers was intensified due to the entry of the Russian company GYCOM Ltd into the world market, which offers devices with “more advanced parameters.” Despite this relative progress, at the beginning of the International Thermonuclear Experimental Reactor (ITER) project, the gyrotron was considered by the expert community only as a radiation source for initiating plasma in a tokamak due to its parameters (maximum power, limited pulse duration, generation efficiency, high cost of power density of the device) and the gyrotron was inferior to sources of other methods of heating and current generation – ion cyclotron and lower hybrid heating, injection of neutral beams. In subsequent years, gyrotron developers solved a number of key problems – the development of highly efficient operating mode converters, energy recovery systems, diamond radiation output windows – which remove the above-mentioned limitations and determine the construction of the modern gyrotron for thermonuclear research. Currently, gyrotrons are capable of continuously (generation duration more than 1000 seconds) generating coherent radiation with a power of up to one megawatt in the frequency range (70–170) GHz with an efficiency of more than 50 percent.

A number of large-scale fusion facilities are equipped now with multi-megawatt ECRH complexes based on similar gyrotrons. The ITER installation under construction is planned to include 24 MW gyrotron complex with a frequency of 170 GHz, the supply of which should be provided by Japan (8 gyrotron systems), Russia (8), EU (6), India (2). Gyrotrons developed in Russia and Japan fully comply with the ITER specification. As part of Russian cooperation between the IAP RAS and GYCOM, 8 gyrotron systems have already been manufactured, which have been accepted by an international organization. In terms of readiness, the ECRH complex is ahead of the ion-cyclotron heating and neutral injection complexes created at ITER. The ECRH is also currently being considered as the primary means of plasma heating and current generation in the DEMO fusion power demonstration prototype designs, which will require significant progress in the development of gyrotron physics and technology to provide the required frequency increases (up to 230–240 GHz) and the desired power increase, efficiency and reliability.

The report provides a brief overview of the operating principles, current state and parameters of megawatt gyrotrons produced in the world. The presented research results are aimed at increasing the generation power, creating multi-frequency gyrotrons, and further advancement in the terahertz range. Options for ensuring stable single-mode oscillation in essentially multimode systems by locking the frequency (phase locking) by an external signal are considered, which in principle opens up also the possibility of coherent radiation from many gyrotrons.

Some examples of non-thermonuclear applications of gyro devices in plasma physics and plasma technologies are also given: high-current ECR ion sources, ceramic sintering, extreme ultraviolet light sources, high-speed deposition of diamond films and single crystals, THz microwave sources for spectroscopy, power amplifiers for modern radars and communications. The use of broadband gyro-amplifiers in combination with a nonlinear saturating absorber in the feedback circuit allows for a very interesting oscillation mode, similar to passive mode-locked lasers: a device with a continuous electron beam produces a sequence of very short coherent pulses with high power, which can exceed the average power of the electron beam.

Acknowledgements. The work supported partly by State Agreement # H.4a.241.19.24.1024 from 20.03.2024, Contract # 1770641334824000019O/37-24/01/45-416 from 22.05.2024.

Key technologies for XCELS

M. V. Starodubtsev

A.V. Gaponov-Grekhov Institute of Applied Physics of the Russian Academy of Sciences, Nizhny Novgorod, Russia,
mstar@ipfran.ru

The XCELS (eXawatt Center for Extreme Light Studies) project [1] aimed to create a large scientific infrastructure based on lasers with giant peak power. The planned infrastructure will include a unique 12-channel light source with a total peak power of 600 PW. The project relies on the significant progress achieved in the last decade in creating extremely high peak power femtosecond laser systems. The talk will provide an overview of the key technologies underlying the XCELS project, which include optical parametric chirped pulse amplification; ultra-wideband phase matching of parametric amplification around the 910 nm wavelength discovered in DKDP (KD_2PO_4, deuterated potassium dihydrogen phosphate) crystals; and the use of a wide-aperture neodymium glass slab laser with multikilojoule pulse energy for pumping the parametric amplifier.

Each of the 12 identical laser channels will produce 20 fs pulses of kilojoule energy, corresponding to a peak power of 50 PW in each channel. When using F/1 focusing optics, the peak intensity achieved when focusing one laser channel will be on the order of 0.44×10^{25} W/cm^2. All 12 beams will be directed to the main target chamber, in which they are focused in a dipole geometry with the focal intensity of almost 10^{26} W/cm^2. The pulses are assumed to be coherently combined, which will increase the focal intensity to 3.2×10^{26} W/cm^2. Thus, the XCELS project implies the creation of a unique laser system with record-breaking total power, while the multichannel nature of the XCELS laser system enables to achieve the highest possible laser field intensity at the focal point.

The interaction of such intense laser radiation with matter and even with vacuum represents a completely new fundamental physics. The direct study of the space–time structure of vacuum and other unknown phenomena at the frontier of high-energy physics and the physics of superstrong fields will be challenged during the proposed experiments at the XCELS laser facility; its multi-channel architecture will also be actively used in the proposed experimental program. Thus, one of the most important goals of the XCELS project, which is of fundamental importance, is research in the field of the physics of strong EM fields, including the quantum electrodynamics (QED) processes in a strong laser field. Among such QED effects, we can single out vacuum polarization in a strong EM field, QED cascades, plasma dynamics with allowance for QED effects, etc.

In addition to QED effects, the experimental program of the project presents experiments aimed at generation and acceleration of particles; generation of secondary EM radiation; laboratory astrophysics; high energy density (HED) processes; diagnostics of HED plasmas and ultra-high-intensity laser fields; and other phenomena.

Expected applications will include the development of compact particle accelerators, the generation of ultrashort pulses of hard X-ray and gamma radiation for material science enabling one to probe material samples with unprecedented spatial and temporal resolution, the development of new radiation and particle sources, etc. Moreover, additional channels can be used both for diagnostic purposes and for generating intense fluxes of secondary radiation and particles, which may be needed in various experiments. Thus, a number of experiments are possible at the XCELS facility, which are inaccessible for other facilities, both existing and under construction.

Acknowledgements. The research was supported by the Ministry of Science and Higher Education of the Russian Federation (Project No. FFUF-2023-0001).

References

1. E. Khazanov, A. Shaykin A, I. Kostyukov, et al. *High Power Laser Science and Engineering*. 2023, **11**, e78.

High intensity ion beams for HIAF: challenges and perspectives

H. Y. Zhao[1,2], L. T. Sun[1,2], H. W. Zhao[1,2], J. B. Li[1,2], L. B. Li[1], L. X. Li[1], W. Lu[1,2], W. Wu[1], Y. T. Lu[1,2] and X. Z. Zhang[1]

[1] Institute of Modern Physics, Chinese Academy of Sciences, Lanzhou, P. R. China
[2] School of Nuclear Science and Technology, University of Chinese Academy of Sciences, Beijing, P. R. China

High Intensity Heavy-ion Accelerator Facility, HIAF, is one of the next-generation heavy ion accelerators, the major scientific goals of which are to explore the frontiers of nuclear physics [1]. It is expected that the facility can deliver heavy ion beams with unprecedented intensities to the experimental stations both in CW mode and in pulsed mode. To attain the expected beam intensities, it requires the ion source to produce very extensive high-charge-state ion beams, which is one of the most critical and also challenging components of HIAF.

To meet the requirements of HIAF for high intensity heavy ion beams, the Fouth generation ECR ion source, FECR [2], has been under intensive development since 2015 and has been fabricated and assembled completely this April. Now the FECR ion source is under commissioning. This talk will present the latest results of the FECR, and the perspectives on more powerful high intensity ion source solution will be discussed.

Acknowledgements. This research was supported by the National Natural Science Foundation of China (Grant Nos. 11427904 and 12025506) and the Key Research of Frontier Sciences (Grant No. 2023YFA1606800).

References

1. X. Zhou, Nucl. Phy. Rev., 2018, 35(4), 339–349.
2. L. Sun, H. W. Zhao, W. Wu et al., Proc. 24th Int. Workshop on ECR Ion Sources, East Lansing, USA, 2020, MOWZO01.

Decay of a strong discontinuity and current filamentation in plasma

Vl. V. Kocharovsky, N. A. Emelyanov, M. A. Garasev, A. A. Kuznetsov, A. A. Nechaev

A.V. Gaponov-Grekhov Institute of Applied Physics of the Russian Academy of Sciences, Nizhny Novgorod, Russia,
kochar@ipfran.ru

The review aims at the classical problem of the decay of a strong plasma discontinuity and a similar problem of the injection of a plasma with hot electrons into a vacuum or a rarefied cold plasma with a magnetic field in the absence of significant particle collisions. The main goal is to elucidate the transient phenomena of the formation of an anisotropic electron velocity distribution leading to quasi-magnetostatic turbulence associated with Weibel-type instabilities. We focus mainly on the formation and decay of current filaments and sheets (see, e.g., Figs. 1, 2) and outline the theoretical and numerical results on this account obtained previously for space and laser plasmas, especially related to the collisionless phenomena.

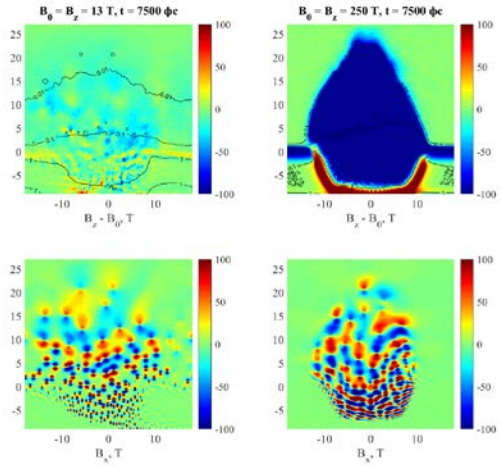

Fig. 1. Two-dimensional (2D) modeling of the magnetic structures after 7.5 ps expansion of a plasma layer with hot electrons into vacuum (the decay of the discontinuity). The initial plasma density is $n_0 = 1.7 \cdot 10^{22}$ cm^{-3}. The horizontal and vertical axes correspond to the x and y coordinates respectively (given in microns). On the left is the simulation with an external magnetic field $B_z = 13$ T orthogonal to the simulation plane: the top panel shows the B_z component of the magnetic field minus the external field (in Tesla) in color, the level lines show the plasma density normalized to the initial one, n/n_0, with gradations of 0.01, 0.1, 1; the bottom panel shows the B_x component of the magnetic field. Right panels show the same for the simulation with an external magnetic field $B_z = 250$ T

We demonstrate and analyze in detail the original results of particle-in-cell modeling of a collisionless expansion of an anisotropic plasma cloud with hot electrons from a flat surface into a background magnetoactive plasma in different settings entailing [1]

(i) a hot-electron spot of a circular or cylindrical form within an initial-value problem or a finite-time injection of electrons from the surface;

(ii) an external magnetic field with three orthogonal orientations: perpendicular to the surface or along it, directed either across or parallel to a long axis of the hot-electron spot; and

(iii) inhomogeneous layers of cold background plasma of different spatial scales and densities.

Bearing in mind typical laser-plasma experiments, we outline the development of the principal structures of currents and highly inhomogeneous magnetic fields linked with distinct forms of the anisotropic electron velocity distribution and sophisticated dynamics of the instability process for diverse sets of attributes (i)–(iii).

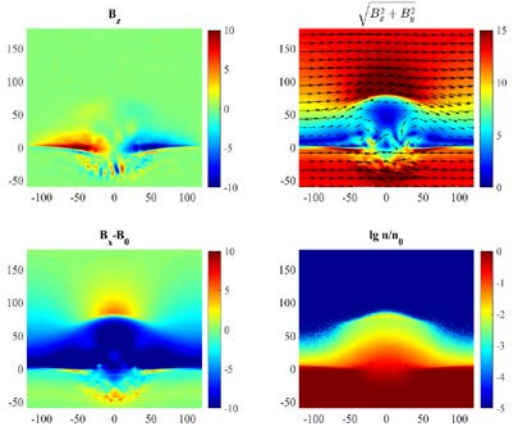

Fig. 2. 2D modeling of the expansion of a plasma with hot electrons (with initial density $n_0 = 10^{20}$ cm^{-3}) into an external magnetic field $B_x = 13$ T at time $t = 20$ ps. Top left panel shows the magnetic field component B_z (in Tesla). Top right panel shows the magnitude of the in-plane magnetic field (in Tesla), arrows show the direction of the in-plane field. Lower left panel shows the field component B_x minus the external field. Lower right panel shows the logarithm of normalized plasma density

Strong magnetic fields generated at the main transition stage are turbulent in nature, can reach, in typical laser experiments, mega-Gauss and higher values, and modify interaction between charged particles notably. In particular, according to the analytical estimates, numerical simulations and laser ablation experiments, the magnetic fields of self-consistent currents of cold and hot electrons quickly lead to the spatial separation of particle counter flows and suppress the beam instability of plasma (Langmuir) waves. This situation is qualitatively different from the well-studied decay of a weak plasma discontinuity, where the electrons obey a Boltzmann distribution and the formation of magnetic turbulence is replaced with the generation of ion-acoustic solitons.

We discribe possible applications of the obtained results to the analysis of laboratory and space plasma problems involving an explosive development of the small-scale magnetic turbulence due to the filamentation of electric currents in the presence of a large-scale magnetic field and an inhomogeneity of plasma density.

References

1. Vl. V. Kocharovsky, A. A. Nechaev, M. A. Garasev, *Reviews of Modern Plasma Physics*, 2024, **8**, 17.

National model of the Earth's climate system: current state, areas of use and development prospects

A. S. Gritsun

Marchuk Institute of Numerical Mathematics RAS, Moscow, Russia, asgrit@mail.ru

In this report we discuss problems related to predictions of the state of the Earth's climate system at various time intervals. The concept of “climate” and “potential predictability” are formulated. We discuss two general sources of predictability – predictability that comes from the right hand side and the one from information provided by the system initial conditions.

We briefly describe the history of creation of the family of climate models INM-CM, developed at the Marchuk Institute of Numerical Mathematics of the Russian Academy of Sciences [1], and representing a complex of coupled models of the dynamics of the atmosphere, the World Ocean, sea ice and the active layer of land soil.

The prospects for the development of the model are discussed, including within the framework of the Research Center “Modeling and Forecasting of Global Climate”, created for the purpose of conducting scientific research in the areas of the Federal Scientific and Technical Program in the field of environmental development of the Russian Federation and climate change and the Government Innovative Project of National Importance “National system for monitoring of climate-active substances.”

Next we present the main experiments of the international program for comparing climate models (CMIP6) [2]. The results obtained using the current version of the Earth system model when simulating climate change in 1850–2014 and forecasting possible climate changes in the 21st century according to IPCC scenarios are discussed. We also discuss the capabilities of the model for seasonal and ten-year prognostic calculations.

References

1. Volodin E., Mortikov E., Kostrykin S., Galin V., Gritsun A., Diansky N., Gusev A., Iakovlev N. 2017, Simulation of the present-day climate with the climate model INMCM5, Climate dynamics, 49, Issue 11–12, 3715–3734, doi:10.1007/s00382-017-3539-7
2. Eyring V., Bony S., Meehl G. A., et al., 2016, Overview of the Coupled Model Intercomparison Project Phase 6 (CMIP6) experimental design and organization, Geosci. Model Dev., 9, 1937-1958, doi:10.5194/gmd-9-1937-2016.

Open type magnetic traps in the World and Russia

P. A. Bagryansky

Budker Institute of Nuclear Physics of Siberian Branch RAS, Novosibirsk, Russia, p.a.bagryansky@inp.nsk.su

Research in the field of open-type magnetic traps for plasma confinement towards controlled nuclear fusion has now received a new impetus due to several successful results obtained at experimental facilities in Russia and the USA in the next fifteen years [1–4]. The results of these experiments showed the possibility of solving key problems of confining hot plasma in such traps, which previously seemed insurmountable and led to an almost complete decrease in activity in this direction throughout the world in the late eighties of the last century.

Key challenges that were successfully overcome are listed below.

1. The possibility of overcoming MHD instabilities and achieving relative plasma pressure $\beta \approx 1$ in an axisymmetric configuration has been demonstrated [3, 4]. This radically reduces the engineering complexity of the magnetic system, makes the physics of transverse transport more transparent and opens up the fundamental possibility of developing fusion reactors that operate with alternative fuels that do not contain radioactive tritium and have a practically inexhaustible production resource.

2. The physical processes that determine longitudinal thermal conductivity have been studied in detail, and a reliable method for limiting it to an energy level of ≈ 6–8 electron temperatures, which is tolerated on average by one electron-ion pair leaving the trap, has been developed [2, 5–7].

3. It has been shown that it is possible to implement hot plasma confinement modes with a nonequilibrium energy distribution function, when the influence of developing kinetic instabilities turns out to be insignificant [3, 4].

These achievements have currently stimulated the emergence of a number of new projects abroad, which are being developed mainly by private companies, for example: Copernicus (TAE Technologies, USA) [8], Wisconsin HTS Axisymmetric Mirror (UW Madison, MIT and Commonwealth Fusion Systems, USA) [9], Novatron (Novatron Group, Sweden) [10, 11]. The planned report will present the status of these and possibly other emerging projects.

Research in the field of hot plasma confinement in open-type traps in Russia is currently mainly concentrated at the Budker Institute of Nuclear Physics SB RAS (BINP), where the gas-dynamic multiple-mirror trap (GDMT) project is being developed [12]. This project is based on both the achievements outlined above and on new ideas proposed and currently being developed at the BINP [13]. To support the GDMT project, several experimental installations have been developed and are in operation, the latest results of which will be presented in the report.

References

1. P. A. Bagryansky, A. V. Anikeev, G. G. Denisov, et al. Nuclear Fusion, Vol. 55, Issue 5 (2015) Article number 053009.
2. P. A. Bagryansky, A. G. Shalashov, E. D. Gospodchikov, et al. *Physical Review Letters*, Vol. 114, Issue 20 (2015) 205001.
3. T. C. Simonen, A. Anikeev, P. Bagryansky, A. Beklemishev, et al. *J. Fusion Energy*, 29, 558 (2010).
4. H. Gota, et al. *Nuclear Fusion* **61** (2021) 106039.
5. E. I. Soldatkina, et al. 2020 *Nucl. Fusion* **60,** 086009.
6. D. Skovorodin 2019 *Phys. Plasmas* **26** (1) 012503.
7. I. S. Abramov, et al. 2019 *Nucl. Fusion* **59** 106004.
8. https://tae.com/
9. https://wippl.wisc.edu/wisconsin-hts-axisymmetric-mirror/
10. novatronfusion.com
11. arXiv:2310.16711v2.
12. D. I. Skovorodin, I. S. Chernoshtanov, V. Kh. Amirov, et al., *Plasma Physics Reports*, 2023, Vol. 49, No. 9, pp. 1039–1086.
13. P. A. Bagryansky, A. D. Beklemishev, V. V. Postupaev, *J. Fusion Energy* , V. 38, № 1, pp.162–181, FEB 2019.

Lightning: more and more puzzles

E. A. Mareev

A.V. Gaponov-Grekhov Institute of Applied Physics Russian Academy of Sciences, Nizhny Novgorod. mareev@ipfran.ru

Lightning is one of the most impressive and at the same time dangerous natural phenomena. Although the history of instrumental observations and theoretical studies of lightning goes back several centuries (see for review, e.g., [1]), a large number of questions related to thunderstorms and lightning still remain open. Moreover, recent decades have brought many new discoveries, achievements, and mysteries in this area. Some of these advances and mysteries are briefly highlighted in this report.

The first part of the report is a brief introduction to the terminology. Different types of lightning discharges and the effects associated with them are discussed here. Particular attention is paid to the differences between cloud-to-ground discharges, intra-cloud discharges and discharges between the cloud and the middle atmosphere and ionosphere (a whole family of such discharges, including jets, giant jets, sprites, halos, and elves, was discovered only at the very end of the 20th century).

The second part of the report is devoted to the problems of describing "classical" cloud-to-ground lightning, transferring a negative or positive charge to the ground. This part covers the problems related to the leader breakdown and to the stepwise propagation of negative and positive leaders, as well as of dart leaders [1, 2]. From the perspective of practical applications, problems associated with the analysis of the so-called main stage of lightning (comprising the return stroke) are of particular interest, and a review of recent experimental and theoretical work on this topic is given here. For example, a two-dimensional model of high-current pulsed arc discharge in air, which takes into account gas dynamics of the discharge channel, real air thermodynamics in a wide range of pressures and temperatures, electrodynamics of the discharge including the pinch effect, and radiation, has recently been proposed [3]; it is especially interesting for the return stroke modelling. When the model was applied to simulate the discharge for the currents in the range 1–250 kA and characteristic rise times in the range 13–25 μs, the results turned out to predict well most characteristics of the discharge (compared to the experimental data).

Much attention has recently been paid to high-energy phenomena associated with thunderstorm and lightning activity, including terrestrial gamma flashes (TGFs) and thunderstorm ground enhancements (TGEs); transient luminous events (TLEs), such as sprites, jets, halos, and elves, are also adjacent to them. The third part of the report is dedicated to a brief analysis of recent work in this direction, including the studies related to observations of lightning from space. Modern investigations in this direction are focused on problems associated with the interpretation of physical mechanisms underlying the generation of hard electromagnetic radiation from lightning discharges, understanding the nature of terrestrial gamma flashes, analyzing the results of satellite observations, and further progress in laboratory experiments with long sparks, which simulate electrical discharges in thunderclouds and lightning (e.g., [4]).

Finally, the fourth part of the report can be entitled "Lightning, climate, and life." This rapidly developing field of knowledge covers the possible role of thunderstorms and lightning in the Earth's climate system. Lightning with extreme parameters and lightning as an indicator of dangerous meteorological phenomena also attracts much attention.

It has now become common to regard the global electric circuit (including both the so-called DC circuit, comprising global quasi-stationary currents maintained by thunderstorms and other electrified clouds, and the so-called AC circuit, comprising Schumann resonances—that is to say, global electromagnetic resonances excited by lightning in the Earth—ionosphere cavity) as part of the Earth system. Recent studies have shown that global circuit parameters reflect climate variability on Earth (responding, in particular, to the El Niño—Southern Oscillation signal [5]).

The fact that Schumann resonances are permanently present in the atmosphere (being supported by global lightning activity) and accompanied the development of living organisms throughout evolution motivates a search for biological effects in living organisms associated with them. This is interesting from both evolutionary and ecological viewpoints, since the spectrum of Schumann resonances can be modified due to changes in lightning activity in a changing climate; in addition, radical changes in the usual electromagnetic environment will take place for artificial ecosystems at space. Recent studies have indicated that the effect of extremely low frequency magnetic fields on light-induced electrical reactions in wheat is more pronounced at the frequency of the second Schumann harmonic (14.3 Hz) than at surrounding non-resonant frequencies [6]. These results in particular support the hypothesis that signaling in plants may be a universal process with the high sensitivity to various low-intensity environmental factors, acting on living systems.

Acknowledgements

This work was supported by the RSF grant no. 23-17-00264.

References

1. V. A. Rakov, Fundamentals of Physics. Cambridge University Press, 2016.
2. B. Zhang, Zhu Y., Zhang X., Popov N.A., et al. *Plasma Sources Sci. Technol.* 2023. V. 32. No 11. P. 115014.
3. A. N. Bocharov, E. A. Mareev and N. A Popov. 2022. *J. Phys. D: Appl. Phys.* **55** 115204.
4. E. A. Mareev, Y. V. Shlyugaev, M. V. Shatalina, et al. 2023. *Astron. Rep.* **67**, 104–114.
5. N. N. Slyunyaev, A. V. Frank-Kamenetsky, N. V. Ilin et al. 2021.*Geophys. Res. Lett*., **48**(21).
6. M. Grinberg, N. Ilin, Yu. Nemtsova, … E. Mareev. 2023. *Plant Signaling & Behavior*, 19(1). 2294425.

Research at ITER, TRT creation and participation in BEST – the next step on the way to creation of thermonuclear fusion reactor in Russia

A. V. Krasilnikov

Institution Project Center ITER, Moscow, Russia, a.krasilnikov@iterrf.ru

With the goal to solve the main problems of designing a thermonuclear tokamak reactor, such as the experimental demonstration of quasi-stationary thermonuclear burning, generation of non-inductive quasi-stationary current; development of plasma technologies and materials of the first wall and divertor, the International Thermonuclear Experimental Reactor ITER [1] is being designed, projects of DEMO demonstration reactors are being developed, and a Tokamak with Reactor Technologies TRT [2] is being developed in Russia (Fig. 1 & Table 1) and tokamak BEST [3] is under construction in ASIPP, China.

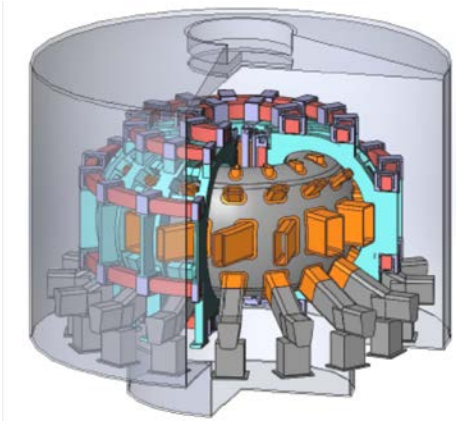

Fig. 1. Tokamak with Reactor Technologies

Table 1

Main characteristics and features of TRT

B (T)	8	High B, HTS
R/a	2.15 / 0.57	Classical tokamak, compact, low cost
Δt (c)	> 100	Quasi-stational
First wall		Options: Be, W coved by B_4C TiB_2-AlN
Divertor		Innovative, W, gas puff
I_p (MA)	4–5	High Current
n_e (10^{20}м$^{-3}$)	1–2	High density
P_{aux} (МВт) NBI ECRH ICRH	30~40 20–25 10 5	Reactor relevant 500 keV 230 GHz 60-80 MHz
Q (DT)	> 1	Reactor Plasma

The main components of the technology platforms of ITER (superconducting electromagnetic system (EMS) made of Nb_3Sn and NbTi, the first wall of W coated with a low-Z material, systems for additional plasma heating, experimental modules of a breeder blanket, plasma control systems, etc.), TRT (EMS of high-temperature superconductors, first wall options of: W with B_4C coating, TiB_2-AlN composite and liquid metal lithium, well upgraded additional heating and quasi-stationary non-inductive current drive systems, innovative divertor, experimental breeder and hybrid blanket modules, reactor-compatible diagnostics and remote plasma control systems, etc.) and BEST (superconducting EMS from Nb_3Sn and NbTi, W first wall, systems of additional plasma heating, tritium complex, fusion plasma with Q = 5 and others) are presented. The technological platforms of the ITER being under construction, the TRT being designed and constructing BEST contain an almost complete, according to modern understanding, set of technologies required for the future thermonuclear reactor.

Creation of the TRT is the creation of the largest science and technology project with international participation in Russia. It will provides keeping the Russian leadership in science, engineering, technology and education of new generation of scientists.

Russian participation in BEST will provide participation of Russian scientists and engineers in experimental studies of fusion plasmas with Q = 5 in 2028–2040 (well before full scale ITER DT operation) at biggest and closest to future fusion reactor thermonuclear complex BEST. The number of BEST/CRAFT technologies (HTS and LTS conductors, cryogenics, power supply systems and antennas for ICRH, robots and others) could be efficiently applied at TRT with very high cost containment effect.

Construction and experimental operation of the technology platform of ITER, TRT и BEST, together with experience of the realization of the other large thermonuclear experiments of the ITER partners, will provide at later step the successful creation both the pure thermonuclear fusion and hybrid (fusion-fission) reactor.

References

1. M. Shimada, D. J. Campbell, V. Mukhovatov, M. Fujiwara, N. Kirneva, K. Lackner, M. Nagami, V. D. Pustovitov, N. Uckan, J. Wesley, 2007 Chapter 1: overview and summary. Nucl. Fusion 47 (6), S1–S17.
2. A. V. Krasilnikov, S. V. Konovalov, E. N. Bondarchuk, et.al. “Tokamak with Reactor Technologies (TRT): Concept, Missions, Key Distinctive Features and Expected Characteristics”, Plasma Physics Reports **47** (11):1092–1106, 2021.
3. Tokamak BEST (ASIPP, China) Private communication.

The problem of determination of fermion vacuum content in quantum electrodynamics. The potential experiments with collisions of heavy ions

V. P. Neznamov

FSUE "RFNC-VNIIEF", Sarov, Russia, vpneznamov@mail.ru, vpneznamov@vniief.ru

At present, there are versions of quantum electrodynamics (QED) with empty fermion vacuum. It is the QED in the Foldy-Wouthuysen representation and the QED with the spinor Klein-Gordon-type equations for electrons and positrons.

In the standard QED, the fermion vacuum is a continuum for creation and annihilation of virtual electron-positron pairs. In this case, the spontaneous creation of real electron-positron pairs in intense electromagnetic fields is possible. In particular, in the standard QED, the Schwinger effect in a strong uniform electrical field is realized.

In this report, we suggest to carry out the series of experiments in the colliders with collision of heavy ions for unambiguous determination of fermion vacuum content in quantum electrodynamics. The experimental results will be the significant fundamental achievement in the quantum field theory and in the elementary particle physics.

Acknowledgements. This study was conducted within the framework of the Scientific Program of the National Center for Physics and Mathematics, Section "Particle Physics and Cosmology".

References

1. V. P. Neznamov, *Part. Nucl.*, 2006, **37**, 86–103.
2. V. P. Neznamov, *Part. Nucl.*, 2012, **43**, 36–41.
3. V. P. Neznamov and V. E. Shemarulin, *Int. J. Mod. Phys. A*, 2021, **36**, 2150086.
4. V. P. Neznamov, *Int. J. Mod. Phys. A*, 2021, 2150173.
5. V. P. Neznamov, *"Quantum electrodynamics with empty fermion vacuum. Possibilities of experimental verification"* (submitted to the journal "PhysMath").
6. R. V. Popov, V. M. Shabaev et al., *Phys. Rev. D*, 2020, **102**, 076005.
7. U. Müller, T. de Reus et al., *Phys. Rev. A*, 1988, **37**, 1449.

NICA collider complex at JINR: physics and lyrics

G. V. Trubnikov

Joint Institute for Nuclear Research (JINR, Dubna),
trubnikov@jinr.ru

The present status of the project of NICA project, which is under construction at JINR (Dubna), is given in report. The main goal of the project is to provide ion beams for experimental studies of hot and dense strongly interacting baryonic matter and spin physics. The proposed physics program concentrates on the search for possible manifestations of the phase transitions and critical phenomena in the energy region, where the excited matter is produced with maximal achievable net baryon density, and clarification of the origin of nucleon spin. The NICA collider will provide heavy ion collisions in the energy range of $\sqrt{s_{NN}}$=4÷11 GeV at average luminosity of $L=1\cdot10^{27}cm^{-2}\cdot s^{-1}$ for $^{197}Au^{79+}$ nuclei and polarized proton collisions in energy range of $\sqrt{s_{NN}}$=12÷27 GeV at luminosity of $L \geq 10^{32}cm^{-2}\cdot s^{-1}$. Time-line of the complex construction, details of start-up configuration, challenges of beam parameters and luminosity preservation are presented.

Extreme ultraviolet light source based on xenon plasma: fundamentals, recent results and prospects for lithography

I. S. Abramov[1], S. V. Golubev[1], E. D. Gospodchikov[1], A. G. Shalashov[1], A. A. Perekalov[2], A. N. Nechay[2], N. I. Chkhalo[2]

[1] A. V. Gaponov-Grekhov Institute of Applied Physics of the Russian Academy of Sciences, Nizhny Novgorod, Russia, abramov@ipfran.ru

[2] Institute for Physics of Microstructures of the Russian Academy of Sciences, Nizhny Novgorod, Russia

Narrowband extreme ultraviolet (EUV) light generated as line radiation of highly charged ions and focused by Bragg multilayer mirrors is used in high-volume manufacturing of chips [1]. The only supplier of the EUV lithography equipment now is ASML Holding N.V. In their lithographer, required plasma with multiply charged ions is supported by radiation from CO_2 laser in evaporated tin droplet [2]. The plasma emits EUV light at 13.5±1% nm with about 6% conversion efficiency of the laser pulse energy. Such high efficiency for this narrow wavelength band is obtained due to 4d-4f unresolved transition array (UTA) in spectra of highly charged tin ions which peak is located near 13.5 nm [3].

Xenon plasma is a promising alternative source of EUV light for lithography. For xenon ions, the analogous UTA peak is located near 11 nm. At this wavelength, Ru/Be multilayer mirrors have been developed with reflection coefficient even higher than this of Mo/Si mirrors used to focus EUV light at 13.5 nm [4, 5]. At normal conditions, xenon is gaseous and chemically inert. This prevents mirror contamination which is a major problem for the sources based on tin droplet evaporation [6].

Xenon EUV light source may be realized as a discharge supported by focused beam of laser radiation in high-pressure xenon jet. In a series of experiments, it was shown that the discharge is characterized by a high conversion efficiency of up to 4% into light at 11.2±1% nm [7–10]. Spatial structure of the EUV emitting region was studied with purposely developed microscope [11]. It was demonstrated that the emitting region had dimensions of several hundred microns meeting the requirements to EUV light source size [1].

In this paper, we discuss fundamentals of the laser discharge in high-pressure jet of xenon, review recent experiments, develop a relevant theoretical description and verify it on available experimental data. We pay special attention to discovered effect of the discharge expansion beyond laser focal spot due to photoionization of a surrounding neutral xenon and consecutive electron heating by a conductive thermal flux from the region of the laser power deposition [11, 12]. Basing on the theory, we propose a strategy to maximize EUV emission. In this context, we introduce Alpha-Machine, a project aimed at demonstration of a working lithographer based on xenon EUV light source supported by Yb:YAG laser and Ru/Be optics, being under development at IPM/IAP RAS. The results of simulation with the developed theoretical model allow us to obtain parameters that ensure optimal source performance for Alpha-Machine (see Table 1).

Acknowledgements. The work was supported by the Russian Science Foundation grant No. 23-22-00270.

Table 1

Optimization of xenon EUV light source for Alpha-Machine

Source parameters	
Laser pulse energy/duration	60 mJ / 1.2 ns
Laser focal waist ($D4\sigma$)	110 μm
Laser focal distance (2×Rayleigh length)	500 μm
Radius of xenon jet	600 μm
On-axis jet gas density	1.0×10^{19} cm^{-3}
Calculated discharge characteristics	
Average ion density*	0.7×10^{19} cm^{-3}
Average electron density	7.1×10^{19} cm^{-3}
Average electron temperature	40 eV
Energy balance (% of laser energy per pulse)	
Absorbed laser energy	80%
Total radiation losses	72%
EUV radiation at 11.2 ±1% nm into 2π (conversion efficiency)	7.5%

*Of which, 40% Xe^{9+}, 33% Xe^{10+}, 23% Xe^{11+}, 2% Xe^{12+}.

References

1. V. Bakshi, *EUV Sources for Lithography*, SPIE Press, 2006.
2. J. van Schoot, *IEEE Electron Devices Magazine*, 2024, **2**(1), 8–22.
3. H. Tanuma, H. Ohashi, S. Fujioka et al. *J. Phys. Conf. Ser*., 2007, **58**, 231–234.
4. N. I. Chkhalo and N. N. Salashchenko, *AIP Adv.*, 2013, **3**, 082130.
5. R. M. Smertin, N. I. Chkhalo, M. N. Drozdov et al. *Opt. Express*, 2022, **30**(26), 46749–46761.
6. N. Böwering, C. Meier, *J. Vac. Sci. Technol. B*, 2020, **38(**6), 062602 .
7. N. I. Chkhalo, S. A. Garakhin, A. Ya. Lopatin et al. *AIP Advances*, 2018, **8**, 105003.
8. S. G. Kalmykov, P. S. Butorin, and M. E. Sasin, *J. Appl. Phys.*, 2019, **126**, 103301.
9. S. G. Kalmykov, P. S. Butorin, M. E. Sasin, and V. S. Zakharov, *J. Phys. D: Appl. Phys.*, 2022, **55**, 105203.
10. V. E. Guseva, A. N. Nechay, A. A. Perekalov, N. N. Salashchenko, and N. I. Chkhalo, *Appl. Phys. B*, 2023, **129**, 155.
11. I. S. Abramov, S. V. Golubev, E. D. Gospodchikov, and A. G. Shalashov, A. A. Perekalov, A. N. Nechay, N. I. Chkhalo, "*Laser discharge in high-pressure jet of heavy noble gas: expansion of emitting volume promises efficient source of EUV light for lithography"*, yet unpublished.
12. I. S. Abramov, S. V. Golubev, E. D. Gospodchikov, and A. G. Shalashov, *Appl. Phys. Lett.*, 2023, **123**, 193502.

Climate network analysis of extreme events: Tropical Cyclones

N. Gupte, R. Sonone

Department of Physics, Indian Institute of Technology Madras, Chennai, 600036, India

We construct climate networks based on surface air temperature data to identify distinct signatures of tropical cyclones in the region of the Indian Ocean, which have serious economic and ecological consequences. The climate network shows a discontinuous phase transition in the size of the normalised largest cluster and the susceptibility during cyclonic events. We analyze these quantities for a year (2016) which had three successive cyclones, viz. Cyclone Kyant, cyclone Nada and cyclone Vardah, and compare these with a year (2017) where a single cyclone, cyclone Ockhi was seen. The microtransitions in these two cases show distinct patterns. The signatures of the cyclones can be seen in other quantities like the degree distributions and other network characterizers. The distribution of teleconnections show a distinct behaviour in the cyclonic periods. Similarly, the distribution of nodes of high degree shows distinct behaviour in cyclonic and recyclonic periods. These three cyclones were seen in the Bay of Bengal. We also compare these with a cyclone, cyclone Ashoba (2015), seen in the Arabian sea where cyclones are rarer. We discuss the implications of these results for further analysis.

The maser effect in molecular crystals

Valery Kovalev[1], Anton Sinko[2] and **Alexander Shkurinov[2,*]**

[1] Lebedev Physical Institute, RAS, Moscow, Russia
[2] Lomonosov Moscow State University, Moscow, Russia
*ashkurinov@physics.msu.ru

The invention of maser by N. Basov and A. Prokhorov marked the beginning of a laser era. The principle of stimulated emission was brilliantly implemented in microwave radiation in molecular beams. Nowadays, solid state media are used to obtain visible and NIR laser radiation. At the same time, obtaining coherent microwave radiation has been neglected. In recent years, rapid development of molecular crystal growth technology has enabled to describe new mechanisms of maser origin for generating coherent microwave radiation in solid state. In my lecture I'm going to give the historical overview of the development of ideas in microwave and later THz radiation in solid state. I'll speak about the unique properties of molecular crystals as if specially created for the development of coherent THz radiation. The special role in such crystals is played by time resolved behavior of phonons and polaritons. In some cases they are capable of emitting electromagnetic radiation, and in some cases even enhance it. I'll also discuss the main mechanisms for narrow- and broadband coherent THz radiation. Sometimes such processes require phase-matching conditions. In the concluding part of the lecture I'll talk about the application of molecular crystals for the creation of broadband metamaterial-based chemical sensors.

Post compression experiments for the intensity increase of TW and PW scale

Gabriel P. Bleotu[1], Sergey Mironov[2], Efim Khazanov[2], Gerard Mourou[3]

[1] Extreme Light Infrastructure-Nuclear Physics and University of Bucharest, Romania
[2] A.V. Gaponov-Grekhov Institute of Applied Physics of the Russian Academy of Sciences, Russia
[3] Ecole Polytechnique, France

Various high-power laser experiments, including those involvinglight matter interaction, vacuum nonlinearities, quantum electrodynamics, and nuclear transmutation, requires lasers pulses with irradiance levels surpassing $10^{23}\,\mathrm{W/cm^2}$. Post-compressing ultrashort, ultra-intense laser pulses offers a versatile solution to this requirement. This study delves into the post-compression methods ranging from terawatt (TW) to petawatt (PW) scale, aiming to demonstrate reliable and reproducible few cycle pulses.

We will present the development and a complete characterization (nonlinear response, wavefront deformation, dispersion) of the nonlinear materials used for spectral broadening which includes various glass and plastic materials. Using these materials for spectral broadening up to 5-fold compression at 100s TW peak power was achieved. Therefore, we succeed to post compress laser pulses ranging from 350 fs–25 fs [1–4] down to sub 10 fs for J level input energies.

The wavefront distortions, small scale self-focusing, temporal and spatial shape, temporal and spatial Strehl ratio will be discussed in details while showing the progress towards single cycle regime at J level.

Insights gained can be further applied to lasers of different parameters, revealing method constraints and applicability [5], aiding high-power lasers advance towards implementation at 10 PW power level.

References

1. J. Wheeler et al., Photonics **9**, 715, (2022).
2. P.-G. Bleotu et al., High Power Laser Sci. Eng., **11**, 30, (2023).
3. P.-G. Bleotu et al., High Power Laser Sci. Eng. **10** (2022).
4. P.-G. Bleotu et al., Four cycles, focused post-compressed 100 TW laser pulses, in preparation.
5. V. Horný, et al., Jan. 15, 2024. doi: 10.21203/rs.3.rs-3856955/v1.

SECTION 1

NONLINEAR DYNAMICS AND ITS APPLICATIONS IN GEOPHYSICS AND ASTROPHYSICS

Fast radio bursts in binary systems

M. V. Barkov

Institute of Astronomy of the Russian Academy of Sciences, Moscow, Russia, barmv05@gmail.com

We consider a magnetar flare model for fast radio bursts (FRBs). We show that millisecond bursts of sufficient power can be generated by synchrotron maser emission ignited at the reverse shock propagating through the weakly magnetized material that forms the magnetar flare. If the maser emission is generated in an anisotropic regime (due to the geometry of the production region or presence of an intense external source of stimulating photons), the duration of the maser flashes is similar to the magnetar flare duration even if the shock front radius is large. Our scenario allows for relaxing the requirements for several key parameters: the magnetic field strength at the production site, luminosity of the flare, and the production site bulk Lorentz factor. To check the feasibility of this model, we study the statistical relation between powerful magnetar flares and the rate of FRBs. The expected ratio is derived by convoluting the redshift-dependent magnetar density with its flare luminosity function above the energy limit determined by the FRB detection threshold. We obtain that only a small fraction, $\sim 10^{-5}$, of powerful magnetar flares trigger FRBs. This ratio agrees surprisingly well with our estimates: we obtained that 10% of magnetars should be in the evolutionary phase suitable for the production of FRBs, and only 10^{-4} of all magnetar flares in the Universe are expected to be weakly magnetized, which is a necessary condition for the high-frequency maser emission.

It is shown that only during a fraction of the orbital period, radio emission can escape the system independently of the emission machanism. This explains the duty cycle of the three repeating FRB sources with periodic activity. The width of the transparency window depends on the eccentricity, stellar wind properties, and the viewing angle. To describe the properties of the known sources, it is necessary to assume large eccentrici ties $\gtrsim 0.5$. We apply the maser cyclotron mechanism of the radio emission generation to model spectral properties of the sources. The produced spectrum is not wide: $\Delta\nu/\nu \sim 0.2$ and the typical frequency depends on the radius of the shock where the emission is generated. The shock radius changes along the orbit. This, together with changing parameters of the medium, allows us to explain the frequency drift during the phase of visibility.

The nonlinear Schrödinger equation and canonical transformation

A. I. Dyachenko

Landau Institute for Theoretical Physics, Chernogolovka, Russia, alexd@itp.ac.ru
Skolkovo Institute of Science and Technology, Moscow, Russia
Higher School of Economics, Moscow, Russia

Consider 1D NLSE for the field $q(x,t)$

$$i\dot{q} + q_{xx} + |q|^2 q = 0 \quad (1)$$

in the periodic domain of 2π. Making Fourier transformation of (1) one can get:

$$i\dot{q}_n - n^2 q_n + \sum_{n_1,n_2,n_3} q^*_{n_1} q_{n_2} q_{n_3} \delta_{n+n_1,n_2+n_3} = 0. \quad (2)$$

Here

$$q(x,t) = \sum_n q_n(t) e^{inx},$$

$$q_n(t) = = \frac{1}{2\pi}\int_0^{2\pi} q(x,t) e^{-inx} dx.$$

Wave numbers are integers in the periodic domain of 2π. The Hamiltonian of the equation is the following:

$$H = \sum_n n^2 |q_n|^2 - \frac{1}{2}\sum_{n,n_1,n_2,n_3} q^*_n q^*_{n_1} q_{n_2} q_{n_3} \delta_{n+n_1,n_2+n_3}$$

Some canonical transformation $q_n \to b_n$ is applied to (2). This transformation has the following form of infinite series:

$$q_n = b_n + \\ + \sum_{n_1,n_2,n_3} B^{nn_1}_{n_2 n_3} b^*_{n_1} b_{n_2} b_{n_3} \delta_{n+n_1-n_2-n_3} + \ldots \quad (3)$$

The transformation was constructed using the technique described in.

The series converges only for small values of b_n:

$$\frac{|b_n|}{\Delta k} < 1, \quad (\Delta k = 1 \quad \text{for domain} \quad 2\pi)$$

Coefficients $B^{nn_1}_{n_2 n_3}$ (and others) of the canonical transformation are chosen to simplify the Hamiltonian. The transformation removes all nonresonant terms in the Hamiltonian and (what is the most important thing) simplifies the fourth order term. So, that

$$H = \frac{1}{2}\sum_n k_n^2 |b_n|^2 - \sum_{n,n_1} D_{nn_1} |b_n|^2 |b_{n_1}|^2 + \mathcal{O}(b^8) \quad (4)$$

$$D_{nn_1} = \begin{cases} 2 & if \quad n \neq n_1 \leq 0, \\ 1 & if \quad n = n_1. \end{cases}$$

Six order term in the Hamiltonian vanishes also (See [2]). For small values of b_n one can consider a reduced Hamiltonian in which only the terms of the fourth order are kept. Then the equation for b is also very simple:

$$i\dot{b}_n - n_n^2 b_n + 2[\sum_{n_1} D_{nn_1} |b_{n_1}|^2] b_n \quad (5)$$

The solution of the equation (5) is trivial:

$$b_n(t) = b_n(0) e^{i(\delta K n - n^2)t} \quad (6)$$

Here

$$\delta K n = 2[\sum_{n_1} D_{nn_1} |b_{n_1}|^2]$$

does not depend on x and is defined by initial conditions only.

Acknowlegements. The work was supported by the Russian Science Foundation grant no. 19-72-30028.

References

1. V. E. Zakharov, V. S. Lvov and G. Falkovich. *Kolmogorov Spectra of Turbulence I*, Springer-Verlag, 1992.
2. A. I. Dyachenko, D. I. Kachulin and V. E. Zakharov. *JETP. Lett.* 2013, 98(1), 43–47.

A model of electron acceleration in the chromosphere of the Sun. Generation of super-Dreicer electric field by a nonlinear Alfven wave in footpoints of magnetic loops

N. A. Emelyanov, **V. V. Zaitsev** and **Vl. V. Kocharovsky**

A.V. Gaponov-Grekhov Institute of Applied Physics of the Russian Academy of Sciences, Nizhny Novgorod, Russia,
n.emelyanov@ipfran.ru

Particle acceleration plays a crucial role in the explanation of observed hard X-ray and gamma emission during solar flares. However, a pointing out the accelerating mechanism and localization of the accelerating area is still challenging. According to the observational data [1, 2], in some cases a number of accelerated particles exceeds a total number of particles occupying a typical coronal loop. So, the models of solar flares face with a problem of high efficiency of the acceleration process. Necessary amount of particles, for example, is contained in a chromospheric part of magnetic loops, namely, in area between the temperature minimum and the transition region, where plasma is much denser than in the corona. Moreover, combined observational data from New Solar Telescope (NST) in the Big Bear Solar Observatory (BBSO) and Atmospheric Imaging Assembly (AIA) on the Solar Dynamics Observatory (SDO) [3] revealed injection of hot dense plasma from footpoints of magnetic loops to their coronal parts. It indicates that particle acceleration and plasma heating can take place directly in the chromosphere.

A model of chromospheric accelerator based on a generation of super-Dreicer electric field by a nonlinear Alfven pulse, which was excited due to Rayleigh — Taylor instability in a footpoint of a magnetic loop, was first considered by V. V. Zaitsev et al. in [4, 5]. However, it was done without taking into account an expansion of magnetic loops with increase of height and, hence, the results can be applied only for bases of magnetic tubes.

This model is developed in the present work. A propagation of an Alfven wave in an exponentially expanding magnetic tube, which is expected to be close to the real conditions, is analytically investigated within a magnetohydrodynamic (MHD) approach. A differential equation, describing the propagation of the Alfven pulse under the abovementioned restrictions, is obtained and its "self-similar" solution is found. Analytical estimation of the electric field, which is generated by this nonlinear pulse and has a component along the ambient magnetic field lines, is given. It is found, that the value of the induced electric field exceeds the super-Dreicer limit [6]:

$$E_D = \frac{e}{r_D^2}\ln\Lambda \qquad (1)$$

Here e is an electron charge, r_D the Debye length, and $\ln\Lambda$ the Coulomb logarithm.

Therefore, almost all particles can be involved in the acceleration process in a footpoint region that guarantees a strong injection of energetic electrons into a coronal part of the magnetic loop. Also, the exponential expansion of a magnetic tube leads to an increase of the value of generated electric field with increase of height.

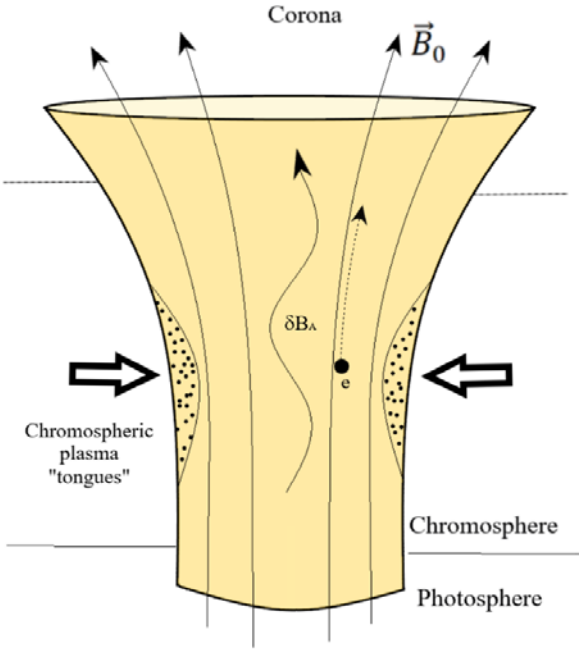

Fig. 1. Schematic illustration of the electron acceleration by the Alfven wave, propagating in the footpoint of the magnetic loop

Thus, we confirm the general conclusions that were made in [4, 5] and discuss possible outcomes of the described scenario in all perspectives, paying particular attention to a modification of the electric current and magnetic field structure by the energetic electrons injected in the coronal loop.

Acknowledgements. This research was supported by the Russian Science Foundation, Grant No.22-12-00308.

References

1. Miller J. A., et al. 1997, J. Geophys. Res. 102, 14631.
2. Emslie A. G., Hénoux J. C. 1995, Astrophys. J. 446, 371.
3. Ji H., Cao W., Goode P. R. 2012, Astrophys. J. Lett. 750, L25.
4. Zaitsev V. V., Stepanov A. V. 2015, Solar Physics 290, 3559.
5. Zaitsev V. V., Kronshtadtov P. V., Stepanov A. V. 2016, Solar Physics 291, 3451.
6. Landau L. D., Lifshitz E. M. Course of Theoretical Physics, M., Nauka, V. 10, p. 222.

Analysis of sprite activity in Russia

A. A. Evtushenko

A.V. Gaponov-Grekhov Institute of Applied Physics of the Russian Academy of Sciences, Nizhny Novgorod, Russia,
a_evtushenko@inbox.ru

Various types of high-altitude discharges were discovered relatively recently, and by now there is an understanding of the basic mechanisms of initiation and there is a generally accepted classification. High-altitude discharges of all types are associated with lightning activity in the troposphere, and naturally in the equatorial regions their number is significantly higher than in the middle latitudes. This work is devoted to the analysis of the distribution of sprites over the territory of Russia, which can be used to plan field observations and estimate the total number of high-altitude discharges. Previously, a parameterization for studying the global distribution of sprites based on data from the WWLLN lightning detection system was proposed and applied to analyzing sprite activity in 2016 [1]. The initiation of each sprite is associated with a powerful lightning discharge, which is called the parent, which makes it possible to propose a parameterization for the distribution of sprites based on the lightning detection data. In this work, a similar approach is applied to study sprites over the territory of Russia for the period 2015–2021 [2].

Due to the location of the Russian Federation in the mid-latitudes of the Northern Hemisphere, the seasonality of thunderstorm activity here is more pronounced than the global average. The total number of lightning discharges for the period November–March in each of the years under study is in the range of 1000–2000 discharges, i.e., no more than 0.3% of the annual number of discharges; thus, these months can be excluded from consideration.

For the study, only lightning discharges with a current of more than 15 kA were taken, as for the global distribution. Maximum currents were observed in 2015–2016 (70–80 kA), with minimums in 2019 and 2020 (40–45kA). Due to its geographical location in the mid-latitudes of the Northern Hemisphere, average currents in the Russian Federation only in the summer months are comparable to average global currents; in the spring-autumn periods, they are 20% lower, which directly influences the number of sprites.

The study shows that the number of sprites over Russia varies significantly from year to year: from 394 in 2019 to 2354 in 2015, which could be assumed immediately from the analysis of the WWLLN data. The dynamics of the number of sprites over Russia is unexpectedly close to the global one: from 2015 to 2019, there was a gradual decline in the number of sprites, with a subsequent increase in 2020–2021. One might expect that the change in sprite activity in mid-latitudes has a larger amplitude, but comparison with the global sprite distribution shows that the trend is quite close to the global trend.

Sprite activity over Russia has a pronounced seasonality (fig. 1): the largest number of high-altitude discharges occurs from June to August, while the number of sprites from November to March is negligible and amounts to less than 2% of the total.

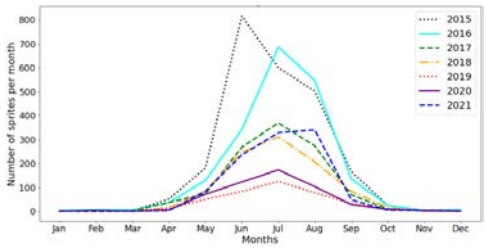

Fig. 1. Seasonal dynamics of the sprite number for 2015–2021

An increase in the number of sprites with decreasing latitude is clearly visible, which is typical for atmospheric electricity phenomena in general since lower humidity and the intensity of convection at higher latitudes do not allow active separation of charges (fig. 2). Taking into account the calculation data for different years, we can conditionally distinguish three areas with high sprite activity: Krasnodar Territory, Altai, and the Far East. It is well known that mesoscale convective systems, due to their structure and large horizontal dimensions, are capable of accumulating large charges, which, on the one hand, contribute to high lightning activity and, on the other hand, allow the development of positive lightning discharges, characterized by high current and transferred charge. Due to the characteristics of the relief and underlying surface in Altai (forest-swamp and forest-steppe zones with a high degree of swamping are complemented by a mountain system in the southeast), conditions for the formation of MCS and high sprite activity are created annually, and in the Far East and Krasnodar Territory, sprite activity is determined by incoming convective systems and has high year-to-year variability.

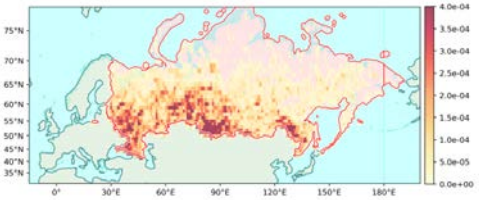

Fig. 2. Sprite density over Russia in 2016

Acknowledgements. The work was supported by the state assignment of the Institute of Applied Physics of the Russian Academy of Sciences (Project FFUF-2023-0004).

References

1. A. Evtushenko, N. Ilin, E. Svechnikova, *Atmos. Res.*, 2022, **276**, 106272.
2. A. Evtushenko, E. Svechnikova, A. Kudryavtsev, *Atmosphere*, 2024, **15**(169).

Statistical physics approaches to the complex Earth system

J. Fan

Beijing Normal University, Beijing, China, j.fang.fan@gmail.com

The 2021 Nobel Prize in Physics was awarded to Syukuro Manabe, Klaus Hasselmann, and Giorgio Parisi for their “pioneering contributions to our understanding of complex physical systems”. The first two made significant achievements in the area of physical modeling of Earth’s climate, quantifying variability, and reliable predictions of global warming. As a complex adaptive system, the Earth may have multiple potential tipping elements. The interactions among these elements can have stabilizing or destabilizing effects on other subsystems, potentially leading to abrupt cascading failures, thereby increasing the threat of sudden and irreversible climate changes. It is imperative that effective actions are taken to mitigate the negative impacts of climate change. However, the complex structure of the Earth's system and the presence of numerous nonlinear interactions make it exceedingly difficult to understand and predict such catastrophic events. This is a topic of great concern to both the scientific community and policymakers. In this report,I will elaborate and discuss recent applications of statistical physics and network theory to Earth's complex systems.

Estimation of forced climate response in ensembles of realizations

A. S. Gavrilov[1], S. V. Kravtsov[2,3], A. M. Feigin[1]

[1] A.V. Gaponov-Grekhov Institute of Applied Physics of the Russian Academy of Sciences, Nizhny Novgorod, Russia, gavrilov@ipfran.ru
[2] University of Wisconsin-Milwaukee, Milwaukee, USA
[3] Shirshov Institute of Oceanology of Russian Academy of Sciences, Moscow, Russia

Earth climate is a complex nonlinear system with a lot of feedbacks on different time scales, subjected to external forcing. For example, in the 20^{th} – 21^{st} centuries the forcing can be associated with the growth of greenhouse gas concentration in the atmosphere (global warming), global aerosol variations due to volcanic activity, anthropogenic CO_2 emissions, solar activity etc. Detection and attribution of forced and internal dynamics in this system is an important problem which is hard to solve primarily because there is only one single realization of this system available for observation.

One possibility to move forward in this problem is to use state-of-the-art Earth system models which are able to generate many climate simulations under the same forcing. Although each of these models has its own climate, altogether they can be used to extract the dynamical laws which are common in different model climates, and, hopefully, in real climate. In this work we focus on the problem of forced climate response detection. Hereinafter, we think of the forced response as the mean signal across the (infinite) ensemble of realizations which can be generated by the system starting from infinitely far (in time) random initial conditions, if it exists and unique. Note that for a linear system it would be equivalent to its forced solution, while for nonlinear system it is just an additive signal which the system evolves around in average, but it still may be useful for some applications. We develop a two-step method able to extract information about forced responses from given ensemble of realizations of many models and then estimate forced response in a new (unseen) climate realization.

As a first step, our method analyses multi-model ensemble of spatially distributed realizations (training set) and estimates the forced response in each model. This is done by modification of a recently developed Bayesian ensemble linear dynamical mode (LDM) decomposition [1–3] which is able to disentangle components of forced and internal variability in ensembles of realizations of a single model, assuming that the forced components are the same in all realizations while the internal components are independent of each other. Essentially, the time scales of all components are optimized during the procedure. Here we generalized LDMs for the multi-model ensemble case by assuming that the forced components are only the same within sub-ensembles corresponding to particular models, and after that the same Bayesian optimization procedure is applied.

The second step of our method approximates a mapping from one single realization to the forced LDM components corresponding to it. To do it, initial single realization is at first smoothed in time by boxcar running-mean filter, and then each forced component is linearly regressed on it. The smoothing time scale is optimized separately for each forced component, and altogether this procedure is called smoothed linear regression (SLR). Note that due to training across many models and single-model realizations SLR tends to be *robust* with respect to both internal variability and inter-model differences, and can be applied to new unseen data after training.

Altogether, our method is called LDM-SLR. We also developed an alternative method in which the first step is simpler but much more computationally fast: the forced components are determined there by ensemble model-wise empirical orthogonal function (EOF) decomposition; it is called EOF-SLR. Being conceptually simpler, it is also expected to have good performance for large training ensembles. Fig. 1 exemplifies the first results of both methods tested on the ForceSMIP [4] ensemble of 5 models. The first 10 realizations of each model were used to train LDM-SLR and EOF-SLR. The other 135 members were used for testing. In general, both of our methods give good results and can be compared with other statistical approaches.

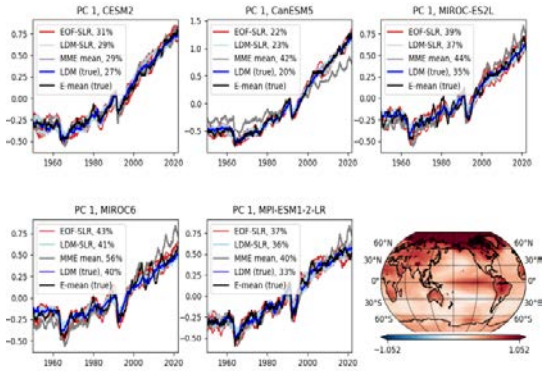

Fig. 1. Forced signal estimation (projected onto leading EOF) by LDM-SLR, EOF-SLR and simple multi-model ensemble mean (MME mean) from testing realizations. Black: "true" forced signal estimation (from all realizations). Blue: LDM forced signal estimation from 10 realizations of each model

Acknowledgements. The research was supported by the state assignment of the Institute of Applied Physics of the Russian Academy of Sciences (Project No. FFUF-2022-0008).

References

1. Gavrilov, A., Kravtsov, S., Buyanova, M., Mukhin, D., Loskutov, E., Feigin, A., *Clim. Dyn.*, 2024, **62**, 1783–1810.
2. Gavrilov, A., Seleznev, A., Mukhin, D., Loskutov, E., Feigin, A., Kurths, J., *Clim. Dyn.*, 2019, 52, 2199–2216.
3. Gavrilov, A., Kravtsov, S., Mukhin, D., *Chaos*, 2020, 30, 123110.
4. Wills, J. R., C. Deser, K. McKinnon, A. Phillips, and S. Po-Chedley, *EGU General Assembly 2024*, EGU24-1962.

Ocean turbulence at large Richardson number

D. S. Gladskikh[1,2,3] and **L. A. Ostrovsky**[1,4]

[1] A.V. Gaponov-Grekhov Institute of Applied Physics of the Russian Academy of Sciences, Nizhny Novgorod, Russia, daria.gladskikh@gmail.com
[2] Research Computing Center, Moscow State University, 119991 Moscow, Russia
[3] Moscow Center for Fundamental and Applied Mathematics, Moscow, Russia
[4] University of Colorado, Boulder, USA

In this study, the theory of stratified turbulent flow developed and discussed earlier by the authors [1–2] is applied to data from different areas of the ocean. The kinetic model of turbulence is used to describe the evolution and structure of the upper turbulent layer with the parameters taken from in situ observations. Particular attention is paid to the cases of the large Richardson number and the role of turbulent potential energy in explaining the observation data. It is shown that turbulence can be amplified and supported even at large gradient Richardson numbers. The cause of that is the exchange between kinetic and potential energies of turbulence.

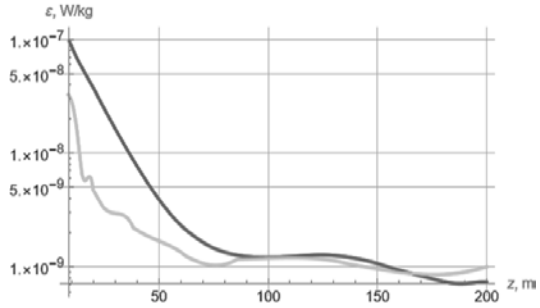

Fig. 1. Profiles of turbulent kinetic energy dissipation rate for cruise D306. Light grey – interpolated data of [3]. Dark grey – theory

As an example, we used some data from the paper [3] that provided a relatively detailed set of measurements for three cruises taken in 2006-2009 in different areas of the world ocean: North Atlantic (cruise D306, June-July 2006 and cruise D321, July – August 2007) and Southern Ocean (cruise JC29, November – December 2008). These experiments were aimed at studying turbulent mixing in the presence of a stratified shear flow associated with mesoscale motions such as eddies and fronts. With the given profiles of current shear and buoyancy frequency taken from [3], the theory developed in [1] yields the results that satisfactorily agree with the measurements of the turbulent dissipation rate given in [3] (see, for example, Fig. 1).

These results were obtained in neglection of vertical turbulence diffusion. To verify this approximation, we solved the full system, adding boundary conditions for fluxes of kinetic and potential energy. In all cases, the local and full models are practically identical.

We demonstrated that including the potential energy of turbulence (associated with density fluctuations in the presence of stratification) in the semi-empirical, Reynolds-type equations of a turbulent flow allows to explain the existence and evaluate the parameters of small-scale turbulence at large Richardson numbers. We have also shown that the contribution of turbulent diffusion to the level of turbulent pulsations is insignificant in the above case.

Acknowledgements. The work was supported by FSTP project “Study of processes in the boundary layers of the atmosphere, ocean and terrestrial waters and their parameterization in Earth system models” within the project “Improvement of the global world-level Earth system model for research purposes and scenarios forecasting of climate change”.

References

1. Ostrovsky, L. A., and Troitskaya, Y. I., *Izvestiya Akademii Nauk Sssr Fizika Atmosfery I Okeana*, 1987, **23**(10), 1031–1040.
2. Gladskikh, D., Ostrovsky, L., Troitskaya, Y., Soustova, I., and Mortikov, E., *Journal of Marine Science and Engineering*, 2023, **11**(1), 136.
3. Forryan, A. et al, *Journal of Geophysical Research: Oceans*, 2013, **118**(3), 1405–1419.

High-order schemes of exponential time differencing for stiff systems with nondiagonal linear part

D. S. Goldobin[1,2] and **E. V. Permyakova**[1]

[1] Institute of Continuous Media Mechanics UB RAS, Perm, Russia, Denis.Goldobin@gmail.com
[2] Perm State University, Perm, Russia

In condensed matter physics, fluid dynamics, chemical and biological physics, many systems are governed by the mathematical models which can be called "stiff" systems – the systems where some modes are fast oscillating or decaying. The topics dealing with such systems include, but not limited to: problems of Anderson localization [1], macroscopic description of spinodal decomposition [2, 3], heat-masstransfer in active media [4, 5], Fokker-Planck dscription for chemical oscillations [6] and neuronal networks [7].

Numerical simulation of these systems with conventional methods is generally too much CPU-time consuming. Two-three decades ago, a family of nonconventional methods was introduced – exponential time differencing (ETD) ones [8] – which is a tool for very accurate high-performance simulation for conservative systems, and stable high-performance simulation for dissipative systems. However, practical implementation of these methods for the systems with nondiagonal linear part of equations is exacerbated by infeasibility of an analytical calculation of the exponential of a nondiagonal linear operator; in this case, the coefficients of the exponential time differencing scheme cannot be calculated analytically. We develop a universal approach for fast and easy practical implementation of the ETD methods [9, 10].

We suggest an approach, where these coefficients are numerically calculated with auxiliary problems. We rewrite the high-order Runge – Kutta type schemes in terms of the solutions to these auxiliary problems and practically examine the accuracy and computational performance of these methods for a heterogeneous Cahn – Hilliard equation, a sixth-order spatial derivative equation governing pattern formation in the presence of an additional conservation law, and a Fokker – Planck equation governing macroscopic dynamics of a network of neurons.

Employment of the presented approach greatly helped us with numerical studies of several problems of nonlinear dynamics: a conclusive study with demanded accuracy was simply infeasible with conventional methods or required many months of simulation on high-performance computer clusters.

Algorithms

For the numerical integration of equation system

$$\dot{\mathbf{u}} = \mathbf{L}\cdot\mathbf{u} + \mathbf{f}(\mathbf{u},t)\,, \qquad (1)$$

auxiliary problems are to be integrated numerically over a reasonably small time interval τ in order to calculate matrices $\mathbf{Q}$ and $\mathbf{M}_n$:

$$\mathbf{u}(t=\tau \mid \mathbf{u}(0),\mathbf{f}=0) = \mathbf{Q}(\tau)\cdot\mathbf{u}(0)\,, \qquad (2)$$

$$\mathbf{u}(t=\tau \mid \mathbf{u}(0)=0,\mathbf{f}(t)=\mathbf{g}t^{n-1}) = \mathbf{M}_n(\tau)\cdot\mathbf{g}\,. \qquad (3)$$

Technically, one calculates these matrices from the following definition:

$$Q_{jk}(\tau) = u_j(t=\tau \mid u_l(0)=\delta_{lk},\, \mathbf{f}=0)\,,$$
$$(\mathbf{M}_n(\tau))_{jk} = u_j(t=\tau \mid \mathbf{u}(0)=0,\, f_l(t)=\delta_{lk}t^{n-1})\,.$$

With calculated matrices $\mathbf{Q}$ and $\mathbf{M}_n$ one can employ the multi-step Runge–Kutta type schemes for exponential time differencing. For instance a fourth order scheme ETD4RK:

$$\begin{aligned}
\mathbf{a} &= \mathbf{Q}_{\tau/2}\cdot\mathbf{u}(t) + \mathbf{M}_{1,\tau/2}\cdot\mathbf{f}(\mathbf{u}(t),t)\,,\\
\mathbf{b} &= \mathbf{Q}_{\tau/2}\cdot\mathbf{u}(t) + \mathbf{M}_{1,\tau/2}\cdot\mathbf{f}(\mathbf{a},t+\tau/2)\,,\\
\mathbf{c} &= \mathbf{Q}_{\tau/2}\cdot\mathbf{a} + \mathbf{M}_{1,\tau/2}\cdot[2\mathbf{f}(\mathbf{b},t+\tau/2)-\mathbf{f}(\mathbf{u}(t),t)]\,,\\
\mathbf{u}(t+\tau) &= \mathbf{Q}\cdot\mathbf{u}(t) + \left[\frac{2\mathbf{M}_3}{\tau^2} - \frac{3\mathbf{M}_2}{\tau} + \mathbf{M}_1\right]\cdot\mathbf{f}(\mathbf{u}(t),t)\\
&\quad - \left[\frac{2\mathbf{M}_3}{\tau^2} - \frac{2\mathbf{M}_2}{\tau}\right]\cdot\Big(\mathbf{f}(\mathbf{a},t+\tau/2)+\mathbf{f}(\mathbf{b},t+\tau/2)\Big)\\
&\quad + \left[\frac{2\mathbf{M}_3}{\tau^2} - \frac{\mathbf{M}_2}{\tau}\right]\cdot\mathbf{f}(\mathbf{c},t+\tau)\,,
\end{aligned}$$

where subscript $\tau/2$ for matrices indicates that they are calculated for a half stepsize of the ETD scheme.

Acknowledgements. The authors acknowledge financial support by the Ministry of Science and Higher Education of the Russian Federation (Theme No. 124021600038-9).

References

1. A. S. Pikovsky and D. L. Shepelyansky, *Phys. Rev. Lett.*, 2008, **100**(9), 094101.
2. A. A. Golovin, A. A. Nepomnyashchy, S. H. Davis, and M. A. Zaks, *Phys. Rev. Lett.*, 2001, **86**, 1550–1553.
3. S. J. Watson, F. Otto, B. Y. Rubinstein, and S. H. Davis, *Physica D*, 2003, **178**(3), 127–148.
4. P. C. Matthews and S. M. Cox, *Nonlinearity*, 2000, **13**(4), 1293–1320.
5. P. C. Matthews and S. M. Cox, *Phys. Rev. E*, 2000, **62**(2), R1473–R1476.
6. R. Erban, S. J. Chapman, I. G. Kevrekidis, and T. Vejchodsky, *SIAM J. Appl. Math.*, 2009, **70**(3), 984–1016.
7. M. di Volo, M. Segneri, D. S. Goldobin, A. Politi, and A. Torcini, *Chaos*, 2022, **32**(2), 023120.
8. S. M. Cox and P. C. Matthews, *J. Comput. Phys.*, 2002, **176**(2), 430–455.
9. E. V. Permyakova and D. S. Goldobin, *J. Appl. Mech. Tech. Phys.*, 2020, **61**(7), 1227–1237.
10. E. V. Permyakova and D. S. Goldobin, *SSRN*, 2024, DOI: 10.2139/ssrn.4768118.

Neuromorphic memory in spiking neuron-astrocyte network

S. Yu. Gordleeva

Lobachevsky State University, Nizhny Novgorod, Russia, gordleeva@neuro.nnov.ru

Modeling the neuronal processes that underlie short-term working memory represents a persistent challenge and a focal point for numerous theoretical investigations in neuroscience. Recently, we present a novel mathematical model featuring a spiking neural network integrated with astrocytes [1]. This model effectively simulates the maintenance of a fragment of information as a resilient activity pattern over several seconds, while elucidating the mechanisms by which this pattern dissipates in the absence of additional stimuli. Our findings shed light on the potential neuro-astrocytic mechanisms governing working memory and provide insights into the functional role of astrocytes in this cognitive process (the prolegomena to this work were published earlier in [2]).

Working memory, often referred to as the brain's "operative memory", plays a pivotal role in rapidly storing and managing information patterns during cognitive tasks. While the conventional belief centered around synaptic connections and plasticity among neurons as the primary carriers of memory functions, a critical element seemed to be missing in the construction of mathematical models attempting to replicate these phenomena.

Astrocytes, cells that accompany neurons and provide trophic and metabolic support, have emerged as crucial players in the working memory process. Not only do they function as slow buffers with signals lasting seconds – thousands of times longer than neuronal spikes – but they also modulate synaptic transmission, akin to synaptic plasticity. Decoding the spatial-temporal calcium signaling in astrocytes and understanding its impact on neuronal signaling present major challenges in modern neurobiology. We proposed a novel bio-inspired two-net spiking neuron-astrocyte network (SNAN) for more complex learning tasks. The concept of the proposed situation-based memory model is schematically summarized in fig. 1. This SNAN, implemented for associated learning, was designed to address issues related to overlapping patterns and enhance memory performance. The model was tested using a novel approach to temporal non-IID data organization for machine learning in spiking neuronal networks. The synergistic interplay between the fast spiking neuronal network and slow astrocytic events demonstrated a remarkable enhancement in memory performance. We believe that the team's findings [1, 2], not only deepen our understanding of the brain's working memory but also pave the way for the development of brain-inspired artificial intelligence systems.

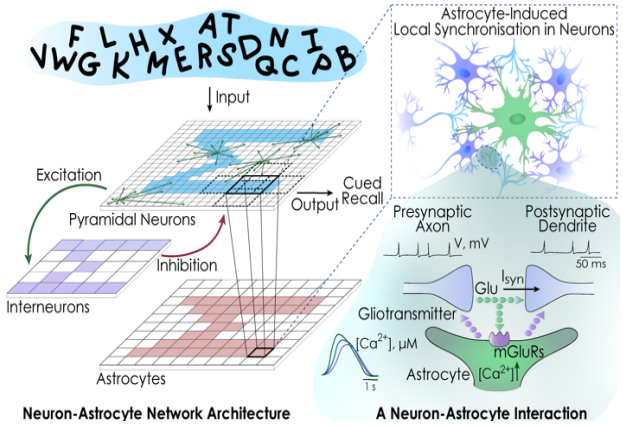

Fig. 1. Concept of the situation-based memory operation in the SNAN model. SNAN topology. The SNAN includes three layers: the layes of pyramidal neurons, the layer of interneurons, and the astrocytic layer. The first layer (79 × 79) consists of synaptically coupled pyramidal neurons. The pyramidal neurons bidirectionally communicate with the interneurons from the second layer (40 × 40). The ratio of pyramidal neurons to interneurons in the model is chosen in accordance with the experimental observations and computational model of the cortex, where 80% of the CSN neurons are pyramidal neurons and 20% are interneurons. Astrocytes are connected by a local gap junction diffusive couplings and represent a 2-D square lattice with a dimension 26 × 26. We focus on the bidirectional interaction between the first neuronal and astrocytic layers. Each astrocyte is interconnected with an ensemble of Na = 16 pyramidal neurons with dimensions 4 × 4 (red lines) overlapping in one row and one column. An input signal encoded as a 2-D pattern is applied to the first layer

Acknowledgements. This work was supported by the Ministry of Science and Higher Education of the Russian Federation according to research project No. FSWR-2023-0029.

References

1. Gordleeva S., Tsybina Y. A., Krivonosov M. I., Tyukin I. Y., Kazantsev V. B., Zaikin A., Gorban A. N. Situation-Based Neuromorphic Memory in Spiking Neuron-Astrocyte Network. IEEE Trans Neural Netw Learn Syst. 2023 Dec 4;PP. doi: 10.1109/TNNLS.2023.3335450
2. Gordleeva S. Y., Tsybina Y. A., Krivonosov M. I., Zaikin A. A., Ivanchenko M. V., Kazantsev V. B., Gorban A. N. Modelling working memory in spiking neuron network accompanied by astrocytes, Frontiers in Cellular Neuroscience. 2021, 15, 631485. doi: https://doi.org/10.3389/fncel.2021.631485.

Signaling is the most sensitive process of plants when influenced by low-intensity astro- and geophysical factors

M. A. Grinberg[1,2], **Y. A. Nemtsova**[1], **A. V. Ivanova**[1], **P. A. Pirogova**[1], **N. V. Ilin**[2], **E. A. Mareev**[2] and **V. A. Vodeneev**[1]

[1] Lobachevsky State University of Nizhny Novgorod, Nizhny Novgorod, Russia, mag1355@yandex.ru
[2]A.V. Gaponov-Grekhov Institute of Applied Physics of the Russian Academy of Sciences, Nizhny Novgorod, Russia

During growth and development, plants are exposed to environmental factors that can affect the activity of various processes occurring in a living organism. Some of these factors, such as, for example, ionizing radiation (IR) and magnetic fields (MF), are relatively stable under normal conditions, but their parameters can vary greatly due to natural and man-made disasters [1]. Significant differences also occur in space station environments, where sustainable plant growing is a major challenge [2]. According to established tradition, the study of the influence of such factors on living organisms is carried out in the range of factor intensities that significantly exceed natural limits [3]. The possibility of extrapolating such data is limited, since for many physiological processes in the range of low intensities of the acting factor there is a loss of linear connection. In addition, different physiological processes in the low-intensity and low-dose range demonstrate different sensitivity to factors. The purpose of this work was to identify the most sensitive plant processes to ionizing radiation and magnetic fields in the Schumann resonance range.

Experiments were performed on 14-15-day-old wheat plants (*Triticum aestivum* L). At the first stage of the experiment, plants were subjected to acute irradiation (IR) in high doses to identify the sensitivity of various processes. Irradiation of dry seeds was performed on a Novalis Tx linear accelerator (Varian, USA) at the Nizhny Novgorod Regional Clinical Hospital named after N. A. Semashko. Irradiation was carried out in doses of 25, 50, 75, 100 Gy, the dose rate was 10 Gy/min. At the second stage, the identified most sensitive processes were tested under the chronic action of low-intensity factors. Irradiation (IR) was carried out using a β-radiation source (^{90}Sr–^{90}Y) with a dose rate of approximately 0.52 μGy/min. The MF was set by Helmholtz coils. The field frequency was 14.3 Hz, the magnitude was 18 μT. The plants were exposed to low-intensity exposure to IR and MF throughout the entire growing period.

The status of plants was assessed based on morphometric indicators, photosynthetic activity and parameters of stress signaling systems. Chlorophyll fluorescence indicators, reflecting the activity of the light stage of photosynthesis, were recorded using a PlantExplorer^{Pro+} PAM fluorometer (PhenoVation, the Netherlands). To measure the level of CO_2 assimilation, an infrared gas analyzer GFS-3000 with a Dual-PAM gas-exchange Cuvette 3010-Dual measuring head (Heinz Walz GmbH, Germany) was used. The parameters of the signaling systems were assessed by the amplitude of electrical reactions caused by an additional stimulus. Electrical reactions were recorded extracellularly using glass macroelectrodes. Changes in illumination and a local increase in temperature were used as model stimuli causing electrical reactions.

It has been shown that morphometric parameters, activity of physiological processes and signaling processes of plants differ in their sensitivity to IR over a wide range of doses. Signaling systems have been the most impacted by IR. Electrical reactions parameters began to show differences with non-irradiated controls even at the lowest doses tested. To change the parameters of photosynthesis and the linear size of plants, many times larger doses of IR are required.

For experiments with low-intensity chronic exposure, a range of IR doses was used in which there is no effect of radiation on morphometric parameters and photosynthetic activity. Under such conditions, a significant increase in the amplitude of heating-induced electrical signals was shown.

For plants exposed to low-intensity MF, similar effects are shown. At field values at which there is no pronounced effect on morphometric parameters and photosynthetic activity, a significant increase in light-induced electrical reactions was found.

Thus, signaling may be a universal process with the highest sensitivity to various low-intensity environmental factors. The high sensitivity of signaling systems can lead to the formation of altered plant resistance to unfavorable conditions under the influence of astro- and geophysical factors.

Acknowledgements. This work was supported by program 10 Experimental Laboratory Astrophysics and Geophysics NCPM.

References

1. G. M. Ludovici, S. Oliveira de Souza, A. Chierici et al., *J. Environ. Radioact.*, 2020, **222**, 106375.
2. E. N. Baranova, M. A. Levinskikh and A. A. Gulevich, *Life*, 2019, **9**(4), 81.
3. S. V. Gudkov, M. A. Grinberg, V. S. Sukhov et al., *J. Environ. Radioact.*, 2019, **202**, 8-24.

A model dataset to test a method for detection of synchronization between the low-frequency oscillations in the cardiovascular signals

A. V. Kurbako[1], Yu. M. Ishbulatov[2], A. M. Vahlaeva[1], M. D. Prokhorov[1,2], V. I. Gridnev[1,3], B. P. Bezruchko[1,2], A. S. Karavaev[1,2,3]

[1] Institute of Physics, Saratov State University, Saratov, Russia, ishbulatov95@mail.ru
[2] Saratov Branch of Kotelnikov Institute of Radio Engineering and Electronics of Russian Academy of Sciences, Saratov, Russia
[3] Institute of Cardiology, Saratov State Medical University, Saratov, Russia

The autonomic control of circulation, attributed to the sympathetic and parasympathetic branches of the autonomic nervous systems, is important for maintaining homeostasis. Dysfunction of the autonomic control could lead to the development of various cardiovascular and other diseases, including myocardial infarction and arterial hypertension, therefore diagnostics of the autonomic control is important for prevention and therapy of cardiovascular diseases [1, 2].

The dynamics of the sympathetic branches can be described using time-delayed feedback oscillators with ~0.1 Hz frequency [3]. The oscillations are evident in the real RR-intervalograms (sequence of the time intervals between the electrocardiogram R-spikes) and photoplethysmogram. Several experimental and model studies [4] suggest that the 0.1 Hz exhibit intervals of phase synchronization, which can last up to hundreds of seconds and alternate with the intervals of asynchronous behavior. Relative duration of the synchronous intervals is smaller in people with impaired autonomic control and is perspective for medical diagnostics and therapy of myocardial infarction and arterial hypertension [4].

However, the real-world signals of the cardiolocial origin are heavily influenced by the noises of central origin and artifacts, the signals are nonstationary, multimodal and broadband, making introduction of the phases, needed to detect the phase synchronization, a non-trivial task.

Careful selection and parameterization of the data analysis techniques is necessary.

Therefore, we proposed mathematical models for the electrocardiogram and photoplethysmogram signals with functionality to preset the pattern of synchronization between the phases of the ~0.1 Hz oscillations. The simulated phase difference reproduce the statistical and spectral characteristics of the experimental data, including the alternating horizontal and sloped sections, corresponding to the intervals of synchronous and asynchronous behavior [6]. The shape of the model signals also closely resembles experimental electrocardiogram and photoplethysmogram time series. The developed models were used to generate the testing dataset.

The previously proposed method [4] for detection of phase synchronization between the abovementioned ~0.1 Hz oscillations, based on automated detection of the horizontal sections of the phase difference, was tested against the model dataset. The parameters of the method were refined to achieve better accuracy. The refined method reached the sensitivity of 0.69, specificity of 0.60, and AUC of 0.75. The performance improved, since the unmodified approach reached the sensitivity of 0.64, specificity of 0.63, and AUC of 0.71.

The results suggest that accuracy of the method is lower, than previously assumed, but we consider this estimation to be more credible, due to a more accurate simulation of the real data processing routine, including filtration of the broadband experimental signals and introduction of the phases using the Hilbert Transform.

Acknowledgements. This work was supported by the Russian Science Foundation, project No. 23-12-00241

References

1. N. Wessel, K. Berg, J. F. Kraemer, A. Gapelyuk, K. Rietsch, T. Hauser, J. Kurths, D. Wenzel, N. Klein, C. Kolb, R. Belke, A. Schirdewan, and S. Kääb, *Front. Physiol.*, 2020, 11.
2. N. M. De Souza, L. C. M. Vanderlei, and D. M. Garner, *Complexity*., 2015, 20(3), 84–92.
3. J. V. Ringwood, S. C. Malpas, *Am J Physiol Regul Integr Comp Physiol.*, 2001, 280, R1105-R1115.
4. A. S. Karavaev, M. D. Prokhorov, V. I. Ponomarenko, A. R. Kiselev, V. I. Gridnev, E. I. Ruban, and B. P. Bezruchko, *CHAOS.*, 2009, 19, 033112.
5. A. R. Kiselev, S. A. Mironov, A. S. Karavaev, D. D. Kulminskiy, V. V. Skazkina, E. I. Borovkova, V. A. Shvartz, V. I. Ponomarenko, and M. D. Prokhorov, *Physiol. Meas.*, 2016, 37, 580–595.
6. A. V. Kurbako, Yu. M. Ishbulatov, A. M. Vahlaeva, M. D. Prokhorov, V. I. Gridnev, B. P. Bezruchko, A. S. Karavaev, *Eur. Phys. J. Spec. Top.*, 2024.

Asymptotic integrability of nonlinear wave equations

A. M. Kamchatnov

Institute of Spectroscopy, Russian Academy of Sciences, Troitsk, Moscow, Russia, kamch@isan.troitsk.ru

It is well known that the concept of complete integrability of nonlinear wave equations plays an extremely important role in nonlinear physics. In this talk, we shall consider a much weaker property of nonlinear wave equations called their *asymptotic integrability*. In physical terms, it means that two asymptotic limits of the wave motion, namely, the dispersionless evolution of smooth pulses and the propagation of high-frequency wave packets, are consistent in the following sense: The Hamiltonian dynamics of a wave packet is preserved by the dispersionless evolution of the background flow [1]. Being weaker than the condition of complete integrability, asymptotic integrability turns out to be more flexible and has important consequences in various areas of nonlinear physics. (i) It allows one to develop a quite detailed analytical theory of the propagation of high-frequency wave packets along large-scale smooth waves [2]. (ii) Combined with the Stokes expression for a soliton's velocity in terms of the dispersion law for linear waves, it leads to the theory of propagation of narrow solitons along large-scale background waves. After adding some plausible assumptions, this theory can be generalized to the Hamiltonian dynamics of solitons under the action of smooth potentials [3–5]. (iii) It is shown that the condition of asymptotic integrability applied to completely integrable equations in the Ablowitz-Kaup-Newell-Segur scheme yields the quasi-classical limit of the corresponding Lax pair [6]. An approximate extension of this property to non-integrable equations allows one to formulate the generalized asymptotic "Bohr-Sommerfeld quantization rule," which determines the asymptotic velocities of solitons produced from an initially intensive and smooth wave pulse. We illustrate the different aspects of the theory with concrete examples of nonlinear wave dynamics.

References

1. A. M. Kamchatnov, *Chaos*, 33, 093105 (2023).
2. D. V. Shaykin, A. M. Kamchatnov, *Phys. Fluids*, **35,** 062108 (2023).
3. A. M. Kamchatnov, D. V. Shaykin, *Phys. Rev. E*, **108,** 054205 (2023).
4. A. M. Kamchatnov, D. V. Shaykin, *arXiv:*2402.12776 (2024).
5. A. M. Kamchatnov, *arXiv:*2403.19199 (2024).
6. A. M. Kamchatnov, D. V. Shaykin, *Physica D*, **460,** 134085 (2024).

Assessing the level of cognitive workload and stress using biosignal analysis

A. S. Karavaev[1,2], E. I. Borovkova[1,3], A. N. Hramkov[1], V. I. Ponomarenko[1,2] and **M. D. Prokhorov[1,2]**

[1] Saratov State University, Saratov, Russia, karavaevas@gmail.com
[2] Saratov Branch of Kotelnikov Institute of Radio Engineering and Electronics of Russian Academy of Sciences, Saratov, Russia
[3] National Medical Research Center for Therapy and Preventive Medicine, 101990 Moscow, Russia

Application of the methods of nonlinear dynamics to study the coupling of oscillations in the signals of the objects of biological nature has important fundamental and applied significance. The functioning of the body involves various complex interacting oscillatory processes that ensure the adjustment of the body's systems to changing external conditions. Analysis of the strength and structure of couplings between such processes is a useful tool for constructing quantitative indices that characterize changing physical and psychophysiological states [1, 2]. Methods for detecting the interaction of various body systems have been successfully applied to estimation of the biological age [3], classification of sleep stages [4–6], diagnostics of the severity of diseases of the cardiovascular system [7–9], and stress diagnostics [1, 2]. The latter is important for the implementation of continuous monitoring of the level of stress in everyday life, and the identification of people who are at risk of developing stress-related disorders.

A change in a human psychophysiological state, in particular, caused by stress, affects the processes of autonomic control. The activity of the processes of autonomic control is reflected in infraslow oscillations of brain potentials with a frequency of less than 0.5 Hz and in low and high oscillations in the signals of a sequence of RR-intervals, the photoplethysmogram (PPG) and respiratory signal. We studied the low and high oscillations in the signals in the frequency ranges of 0.05–0.15 Hz and 0.15–0.50 Hz in healthy subjects at rest and during stress-inducing cognitive tasks. This oscillations associated with the processes of sympathetic and parasympathetic control.

We analyzed the power spectra of EEG signals, a sequence of RR-intervals and the PPG in different frequency ranges. We revealed that, compared with the state of rest, the stress state during stress-inducing cognitive tasks is characterized by a significant decrease in the power of infraslow oscillations in EEG, increase in the power of low oscillations in RR-intervals, decrease in the power of high oscillations in PPG. We analyzed the phase coherence coefficients and indices of directional coupling between oscillations in the signals of different EEG leads, RR-intervals and the PPG in different frequency ranges. We found the change of structure of couplings between the infraslow oscillations in EEG leads. In particular, under stressful conditions, a decrease both of intrahemispheric and interhemispheric couplings between EEG leads takes place in the range of 0.05–0.15 Hz, while in the range of 0.15–0.50 Hz, a decrease of intrahemispheric and an increase of interhemispheric couplings is observed. Also we found decrease the couplings between of the respiratory and cardiovascular systems during stress-inducing cognitive tasks.

Acknowledgements. This work was supported by the Russian Science Foundation, project No 23-12-00241.

References

1. R. Katmah, F. Al-Shargi, U. Tariq, F. Babiloni, Al- F. Mughairbi, H. Al-Nashash. *Sensors*, 2021, 21(15), 5043.
2. G. Giannakakis, D. Grigoriadis, K. Giannakaki, O. Simantiraki, A. Roniotis, M. Tsiknakis. *IEEE Transactions on Affective Computing*, 2019, 1, 1.
3. V. I. Ponomarenko, A. S. Karavaev, E. I. Borovkova, A. N. Hramkov, A. R. Kiselev, M. D. Prokhorov, T. Penzel, *Chaos*, 2021, 31, 073105
4. E. I. Borovkova, A. N. Hramkov, .S. Karavaev, M. D. Prokhorov, Yu. M. Ishbulatov, T. Penzel, *Annu Int Conf IEEE Eng Med Biol Soc*., 2021.
5. E. I. Borovkova, M. D. Prokhorov, A. R. Kiselev, A. N. Hramkov, S. A. Mironov, M. V. Agaltsov, V. I. Ponomarenko, A. S. Karavaev, O. M. Drapkina, T. Penzel, *Frontiers in Network Physiology*, 2022, 2, 942700.
6. A. S. Karavaev, V. V. Skazkina, E. I. Borovkova, M. D. Prokhorov, A. N. Hramkov, V. I. Ponomarenko, A. E. Runnova, V. I. Gridnev, A. R. Kiselev, N. V. Kuznetsov, L. S. Chechurin, T. Penzel, *Frontiers in Neuroscience*, 2022, 15, 791510.
7. A. S. Karavaev, M. D. Prokhorov, V. I. Ponomarenko, A. R. Kiselev, V. I. Gridnev, E. I. Ruban, B. P. Bezruchko, *Chaos*, 2009, 19, 33112.
8. O. L. Bockeria, V. A. Shvartz, A. A. Akhobekov, L. A. Glushko, T. G. Le, A. R. Kiselev, M. D. Prokhorov, L. A. Bockeria , *Cor et Vasa*, 2017, 59(3), e266-e271.
9. R. Kiselev, V. I. Gridnev, M. D. Prokhorov, A. S. Karavaev, O. M. Posnenkova, V. I. Ponomarenko, B. P. Bezruchko, V. A. Shvartz, *Annals of Noninvasive Electro-cardiology*, 2012, 17(3), 204-213.
10. N. A. Aladjalova, *Nature*, 1957, 179, 957.
11. G. G. Knyazev, *Neurosci. Biobehav.* Rev., 2012, 36, 677.
12. M. L. Lorincz, F. Geall, Y. Bao, V. Crunelli, S. W. Hughes, *PLoS ONE*, 2009, 4, e4447.
13. S. Karavaev, A. R. Kiselev, A. E. Runnova, M. O. Zhuravlev, E. I. Borovkova, M. D. Prokhorov, V. I. Ponomarenko, S. V. Pchelintseva, T. Yu. Efremova, A. A. Koronovskii, A. E. Hramov, *Chaos*, 2018, 28, 081102.
14. R. Stroop, *J. Exp. Psychol.*, 1935, 18, 643–662.
15. G. M. Schneider, D. W. Jacobs, R. N. Gevirtz, D. T. O'Connor, J. Hum, *Journal of Human Hypertension*, 17(12), 829–840.
16. E. I. Borovkova, A. N. Hramkov, E. S. Dubinkina, V. I. Ponomarenko, B. P. Bezruchko, Yu. M. Ishbulatov, A. V. Kurbako, A. S. Karavaev, M. D. Prokhorov, *The European Physical Journal Special Topics Pl*us, 2023, 232, 625–633.
17. M. D. Prokhorov, E. I. Borovkova, A. N. Hramkov, E. S. Dubinkina, V. I. Ponomarenko, Y. M. Ishbulatov, A. V. Kurbako, A. S. Karavaev, *Applied Sciences*, 2023, 13, 8390.

On robustly chaotic attractors in systems from applications

A. O. Kazakov

University Higher School of Economics, Nizhny Novgorod, Russia, kazakovdz@yandex.ru

One of the most fundamental problems in multidimensional chaos theory is the study of strange attractors which are robustly chaotic (i.e., they remain chaotic after small perturbations of the system). It was hypothesized in [1] that the robustness of chaoticity is equivalent to the pseudohyperbolicity of the attractor. Pseudohyperbolicity is a generalization of hyperbolicity. The main characteristic property of a pseudohyperbolic attractor is that each of its orbits has a positive maximal Lyapunov exponent. In addition, this property must be preserved under small perturbations. The foundations of the theory of pseudohyperbolic attractors were laid by Turaev and Shilnikov, who showed that the class of pseudohyperbolic attractors, besides the classical Lorenz and hyperbolic attractors, also includes wild attractors which contain orbits with a homoclinic tangency.

In this talk, using the pseudohyperbolicity notion, we will explain how to check whether the attractor is robustly chaotic or not. We will describe the corresponding numerical methods and apply them for the study of model systems (the Lorenz and Shimizu-Morioka systems) as well as systems arising in applications (optical laser model, model of thermal convection, ensembles of oscillators, etc.)

References

1. Gonchenko S., Kazakov A. and Turaev D., 2021. Wild pseudohyperbolic attractor in a four-dimensional Lorenz system. Nonlinearity, 34(4), p.2018.

Prediction of solar activity using a neural network controlled by a solar dynamo model

N. Kleeorin[2,3], K. M. Kuzanyan[1,2], N. T. Safiullin[2,4], V. N. Obridko[1,2], I. Rogachevskii[3], S. V. Porshnev[4], R. A. Stepanov[2]

[1] Pushkov Institute of Terrestrial Magnetism, Ionosphere and Radio Wave Propagation Russian Academy of Sciences, Moscow, Russia
[2] Institute of Continuous Media Mechanics of the Ural Branch of Russian Academy of Science, Perm, Russia, nat@bgu.ac.il
[3] Ben Gurion University, Beer-Sheva, Israel
[4] Ural Federal University, Ekaterinburg, Russia

A nonlinear dynamic model of the alpha-Omega dynamo has been developed that takes into account the evolution of magnetic helicity. The model is directly based on systematic observations of solar activity [1]. Based on this model, we have developed a method that allows us to predict 13-month smoothed sunspot numbers with high accuracy. Our method uses a nonlinear dynamic dynamo model as a control signal source for the neural network. The developed neural network actually plays the role of an additional link connecting our dynamo model with an array of existing and newly arriving observational data.

The monthly forecast has been produced since the end of 2017 (and posted monthly online https://github.com/rodionstepanov/SolarActivityPrediction since October 2021) and indeed demonstrates high accuracy. We qualitatively compared our results with those of other forecasting methods.

We have shown that it is quite possible to forecast 13-month smoothed averages with a lead time of 6–12–18 months, even in the absence of correction of these forecasts based on current observations; its accuracy remains on par with existing methods developed by other authors. It is noteworthy that the use of a neural network in conjunction with a nonlinear dynamic dynamo model to correct these forecasts based on current observations of 13-month smoothed averages allows us to achieve prediction accuracy over a horizon of 6–18 months, comparable to the accuracy of monthly forecasts.

Acknowledgements. The work was supported by the Russian Science Foundation grant No. 21-72-20067.

References

1. Safiullin N., Kleeorin N., Porshnev S., Rogachevskii I., Ruzmaikin A. // Journal of Plasma Physics, 2018, Volume 84, Issue 3, article id. 735840306.

Neural mass models for the simulation of brain dynamics

V. V. Klinshov, **A. A. Zlobin, S. Yu. Kirillov** and **V. I. Nekorkin**

A.V. Gaponov-Grekhov Institute of Applied Physics of the Russian Academy of Sciences, Nizhny Novgorod, Russia,
vladimir.klinshov@ipfran.ru

Electrical activity of neuronal populations provides a substrate for information processing and cognitive functions in central neural system. Mathematical modelling has been a guide on this way for more than 30 years. One of the promising approaches in mathematical modeling of neural networks is the development of reduced models describing large populations of coupled neurons in terms of low-dimensional dynamical systems for the averaged variables. Such macroscopic or "neural mass" models can be obtained heuristically or derived from the microscopic dynamics using the refractory density approach, master equation formalism or other techniques. Recently, the so-called next generation of neural mass models won much attention of the researchers. The theoretical ground for this type of models is provided by the application of Ott-Antonsen theory to populations of theta-neurons or quadratic integrate-and-fire neurons [1]. A distinctive feature of these models is their capability to account for the degree of synchrony in neuronal populations. Next-generation models were proved useful in a number of contexts including the whole-brain simulations.

Being exact in the thermodynamic limit, neural mass models are considered as a good proxy of finite neuronal populations of sufficiently large size. However, whether and to what extend the population dynamics is amendable to finite-size effects is an open question. We address this point and consider the effect of the network size on the output signal it generates [2]. We demonstrate that in analogy to electronic circuits, the discrete rather than continuous nature of neurons constituting the network leads to the emergence of the shot noise. We show that adding this noise to the neural mass model transforms the latter into a system of stochastic differential equations reproducing the dynamics of a finite-size population. The core ingredient of the theory is calculation of the power spectrum of the shot noise, which consists of the shot noise for an uncoupled network plus macroscopic fluctuations induced by coupling, as demonstrated in Fig. 1. Our results allow to obtain a modified neural-mass model in the form of a stochastic differential equations which describes the coarse-grained dynamics of the finite-size network.

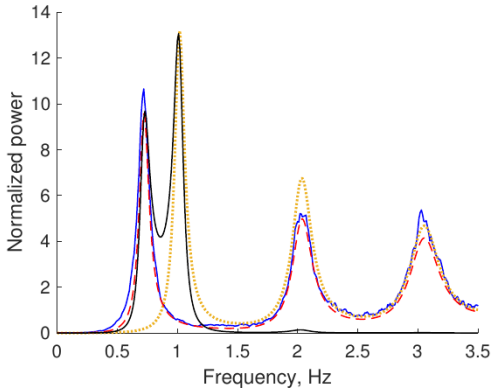

Fig. 1. Power spectrum of the shot noise of a network from Ref. 1 with the parameters $J = 10$, $\eta = 0$, $\Delta = 1$. Red dashed line: theoretical predictions. Blue solid line: numerical results for $N = 10^4$. Ocher dotted line: the noise of the uncoupled network. Black solid line: coupling-induced fluctuations

Another key approximation often used assumption is the Lorentzian distribution of the parameters of neurons inside the population which makes the reduction especially efficient. However, the Lorentzian distribution is often implausible as having undefined moments, and the collective behavior of populations with other distributions needs to be studied. We propose a method which allows effective reduction for an arbitrary distribution and show how it performs for the Gaussian distribution. We demonstrate that the dynamics of the population depends significantly on the form of the distribution. Namely, the dynamics of the populations with Lorentzian and Gaussian distributions differ drastically even if their mean and width are equal.

Acknowledgements. The work is supported by the Russian Science Foundation, grant no. 24-12-00245.

References

1. E. Montbrio, D. Pazo, A. Roxin, *Phys. Rev. X.*, 2015, **5**, 021028.
2. V. Klinshov, and S. Kirillov, *Phys. Rev. E*, 2022, **106**(6), L062302.
3. V. Klinshov, S. Kirillov, and V. Nekorkin, *Phys. Rev. E*, 2021, **103**(4), L040302.

The numerical simulations of reflection index dynamics of incident radio wave coursed by an electromagnetically driven Langmuir turbulence in a smoothly inhomogeneous plasma layer

A. V. Kochetov

A.V. Gaponov-Grekhov Institute of Applied Physics of the Russian Academy of Sciences, Nizhny Novgorod, Russia,
kochetov@ipfran.ru

The numerical simulations of reflection index dynamics coursed by an electromagnetically driven Langmuir turbulence is carried out in the frameworks of nonlinear Schrodinger equation which we supplement by boundary condition for an incident and reflected wave calculation. The incident wave is responsible for an electromagnetic field pumping into a smoothly inhomogeneous plasma layer, which we consider to be with unperturbed linear density profile and partial inverse radiation losses. The inverse radiation losses are added with the volume field dissipation in turbulence regions. The nonlinear Schrodinger equation in inhomogeneous plasma layer

$$iu_t + u_{xx} + \varepsilon_0 + |u|^2 u = 0 \qquad (1)$$

with incident electromagnetic wave pumping and back scattered radiation damping [1, 2]

$$u_x = -iu + 2iu_0(t)\,|_{x=-l} \qquad (2)$$

is extended with the imaginary part of plasma dielectric constant ε_0 (volume damping), which is should be taken into account in strong electromagnetic field plasma regions and results the energy transformation from electromagnetic waves to plasma ones at resonance interaction [3]. Electromagnetic wave volume field dissipation due to electromagnetically driven Langmuir turbulence we simulate by the nonlinear one, dependent on the local field amplitude and plasma-field evolution.

$$\varepsilon_0 = 1 - n_0(1 - i\nu/\omega), \qquad (3)$$

n_0 is normalized density profile and the volume damping ν at the vicinity of the turning region reproduces the basic wave-particle energy transformation peculiarities: hard excitation, nonlinearity, hysteresis [4]. We also take into account the "on" and "off" absorption thresholds different in several times and the volume damping hysteresis as well.

$$\nu/\omega = \gamma\Theta(|u|^2 - u_{th})|u|^{\alpha}, \qquad (4)$$

where the parameter γ determines the amplitude of the effective collision frequency, u_{th} is the normalized threshold field, and Θ is a Heaviside (step) function. As a result the dependence of the thresholds of the steady-state, periodic and chaotic regimes of plasma-incident wave interaction is obtained and the number of scenario of reflection and absorption dynamics and turbulence evolution is demonstrated, for example, on the Fig. 1, 2. The obtained results may be used to interpret the experiments on the observations of Langmuir stage ionosphere modification.

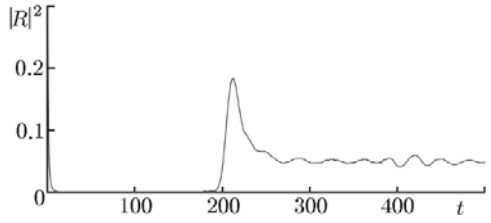

Fig. 1. Dynamics of the reflection coefficient $|R(t)|^2$ for $u_0 = 0.15$, $u_{th} = 0.12$, and $\gamma = 0.1$, $\alpha = 2$

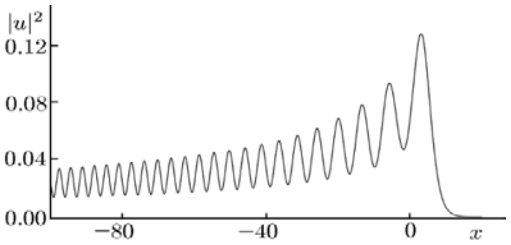

Fig. 2. Distribution $|u(x, t = 500)|^2$ for the same as Fig. 1 parameters: $u_0 = 0.15$, $u_{th} = 0.12$, and $\gamma = 0.1$, $\alpha = 2$

Acknowledgements. The work was supported by the state assignment of the Institute of Applied Physics of the Russian Academy of Sciences (Project FFUF-2024-0044 "Analysis and modeling of electrodynamic processes in the Earth's lithosphere, atmosphere and space").

References

1. *Kochetov A. V. Mironov V. A.*, et al, Adv. Space Res., 29, 1369, 2002.
2. *Kochetov A. V. Terina G. I.* 38, 2490, 2006.
3. *Shapiro D. V., ShevchenkoV. I.* in Handbook of Plasma Physics 2, eds. A. A Galeev, R. N. Sudan. Elsevier, Amsterdam, 1984.
4. *Kochetov A. V., Mjoelhus E.* Proc. of IV Intern. Workshop "SMP", Ed. A.G. Litvak, Vol.2, N. Novgorod, 491, 2000.

Theory-guided ML for accurate prediction of summertime Arctic Sea ice

D. Kondrashov

University of California, Los Angeles, USA, dkondras@atmos.ucla.edu

Decline in the Arctic sea ice due to global warming has profound socio-economic implications and is a focus of active scientific research. Of particular interest is prediction of September Arctic sea ice on subseasonal time scales, i.e. from early summer into fall, when sea ice coverage in Arctic reaches its minimum. Forecasting of September Arctic sea ice is very challenging due to the high variability of ocean and atmosphere over Arctic in summer, shortness of observational data to develop robust statistical and ML models, as well as inadequacies of the physics-based models to simulate sea-ice dynamics.

Here we present retrospective forecasts of regional summertime Arctic sea ice as part of Sea Ice Outlook (SIO) assessment of the multi-model predictive skill [1]. using theory-informed ML method of data-adaptive harmonic decomposition (DAHD) [2–5], see Fig. 1.

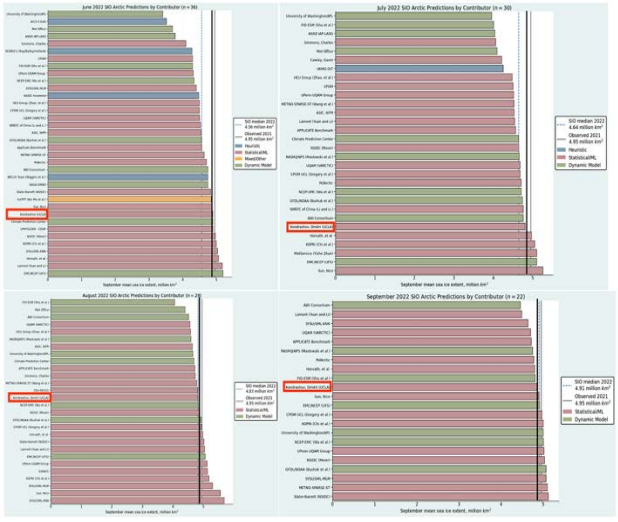

Fig. 1. Real-time predictions of monthly averaged September 2022 pan-Arctic Sea Ice Extent (SIE) by the nonlinear stochastic DAHD-based model [4] (annotated by box) at the beginning of June, July, August and September, respectively, and adapted from the 2022 SIO report [9]. The observed September 2022 SIE was 4.87 million square kilometers, annotated by thick black line in the figure

Unlike standard statistical and ML methods, DAHD-enabled modeling explicitly incorporates nonlinear, memory and synoptic (stochastic-like) weather effects within a universal parametric family of simple nonlinear stochastic models – coupled Stuart-Landau oscillators synchronized at different frequencies by the noise. It is theoretically guided by Mori-Zwanzig formalism of statistical mechanics and Koopman theory aimed at optimal modeling of partially observed complex and nonlinear dynamical systems [6–8], – such as dynamics of Arctic sea ice as subsystem of ice-atmosphere-ocean climate system.

Our results provide yet another evidence, that DAHD is very competitive, and are consistent with its real-time SIO predictions over the past 7 years. The average of summertime DAHD-based predictions (June, July, and August) was within 0.3 million km^2 of the observed September pan-Arctic Sea Ice Extent (SIE), and typical multi-model SIO spread of lower–upper quartiles ≈ 0.6 million km^2. Figure 1 shows multi-model Pan-Arctic SIO submissions in 2022 and adapted from its post-season report [9], where DAHD-based predictions were very accurate and consistent from early through late summer.

References

1. M. Bushuk et al. *BAMS*, 2024, in press, doi:10.1175/BAMS-D-23-0163.1.
2. D. Kondrashov, M. D. Chekroun, and M. Ghil, *Physica D*, 2015**, 297**, 33–55.
3. D. Kondrashov, M. D. Chekroun, and P. Berloff. *Fluids*, 3(1):21, 2018.
4. D. Kondrashov, M. D. Chekroun, and M. Ghil. *Dynamics and Statistics of the Climate System*, 2018.
5. D. Kondrashov, E. Ryzhov, and P. Berloff, *Chaos*, 30:061105, 2020.
6. V.Lucarini and M.D.Chekroun, *Nature Reviews Physics*, 5(12):744–765, 2023.
7. M. Santos Gutierrez, V. Lucarini, M. D. Chekroun, and M. Ghil, *Chaos*, 31(5):053116, 2021.
8. Y. Zhen, B. Chapron, E. Memin, and L. Peng. *Phys. Rev. E*, 105:034205, 2022.
9. Bhatt, U., Sea Ice Outlook: 2022 Post Season Report., *https://www.arcus.org/sipn/sea-ice-outlook/2022/post-season*.

Mean flow induced by longitudinal libration of a fluid-filled rotating container bounded by two conical surfaces

M. V. Kurgansky

A.M. Obukhov Institute of Atmospheric Physics, Russian Academy of Sciences, Moscow, Russia, kurgansk@ifaran.ru

The problem of determining a mean flow induced by longitudinal libration of a rapidly rotating fluid-filled container bounded by the surfaces of two oppositely oriented right circular cones is considered. The effect under consideration is due to nonlinearities in the Ekman boundary layers, which develop on the librating conical surfaces. It is shown that the problem is reduced, through introducing a cosine of the angle between the normal to the conical surfaces and the axis of rotation, to the problem of determining a mean flow induced by libration of a fluid-filled rotating cylindrical container of infinite radius. A theoretical scenario is proposed of how the solved problem can be applied to the approximate determination of the differential mean rotation in a significant part of a rotating spherical and/or oblate spheroidal cavity under the action of longitudinal libration forcing.

In a plane passing through the axis of rotational symmetry, the geometry considered in this work can also be seen as a low-order polygonal approximation to an ellipse, and a container bounded by two oppositely directed conical surfaces can be seen as a rough first approximation to a spheroidal cavity. Besides possible technical applications, the results of this work can also be used in geophysics and astrophysics for a rough estimation of differential mean rotation characteristics within celestial bodies subjected to longitudinal libration without needing to invoke the full spherical/spheroidal geometry [1].

References

1. Kurgansky M. V. Mean flow induced by longitudinal libration of a fluid-filled rotating container bounded by two conical surfaces // European Journal of Mechanics / B Fluids 105 (2024) 357–367. https://doi.org/10.1016/j.euromechflu. 2024.02.008.

Quasilinear approach to magnetic turbulence in anisotropic plasma

A. A. Kuznetsov, N. A. Emelyanov, M. A. Garasev, A. A. Nechaev, Vl. V. Kocharovsky

A.V. Gaponov-Grekhov Institute of Applied Physics of the Russian Academy of Sciences, Nizhny Novgorod, Russia,
kuznetsov.alexey@ipfran.ru

Anisotropic velocity distributions of electrons subject to aperiodic instability of the Weibel type are characteristic of various problems in the physics of space collisionless plasma, including the solar wind and the magnetospheres of stars and planets. The instability leads to the formation of small-scale current filaments and quasi-magnetostatic turbulent fields consistent with them, which significantly change the particle kinetics in plasma.

This report is devoted to the study of the evolution of the spatial spectrum of Weibel turbulence in two-dimensional approximation for a nonrelativistic plasma with an axially symmetric anisotropic electron velocity distribution. We focus on the quasilinear collective effects in the dynamics of the spectrum [1, 2]. For certainty, we choose the bi-Maxwell initial particle distribution with higher temperature along one direction (the axis of anisotropy) and lower temperature along the other two.

An original quasilinear system of equations is derived from the Maxwell-Vlasov equations and describes the evolution of spatial modes (harmonics) of particle velocity distribution and associated electromagnetic fields. The interaction of modes is taken into account through their integral effect on the particle-velocity distribution homogeneous in space. In a wide range of the initial electron-velocity anisotropy, including both small and large values compared to unity, the equations are solved for many hundreds of modes with the help of Leapfrog method. The selected modes tightly cover the two-dimensional calculation plane, which is taken in two ways. In one case, the anisotropy axis is perpendicular to the calculation plane, and in the other – belongs to it.

The obtained solutions of the quasilinear system were compared with the results of similar calculations using the particle-in-cell code EPOCH, which takes into account the direct nonlinear interaction of modes. It is found that in the first case, when a calculation plane is perpendicular to the axis of anisotropy, the quasilinear interaction is a decisive factor of nonlinear turbulence development over a long period of time. In the second case the two-dimensional quasilinear approach works not so well, presumably, due to specific role of the oblique modes. Comparing with EPOCH modeling, we find the contribution of direct interaction of modes to some parts of the turbulence spectrum at some stages of its evolution, e.g., at the saturation stage, especially in the second case. Also, the modeling confirms validity of the recently found integral relation linking the root-mean-square turbulent magnetic field, the anisotropy parameter, and the characteristic wavenumber of turbulence [2]; see Fig. 1.

The advantage of our quasilinear approach is a very low noise level as compared to the particle-in-cell code, which does not allow one to calculate the spectrum of turbulence with the same accuracy as we do when studying the dynamics of individual modes. This made it possible for the first time to establish and study various stages of their evolution, including exponential, superfast and power-law growth as well as their oscillatory decay. Some properties of the nonlinear evolution of the whole turbulence spectrum have also been established, including its quasi-self-similar character and well-defined power-law slopes at the long- and short-wavelength wings. Also, typical patterns of deformation (flattening) of the particle velocity distribution are picked out and typical evolution of both the electron anisotropy parameter and magnetic field energy are investigated (Fig. 1).

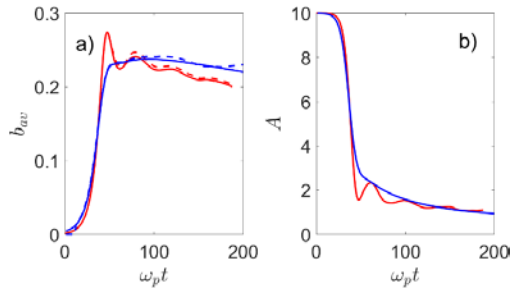

Fig. 1. Typical evolution of (a) the root-mean-square magnetic field, b_{av}, [1] (solid lines) and estimates of this quantity [2] (dashed lines) and (b) the anisotropy parameter, A, according to numerical modeling by means of the quasilinear approach (red lines) and the particle-in-cell code EPOCH (blue), respectively

The scattering of particles by the turbulent magnetic fields is essential for the direct nonlinear interaction of modes, including both the resonant or non-resonant interaction, which is not accounted for in the quasilinear approximation. To describe this process in the quasilinear modeling, we estimate analytically a scattering cross-section and add the anomalous collisions to the Vlasov equation within the simplest BGK tau-approximation. For the simulation in the case when the calculation plane is perpendicular to the anisotropy axis, the result shows only minor refinements of the turbulence dynamics. For another case when the anisotropy axes lies in the calculation plane and the influence of direct nonlinear interaction of modes is stronger, the result of the improved quasilinear modeling is changed notably and becomes more close to the result of the particle-in-cell modeling.

All the results obtained indicate the prospects of using a quasilinear approach for a detailed study of the dynamics of magnetic-turbulence spectrum, especially in plasma with a low anisotropy, where the particle-in-cell method is difficult to apply due to a high level of noise.

The work was supported by the Russian Science Foundation (project No. 20-12-00032).

References

1. A. A. Kuznetsov, A. A. Nechaev, M. A. Garasev, Vl. V. Kocharovsky, *JETP*, 2023, 137 (6), 966-985.
2. A. A. Nechaev, A. A. Kuznetsov, and Vl. V. Kocharovsky, *J. Plasma Phys.*, 2023, 89 (6), Art. id. 175890601.

Waves and atmosphere modeling in severe weather conditions

A. M. Kuznetsova, A. S. Dosaev, Yu. I. Troitskaya

A.V. Gaponov-Grekhov Institute of Applied Physics of the Russian Academy of Sciences, Nizhny Novgorod, Russia, alexandra@ipfran.ru

At high wind speeds, a large amount of sea aerosol is formed, containing droplets of sea spray of various sizes and formation mechanisms. The presence of these droplets changes the state of the air-sea interface in the sea surface boundary layer, affecting the processes of momentum and heat exchange between air and sea and changing the drag coefficients of the sea surface. Accurate description of air-sea interaction processes is important for improving the forecast of the development of severe storm systems.

Today in the atmosphere and wave models the exchange coefficients for momentum, C_D, don't consider the influence of sea aerosol at high wind speeds. Additionally, the spray generation function can also be taken into account in emission and aerosol transport models.

Taking into account the designated importance of small-scale processes in extreme weather events (storms and hurricanes), detailed studies have recently been carried out in the framework of laboratory modeling on experimental stands. The obtained results demonstrated the great influence of marine aerosol on the Earth system, including the physics and chemistry of the atmosphere above the oceans, and marine geochemistry and biogeochemistry in general. It affects atmospheric transparency, remote sensing and air quality. The effect of sea spray can be considered as a plausible reason for the decrease in the surface drag coefficient in hurricane-force winds. For the calculations, the parameterization of the aerosol particle size distribution function proposed in [1] is used. This spray generation function (SGF) depends on the dynamic wind speed, radius of the drop, Reynolds number and Weber number.

The WRF-Chem model is modified to account for sea spray droplets of different sizes. The particles radius range values are considered in bins (10–30, 30–75, 75–200, 200–500 μm). The parameterization of the aerosol particle size distribution function in the WRF-Chem model was refined using the GOCART module. In addition to the splash size distribution function, a spray distribution function has been added to the sea salt concentration distribution calculation module, taking into account drops from “bags” and floating bubbles.

Results

The implementation of the obtained parameterization of the size distribution function of aerosol particles is implemented; Hurricane Irma simulations in WRF-Chem model are made [2]. In addition, model calculations are performed using a new drag parameterization using GOCART chemistry model. For data on wind speed U10, a comparison of the data obtained at the buoy location in the Atlantic Ocean with the data obtained at buoy 41043 location is made, and at the same point the data on wind friction speed u_* is compared. The results of WRF calculation without taking into account aerosol, taking into account aerosol using the GOCART method, taking into account aerosol using the GOCART method with an implemented parameterization of the aerodynamic drag coefficient, taking into account aerosol using the GOCART method with an implemented spray generation function are shown. For wind speed U_{10}, a comparison is given with measurement data from NDBC buoy No. 41043.

All calculation results overestimate the buoy measurements. The implementation of the spray generation function leads to a slight decrease in wind friction speed values, while the results of wind speed calculations differ from the default GOCART aerosol module to a lesser extent, since they are regularly use as input to the calculation model from wind reanalysis data. The calculation of the WRF-Chem model taking into account aerosol using the GOCART method with the implemented parameterization of the aerodynamic drag coefficient C_D demonstrates at the location a rapid increase in wind speed and a sharp peak, followed by a sharper decrease in wind speed than in the case of using other calculation methods.

Acknowledgements. The research is supported by the RSF grant 24-17-00299.

References

1. Troitskaya, Y., Kandaurov, A., Ermakova, O., Kozlov, D., Sergeev, D., & Zilitinkevich, S. (2018). The “bag breakup” spume droplet generation mechanism at high winds. Part I: Spray generation function. *Journal of physical oceanography, 48*(9), 2167–2188.
2. Kuznetsova A., Baydakov G., Dosaev A., and Troitskaya Y. “Drag Coefficient Parameterization under Hurricane Wind Conditions”. *Water* 15, no. 10 (2023): 1830.

Using empirical modeling approach for the estimation real-world system's stability to strong perturbations: stability of the paleoclimate in the Pleistocene epoch

E. M. Loskutov, V. V. Vdovin, V. V. Klinshov, A. S. Gavrilov, D. N. Mukhin and **A. M. Feigin**

A.V. Gaponov-Grekhov Institute of Applied Physics of the Russian Academy of Sciences, Nizhny Novgorod, Russia, loskutov@ipfran.ru

In this work we using relatively recent development non-local stability measure (interval stability) to real-world systems, based on their observational data, for the study of changes in the global stability of the Earth's climate during the Pleistocene epoch. Interval stability [1] is a method for the estimation complex system's stability to strong perturbations. This method describes how large perturbation should be to disrupt the stable dynamical regime of the system. The main interval stability method remains unaltered but we propose to use an empirical modelling approach [2] to apply the interval stability measure for the characterization of real-world systems. An empirical model let us possibility to study the response of the investigated system to strong perturbations, to analyze the structure of various regions in phase space, and to investigate the internal dynamics of a system far from its attractor. Of course, we would not have this possibility if we had only one observable time series of the real-world system in our hands. We used this method for study the properties of a real natural system: to analyze the stability of the Earth's climate system during last 2.6 million years. As a data source we used composite stack LR04 [3] which consists of the time series of the relative content of the δ18O isotope in shells of deep-sea organisms from the group of protists (benthic foraminifera) recorded from 57 cores from deep sea drilling wells at different sites of the world ocean fig. 1a). Based on statistically optimal nonlinear stochastic model (fig. 1b) extracted from observational data (fig. 1a), it is shown that the stability of the global climate to any disturbances decreases throughout the Pleistocene period, enhancing its response to fast (with a millennial scale or less) internal disturbances. This is consistent with the assumption made in the work [2] that a decrease in the stability of the internal dynamics of the Earth's climate is a probable cause of the middle Pleistocene transition [4] that occurred about a million years ago. The proposed approach, combining the interval stability method with optimal empirical reconstruction of the system under study, can be used to study a wide range of complex dynamic systems of various natures.

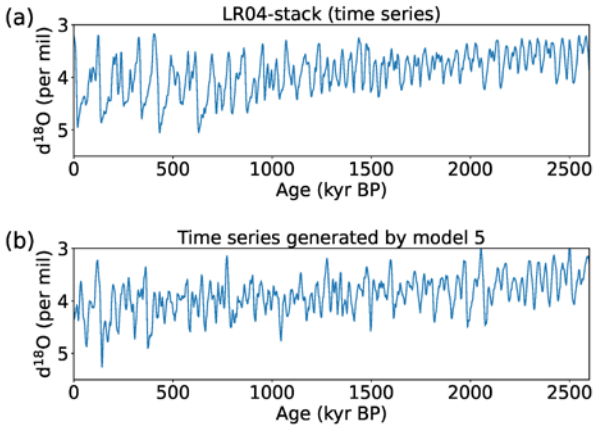

Fig. 1. (a) Oxygen isotopic records over the past 2.6 million years; (b) one of the time series of empirical model based on the LR04 stack

Acknowledgements

This work was supported by the project #075-02-2023-911 of Program for the Development of the Regional Scientific and Educational Mathematical Center "Mathematics of Future Technologies".

References

1. V. V. Klinshov, S. Kirillov, J. Kurths, and V. I. Nekorkin, *New Journal of Physics*, 2018, **20**, 043040.
2. D. Mukhin, A. Gavrilov, E. Loskutov, J. Kurths, and A. Feigin, *Scientific Reports*, 2019, **9**.
3. L. Lisiecki and M. Raymo, *Paleoceanography*, 2005, **20**.
4. N. Pisias and T. Moore, *Earth and Planetary Science Letters*, 1981, **52**, 450–458.

Discrete and semi-discrete multidimensional solitons and vortices – established results and novel findings

B. A. Malomed

Department of Physical Electronics, School of Electric Engineering, Faculty of Engineering, Tel Aviv University, Tel Aviv 69978, Israel, malomed@tauex.tau.ac.il

The talk aims to presents concise survey of basic discrete and semi-discrete nonlinear models which produce two- and three-dimensional (2D and 3D) solitons, and a summary of main theoretical and experimental results obtained for such solitons. The models are based on the discrete nonlinear Schrodinger (DNLS) equations and their generalizations, such as a system of discrete Gross-Pitaevskii (GP) equations with the Lee-Huang-Yang corrections, the 2D Salerno model (SM), DNLS equations with long-range dipole-dipole interactions, a system of coupled discrete equations for the second-harmonic generation with the quadratic nonlinearity, a 2D DNLS equation with a superlattice modulation opening mini-gaps, a discretized NLS equation with rotation, a DNLS coupler and its *PT*-symmetric version, a system of DNLS equations for the spin-orbit-coupled (SOC) binary Bose-Einstein condensate, and others. Following a recent review article [1], the talk presents a review of basic species of multidimensional discrete modes, including fundamental and vortex solitons, their bound states, gap solitons populating mini-gaps, symmetric and asymmetric solitons in the conservative and *PT*-symmetric couplers, cuspons in the 2D SM, discrete SOC solitons of the semi-vortex and mixed-mode types, 3D discrete skyrmions, and some others.

References

1. B. A. Malomed. Discrete and semi-discrete multidimensional solitons and vortices: established results and novel findings, Entropy **26**, 137 (2024). (special issue Recent Advances in the Theory of Nonlinear Lattices).

Exact solutions of shallow water equations over seamounts: generalization of the Carrier-Greenspan transform

I. E. Melnikov and **E. N. Pelinovsky**

National Research University Higher School of Economics, Nizhniy Novgorod, Russia,
A.V. Gaponov-Grekhov Institute of Applied Physics of the Russian Academy of Sciences, Nizhniy Novgorod, Russia,
e-mail: melnicovioann@gmail.com

The Carrier-Greenspan (CG) transform has become incredibly popular for describing the waves rolling onto the flat slope within the framework of the nonlinear shallow water theory (see, for example, [1, 2]). The amazing fact that this transformation (and its linearization) gives us is that a linear and nonlinear shallow water system will be reduced to the same (Euler-Darboux-Poisson) equation (1) for some function Φ [1]

$$\frac{\partial^2\Phi}{\partial\lambda^2}-\frac{\partial^2\Phi}{\partial\sigma^2}-\frac{1}{\sigma}\frac{\partial\Phi}{\partial\sigma}=0 \qquad (1)$$

through which all elements of the wave field are expressed (u is the depth-averaged flow velocity, η is the water surface displacement), as well as variables (x is a spatial coordinate, t is time)

$$u=\frac{1}{\sigma}\frac{\partial\Phi}{\partial\sigma},\quad \eta=\frac{1}{2g}\left[\frac{\partial\Phi}{\partial\lambda}-u^2\right]$$
$$x=\frac{1}{2\alpha g}\left[\frac{\partial\Phi}{\partial\lambda}-u^2-\frac{\sigma^2}{2}\right],\quad t=\frac{1}{\alpha g}\left[\lambda-\frac{1}{\sigma}\frac{\partial\Phi}{\partial\sigma}\right] \qquad (2)$$

We decided to generalize this approach for arbitrarily change the bottom $h(x)$, while considering the linear version of the shallow water equations (3)

$$\frac{\partial u}{\partial t}+g\frac{\partial\eta}{\partial x}=0,\qquad \frac{\partial\eta}{\partial t}+\frac{\partial}{\partial x}(h(x)u)=0 \qquad (3)$$

by representing the components of the wave field as

$$\eta=\phi(\lambda)\frac{\partial\Phi}{\partial\lambda},\ u=\psi(\sigma)\frac{\partial\Phi}{\partial\sigma},\ x=Lf(\sigma),\ t=T\lambda \qquad (4)$$

where φ, ψ and Φ are new arbitrary functions, λ and σ are new variables (T and L are dimensional constants). After applying certain conditions to the new introduced functions, we get that our system (3) can be reduced to a single equation (5) from which solutions of the system (3) can be obtained

$$\frac{\partial^2\Phi}{\partial\lambda^2}-\frac{\partial^2\Phi}{\partial\sigma^2}+\frac{\psi'}{\psi}\frac{\partial\Phi}{\partial\sigma}=0 \qquad (5)$$

However, in the general case, it is not so easy to obtain [3] an accurate analytical solution of equation (5). For certain functions ψ, this equation (5) becomes the Euler-Darboux-Poisson equation, which is easily solved precisely, and its solutions coincide with the results obtained in the works [4, 5], however, in a different way. Thus, a solution has been obtained for a countable family of power-law profiles, as well as for some configurations of seamounts (Fig. 1) that are set parametrically.

The report discusses the behavior features of waves over seamounts. It is shown that when moving from a more gentle slope to a sharper one, the waveform will integrate a certain number of times, and the maximum amplitude is not reached at the very top of the mountain. The solution for such seamounts is presented in the form of two generalized traveling waves, which indicates a non-reflective spread of waves (and energy) over such a bathymetry. Thus, this study demonstrates that the presence of seamounts in the coastal zone does not guarantee protection from tsunami waves.

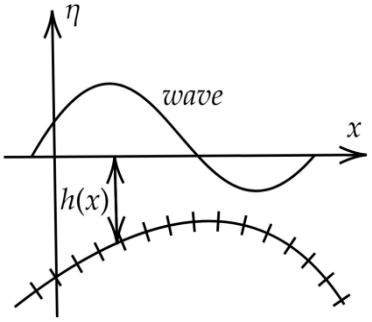

Fig. 1. Wave propagation over an underwater mountain

It is possible that for the obtained profiles, as well as for the linear slope profile, it will be possible to find a nonlinear analogue of the generalization of CG transform. At the same time, we have already found the linear parts of these transformations for mapping into the Euler-Darboux-Poisson equation. In that way the authors hope that it will be possible to correctly determine the nonlinear parts of this transformation in the future.

Acknowledgements. The authors gratefully acknowledge financial support by the RSF grant 24-47-02007.

References

1. G. F. Carrier and H. P. Greenspan, “Water waves of finite amplitude on a sloping beach,” Journal of Fluid Mechanics 4, 97–109 (1958).
2. G. F. Carrier, T. T. Wu and H. Yeh, “Tsunami run-up and draw-down on a plane beach,” Journal of Fluid Mechanics 475, 79 – 99 (2003).
3. O. V. Kaptsov and D. O. Kaptsov, “Solutions of some wave mechanics models,” Fluid Dynamics 58, 1227–1234 (2024).
4. E. N. Pelinovsky and O. V. Kaptsov, “Traveling waves in shallow seas of variable depths,” Symmetry 14, 1448 (2022).
5. I. E. Melnikov and E. N. Pelinovsky, “Linear Waves on Shallow Water Slowing Down near the Shore over Uneven Bottom” Fluid Dynamics 59(2), 260–269 (2024).

Identification and analysis of mid-latitude atmospheric regimes with hidden Markov models

D. N. Mukhin[1], **R. S. Samoilov**[1] and **A. Hannachi**[2]

[1] A.V. Gaponov-Grekhov Institute of Applied Physics of the Russian Academy of Sciences, Nizhny Novgorod, Russia, mukhin@ipfran.ru

[2] Stockholm University, Stockholm, Sweden

Low-frequency variability (LFV) of the atmosphere, that is behavior on time scales greater than meteorological forecasting time, is poorly understood and hardly predictable. The LFV of the extratropical atmosphere involves hemispheric-scale recurring, often persistent, structures of atmospheric circulation known as teleconnection patterns or regimes, which form the backbone of low-frequency atmospheric variability and can have a profound impact on predictability on intraseasonal and longer timescales [1–3]. Having the spatial scales of circulation anomalies of the order of 10,000 km, they strongly modulate the routes and intensity of synoptic structures in the atmosphere, and hence determine long-term weather over large areas. Although modeling and analysis of the mid-latitude climate is closely related with modeling regimes, both the identification and the understanding of their dynamics continue to be a controversial issue due to different definitions of regimes and many different methods used.

According to quasi-geostrophic theory of large-scale baroclinic atmospheric motions, the LFV is largely driven by essentially nonlinear dynamical system. Experiments with quasi-geostrophic atmospheric models uncovered high-dimensional chaotic dynamics of the atmospheric flows, that includes a set of metastable states which manifest themselves as the persistent patterns [4, 5]. Relying on this, we treat the regimes as metastable states in the phase space of the system and use an approach of hidden Markov models (HMM) [6] to find and analyze them. A method we present here consists of three main steps: (1) constructing of a low-dimension embedding space efficient for the LFV representation, based on nonlinear principal component analysis, (2) training and optimizing the structure of the HMM, and (3) using an original method for decomposing the HMM state space into a set of metastable subsets associated with the regimes. A thorough analysis of the significance of the detected regimes is an integral part of the proposed method. In addition to detecting regimes, the method allows one to estimate the expected lifetime of each regime, the probabilities of transitions between regimes, and the probability that an observed pattern belongs to a certain regime. The results of applying the method to analysis of geopotential heights of the troposphere (500 hPa) and stratosphere (100 hPa) over the winter Northern Hemisphere are demonstrated, the properties and impact on the weather of the obtained regimes as well as the interannual evolution of their statistics are discussed.

Acknowledgements. The work is supported by the Russian Science Foundation, grant #22-12-00388.

References

1. Hannachi, A., et al. *Reviews of Geophysics*, 2017, 55(1), 199–234.
2. Ghil, M., et al. (2019). Sub-Seasonal to Seasonal Prediction. Elsevier, 119–142.
3. D. Mukhin, A. Hannachi, T. Braun, and N. Marwan, *Chaos* 32, 2022, 113105
4. S. Vannitsem, and C. Nicolis, *Journal of the Atmospheric Sciences*, 1997, 54(2), 347-361
5. A. Gritsun, V. Lucarini, Physica D: *Nonlinear Phenomena*, 2017, Volume 349
6. C. Franzke, T. Woollings, O. Martius, *Journal of the Atmospheric sciences*, 2011, vol. 68, pp. 2809-2825.

Bayesian stochastic recurrent neural network for modeling atmospheric regimes

D. N. Mukhin and **A. S. Gavrilov**

A.V. Gaponov-Grekhov Institute of Applied Physics of the Russian Academy of Sciences, Nizhny Novgorod, Russia,
mukhin@ipfran.ru; gavrilov@ipfran.ru

Complex multiscale dynamics of the atmosphere in extratropical latitudes includes various persistent atmospheric regimes with the residence time up to several weeks. Identification, modeling and prediction of such regimes remains one of the unsolved problems. Rapid development of statistical methods and algorithms allows to tackle this problem with the help of modern machine learning approaches. In the current work we develop a Bayesian stochastic model for large-scale atmospheric dynamics based on recurrent neural networks (RNNs).

RNN is a network which has a hidden state reflecting the dynamical properties of the observed system which are helpful for the prediction of the next system's state (target variable). The core element of RNN structure is recurrent cell which allows to update the current hidden state using the current observed state. It has a fixed number of trainable parameters and can be applied recursively many times, allowing to model dependencies with large memory depth (and thus multiscale dynamics) without increasing the number of RNN parameters, i.e. without overfitting. However it becomes more tricky to train because of arising deep learning challenges. Here we construct a model in the form of evolution operator with the sum of RNN as deterministic part and multidimensional Gaussian stochastic part, generalizing Bayesian stochastic model framework from our previous works [1–3]. To train the model, we employ the same Bayesian posterior probability density as a cost function, but change the numerical algorithm and optimization criterion: instead of Laplace approximation of Bayesian evidence optimality (which becomes bad for deep networks), we cross-validate the model likelihood to choose optimal hyperparameters; and we use stochastic gradient algorithm with cross-validation-based early stopping during the maximization of the Bayesian posterior. Both strategies are well-known in deep learning but the chosen cost functions are taken from the Bayesian framework.

The proposed model involves variables obtained by nonlinear dimensionality reduction via kernel principal component analysis – kernel principal components (PCs) – and aimed at characterizing the target regimes [4]. At first we construct the "classic" variant of stochastic RNN-based evolution operator which maps a sequence of past values of kernel PCs to their current values. However, we note that kernel PCs are actually defined by an implicit highly nonlinear mapping from high-dimensional space of observed variables which makes them represent a very distorted version of the original phase space and potentially be less appropriate for evolution operator construction. To reflect this idea, we modify the classic variant and use an undistorted linear projection of original variables to form a low-dimensional phase space for RNN. We train the RNN to stochastically map a sequence of the past linear PCs to their current values and, *additionally*, to the current values of kernel PCs. In this way our modified stochastic RNN combines the evolution operator in the undistorted projection of the original space and the *low-dimensional* approximation of mapping from the original space to the target variables – kernel PCs.

As a proof of concept, we illustrate the method for the mid- and high-latitude data in the Northern hemisphere in winter, see e.g. Fig. 1 for the geopotential height at 70 hPa whose kernel PCs represent the main regimes of polar vortex. It is seen that the modified stochastic RNN provides the better representation of the observed density of the system states in the space of kernel PCs, rather then the "classic" one. It can also be shown that it provides a good low-dimensional reconstruction of the mapping from the original variables to kernel PCs. Thus, this model may serve as a good simulator and, possibly, predictor of atmospheric dynamics which also captures the important regimes.

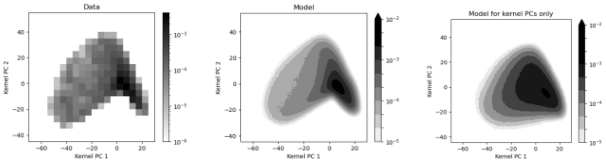

Fig. 1. The density of polar vortex states (invariant measure) in the space of leading kernel PCs for the observed data (*left*), the modified Bayesian stochastic RNN (*middle*), and the classic Bayesian stochastic RNN (*right*), see text for details

Acknowledgements. The research was supported by the Russian Science Foundation, grant #22-12-00388.

References

1. A. Gavrilov, E. Loskutov, D. Mukhin, *Chaos, Solitons and Fractals*, 2017, 104, 327–337.
2. A. Gavrilov, A. Seleznev, D. Mukhin, E. Loskutov, A. Feigin, J. Kurths, *Clim. Dyn.*, 2019, 52(3–4), 2199–2216.
3. A. Gavrilov, E. Loskutov, A. Feigin, *Chaos*, 2022, 32(2), 023111.
4. D. Mukhin, A. Hannachi, T. Braun, N. Marwan, *Chaos*, 2022, 32 (11), 113105.

Analytical model of a magnetopause current sheet with an arbitrary particle energy distribution and its stability

A. A. Nechaev, **M. A. Garasev** and **Vl. V. Kocharovsky**

A.V. Gaponov-Grekhov Institute of Applied Physics of the Russian Academy of Sciences, Nizhny Novgorod, Russia,
a.nechaev@ipfran.ru

We present analytical kinetic models of multicomponent current sheets of a magnetopause type allowing for arbitrary particle energy distributions [1, 2]. These one-dimensional models satisfy stationary Vlasov – Maxwell equations and describe a kinetic-scale distributed boundary between two regions of plasma with different number densities and magnetic field values, e.g., between the solar (stellar) wind and a planet's magnetosphere.

To test the stability of the constructed models, we carry out particle-in-cell numerical simulations, in which the analytically found self-consistent solution to the kinetic equations is set as an initial condition, and the evolution of the magnetoactive plasma is calculated. Analytical estimates predict that, depending on the free parameters of a sheet, the aperiodic Weibel-type instability is completely inhibited within its central part or can successfully develop despite the presence of the self-consistent magnetic field. Both cases are investigated numerically and compared for two choices of the particle energy distribution, Maxwellian and Kappa.

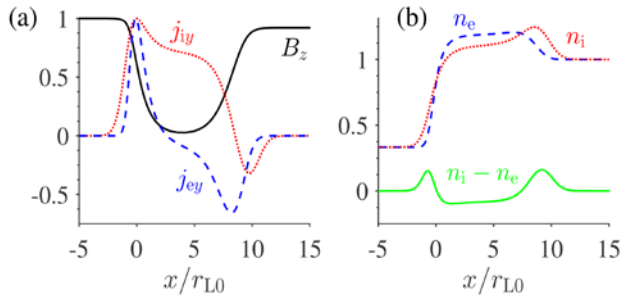

Fig. 1. Initial structure of the 4-component Maxwellian current sheet, comprised of 2 electron and 2 proton components: (a) magnetic field profile B_z (solid line), current densities of ions and electrons in the y direction, j_{ey} and j_{iy} (dots and dashes respectively), all normalized to their maxima; (b) normalized number densities of current-carrying ions and electrons, n_e and n_i (dots and dashes respectively), and their difference (solid line), proportional to the charge density. Model ion-electron mass ratio is 18.

Simulations confirm the theoretical predictions and show that the simplest sheets without particle countercurrents are stable against the Weibel instability. In a model with countercurrents (Fig. 1) the magnetic field of the sheet can be made weak enough, so that the particles areunmagnetized and the Weibel perturbations can grow effectively (Fig. 2). However, the instability saturates at a relatively low level and is confined within the region of suppressed magnetic field between the countercurrents, so the large-scale current structure remains stable.

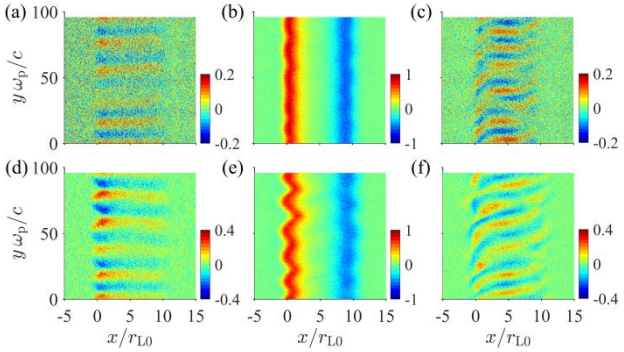

Fig. 2. Snapshots of the simulated evolution of the sheet presented in Fig. 1 at the moments of time (a)–(c) $t \approx 3400/\omega_p$, (d)–(f) $t \approx 7500/\omega_p$. Panel columns show normalized total current density in projections on axes x, y, z (from left to right)

We show that for both Maxwellian and Kappa particle energy distributions, the global structure of the current sheet and the character of the Weibel-type instability in its inner part are similar. The presence of the inhomogeneous self-consistent magnetic field and gradients of the plasma's local properties significantly influence the evolution of the Weibel turbulent spectrum from short to long wavelengths in comparison with the case of a homogeneous magnetoactive plasma.

The proposed current sheet models and the results on their small-scale instability can be used to interpret phenomena observed in the vicinity of planetary magnetopauses and the coronas of late-type stars.

Acknowledgements. The work was supported by the RSF (project No. 20-12-00268). Computational resources were provided by the Joint Supercomputer Center of the Russian Academy of Sciences.

References

1. A. A. Nechaev et al., *JETP Lett.*, 2023, **117**, 214–221.
2. V. V. Kocharovsky et al., *Astron. Lett.*, 2019, **45**, 551–564.

Cortical traveling waves and space-time non-separable inverse modeling in functional time resolved neuroimaging

A. E. Ossadtchi

Higher School of Economics, Nizhny Novgorod, Russia

Cortical traveling waves paradigm has relatively recently replaced the more traditional point view stating that neuronal sources and the recordings of brain's electrical activity can be modeled as a linear superposition of space-time separable rank-1 components. Cortical traveling waves of electrical activity accompany both normal and pathological workings of the brain. Most of the current studies of cortical traveling waves are performed using invasive recordings as the methods for detecting and localizing traveling waves in the non-invasively collected electroencephalographic data are missing.

I will present two approaches solving this problem and demonstrate their utility in both simulated and real EEG and MEG data analysis. The first approach is based on representing the observed vector time series data as a mixture of traveling waves propagating over cortex in various directions regularized by the L1 norm on the mixture coefficients which ensures sparsity of the traveling wave directions. I will show the results of applying this method to identify seizure onset zones in MEG data recorded in patients with pharmacologically intractable epilepsy. The second technique is based on the state space modeling approach operationalized by the unscented Kalman filter technique to infer the spatial and temporal components of the non-linearly observed cortical rhythms. The method allows us to resolve the controversy behind possible generative mechanisms of non-invasively observed traveling wave-like patterns.

Study of the reproducibility of mid-latitude atmospheric circulation regimes by the Earth System model of the INM RAS

R. S. Samoilov and **D. N. Mukhin**

A.V. Gaponov-Grekhov Institute of Applied Physics of the Russian Academy of Sciences, Nizhny Novgorod, Russia,
samoilov@ipfran.ru

Introduction

The dynamics of the mid-latitude atmosphere has complex multiscale behavior. While modern meteorology successfully copes with forecasting the atmosphere for 1-2 weeks, the predictability of atmospheric processes with large time scales is extremely low. Such time scales constitute so-called low-frequency atmospheric variability. Experiments with atmospheric models of different complexity levels and with observations show that low-frequency atmospheric variability is characterized by repeating states - planetary-scale circulation structures (regimes). The lifetime of each state can reach 3-4 weeks. These structures determine dominant paths of evolution of synoptic eddies, which strongly influence on weather regimes over vast territories. Currently, a large number of studies are devoted to identifying and modeling repeating states of the mid-latitude atmosphere, but the results obtained are contradictory and strongly depend on the choice of identification method.

Methods

This report proposes an original method for identifying and analyzing regimes, based on the understanding of regimes as regions of slowing down of phase trajectories in the phase space of the system, or neighborhoods of metastable states [1]. The idea of the method is to construct a Gaussian hidden Markov model from observed data and identify special subsets of model states. These subsets have a following property by definition. Their probability to leave themselves is abnormally low. Within the framework of this model, the dynamics of the system is parameterized by a Markov process, while both the set of hidden (not directly measured) states of the system and the probabilities of transitions between them are unknown a priori. The probabilistic connection of the hidden state with the measured values is specified by normal distribution with trainable parameters. To train the model, the Baum-Welsh algorithm [2] is used, which uses the forward-backward method. After constructing the model, the set of states is divided into communities maximizing average difference between two probabilities. First one means that the system will remain in the current community significantly. Second means the same but for random process which has stationary distribution similar to the system's one. For purpose of identification communities, the transition matrix is divided into blocks using an approach specially generalized for this task, based on the spectral method of graph partitioning [3].

Implementations and results

The report examines the reproducibility of winter atmospheric circulation regimes in the mid-latitudes of the Northern Hemisphere by the INM RAS Earth System Model (INMCM) based on data from historical and pre-industrial experiments. It means that an analysis of characteristics of atmospheric circulation regimes in the INMCM model is made in comparison with regimes found from reanalysis data (time series of geopotential height fields in the troposphere and stratosphere are used). In addition, the role of the own variability of model and the role of forcings in the formation and evolution of regimes are explored.

Plans

It is planned to generalize the model to the non-stationary case and apply it to data with seasonal variability. There is also the task of improving optimization by the number of hidden states. In this report the Akaike information criterion (AIC) is used for that purpose and it can be changed.

Acknowledgements

This work was supported by the Russian Science Foundation (Grant No. 22-12-00388).

References

1. Franzke C., Woollings T., Martius O. Persistent Circulation Regimes and Preferred Regime Transitions in the North Atlantic // Journal of the Atmospheric sciences. – 2011. – Vol. 68. – P. 2809–2825.
2. Leonard E. Baum, Ted Petrie, George Soules, Norman Weiss A maximization technique occurring in the statistical analysis of probabilistic function of markov chains // The Annals of Mathematical Statistics. – 1970. – Vol. 41, no. 1. – P. 164–171.
3. M. E. J. Newman Modularity and community structure in networks // The Annals of Mathematical Statistics. – 2006. – Vol. 103, no. 23. – P. 8577–8582.

Observed and simulated nonlinearity of ENSO

A. F. Seleznev and **D. N. Mukhin**

A.V. Gaponov-Grekhov Institute of Applied Physics of the Russian Academy of Sciences, Nizhny Novgorod, Russia,
aseleznev@ipfran.ru

El Niño–Southern Oscillation (ENSO) is the most prominent mode of interannual climate variability, which originates in the tropical Pacific, but has a global impact. Some fundamental features of observed ENSO are still not satisfactorily simulated by the most of state-of-the-art Earth system models [1]. One of that feature is the asymmetry between hot (El Niño) and cold (La Niña) states of ENSO: El Niño events are often stronger than La Niña events, while the last ones tend to be more persistent. Such an asymmetry is generally attributed to nonlinear feedbacks between sea surface temperatures, thermocline and winds in the tropical Pacific [2, 3]. At the same time, there are alternative conceptions highlighting the role of fast atmospheric processes associated with irregular zonal wind anomalies [4].

In this study we identify ENSO asymmetry via the analysis of upper ocean heat content (OHC) variability in the tropical Pacific from both high-resolution reanalysis dataset and ensemble datasets, produced by the Earth system models participating in the Coupled Model Intercomparison Project (CMIP). It was demonstrated [5, 6] that observed tropical Pacific OHC variability is captured well by two leading modes, obtained using conventional empirical orthogonal functions (EOF) decomposition of OHC anomalies data. These modes reflect the fundamental recharge-discharge mechanism of ENSO [7] involving a recharge and discharge of OHC along the equator caused by a disequilibrium between zonal winds and zonal mean thermocline depth. Here we reveal and analyze interannual dependencies in ENSO dynamics from these leading empirical OHC modes. We obtain that corresponding interannual dependencies revealed from reanalysis OHC data are truly nonlinear that reflects El Niño/La Niña asymmetry. We also examine how some Earth system models from CMIP reproduce the observed ENSO nonlinearity. Finally, we demonstrate that in context of the conventional conceptual theory of ENSO [7] the observed nonlinear interannual dependencies are attributed to nonlinear feedbacks inherent to internal ENSO dynamics rather than fast external forcing.

Acknowledgements. The study was supported by the Russian Science Foundation, grant #23-62-10043.

References

1. Y. Zhao and D.-Z. Sun, ENSO asymmetry in CMIP6 models. Journal of Climate 35 (2022), No. 17, 5555–5572.
2. S.-I. An and F.-F. Jin, Nonlinearity and asymmetry of ENSO. Journal of Climate 17 (2004), No. 12, 2399–2412.
3. F.-F. Jin, S.-I. An, A. Timmermann, and J. Zhao, Strong El Niño events and nonlinear dynamical heating. Geophysical Research Letters 30 (2003), No. 3, 20–21.
4. J.-S. Kug, F.-F. Jin, K. P. Sooraj, and I.-S. Kang, State-dependent atmospheric noise associated with ENSO. Geophysical Research Letters 35 (2008), No. 5, L05701.
5. A. Seleznev and D. Mukhin, Improving statistical prediction and revealing nonlinearity of ENSO using observations of ocean heat content in the tropical Pacific. Climate Dynamics 60 (2023), No. 1-2, 1–15.
6. Seleznev, Aleksei F., Gavrilov, Andrey S., Mukhin, Dmitry N., Gritsun, Andrey S. and Volodin, Evgenii M.. "ENSO phase locking, asymmetry and predictability in the INMCM Earth system model" Russian Journal of Numerical Analysis and Mathematical Modelling, vol. 39, no. 1, 2024, pp. 35-46.
7. F.-F. Jin, An equatorial Ocean recharge paradigm for ENSO. Part I: Conceptual model. Journal of the Atmospheric Sciences 54 (1997), No. 7, 811–829.

Microphysics of the air-sea interaction at high winds and its role in the dynamics and thermodynamics of severe sea storms

D. A. Sergeev and **Yu. I. Troitskaya**

A.V. Gaponov-Grekhov Institute of Applied Physics of the Russian Academy of Sciences, Nizhny Novgorod, Russia, daniil@ipfran.ru

Showing the record strengths and growth-rates, a number of recent hurricanes have highlighted needs for improving forecasts of tropical cyclone intensities most sensitive to models of the air-sea coupling. Especially challenging is the nature and effect of the very small-scale phenomena, the sea-spray and foam, supposed to strongly affecting the momentum- and heat- air-sea fluxes at strong winds. The present work is focused on our progress in understanding and describing these "micro-scale" processes, their physical properties, the spray and foam mediated air-sea fluxes and the impact on the development of marine storms.

Fig. 1. Photographs of TSWiWaT (a) and AELOTRON (b) facilities

The starting points for this study were two series of laboratory experiments. The first one was designed for investigation of the spray generation mechanisms at high winds. The experiments were carried out on the two different wind-wave facilities: Thermostratified Wind-Wave Tank (TSWiWaT) of IAP RAS and AELOTRON circular wind-wave facility of Heidelberg university (Fig. 1). It allows us to obtain results for a wide range of wind rates and fetches conditions. We detected 3 dominant spray generating mechanisms: stretching liquid ligaments, bursting bubbles, splashing of the falling droplets and "bag-breakup". We investigated the efficiency spray-production mechanisms and developed the empirical statistics of the numbers of the spray generating events of each type (see [1]). Basing on the "white-cap method" we found out the dependence of the spray-generating events on the wind fetch. The main attention was paid to the "bag-breakup" mechanism. Here we studied in detail the statistics of spray produced from one "bag-breakup" event. Basing on these developments, we estimated heat and momentum fluxes from the spray-generating events of different types and found out the dominant role of the "bag-breakup" mechanism.

To estimate the direct heat and momentum fluxes from the ocean surface to the atmosphere, we studied in the special experiment the foam impact on the short-wave part of the surface waves and the heat momentum exchange in the atmospheric boundary layer at high winds. Based on these results, we suggest a simple model for the aerodynamic and temperature roughness and the eddy viscosity in the turbulent boundary layer over a fractionally foam-covered water surface (see [2]).

The synergetic effect of foam at the water surface and spray in the marine atmospheric boundary layer on ocean surface resistance at high winds is estimated so as to be able to explain the observed peculiarities of the air-sea fluxes at stormy conditions (see Fig. 2). Calculations within the nonhydrostatic axisymmetric model show, that the "microphysics" of the air-sea coupling significantly accelerate development of the ocean storm.

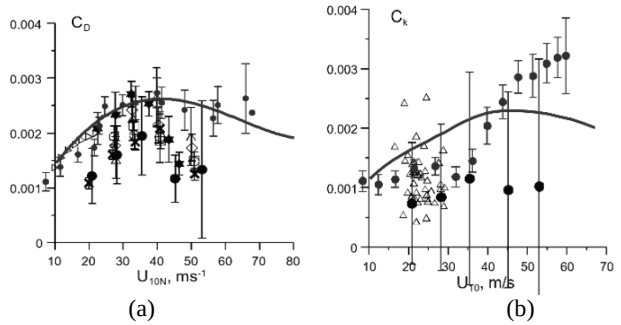

(a) (b)

Fig. 2. Aerodynamic drag coefficient (a) and enthalpy exchange coefficient (b) dependencies on the equivalent wind speed velocity U_{10}. Symbols – available data of field measurements. Lines – results of present work

Acknowledgements. This work was supported by the RSF project № 23-77-10060.

References

1. Yu. Troitskaya, A. Kandaurov, O. Ermakova, D. Kozlov, D. Sergeev, & S. Zilitinkevich, *J. Phys. Ocean.*, 2018, **48**, 2167–2188.
2. Yu. Troitskaya, A. Kandaurov, M. Vdovin, D. Sergeev, S. Zilitinkevich, *J. Phys. Ocean*., 2019, **49**, 959–981.

Experimental observation of super anti-cyclone in rotating cube

D. D. Tumachev, A. A. Levchenko, S. S. Vergeles and **S. V. Filatov**

Landau Institute for Theoretical Physics Russian Academy of Sciences, Chernogolovka, Russia, d.tumachev@issp.ac.ru

The main feature of fluid motion in a rotating system is the two-dimensionalization along the axis of rotation. Due to the action of Coriolis forces, the flow becomes quasi-two-dimensional and directed in a plane perpendicular to the axis of rotation, while being homogeneous along this axis. Similar to a purely two-dimensional flow [1], long-lived coherent vortices can form in a quasi-two-dimensional flow [2–4].

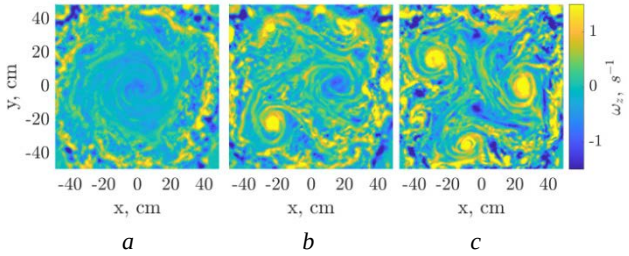

Fig. 1. The spatial distribution of vorticity for a regime with a large anticyclone in the center of the cube. Cube rotation speeds 3.6, 6.8, 10.8 rpm. The cube rotates counterclockwise

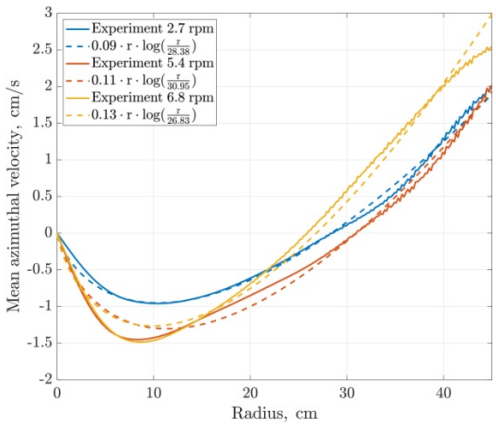

Fig. 2. Azimuthal velocity profile for anticyclones at different cube rotation speeds. The dotted line indicates the fit of the theoretical curve from the work [5]

An experimental study of the characteristics of these vortices was carried out in [4]. In this experiment, flow was excited by mixers installed in the vertical corners of a rotating hermetically closed cube with water. As the speed of the cube decreased and the mixers mode remained constant, an increase in size of cyclones and energy was observed, as well as a decrease in vortex number. Works aimed at theoretical [5] and numerical [1] studies of vortices in a quasi-two-dimensional system predict the presence of a single or pair of vortex condensates, which conflicts with experimental observations. A possible reason is that, due to the nature of the excitation, a regime was observed that does not match the parameters of the proposed models. It would be interesting to investigate what happens as the rotation rate continues to decrease relative to the intensity of turbulent pumping.

It could be assumed that, as a result of an increase in forcing intensity, one cyclone would remain, with its center located in the center of the flow. However, experimental observations suggest otherwise. An super anti-clone has been observed in the middle of the cube, whose lifetime is significantly longer than the dissipation time (Fig. 1, *a*). Around the anti-cyclone, a peripheral movement in a cyclonic direction has formed. As the rotation rate increases, cyclones start to appear on the periphery and are carried away by the mean current (Fig. 2, *b*). At a certain threshold rotation rate, the anti-cyclonic structure disappears (Fig. 3, *b*).

The report presents the results of an experimental study of a super anti-cyclone. In particular, the parameters of the occurrence of this phenomenon have been studied, and it has also been shown that at low rotational speeds of the cube, the azimuthal velocity profile (Fig. 2) coincides well with the dependence of the type

$$U^{\varphi} = A \cdot r \cdot \ln(\frac{r}{R}) \qquad (1)$$

presented in [5].

Acknowledgements. This work was supported by the Russian Science Foundation (project no. 23-72-30006).

References

1. Laurie, Jason, et al. "Universal profile of the vortex condensate in two-dimensional turbulence." *Physical review letters* 113.25 (2014): 254503.
2. McEwan, A. D. "Angular momentum diffusion and the initiation of cyclones." *Nature* 260.5547 (1976): 126-128.
3. Godeferd, Fabien S., Frédéric Moisy. "Structure and dynamics of rotating turbulence: a review of recent experimental and numerical results." *Applied Mechanics Reviews* 67.3 (2015): 030802.
4. Tumachev D., Filatov S., Vergeles S., Levchenko A., Two dynamical regimes of coherent columnar vortices in rotating fluid, JETP Letters 118, 426–432 (2023).
5. Kolokolov, I. V., L. L. Ogorodnikov, and S. S. Vergeles. "Structure of coherent columnar vortices in three-dimensional rotating turbulent flow." *Physical Review Fluids* 5.3 (2020): 034604.

Periodic principal component method unveiling spectral dynamics of the PSR B0329+54 radio emission

V. V. Vdovin[1], A. S. Gavrilov[1], E. R. Kocharovskaya[1], S. V. Logvinenko[2], E. M. Loskutov[1], V. M. Malofeev[2] and **V. V. Kocharovsky[1]**

[1] A.V. Gaponov-Grekhov Institute of Applied Physics of the Russian Academy of Sciences, Nizhny Novgorod, Russia
[2] Pushchino Radio Astronomy Observatory, Astro Space Center, Lebedev Physical Institute, Russian Academy of Sciences, Pushchino, Moscow obl., Russia

Introduction

We analyze the spectral–correlation features (principal components) of the dynamic spectra of the radio pulsar PSR B0329+54 observed near a frequency of 111 MHz in a band of almost 2.5 MHz at Pushchino Radio Astronomy Observatory (PRAO) [1]. The simple time-dependent spectral features of the PSR B0329+54 have been investigated previously and demonstrate up to 9 emission components [2, 3] and their Faraday modulation [4, 5], i.e., the rotation of the plane of linear polarization of the broadband emission. Our observing band contains about 6 Faraday periods of the pulsar emission. We develop the Periodic Principle Component (PPC) method which makes it possible to distinguish them very well using only a few minutes of observations. Yet, we find the period and dispersion measure of the pulsar, resolve nine spectral-correlation components and their Faraday structure, including rotation measure in each of them, their relative phases and the rates of frequency drift.

Methods

We convert the original 0.2 μs time series of the emission near a frequency of 111 MHz with duration of about several minutes into a dynamic spectrum which has a time resolution of about 0.2 ms and contains about 500 frequency channels. Then we compensate the dispersion measure of the pulsar, do some other preprocessing [1], match the pulsar pulse repetition period (about 715 ms) to our data, and finally convert the 15-minute dynamic spectrum into a series of about 1350 smaller dynamic spectra of about 120 ms duration, one for each pulse.

Then we generalize the Principal Component Method, which is widely used in mathematical statistics [6], to the PPC method, which is not so common and has not ever been applied to pulsar dynamic spectra. Both ordinary and periodic methods are described in [7, 8].

Our PPC method treats the data as a matrix of “pulse number” and “frequency-time” dimensions, finds the data correlation and defines the best “spectral” functions that are orthogonal to each other and describe the maximum variation of the data. We decompose the data into them, multiplying each function by some time-dependent amplitude, and keep some of the first (most informative) of these functions, making a low-dimensional approximation to the data and investigating it. When we study empirical data as a time series, we often call these functions as empirical orthogonal functions (EOFs), no matter what are actual (different) units of measurement of the data.

In our case of the PPC method, both the time and frequency of the dynamic spectrum for a given pulse play on the same footing. So, we have about 1350 “pulse” points and about 300000 “frequency-time” points in our data. Although the pulses vary greatly, the pulsar's emission is periodic with fine precision, so the PPC method is well suited to the spectral-dynamical features. For the PSR B0329+54, we find about 20 EOFs that contain information concerning the pulsar emission components. The computer implementation of the PPC method is based on standard libraries of the Python programming language and provides data preprocessing, validation of the dispersion factors and the time scale, and an effective calculation of EOFs for data of several tens of gigabytes.

Results

By means of the PPC method applied to the radio emission of the pulsar PSR B0329+54, we (i) determine the dispersion measure of the pulsar, (ii) identify nine pulse (spectral-correlation) components with essential linear polarisation, (iii) investigate their mutual correlations, (iv) evaluate an efficient frequency period of Faraday rotation for each of these components, (v) carry out their relative phases (which remain constant even though these frequency phases themselves change randomly), and (vi) discover the frequency-time chirp (drift) of various elements in the dynamic spectrum of the pulsar.

The PPC methods can be applied to the data of pulsar’s observations by various radio telescopes in various frequency ranges, and may prove very useful in solving the more than half a century old problem of the origin of the radio emission from the rotating neutron stars.

Acknowledgements. This work is based on the observational data obtained with the PRAO radio telescope. The study was supported by a grant from Russian Science Foundation (project no. 23-62-10043, https://rsci.ru/project/23-62-10043/).

References

1. V. V. Kocharovsky, V. V. Vdovin, A. S. Gavrilov, et al., Astronomy Letters, 2024, **50**, p. 120.
2. R. T. Gangadhara, Y. Gupta, Astrophys. J., 2001, **555**, p.31.
3. T. E. Hassall, B. W. Stappers, J. W. T. Hessels, et al., Astron. Astrophys., 2012, **543**, p. A66.
4. S. A. Suleimanova and V. D. Pugachev, Astron. Rep., 2002, **46**, p. 309.
5. C. Sobey, S. Johnston, S. Dai, et al., Mon. Not. R. Astron. Soc., 2021, **504**, p. 228.
6. J. V. Wall and C. R. Jenkins, *Practical Statistics for Astronomers*, 2nd ed., Cambridge Univ. Press, 2012.
7. D. Mukhin, A. Gavrilov, A. Seleznev, and M. Buyanova, Geophys. Res. Lett., 2021, **48**, p. 6.
8. A. Seleznev and D. Mukhin, Clim. Dyn., 2023, **60**, p. 1.

On the analysis of the acoustic field during scattering at a periodically uneven interface

Yu. M. Zaslavsky and **V. Yu. Zaslavsky**

A.V. Gaponov-Grekhov Institute of Applied Physics of the Russian Academy of Sciences, Nizhny Novgorod, Russia,
zaslav@ipfran.ru

Sound scattering (according to Kirchhoff) is simulated, which occurs at the boundary of two media with a periodically grooved (sinusoidal, combed) surface shape of the contact boundary and sharply differing in sound velocity. The problem under discussion is in demand, for example, when searching for manganese nodules in the water area, during express control of the characteristics of the bottom irregularity in the water-bottom soil area, where hydroacoustic waves are used [1, 2]. The analysis is performed in a simplified formulation – as a two–dimensional problem with an infinitely long boundary – with a sinusoidal comb shape cyclically repeated along the horizontal axis. The scattered field is calculated based on the Kirchhoff approach, using a ray representation of plane waves unlimited along the front – incident, reflected and transmitted [3–6]. Scattered waves penetrating through the boundary into the interior of the medium are also analyzed, both with harmonic and pulsed oscillations. The course of the rays and the reflection-passage coefficients in the Born approximation are regulated by the Snellius law and Fresnel formulas for reflection-passage coefficients. Two models of bordering media are envisaged: 1 – "gluing" – two mutually contacting scalar media and 2 – "slip contact" – the water – solid (hard) bottom boundary. In the first case, the condition of equality of both components of the displacements at the boundary, in the second – the condition of non-flow (equality of the vertical component of the displacements) and the reversal of the shear component of the stress tensor from the solid bottom boundary. The analysis uses constraints based on the small ratio of the height of the sinusoidal ridge corrugation to the spatial period of the border irregularity. In this case, it is permissible to neglect the quadratic corrections describing the orts oriented along the normal at intermediate points on the period of the corrugated boundary and deviating from the axial directions in them. Multiple scattering of rays arising from their deep penetration into the area between the ridges at the interface is also excluded. The multiple scattering of the wave – reflection from the slopes of the ridge significantly complicates the strict description of the scattering process. It is shown that the scattering characteristic in the harmonic oscillation mode has a multi-lobed shape, and the width of the petals is determined by the height of the ridge of the periodic structure of the boundary irregularity. The scattering indicatrix demonstrates the lobe structure of the angular distribution of the wave amplitude.

This characteristic is highly variable and varies with the change of frequency and the ratio of propagation velocities, making it impossible to fix a stable feature for interpreting and diagnosing the properties of the medium. In this regard, the possibility of representing a scattered wave in the form of a short pulse response to a probing parcel is considered. A replica of the pulse is depicted on a panorama in which the polar angle is laid along the abscissa axis, and the duration of the pulse delay in the media in contact is laid along the ordinate axis. In contrast, the panoramic image used for the pulse mode is an integral indicator that is stable and suitable for adequate operational diagnostics of the parameter – the ratio at the boundary of acoustic velocities.

Based on the application of the finite element method, numerical 3-D modeling of waves (analogous to aperture apodization of waves limited along the front), or created by a source of directional radiation, for example, an oscillating acoustic dipole installed near the boundary of media with a sinusoidal comb shape, is carried out. The possibility of angle scanning by the directivity of reflected and refracted scattered waves is demonstrated. The characteristic features in scattering indicatrises and in impulse responses are laid down as informative signs in the bottom soil diagnostic algorithm.

Acknowledgements. This work was supported by the IAP RAS program # FFUF-2024-0041.

References

1. A. N. Ivakin, Proceedings of School-Seminar of Academician L.M. Brekhovskikh on Acoustics of the Ocean, Moscow, 1998, p. 84.
2. A. B. Shmelev, SOVIET PHYSICS USPEKHI, 1972, **15**, 2, pp. 173–183.
3. K. E. Abbakumov, V. A. Konovalov. Abstracts of 10th European conference on Nondestructive testing. – Moscow, 2010, pp. 173–175.
4. Shagapov V. Sh., Sarapulova V. V., Journal Applied Mechanics and Technical Physics, 2015, **56**, 5, pp. 119–129.
5. K. E. Abbakumov, Russ J. Nondestruct Test, 2017, **53**, pp. 475–484.
6. F. G. Bass and I. M. Fuks, Wave Scattering from Statistically Rough Surfaces, Pergamon Press, New York, 1979.

On the parametric interaction of seismic waves emitted by a vibration source

Yu. M. Zaslavsky and **V. Yu. Zaslavsky**

A.V. Gaponov-Grekhov Institute of Applied Physics of the Russian Academy of Sciences, Nizhny Novgorod, Russia, zaslav@ipfran.ru

Seismic vibrations of low difference frequency emitted parametrically when biharmonic waves are excited by a vibrating seismic source installed on the Earth's surface are analyzed. The vibrator acts on the ground with variable force, radiating deep into two coaxial collimated beams of high–frequency longitudinal waves - harmonics close in frequency. Due to the parametric interaction of biharmonics, a difference frequency wave is also generated in the medium. The interaction is caused by the manifestation of nonlinear properties of the medium in the sedimentary column – a quadratic deviation in the linear Hooke stress-strain relationship.

Considering parametric effects during the propagation of seismic, i.e. elastic waves in the geomedium, we will start from the classical description of parametric interaction in coaxial searchlight sonar beams, which can serve as a basic one, and therefore it is mentioned here. It is known that when creating narrowly directed low-frequency sonar signals in an aqueous medium, parametric antennas are used, among other types of receiving and emitting devices, while quadratic nonlinearity is used in their work, characteristic of the compressibility of a liquid and manifested during the propagation of an acoustic wave. The antennas work both for the emission of waves of difference frequency and in the mode of recording low-frequency sonar signals at combination frequencies. According to the literature, the relevant studies were initially carried out by American acoustics [1 – 3], then there were pioneering works by acoustics of the Russian school specializing in receiving antennas [4], as well as a series of studies in the field of parametric radiators, which were carried out, for example, by the authors mentioned in [5, 6].

The main interest is in the characteristics of a low-difference frequency wave: the spatial and angular distribution of the amplitude, the nature of the wave level decline with distance and its frequency dependence. One of the ways to obtain a narrow focus of low-frequency radiation (penetrating deep into the subsurface) is to use the parametric principle of generation. The virtual sourcesthat arise in this case create the effect of a significant aperture. The spatial and angular characteristic of the radiation is graphically presented. Thus, the possibility of generating and emitting seismic vibrations at frequencies from units to several tens of hertz with a high angular directivity significantly exceeding that achievable with small (insignificant dimensions) dimensions of the radiator is being investigated. Estimates of the level of low-frequency vibrations generated parametrically in the soil are performed, while averaged values of the parameter of rock nonlinearity in the area of near-surface layers are used, and the possibility of achieving a radiation range practically acceptable for reliable registration is shown.

Acknowledgements. This work was supported by the IAP RAS program # FFUF-2024-0041.

References

1. P. J. Westervelt, JASA, 1963, **35**, 4, pp. 535-537.
2. H. O. Berktay, J. A. Shooter, JASA, 1973, **53**, 2, pp. 537-556.
3. H. O. Berktay, D. J. Leahy, JASA, 1974, **55**, 2, pp. 539-546.
4. V. A. Zverev, A. I. Kalachev, Acoustic J., 1968, **14**, 2, pp. 214-220.
5. A. S. Alekseev, N. I. Geza, B. M. Glinsky, A. F. Emanov, V. N. Kashun, Kovalevsky V. V., et al., 2004. Active Seismology With Powerful Vibrational Sources. ICM&MG SB RAS, Filial Geo Publishing House of the SB RAS, Novosibirsk (in Russian).
6. V. M. Solovyev, A. F. Emanov, S. A. Elagin, V. S. Seleznev, V. N. Kashun, A. V. Liseikin, V. I. Yushin, In Book: Active Geophysical Monitoring. 2019, pp. 389-404.

Self-similar growth of conic cusps on the liquid metal surface in an electric field

N. M. Zubarev

Institute of Electrophysics, UB RAS, Ekaterinburg, Russia, nick@iep.uran.ru
Lebedev Physical Institute, RAS, Moscow, Russia

A flat horizontal free surface of a conducting liquid (liquid metal for applications) is unstable in a sufficiently strong external vertical electric field. This instability is known as the Tonks–Frenkel (TF) instability. In a supercritical field, boundary perturbations begin to grow, demonstrating a tendency toward unlimited sharpening of the surface. It was experimentally established [1] that a cone with an opening angle close to 98.6^o is formed on the surface in a finite time. This angle arises in the problem of possible stationary configurations of the charged surface of a conducting liquid: in 1964, Taylor [2] showed that, for a cone with the angle of 98.6^o, the electrostatic pressure can be balanced by the capillary pressure. Despite the coincidence of the angle, one should not confuse stationary conical formations (conventional static Taylor cones [2]) on the surface of a liquid in an electric field and dynamic cones arising as a result of the development of TF instability [1]. For the dynamic case, time-dependent self-similar solutions to the equations of motion of an inviscid perfectly conducting fluid were revealed in paper [3]. These solutions are responsible for the formation of conic cusps in a finite time.

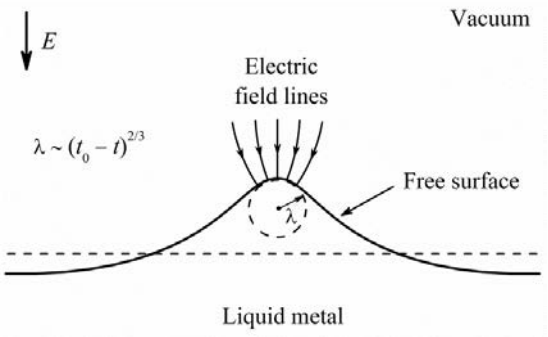

Fig. 1. Sketch of the problem geometry.

For self-similar growth of conic cusps, the spatial scale λ (as such a scale, one can choose, for example, the radius of curvature of the protrusion apex) decreases with time t according to the power law $\lambda \sim (t_0 - t)^{2/3}$, where t_0 is the moment of singularity formation (see Fig. 1). As it turned out, a cone with the Taylor opening angle 98.6^o is the asymptotic shape of the surface close to the singular point, i.e., the self-similar solution resembles in geometry the static Taylor solution.

In the present work, we analytically study the dynamics of the formation of a conic cusp due to the TF instability, taking into account the finite viscosity of the medium. As the system evolves, the Reynolds number (Re) at the tip of an accelerating protrusion decreases from large values, at which the ideal fluid model is applicable, to zero, when viscous effects become dominant.

As it turns out, in terms of the local field strength E at the cusp apex, the process of cusp formation can be divided into two main stages. At the first stage, when $E << E_c$ and $\mathrm{Re} >> 1$, the relations $E \sim u \sim \lambda^{-1/2} \sim \tau^{-1/3}$ between the main parameters of the problem (spatial and temporal scales λ and τ, electric field strength E, fluid velocity u) hold. Here, $E_c = \alpha(\varepsilon_0\rho)^{-1/2}\nu^{-1}$ is a certain threshold value of the electric field strength, α is the surface tension coefficient, ε_0 is the electric constant, ρ is the fluid density, and ν is the kinematic viscosity. At this stage, the cone angle coincides with the angle of the static Taylor cone, 98.6^o. At the second stage, when $E >> E_c$ and $\mathrm{Re} << 1$, we have $E \sim u^{3/2} \sim \lambda^{-3/4} \sim \tau^{-1/2}$ with the limiting angle value of 33.1^o [4]. For the parameters of molten copper, the value E_c is approximately equal to 10^8 V/cm. It is achieved when the characteristic spatial scale (for example, the rounding radius of the protrusion tip) is on the order of tens of nanometers. As an example of a situation where these conditions are realized, we can point out here the paper [5] that examined prebreakdown processes that occur in a cathode microprotrusion with a molten tip exposed to an external electric field.

The obtained analytical result is consistent with the results of numerical modeling [6] of the TF instability development taking into account liquid viscosity, where a tendency was observed toward a decrease in the angle of the formed cone with decreasing Re.

Acknowledgements. This work was supported by the Russian Science Foundation (Grant No. 20-19-00323-P), https://rscf.ru/project/20-19-00323/.

References

1. L. M. Baskin, A. V. Batrakov, S. A. Popov, and D. I. Proskurovsky, *IEEE Trans. Dielectr. Electr. Insul.*, 1995, **2**, 231-236.
2. G. I. Taylor, *Proc. R. Soc. A*, 1964, **280**, 383-397.
3. N. M. Zubarev, *JETP Lett.*, 2001, **73**, 544-548.
4. N. M. Zubarev, *Phys. Fluids*, 2024, **36**, 042102.
5. I. V. Uimanov, D. L. Shmelev, and S. A. Barengolts, *Vacuum*, 2024, **220**, 112823.
6. T. G. Albertson and S. M. Troian, *Phys. Fluids*, 2019, **31**, 102103.

Features of electron runaway in a gas gap with an inhomogeneous electric field

M. I. Yalandin[1,2], N. M. Zubarev[1,2] and O. V. Zubareva[1]

[1] Institute of Electrophysics, UB RAS, Ekaterinburg, Russia, olga@iep.uran.ru
[2] Lebedev Physical Institute, RAS, Moscow, Russia

Free electrons in a gas or plasma may undergo continuous acceleration (i.e., a transition to the runaway mode) if a sufficiently strong external electric field is applied [1]. In a homogeneous or weakly inhomogeneous field, free electrons enter the runaway mode if the field strength E at their origin site exceeds a certain critical value E_c that depends on the type of gas and its pressure [2]. In a strongly inhomogeneous field due to the use of pointed cathodes, this condition is not sufficient for continuous acceleration of electrons within the entire gas gap. The field decays rapidly with distance from the tip, and an electron accelerated in the near-cathode region may start decelerating at the periphery [3].

The present work is devoted to the study of how the degree of inhomogeneity of the electric field distribution in the interelectrode gap affects the conditions for the generation of runaway electrons.

The one-dimensional motion of a free electron along the symmetry axis z of the electrode system can be described by the nonlinear ordinary differential equation

$$d\varepsilon / dz = eE(z) - F(\varepsilon). \qquad (1)$$

Here e is the elementary charge; F is the braking force, which acts on the electron in a medium and depends on its kinetic energy ε. We will use the nonrelativistic Bethe formula [4] for the dependence $F(\varepsilon)$. For the field strength on a scale larger than the tip rounding radius, we can take $E \sim 1/z^{\gamma}$, where the exponent γ characterizes the degree of inhomogeneity of the field distribution (the position of the cathode, from which electrons with initially low energy start, corresponds to $z = 0$). For electrode configurations used in experiments, γ falls within the range from zero (flat cathode) to one (needle cathode). For a conical cathode, the relation between the opening angle α and the exponent γ is given by the following equation [5]: $P_{\gamma}(-\cos(\alpha/2)) = 0$, where P_{γ} is the Legendre function of order γ. For a tubular edge cathode, it can be taken $\gamma = 1/2$ [3].

Analysis of the equation (1) has shown [5] that the dynamics of free electrons is qualitatively different for different degrees of field inhomogeneity, i.e., for different values of γ. Indeed, let us assume that an electron is accelerated at the periphery, i.e., the electric force eE dominates over the braking force F at large z. Then the kinetic energy of the electron is determined by the difference of potentials passed by it, $\varepsilon = e\Phi \sim z^{1-\gamma}$, where we have taken into account that $E = -d\Phi/dz$. The braking force for high ε is estimated as $F \sim 1/\varepsilon$ [4], so that $F \sim z^{\gamma-1}$. Let us compare it with the electric force $eE \sim 1/z^{\gamma}$. It can be seen immediately that, at large z, the condition $eE >> F$ used by us is fulfilled only if $\gamma < 1/2$. Taking into account the inequality $\gamma > 0$, we find that the exponent lies within the range $0 < \gamma < 1/2$. This condition is necessary for continuous acceleration at the limit of large z. At $1/2 < \gamma < 1$, the initial assumption that the accelerating force eE dominates over the decelerating force F at large z is violated. It is possible to conclude that, in this case, the electron will not be continuously accelerated. Its behavior will be more complicated: initially, in the region of low z, it will be accelerated and, after moving far away from the cathode, start to decelerate. In the absence of limitations on z, this will unavoidably result in it turning into a thermal electron.

Hence, our analysis of the asymptotic behavior of free electrons in a gas under inhomogeneous field conditions has shown that their dynamics is radically different at $0 < \gamma < 1/2$ and $1/2 < \gamma < 1$ (in relation to a conical cathode, the boundary case $\gamma = 1/2$ corresponds to the cone angle of 98.6° [5, 6]). It is clear that this will influence the conditions of electron runaway in a gas gap. As it turns out, for a weakly inhomogeneous field distribution ($0 < \gamma < 1/2$), the classical local condition of runaway is quite applicable, namely that the field strength $E(0)$ at the electron starting position must exceed the critical value E_c, which depends only on gas properties. For a strongly inhomogeneous field distribution ($1/2 < \gamma < 1$), this condition does not ensure electron runaway in the entire gap, and a stronger nonlocal condition is required. The voltage U applied to the gap must exceed a certain threshold U_c, which depends both on the properties of the gas and on the geometry of the interelectrode gap (interelectrode distance).

Acknowledgements. This study was supported by the Russian Scientific Foundation, grant no. 23-19-00053, https://rscf.ru/project/23-19-00053/.

References

1. H. Dreicer, *Phys. Rev.*, 1959, **115**, 238-249.
2. G. A. Mesyats, Yu. I. Bychkov, and V. V. Kremnev, *Sov. Phys. Usp.*, 1972, **15**, 282-297.
3. N. M. Zubarev, G. A. Mesyats, and M. I. Yalandin, *JETP Lett.*, 2017, **105**(8), 537-541.
4. H. Bethe, *Ann. Phys.*, 1930, **397**(3), 325-400.
5. N. M. Zubarev, O. V. Zubareva, and M. I. Yalandin, *Dokl. Phys.*, 2023, **68**(9), 279-283.
6. G. I. Taylor, *Proc. R. Soc. A*, 1964, **280**, 383-397.

SECTION 2

EXTREME-FIELD PHYSICS AND NONLINEAR PROCESSES IN LASER-MATTER INTERACTIONS

Experiments and modeling on high energy particles and radiation in relativistic laser-matter interaction

N. E. Andreev

Joint Institute for High Temperatures of RAS, Moscow, Russia, andreev@ras.ru
Moscow Institute of Physics and Technology (State University), Dolgoprudnyi, Moscow region, Russia

Intense beams of photons and particles in the MeV energy range are effective tools in many areas of research, such as the creation and diagnostics of matter in extreme states, nuclear physics and materials science, as well as in other applications. Currently, an efficient concept for creating sources of γ-radiation and neutrons based on the generation of relativistic electrons in the Direct Laser Acceleration (DLA) mode is being discussed. PW-class laser systems capable of generating subpicosecond and femtosecond pulses focused to ultrarelativistic intensity, are good candidates for creating high-current beams of ultrarelativistic electrons in extended plasma with a density close to critical in the DLA process [1–3].

The generation of ultra-bright DLA-based secondary sources of MeV particles and radiation was successfully demonstrated at the sub-PW Nd:glass PHELIX laser facility in Darmstadt. The interaction of the PHELIX sub-ps pulse of ~10^{19} W/cm^2 intensity with pre-ionized low-density polymer foam led to an increase in the effective electron temperature, electron energy and beam charge by a factor of 10–20 compared to shots on conventional foil with the same laser parameters, Fig. 1 [4, 5].

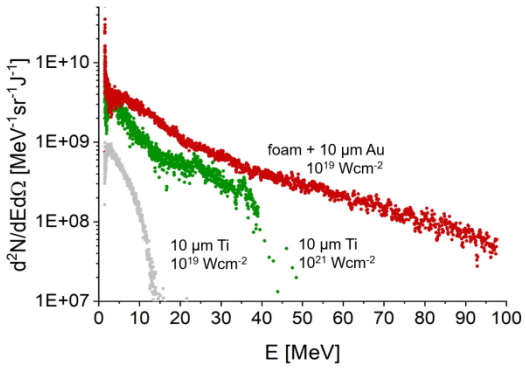

Fig. 1. Electron energy distributions are normalized to the corresponding laser energy inside FWHM of the focal spot in Joules. Shots were made onto the pre-ionized low density foam layer in combination with 10 μm Au-foil at 1.5×10^{19} Wcm^{-2} laser intensity (red) and onto 10 μm thin Ti-foils irradiated by the 9×10^{20} Wcm^{-2} (green) and 1.6×10^{19} Wcm^{-2} (gray) laser intensities. In all cases, spectra were measured along the laser axis

The resulting mega-ampere current beam of DLA electrons penetrates a high-Z converter attached to the foam on the back side and generates directed gamma rays with an effective temperature of 10–15 MeV and photon energies exceeding 50 MeV, Fig. 2, as observed in the detection of short-living isotopes Au192 and Ta176 and high-yield neutrons [6–8].

The dependences of the parameters of laser-generated electron bunches and radiation on the laser intensity and plasma density are obtained and analyzed taking into account current and future experiments [2–10]. The results

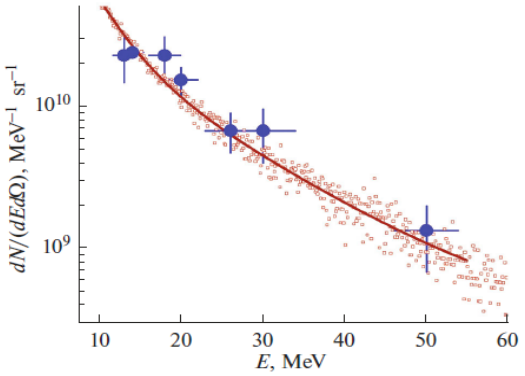

Fig. 2. Spectra of bremsstrahlung γ-rays measured (circles with errors) and simulated using GEANT4 (dots), solid line – two-temperature approximation of the simulated spectrum

obtained show a way to improve the efficiency of a broad class of secondary laser sources, such as sources of electrons, positrons, betatron and bremsstrahlung radiation as well as sources of protons and neutrons for various applications.

References

1. L. P. Pugachev, N. E. Andreev, P. R. Levashov, O. N. Rosmej, *Nucl. Instrum. Methods Phys. Res. A*, 2016, **829**, 88–93.
2. N. E. Andreev, V. S. Popov, O. N. Rosmej, A. A. Kuzmin, A. A. Shaykin, E. A. Khazanov, A. V. Kotov, N. G. Borisenko, M. V. Starodubtsev, A. A. Soloviev, *Quantum Electronics*, 2021, **51**, 1019–1025.
3. X. F. Shen, A. Pukhov, O. N. Rosmej, N. E. Andreev, *Phys. Rev. Applied*, 2022, **18**, 064091.
4. O. N. Rosmej, N. E. Andreev, S. Zaehter, N .Zahn, P. Christ, B. Borm, T. Radon, A. Sokolov, L. P. Pugachev, D. Khaghani, F. Horst, N. G. Borisenko, G. Sklizkov, V. G. Pimenov, *New J. Phys*., 2019, **21**, 043044.
5. O. N. Rosmej, M. Gyrdymov, M. M. Günther, N. E. Andreev, P. Tavana, P. Neumayer, S. Zähter, N. Zahn, V. S. Popov, N. G. Borisenko, A. Kantsyrev, A. Skobliakov, V. Panyushkin, A. Bogdanov, F. Consoli, X. F. Shen, and A. Pukhov, *Plasma Phys. Control. Fusion*, 2020, **62**, 115024.
6. M. M. Günther, O. N. Rosmej, P. Tavana, M. Gyrdymov, A. Skobliakov, A. Kantsyrev, S. Zähter, N. G. Borisenko, A. Pukhov & N. E. Andreev, *Nat. Commun.*, 2022, **13**, 170.
7. P. Tavana, N. Bukharskii, M. Gyrdymov, U. Spillmann, Ş. Zähter, J. Cikhardt, N. G. Borisenko, Ph. Korneev, J. Jacoby, C. Spielmann, N. E. Andreev, M. M. Günther and O. N. Rosmej, *Front. Phys*., 2023, **11**, 1178967.
8. N. E. Andreev, I. R. Umarov, V. S. Popov, *Journal of Surface Investigation: X-ray, Synchrotron and Neutron Techniques*, 2023, **17**, (4), 848–854.
9. N. E. Andreev, I. R. Umarov, V. S. Popov, *Bulletin of the Lebedev Physics Institute*, 2023, **50**, Suppl. 7, S797-S805.
10. J. Cikhardt, M. Gyrdymov, S. Zähter, P. Tavana, M. M. Günther, N. Bukharskii, N. Borisenko, J. Jacoby, X. F. Shen, A. Pukhov, N. E. Andreev, O. N. Rosmej, *Matter Radiat. Extremes*, 2024; **9** (2), 027201.

Effects of nonlinear interaction of modes in CW multicore fiber lasers

S. A. Babin and **E. V. Podivilov**

Institute of Automation and Electrometry SB RAS, Novosibirsk, Russia, babin@iae.nsk.su

Multicore fibers (MCFs) are treated now as a perspective medium which is able to extend limited capacities of singlemode fiber in optical communications, fiber lasers and sensors. With recent implementation of the technology of point-by-point refractive index modification by femtosecond (fs) laser [1] it became possible to inscribe fiber Bragg gratings (FBGs) at arbitrary position in the selected fiber core (both in longitudinal and transverse direction) that offers new opportunities for development of advanced multicore fiber lasers.

Here we review our recent results on the fabrication of FBG arrays in passive and active multicore fibers and their application as complex reflectors of Raman [1] and Yb-doped [2] MCF laser cavities. In such complex cavities the generated waves (transverse and longitudinal modes) behave sufficiently differently from those in singlemode single-core fibers due to specific linear and nonlinear interaction of modes in MCFs. We demonstrate new opportunities of tailoring spatial and spectral characteristics of the continuous-wave (CW) MCF laser generation with an emphasis on intracavity beam combination with single output beam (that means spatial localization) and laser spectrum narrowing due to the interaction of transverse modes of individual cores and supermodes formation and hybridization which results in the collapse of individual core lines into the single narrow line (that means spectral localization), see Fig. 1 [2].

The effects have been studied theoretically and experimentally demonstrating their qualitative agreement. Further development of the theoretical model and potential practical applications of the demonstrated MCF lasers will be discussed.

Acknowledgements. The authors acknowledge financial support by the Russian Science Foundation (21-72-30024).

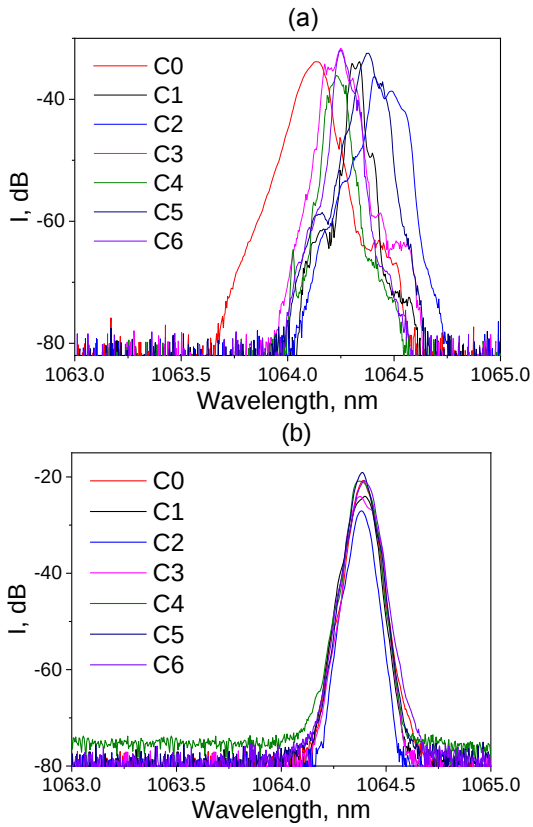

Fig. 1. Individual lines generated in central (C0) and peripherical (C1–C6) cores of Yb-doped MCF laser with FBG cavity in each core without (a) and with (b) core coupling [2]

References

1. A. Wolf, A. Dostovalov, K. Bronnikov, M. Skvortsov, S. Wabnitz, and S. Babin, *Opto-Electronic Advances*, 2022, **5**(4), 210055.
2. A. G. Kuznetsov, A. A. Wolf, A. V. Dostovalov, E. V. Podivilov, S. A. Babin, *Opt. Lett.*, 2023, **48** (13) 3603–3606.

Self-organization of plasma nanostructures during the tightly focused femtosecond laser pulse exposure in the volume of transparent dielectrics

A. V. Bogatskaya[1,2], **E. A. Volkova**[3] and **A. M. Popov**[1,2]

[1] Lebedev Physical Institute, RAS, Moscow, Russia
[2] Faculty of Physics, Moscow State University, Moscow, Russia
[3] Skobeltsyn Institute of Nuclear Physics, Moscow State University, Moscow, Russia

Femtosecond laser writing of birefringent subwavelength nanopatterns in solid dielectrics has been studied for almost two decades since it reveals a number of applications such as optical memory devices, micro-photonic crystals, couplers, binary storage elements etc [1]. Despite extensive both theoretical and experimental research in this area, there is still no universal theoretical model explaining the self-consistent dynamics of field and plasma subsystems in a particular regime of laser exposure. As a result, the obtained data are rather contradictory and their comparison is very complicated due to the very different experimental conditions.

In this work we present the numerical study of dense plasma formation in the volume of fused silica exposed by intense tightly focused femtosecond IR laser pulse to verify the recently proposed hierarchical mechanism of plasma nanopatterns formation which involves the pulse reflection in the pre-focal region and generation of stacks of plasma «sheets» and subsequent excitation of interfacial (at the boundary between weakly/strongly photoexcited dielectric layers) sub-wavelength plasmons [2]. For this purpose, we develop the self-consistent algorithm for the numerical integration of the second-order wave equation in the cylindrical geometry together with the rate equation for the electronic density in diffusion approximation.

It was demonstrated that the plasma object with electron density at a level $\sim 1-2\times 10^{20}$ cm^{-3} arises typicallyin the pre-focal plane, which is in qualitative agreement with the previously developed quasi one-dimensional modelling [3]. The formation of this plasma object is mainly associated with the direct field ionization in multiphoton or tunnel regime while the electron impact ionization is almost negligible. The plasma formed in the near-focal region effectively scatters the incident femtosecond laser pulse producing the region of effective wave interference. As a result, the spatial distribution of the electron production rate is characterized by rather sharp maxima located in the bunches of the standing wave. These maxima lead to the formation of periodic subwavelength regions ofdense plasma both in the ρ- and z-directions (see Fig. 1). It was found that the present mechanism is not associated with the plasmonic one predicted in [2], since the formed electron densities are essentially below critical. Optimal parameters of focused laser radiation were determined for regular plasma self-organized nanostructures. Concretely, it was shown that the most essential for the implementation of such nanostructuring regime is the presence of tight focusing. We also demonstrate that the energy absorbed during the laser pulse is sufficient for strong heating and sub-sequent melting of dielectric sample in the areas of dense plasma formation. Under the conditions of periodic pulse exposure in the volume of fused silica utilized in experiments [4], the processes of melting and solidification of thesubstance will be repeated and accumulated, leading to self-organized modifications of its optical properties. The obtained profiles of plasma nanostructures are found to be in good agreement with SEM images of micromodifications inscribed by Yb-doped fiber laser of 0.3 and 0.6 ps duration and 1030 nm wavelength in accumulation regime[4]. Thus, we believe that the conducted studies shed light on the crucial mechanisms of plasma reorganization under the conditions of tightly focused laser exposure which can force further advancement in laser writing of volume nanopatterns in transparent dielectrics within the suggested regime.

Acknowledgements. This work was supported by the Russian Science Foundation (project no. 22-72-10076).

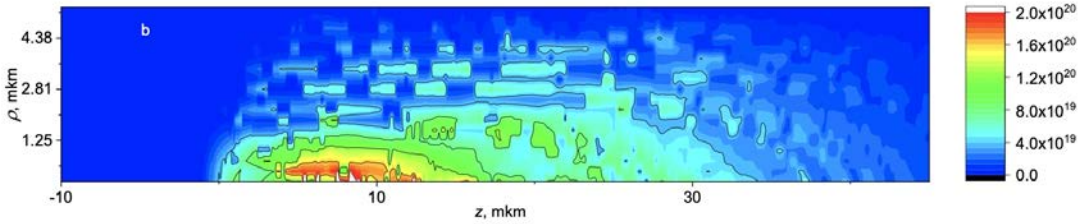

Electron density in the volume of fused silica formed by tightly focused laser pulse with 1030 nm wavelength and 50 fs duration. Pulse energy is 0.24 mkJ, focal spot radius is 2.5 mkm. Pulse moves along the z-axis from the right to left

References

1. E. Mazur, and R. Gattass, *Nature Photon*., 2008, **2**, 219–225.
2. S. I. Kudryashov, P. A. Danilov, M. P. Smaev, A. E. Rupasov, A. S. Zolot'ko, A. A. Ionin, and R. A. Zakoldaev, *JETP Lett*., 2021, **113**(8), 493–497.
3. A. V. Bogatskaya and A. M. Popov. *Optics and Spectroscopy*, 2024, **132**(1), 47–53 (in Russian).
4. Yu. Gulina, A. E. Rupasov, G. K. Krasin, N. I. Busleev, I. V. Gritsenko, A. V. Bogatskaya, and S. I. Kudryashov, *JETPLett.*, 2024, **119**(9), 638–644.

Conversion of intense ultrashort laser pulses into strong electromagnetic fields with the use of profiled micro-targets

N. B. Bukharskii, **Ph. A. Korneev** and **E. O. Dmitriev**

National Research Nuclear University MEPhI, Moscow, Russia, n.bukharskii@gmail.com
P. N. Lebedev Physical Institute, Moscow, Russia

Interaction of relativistically intense ($\gtrsim 10^{18}$ W/cm^2) laser radiation with solid targets is accompanied by the generation of powerful discharge currents caused by the formation of high positive potentials due to the escape of hot electrons from the interaction region into vacuum [1, 2]. Such currents, when excited in a profiled micro-target, hold a promising potential as a source of strong magnetic fields and secondary electromagnetic radiation in the terahertz (THz) frequency range.

Generation of strong magnetic fields may be realized with the use of targets with curved geometry allowing for the formation of enclosed current loops. In this case, the magnetic field generated by the return current may persist on the time-scale greatly exceeding the laser pulse duration. “Snail” targets [3, 4] are one example of the geometry which can be used for efficient magnetic field generation. The results of the performed numerical modeling, as well as the analysis of experimental data, indicates that the amplitude of the magnetic field excited in the inner volume of the “snail” by sub-petawatt ultrashort ($\simeq$ 0,5 ps) laser pulse may reach $\simeq$ 1 kT; the magnetic field is “frozen” into dense plasma and may exist in the target for $\simeq$ 100 ps [3]. Transition to more powerful multi-petawatt laser driver enables the generation of even stronger magnetic fields of up to 10^5 T scale [4]. Some of the parameters of magnetized plasma achieved with the “snail” targets closely reproduce those of certain astrophysical objects, such as accretion disks of close binary systems [5], allowing for their laboratory modeling. In addition, the generated electromagnetic structure can be employed for control of high-energy particle flows enabling their efficient collimation and focusing [4].

Another interesting scenario of laser-matter interaction may be realized with the use of intense laser pulses of femtosecond duration. In this case, the created return current also takes the form of an ultrashort femtosecond pulse, which according to the modeling remains well localized on the target scale [6–8] as the current travels along the target perimeter. Propagation of such a compact current pulse along a curved path is followed by creation of electromagnetic waves. Various target geometries were considered in this context via numerical simulations and analytical estimates, including both the targets where the current pulse propagated along the target surface following an enclosed path, i.e. a circle [6] or an ellipse [7], as well as extended targets where the current pulse propagated along continuous periodically curved trajectories, i.e. a sinusoid [8]. As the calculations showed, the proposed mechanism allowed for the direct control of certain important properties of THz radiation, such as spatio-temporal profiles of emission, radiation spectrum, angular distribution of the emitted power and polarization. The latter can be manipulated by exciting a directed discharge pulse via irradiation of an enclosed elliptic surface at a grazing incidence, since in this case parameters of the polarization ellipse are defined by the parameters of the elliptic surface [7]. More complex polarization states may also be obtained with more complex target geometries. The aforementioned advantages are coupled with the capability of obtaining terawatt levels of power emitted in the THz domain, provided a petawatt femtosecond laser pulse is used as a driver [8]. This makes the considered scheme attractive for various fundamental studies and perspective applications where intense sources of THz radiation with controllable properties are required. The shape of the discharge current pulse, its length and dissipation in the process of propagation along the target remains an open question, assuming more realistic interaction conditions, which, however, is important for further applications such as generation of secondary radiation or particle guiding.

Acknowledgements. The research was supported by the Russian Science Foundation (grant no. 24-22-00402). The authors acknowledge the NRNU MEPhI High-Performance Computing Center and the Joint Supercomputer Center RAS.

References

1. K. Quinn, P. A. Wilson, C. A. Cecchetti *et al.*, *Phys. Rev. Lett.*, 2009, **102**(19), 194801.
2. M. Ehret, M. Bailly-Grandvaux, Ph. Korneev *et al.*, *Phys. Plasmas*, 2023, **30**(1), 013105.
3. M. Ehret, Yu. Kochetkov, Y. Abe *et al.*, *Phys. Rev. E*, 2022, **106**(4), 045211.
4. N. D. Bukharskii and Ph. A. Korneev, *Bull. Lebedev Phys. Inst.*, 2023, **50**, S869-S877.
5. K. F. F. Law, Y. Abe, A. Morace et al., *Phys. Rev. E*, 102(3), 033202.
6. N. Bukharskii, Iu. Kochetkov and Ph. Korneev, *Appl. Phys. Lett.*, **120**(1), 014102.
7. E. Dmitriev, N. Bukharskii and Ph. Korneev, *Photonics*, **10**(7), 803.
8. N. Bukharskii and Ph. Korneev, *Matter Radiat. Extremes*, 8(4), 044401.

On the way to effective laser-based radiation-nuclear sources

V. Yu. Bychenkov

P.N. Lebedev Physical Institute, Moscow, Russia, bychenkovvy@lebedev.ru
Center for Fundamental and Applied Research, Dukhov Research Institute of Automatics, Moscow, Russia

A widely-discussed laser-wakefield acceleration of electrons is replaced by a more promising regime of a relativistic self-trapping (RST) mode when it is necessary to have more sufficiently energetic electrons. Here, a diffraction divergence is balanced by the relativistic nonlinearity such that the laser beam radius stays unchanged during pulse propagation in a plasma over many Rayleigh lengths [1, 2]. Such a stable propagation regime in a rather dense target (near-critical density plasma) is favorable for generation of multi-nC high energy electron bunches with hundred MeV range energy and is of strong demand for numerous radiation-nuclear applications. The way to reach RST, the properties of the generated electrons, and different radiation-nuclear applications is discussed.

Despite the self-focusing regime in a nonlinear medium was predicted in concept almost 60 years ago, the theoretically justified proof of the laser-plasma space matching condition for implementing RST in a plasma with relativistic nonlinearity has appeared only now, although numerical PIC simulations (particle-in-cell) demonstrated this. Here, we present theoretical justification for such matching condition (a_0 – standard dimensionless amplitude of the laser field with the frequency ω)

$$D \sim \frac{c}{\omega}\sqrt{a_0}\,\frac{n_c}{n_e} \qquad (1)$$

using the nonlinear Schrödinger equation (NSE)-based analytical approach. The proposed analytical approach on the basis of NSE relied on the exact self-trapping solutions makes it possible justify the results of PIC-simulations.

The example of the relativistically self-trapped laser pulse from the 3D PIC-simulation is illustrated in Fig. 1 for the matched laser pulse transversal size, $D = 2R$, plasma density, n_e, pulse duration τ and laser field amplitude (red-blue). The space matching condition Eq. (1) is supplemented by the space matching one, i.e.

$$D \sim c\tau \sim \frac{c}{\omega}\sqrt{a_0}\,\frac{n_c}{n_e} \qquad (2)$$

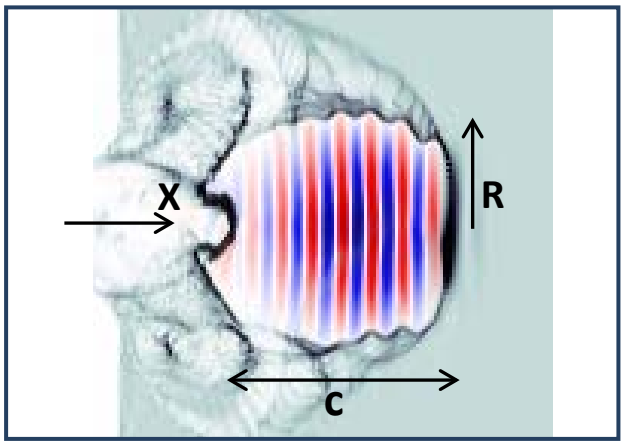

Fig. 1. Self-trapped laser pulse propagation in the x-direction

The condition Eq. (2) guarantees a stability of the RST in relation to its filamentation and self-modulation.

It has been performed the end-to-end coupled 3D PIC and GEANT4 Monte Carlo simulations applied to the final radiation-nuclear sources that is illustrated by Fig. 2.

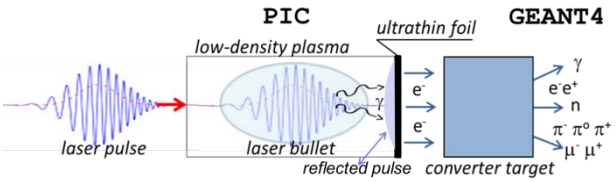

Fig. 2. Laser-targets design for radiation-nuclear applications

As examples, we discuss therapeutic irradiation of the located targeted region in a biological tissue phantom, betatron or Bremsstrahlung gamma sources, gamma-imaging of deeply shielded objects, nuclear gamma fluorescence response of deeply shielded nuclear-hazardous materials, inverse Compton gamma source, medical isotopes production, positron and neutron generation and meson factory to demonstrate in favour of the attractive perspectives offered by the RST regime. Most of these applications are already available using modern short-pulse TW of sub-PW lasers.

Based on the 3D PIC simulations it has been demonstrated how the best efficiency of electron acceleration in terms of the total charge of high-energy electrons and laser-to-electrons conversion rate can be achieved. For given laser pulse energy the universal way is a proper matching of laser hot spot size and electron plasma density to the laser pulse duration. The recommendation to achieve the highest yield of high-energy electrons is to compress laser pulse as much as possible. As example, compression of the few tens fs pulse to the ~ 10 fs pulse leads to generation of the high-energy electron bunch with the highest total charge to exhibit conversion efficiency exceeding 50% for the Joule-level laser pulse energies. Thus, our results have demonstrated good prospects so-called pulse shortening technology CafCA (compression after compressor approach) [3] for different radiation-nuclear applications.

Acknowledgements. The work is supported by the Ministry of Science and Higher Education of the Russian Federation under agreement no. 075-15-2021-1361.

References

1. V. Yu. Bychenkov and M. G. Lobok, *JETP Lett.*, 2021, **114**(10), 579–584.
2. O. E. Vais, M. G. Lobok, A. A. Solov'ev, S. Yu. Mironov, E. A. Khazanov and V. Yu. Bychenkov, *JETP Lett.*, 2023, **118**(12), 871–876.
3. E. A. Khazanov, S. Yu. Mironov and G. Mourou, *Phys.-Usp.*, 2019, **62**(11), 1096–1124.

High dispersive mirrors for ultrafast lasers

Yu Chen[1], **Yanzhi Wang**[1], **Yesheng Lu**[1], **Tianze Xu**[1,2], **Chang Liu**[1,2] and **Jianda Shao**[1,2,3]

[1] Laboratory of Thin Film Optics, Shanghai institute of Optics and Fine Mechanics, Shanghai, China, chenyu4@siom.ac.cn
[2] Center of Materials Science and Optoelectronics Engineering, University of Chinese Academy of Sciences, Beijing, China
[3] Hangzhou institute for advanced study, Hangzhou

Highly-dispersive mirror (HDM) with properties of high reflection and large amount of dispersion has the potential to be used as pulse stretchers and compressors in laser systems. In this work, two kind of HDMs designed for Ti:sapphire lasers and Yb-fiber lasers were developed. A pair of positive and negative HDM with the group delay dispersion (GDD) of ±1000 fs^2 in the spectral range of 750 nm to 850 nm was designed based on the proposed modified Gires–Tournois interferometer (MGTI) structure. Pulse stretching and compression capacity of the positive and negative broadband HDM has been studied theoretically. The femtosecond laser-induced blister structure of the HDMs was observed, the formation and evolution processes of the blister are evaluated. For the narrowband HDM at the wavelength of 1 micrometer, a multi-cavities structure was proposed to design the −20000 fs^2 HDM. The flat bottom pit structure induced by a 1064 nm nanosecond laser was observed. Based on the electric field of the HDM and the damage depth measured by scan probe profiler, the formation of flat bottom pit was explained.

Design and production of HDMs

For the broadband positive and negative HDM, Niobium pentoxide (Nb_2O_5) and silicon dioxide (SiO_2) were chosen as layer materials. A novel starting design based on a modified Gires–Tournois interferometer (MGTI) was employed. The MGTI consists of three parts: a high-reflection stack, multi-G-T cavities, and conjugate cavities, which can be expressed as G/(HL)^n(HxL)^m(HyLH)^o(LyHL)^o/A, where G and A are the substrate and air, respectively, and H and L represent the high- and low-index materials (the optical thickness equals the quarter-wave of the reference wavelength). Based on the MGTI structure, a pair of positive and negative HDM with the GDD of ±1000 fs^2 from 750 nm to 850 nm was designed. Moreover, to further increase the amonut of dispersion, a three cavities structure was proposed to design the narrowband HDM with a GDD of −20000 fs^2 at 1 micrometer.

Both HDMs were deposited on fused silica substrates using a Veeco Spector dual-ion beam sputtering plant. The metallic material was deposited on fused silica substrates by sputtering a pure metal target with O_2, whereas the SiO_2 material was formed by sputtering a SiO_2 target with O_2. Owing to the stable deposition rates, a time-control technique was utilized to monitor the layer thickness.

Characterization of HDMs

The transmittance spectra and GDD were measured using a Perkin-Elmer spectrophotometer and commercial white light interferometer. The comparison between theoretical and measured characteristics are shown in Fig. 1. Great agreement can be observed from Fig. 1.

To study the pulse stretching and compression capabilities of the PHDM and NHDM, output pulses stretched by the PHDM and recompressed by the NHDM were simulated respectively. Pulse analysis showed a nearly Fourier-limited pulse with only a few percent loss after a total of 100 reflections on the PHDM and NHDM were obtained, which proved the great matching between the PHDM and NHDM.

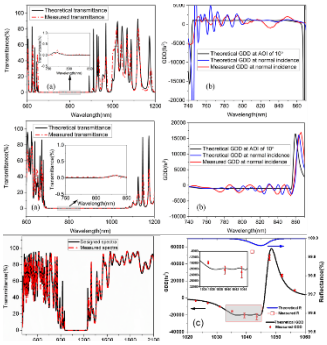

Fig. 1. Comparison of designed and measured characteristics

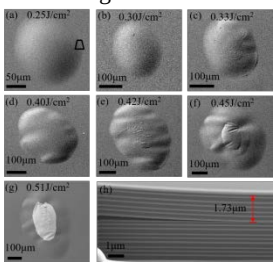

Fig. 2. SEM and FIB images of typical blister in NHDM

Laser induced damage properties of ±1000 fs^2 HDMs were studied under the irradiation of 40 fs laser pulses. The laser-induced damage threshold (LIDTs) are approximately 0.22 J/cm^2 and 0.11 J/cm^2 for the PHDM and NHDM, respectively. A higher damage threshold of the PHDM than that of the NHDM resulting from a lower electric field inside the layer structure, was observed. A blister structure was observed over a wide fluence range for both HDMs, which are shown in Fig. 2. The formation and evolution of laser-induced blisters were demonstrated. Furthermore, the laser-induced damage mechanics of −20000 fs^2 HDM was demonstrated. A flat bottom pit structure was observed at a wide fluence range. The formation of flat bottom pit was successfully explained with the electric field distribution and the damage depth measured by scan probe profiler.

References

1. V. Pervak, et al., Opt. Express, 2012, 20(4), 4503–4508.
2. E. Fedulova, et al., Opt. Express, 2015, 23(11), 13788–13793.
3. Y. Chen, et al., Opt. Express, 2016, 24(17), 19835–19840.

Fractals and human concepts as intermediate asymptotics

Felix Feldchtein

Medical Device Consultant, Shrewsbury MA, USA, felixfel00@gmail.com

This work was inspired by the idea of intermediate asymptotics suggested by Barenblatt and Zeldovich as early as in 70's [1] and further elaborated by Zeldovich and Sokolov in [2]. It was further inspired by Steven Pinker, especially the books [3, 4] offering in-depth analysis of human language semantics and relationship to the real world models and concepts.

Intermediate asymptotics, also known in Western literature as "method of matched asymptotic expansions" [5] is known as finding several different approximate solutions, typically related to a different mathematical submodels, each being accurate for some part of the range of the independent variable, and then combining these different solutions together to give a single approximate solution that is valid for the whole range of values of the independent variable.

In the presentation this approach is expanded and generalized not only beyond the differential equations where it was originally proposed and elaborated, but also outside the mathematical models of the nature in general. All human concepts are considered as an approximate models of the nature. These models are becoming parts of the same continuum (in most cases multi-dimensional continuum), even when they are originally perceived as being separate or mutually exclusive.

With the presented view all concepts are approximate models and they are approximately (albeit sometimes with very good accuracy) valid within some range of parameters and gradually becoming less valid when approaching the periphery if the validity area. As it happens, these concepts are evolving into the alternative concepts, some of them normally considered as not compatible or mutually exclusive with the original models/concepts.

The suggested framework is then illustrated with multiple examples, starting with relatively simple and straightforward and continuing to complex philosophical issues. Then potential implications on scientific methodology, as well as epistemology and philosophy are discussed.

References

1. Г. И. Баренблатт, Я. Б. Зельдович Промежуточные асимптотики в математической физике // Успехи математических наук. 1971. 26(2 (158)):115–129.
2. Я. Б. Зельдович, Д. Д. Соколов Фрактали, подобие, промежуточная асимптотика // Успехи физических наук. 1985. 146(7):493–506.
3. S. Pinker, M. Foster How the mind works: Norton New York; 1997.
4. S. Pinker. The stuff of thought: Language as a window into human nature: Penguin; 2007.
5. R. E. O'Malley. The method of matched asymptotic expansions and its generalizations. Historical Developments in Singular Perturbations. 2014:53–121.

Thermal distortion of broadband high-reflection coatings under high-power continuous laser

Yukang Feng[1,2], **Yanzhi Wang**[1], **Yesheng Lu**[1], **Yu Chen**[1], **Botong Liu**[1] and **Jianda Shao**[1,3]

[1] Thin Film Optics, Shanghai Institute of Optics and Fine Mechanics, Shanghai, China
[2] Center of Materials Science and Optoelectronics Engineering, University of Chinese Academy of Sciences, Beijing, China
[3] CAS Center for Excellence in Ultra-intense Laser Science, Shanghai, China

With the development of laser technology, laser power is continuously increasing. High-power laser irradiation on coatings results in thermal deformation [1, 2] due to the absorption of laser energy. In complex optical systems comprising numerous reflective mirrors, cumulative surface deformations can degrade beam quality. To explore the damage mechanisms of high-reflectivity mirrors caused by high-power continuous laser exposure at different wavelengths, a thermal distortion simulation algorithm was developed to predict temperature rise, thermal distortion, and the stress distribution in coatings. The ultra-wideband, low-absorption, and high-reflectivity thin film (R>99.9% λ = 500–1100 nm) with various multilayer film structure was investigated, integrating algorithms to validate simulation predictions. Theoretical investigations revealed that high-power laser beams could induce deformation at the center of coatings surfaces. Laser irradiation of different wavelengths on the same thin film structure will result in different temperature increases. The thermal optical and thermal expansion coefficients of materials play vital roles in determining the optical and mechanical characteristics of thin films when subjected to laser-induced temperature fluctuations.

$$L_x = L_y = L_0[1 + t(1-s)/E]$$
$$L_z = L_0(1 - 2st/E) \quad (1)$$

Eq. 1 describes the deformation of the film. L_x, L_y, and L_z are the strain in the x, y, and z directions, respectively, E is the Young's modulus, t is the stress, and s is the Poisson's ratio.

$$t(1-s)/E = (\alpha - \beta)(T - T_0) \quad (2)$$

Where α and β are the thermal expansion coefficients of the substrate and the film, respectively [3–5]. The thermal distortion of the film at different temperature shifts ($T - T_0$) is obtained from Eq. 2. Using this distortion, we can then compute the optical performance of the film through its optical matrix.

Acknowledgements. This work was supported by National Key R&D Program of China (2022YFB3605903), the China Postdoctoral Science Foundation (2022M723268), the International Partnership Program of the Chinese Academy of Sciences (181231KYSB20200040), the Youth Innovation Promotion Association of the Chinese Academy of Sciences (Y2021072), and the Strategic Priority Research Program of CAS (XDB1603).

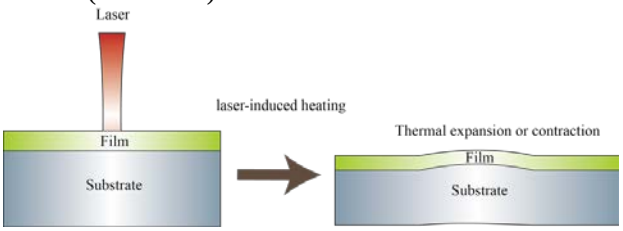

Fig. 1. Thermal distortion of film caused by laser-induced temperature rise

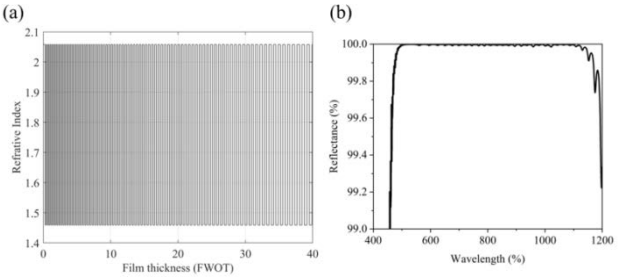

Fig. 2. (a) Layer refractive index distribution of coating; (b) Reflectance of coating

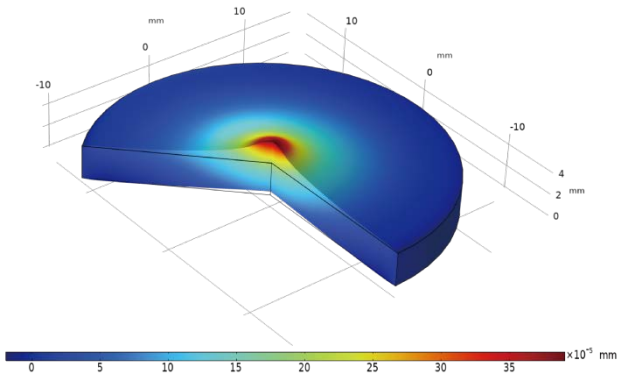

Fig. 3. (a) Film deformation diagram under laser irradiation

References

1. E. Suhir. J. Appl. Phys. 88 (5): 2363–2370 (2000).
2. Haruo Takashashi. Appl. Opt. 34, 667-675 (1995).
3. Claude A. Klein, Opt. Eng. 40(6), (2001).
4. H. Angus Macleod, Thin-film optical filters. CRC press, (2010).
5. Jeffrey L. Braun, et al. J. Heat Transfer .052801(2018).

Development and initial findings of a few-cycle CEP-stable femtosecond laser source

K. A. Glushkov and **I. B. Mukhin**

A.V. Gaponov-Grekhov Institute of Applied Physics of the Russian Academy of Sciences, Nizhny Novgorod, Russia,
k.glushkov@ipfran.ru

Optical parametric amplifiers have the potential to simultaneously increase the energy and average power of low-cycle pulses due to their wide bandwidth, high gain and low heat dissipation [1].

A parametric femtosecond laser system of 2-μm spectral range has been developed based on a sub-picosecond ytterbium laser. The generation of a wide spectrum occurs when using the second harmonic of fundamental radiation, and the generation of a difference frequency allows for adjustment to the infrared range and passive phase stabilization relative to the envelope (CEP). Subsequent parametric amplification in the region of 2 microns leads to an increase in pulse energy up to 20 μJ. The generated radiation has a spectral width of more than 500 nm (Fig. 1.), and the pulse duration is close to spectrally limited and is 22 femtoseconds (Fig. 2.) or 2.7 field oscillations. The CEP stability measurement performed by the f-2f interferometry method showed a standard deviation of 300 mrad. A parametric amplifier is being developed to amplify this signal to the mJ energy level.

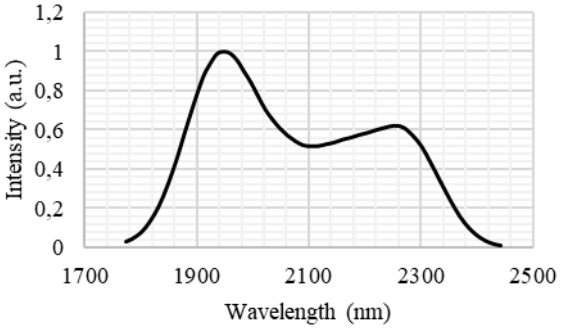

Fig. 1. Femtosecond pulse spectrum

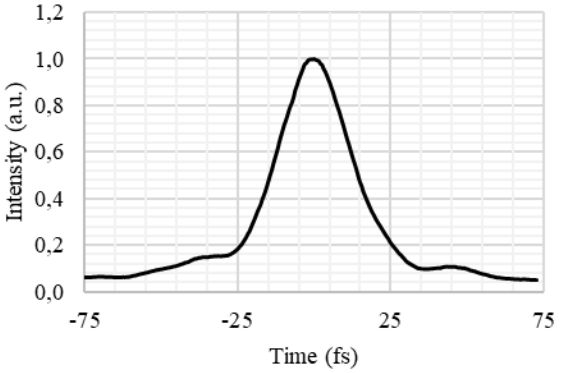

Fig. 2. Autocorrelation function

The optical scheme described above with the addition of a second harmonic generation node from the difference frequency was tested on the PEARL complex as a femtosecond part of the starting system [2]. The synchronism angle of the nonlinear BBO crystals of the femtosecond system has been changed to form laser pulses with a central wavelength of 1820 nm. This approach has an important advantage, since starting with an ytterbium femtosecond generator makes it easy to implement precision optical synchronization between the pulses of the pump channels and the femtosecond signal using fiber optics elements. Additionally, the use of a 2nd harmonic generation node allows you to increase the contrast of laser pulses. After the introduction of this system into the laser complex, the short-term energy stability increased from 40% to 3% RMS, and the duration of the fs pulse decreased by more than 2 times, to 30 fs. These studies formed the basis for the design of the launch part of the XCELS megascience installation.

Another important application of the developed femtosecond laser system is the generation of high harmonics of radiation, since the pulse duration in 2.3 field oscillations in combination with CEP stabilization potentially allow the formation of single attosecond pulses. The first studies of the generation of high-order harmonics in solid-state targets allowed the formation of harmonics up to the 11th (with a wavelength of 190 nm). Another direction of development of the created femtosecond system is the formation of femtosecond pulses in the region of 10 microns by generating a difference frequency between the spectral ranges of 1940 nm (wavelength of amplification of tullium lasers) and 2400 nm. Further, such radiation can be amplified in a high-pressure CO_2 amplifier.

Acknowledgements

This work was supported by Russian Science Foundation No. 24-12-00461, https://rscf.ru/project/24-12-00461/.

References

1. H. Fattahi, H. Wang, A. Alismail, G. Arisholm, V. Pervak, A. M. Azzeer, F. Krausz, Opt. Exp., 2016, 24(21), 24337–24346.
2. I. Mukhin, K. Glushkov, A. Soloviev, A. Shaykin, V. Ginzburg, I. Kuzmin, M. Martyanov, S. Stukachev, S. Mironov, I. Yakovlev, E. Khazanov, Appl. Opt., 2023, 62(10), 2554–2559.

Reflection pulse compression grating: a new look at an old problem

Yuxing Han, Yunxia Jin, Jianda Shao

Laboratory of Thin Film Optics, Shanghai Institute of Optics and Fine Mechanics, Chinese Academy of Sciences, China

The pulse compressor has evolved to be a core module of 100 petawatt (PW) or exawatt laser facilities; however, the diffraction efficiency bandwidth, laser-induced damage threshold (LIDT), and aperture of its currently deployed gratings strongly restrict the ultra-intense and ultrashort pulse compression. Maximizing the energy-loading capability of gratings is a world-wide challenge in the high-peak-power laser field. Here, for 10's femtosecond-PW pulse compression, an ultra-broadband gold grating was developed to dramatically broaden the high diffraction efficiency bandwidth from 100–200 nm to 400 nm. Moreover, a core mechanism was elucidated whereby the high diffraction efficiency combined with the deep penetration effect of electrons under high-energy laser irradiation can tap the LIDT potential of metal grating. Accordingly, the electrum grating was invented and demonstrated experimentally with superior performance in terms of diffraction efficiency bandwidth and LIDT compared with normal gold gratings. In addition, for picosecond-PW pulse compression, a multilayer dielectric grating (MDG) design paradigm was proposed. The grating solution regions were classified into four regions based on the line density: incompatible, stable, anomalous, and turbulent. Importantly, TM-polarized MDGs had the superiority of a high LIDT owing to the low electric field intensity. An energy scaling factor 7.09 times larger than that of NIF-ARC was obtained by taking advantage of TM polarization and a small incident angle. Meanwhile, the meter-scale grating fabrication campaign is well underway. These results make a pioneering technical reserve to facilitate future 100 PW-class ultrafast laser systems.

Keywords: Ultra-intense and ultrashort laser, ultra-broadband gold grating, electrum grating, multilayer dielectric grating, TM polarization, LIDT.

Grating compressor optimization aiming maximum focal intensity

E. A. Khazanov

A.V. Gaponov-Grekhov Institute of Applied Physics of the Russian Academy of Sciences,
efimkhazanov@gmail.com

To reach maximum focal intensity, the laser radiation should be Fourier-limited not only in time, but also in space. For this purpose, an acousto-optic programmable dispersive filters and adaptive mirrors are used. But these technologies cannot compensate for space-time coupling in principle. Since diffraction gratings are not perfectly plane, any compressor inevitably introduces space-time coupling phase distortions, which reduce the focal intensity. This reduction has been numerically studied in many works, for example [1], for specific compressor parameters, but we are not aware of any analytical results.

In this work, the focal intensity is found analytically. An expression has been obtained in the most general form for an arbitrary compressor – an asymmetric out-of-plane compressor with gratings of arbitrary surface shape. The focal intensity is most strongly affected by the linear angular chirp caused by the spatial shift of different frequencies on the second and third gratings. The second effect is that the shape of the wave front reflected from the grating repeats the shape of the grating, but the proportionality coefficient is frequency dependent. This effect to the best of our knowledge, has not been studied in the literature before.

In addition, a simple method of compensating for space-time coupling is proposed, which consists in two-angle adjusting of the fourth grating, which allows us to significantly increase the focal intensity and/or reduce the requirements for the accuracy of grating manufacturing. The focal intensity of the compressor for the XCELS Project is shown in Fig. 1.

It has been shown that the decrease in the focal intensity depends on the product of the grating surface rms σ and the spectrum bandwidth Δω. For a given value of σ, with increasing Δω, the focal intensity changes in two ways: it increases in proportion to 1/Δω due to the shortening of the Fourier-limited pulse, but decreases due to an increase in space-time coupling. As a result, a decrease in Δω may not reduce the focal intensity, it may even lead to its slight increase.

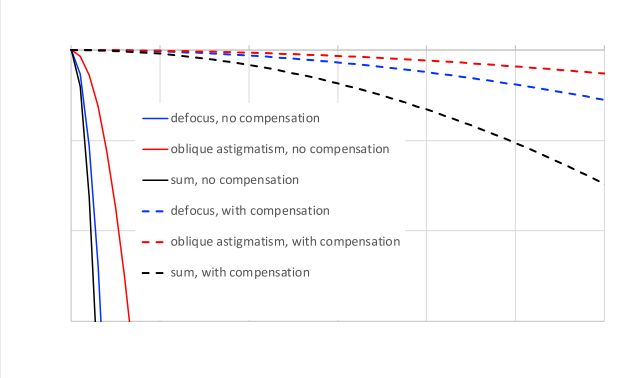

Fig. 1. Focal intensity without (solid line) and with (dashed line) compensation for the grating shaped as defocus or vertical astigmatism (blue), oblique astigmatism (red) and the sum of three Zernike polynomials (black)

Acknowledgements. The research was supported by the Ministry of Science and Higher Education of the Russian Federation (Project No. FFUF-2023-0001).

References

1. Z. Li, J. Liu, Y. Xu, Y. Leng, and R. Li, Optics Express, **30**, 41296 (2022).

Smoothing of fluence fluctuations of intense femtosecond laser beams in asymmetric compressors

D. E. Kiselev, A. A. Kochetkov, I. V. Yakovlev and **E. A. Khazanov**

A.V. Gaponov-Grekhov Institute of Applied Physics of the Russian Academy of Sciences, Nizhny Novgorod, Russia, dimakiseloff@yandex.ru

All high-power femtosecond laser systems use chirped pulse amplification methods [1], the key element of which is an optical compressor. Traditionally, the Tracy compressor [2] with two pairs of parallel diffraction gratings is used. In this case, the last fourth grating is in more severe conditions from the point of view of laser impact, since the diffraction gratings have a lower threshold of breakdown by femtosecond pulses compared to nanosecond pulses. As a rule, the fluence in broad beams of high-power lasers is not uniformly distributed. “Hot spots” caused by defects in the optics upstream of the compressor limit the maximum energy of the output radiation pulses, requiring its reduction below the optical breakdown threshold at these points.

This paper presents the results of the study of the possibilities of smoothing the spatial modulation of fluence in laser beams due to the use of asymmetric nonplanar compressors of chirped pulses [3].

In the experiments performed, a Ti:sapphire laser in the femtosecond mode generated radiation pulses with a central wavelength of 905 nm and a spectral width at half-height of about 40 nm. The beam coming out of the laser was expanded by a telescope and passed through a 4 mm diameter aperture, which provided a quasi-homogeneous beam profile. The beam was then directed into a compressor. The compressor was a single-lattice analog of the four-lattice compressor of the PEARL laser system.

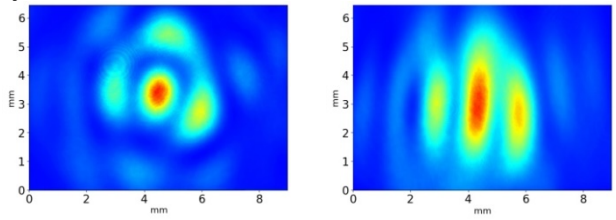

Fig. 1. Profiles of beams that passed (a) a symmetric compressor ($\gamma_3 = 0$), as well as (b) an asymmetric compressor, at γ_3 =1.11°

The scheme of a single-lattice compressor is very convenient for its reconfiguration into a non-symmetric scheme, in which the beam direction on the return passage by means of an additional flat mirror can be deviated from the direction corresponding to the symmetric scheme. In particular, the scheme of a nonplanar compressor was investigated when the angle γ3 of the third beam incidence on the grating in the vertical plane is not equal to zero.

In practice, the spatial distribution of fluence in the beam is irregular. To investigate the efficiency of beam smoothing by an asymmetric compressor, we introduced into the beam an amplitude mask, which is a transparent glass plate with several opaque points of 0.5–1 mm diameter applied to it in random places. Figures 1a and 1b show the profiles of beams that passed the symmetric and asymmetric compressors, Ti:sapphire laser operated in femtosecond mode.

In Fig. 1b, the effect of smoothing the non-uniformity along the y-axis at non-zero angle γ_3 is clearly visible.

For quantitative analysis, we compared the spatial fluence spectra obtained experimentally and theoretically. Fig. 2 shows the one-dimensional fluence spectra $S_y(k_y)$ calculated from the two-dimensional Fourier spectrum $S(k_x, k_y)$ using the formulas:

$$S(k_x, k_y) = \left| \int_{-\infty}^{\infty} w(x,y) e^{i(k_x x + k_y y)} dxdy \right|^2,$$

$$S_y(k_y) = \int_{-\infty}^{\infty} S(k_x, k_y) dk_x,$$

and the coefficient of suppression (transmission) of fluence fluctuations in the y plane:

$$T(k_y, \gamma) = \frac{S_y(k_y, \gamma)}{S_y(k_y, \gamma = 0)}.$$

To calculate the theoretical spectra $S(k_x, k_y)$, we used the experimentally measured spectrum at γ_3=0 and multiplied it by the suppression factor.

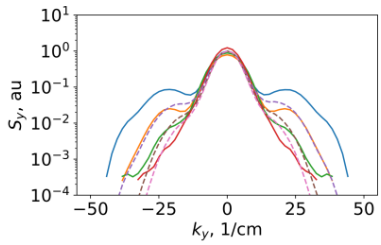

Fig. 2. Experimental (solid lines) and theoretical (dashed lines) fluence spectra of $S_y(k_y)$

In the horizontal plane, the fluctuations were practically independent of γ_3. In the y plane, effective filtering occurred, and the larger the angle γ_3, the larger spatial scales were filtered.

Acknowledgements. The research was supported by the Ministry of Science and Higher Education of the Russian Federation (Project No. FFUF-2023-0001).

References

1. D. Strickland and G. Mourou, Compression of amplified chirped optical pulses, *Optics Communications*, 56, 219–221 (1985).
2. E. B. Treacy, Optical pulse compression with diffraction gratings, *IEEE Journal of Quantum Electronics QE-5*, 454–458 (1969).
3. E. Khazanov, 2D-smoothing of laser beam fluctuations in optical compressor, *Laser Phys. Lett.*, 20, 125001 (2023).

Orbital Angular Momentum exchange in interaction of structured laser beams with electrons and low-density plasma

E. O. Dmitriev and **Ph. A. Korneev**

National Research Nuclear University MEPhI, Moscow, Russia,
P. N. Lebedev Physical Institute, Moscow, Russia

The problem of energy, momentum and orbital momentum exchange between light and charged particles is one of the fundamental problems with a long history. For simple models like, e.g. a plane wave and single particle, there are analytical solutions, though for realistic situations, like the case of irradiation plasma by focused laser beams or with applied stationary external fields, the lack of known integrals of motions makes even interaction with individual particles a nontrivial problem, where irreversible changes of dynamical particle characteristics, such as momentum and angular momentum may occur. In case when the light has an internal structure defining its orbital angular momentum, this nontrivial problem becomes specially intriguing due to the initial absence of the axial symmetry in the system.

Recent numerical studies [1–3] demonstrate the possibility of the Orbital Angular Momentum (OAM) transfer from a structured laser beam to a low-density plasma and generation of a strongly magnetized plasmoid with the poloidal magnetic field geometry. The actual transfer mechanism however is not evident, though an important role of the longitudinal particle motion was unraveled [2]. The problem of analysis of the OAM transfer is additionally complicated by the need of accurate analytical expressions for the driving electromagnetic fields, as the main paraxial approximation and the simple approximation of the temporal envelope appear to be insufficient. This was demonstrated with use of a special case of the OAM beam, where the orbital momentum and the polarization momentum of light were opposite, so that the integral of motion exists in the wave-particle system [4].

To understand the overall OAM transfer to a system of interacting particles, a more simple case of the light wave interaction with a single particle was considered numerically in several works, see, e.g. [2, 5, 6]. The system of non-interacting particles, which is the limiting case of low-density plasma, then can be achieved by averaging over the initial particle positions. Form the known numerical results it follows, that in this case, the transferred angular momentum for an axially symmetrical particle distribution is the relativistic phenomenon, so for the analysis, the lowest order perturbation theory is insufficient. The case of relativistic intensities corresponds also to the simulation setups [1–3], where the average transferred OAM was high enough to generate the strong quasi-stationary magnetic fields.

As an initial step in the analytical study of the OAM transfer to single particles, the perturbation theory on the amplitude of the driving laser pulse was developed up to higher orders [8]. It was found, that in general, i.e. for arbitrary spatially structured pulses with a slow time dependence, for an axially symmetric initial particle distribution, the OAM transfer may occur in the fourth order on the laser field amplitude. In the obtained general result, the approximate analytical expressions for the driving laser pulse, obtained in frames of the paraxial approximation and the approximation of the slowly-varying temporal amplitude, were used to estimate the rate of the OAM transfer. It was found, that the actual parameter which defines the overall transfer rate, is a combination, which includes the laser wave amplitude and the paraxial parameter, which may be interpreted as a relation of the particle oscillation amplitude in the laser wave to the beam waist. This effectively extends the applicability range of the obtained result to the case of moderately relativistic interaction. The obtained analytical results were examined with the Monte-Carlo numerical simulations, where the electromagnetic fields were obtained numerically with the Maxwell Yee solver incorporated in the open-source Partical-in-Cell code Smilei [9].

The obtained expressions for the single-particle absorption allows for estimates for the OAM absorption in low-density plasmas and consideration of some more complex collective effects in a system of weakly-interacting charged particles including generation of the magnetic fields and waves interaction [10, 11].

References

1. R. Nuter, Ph. Korneev, I. Thiele, and V. Tikhonchuk, Physical Review E, **98**, 033211 (2018).
2. R. Nuter, Ph. Korneev, E. Dmitriev, I. Thiele, and V. Tikhonchuk, Physical Review E, **101**, 053202 (2020).
3. A. Longman and R. Fedosejevs, Physical Review Research, **3**, 043180 (2021).
4. E. Dmitriev and Ph. A. Korneev, Bulletin of the Lebedev Physics Institute, **49**, 48 (2022).
5. V. T. Tikhonchuk, P. Korneev, E. Dmitriev, and R. Nuter, High Energy Density Physics, **37**, 100863 (2020).
6. P.-V. Toma, S. Miclut a-Campeanu, M. Boca, A. Nicolin, and V. Baran, in AIP Conference Proceedings, **2843** (AIP Publishing, 2023).
7. E. Dmitriev and Ph. A. Korneev, Bulletin of the Lebedev Physics Institute, **50**, S891 (2023)
8. E. Dmitriev and P. Korneev, arXiv:2405.00907.
9. J. Derouillat, A. Beck, F. Perez, T. Vinci, M. Chiaramello, A. Grassi, M. Fle, G. Bouchard, I. Plotnikov, N. Aunai, J. Dargent, C. Riconda, and M. Grech, Computer Physics Communications, 222, 351 (2018)
10. D. R. Blackman, R. Nuter, Ph. Korneev, A. Arefiev, and V. T. Tikhonchuk, Physics of Plasmas, **29**, 072105 (2022).
11. R. Nuter, Ph. Korneev, and V. T. Tikhonchuk, Physics of Plasmas, **29**, 062101 (2022).

QED cascade multiplicity at laser-solid interaction

M. A. Serebryakov, E. N. Nerush, I. Yu. Kostyukov

A.V. Gaponov-Grekhov Institute of Applied Physics of the Russian Academy of Sciences, Nizhny Novgorod, Russia,
kost@ipfran.ru

QED cascading in a strong EM field is one of the striking phenomena that is still poorly studied in laboratory conditions. This manifests itself in the exponential growth of electron-positron pairs over time. It is generally believed that QED cascades develop in the polar cap of neutron stars while electron-positron plasma plays a key role in many astrophysical processes [1]. Progress in laser technology opens route to convert laser energy into electron-positron plasma and gamma rays through QED cascading.

There are a number of configurations were proposed to study QED cascade in the laser field experimentally [2, 3]. It is known that the cascade does not develop in the plane EM field if it is initiated from a few seed particles. That is why the proposed schemes implies many laser pulses forming standing-wave-like configurations. However, such schemes require a space-time synchronization of the laser pulses which greatly complicates the proposed schemes. Yet the standing wave configuration can be formed by the reflection of a single laser pulse from the solid targets. In this case there is no need in the synchronization. Moreover, as a result of ponderomotive pressure of the incident laser pulse, the reflection surface turns into a concave mirror there by providing additional focusing of the reflected laser radiation. This may increase the laser intensity at the region of the superposition of incident and reflected radiation.

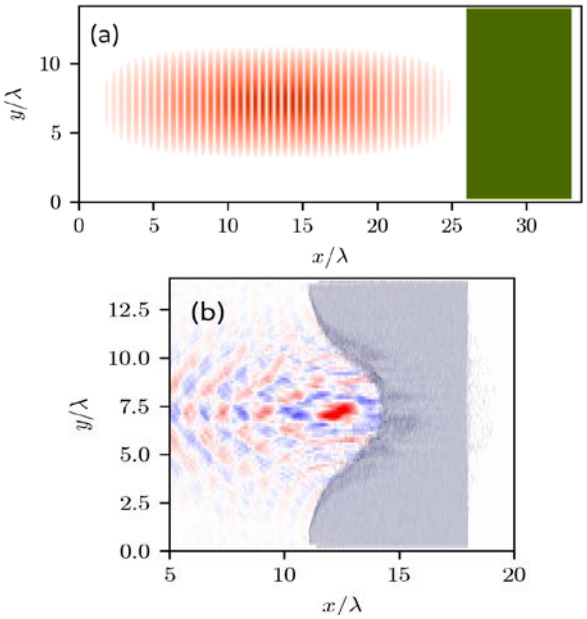

Fig. 1. (a) The initial distribution of the laser intensity and the target plasma density; (b) the distribution of E_y-B_z field and the ion density in the simulation with $a_0 = 900$, $n_e = 500\ n_{cr}$, $ct/\lambda = 15$

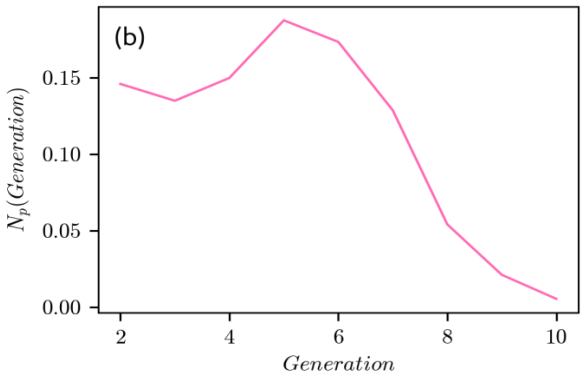

Fig. 2. The distribution of the positron number on the generation number for $a_0 = 900$, $n_e = 500\ n_{cr}$, $ct/\lambda = 20$ and the laser pulse duration is 30 fs

In this work we numerically study the development of theQED cascade in the field formed by superposition of the incident laser radiation and the radiation reflected from the solid target. To demonstrate that the positrons formed in the simulationarise exactly in the QED cascade, the QUILL codewas modified so that the quasi-particles have an additional parameter which is their generation number. This parameter also represents the cascade multiplicity. The initial plasma electrons belong to the zero generation.

The result of simulation is shown in Figs. 1 and 2 for parameters $a_0 = 900$, $n_e = 500\ n_{cr}$, where a_0 is the normalized strength of the laser field and the n_e is the electron density in the target, n_{cr} is the critical density. It is seen from Figs. 2 that the cascade multiplicity exceeds 9 for the considered parameters. Therefore, the observation of QED cascade is feasible for the configuration with laser reflection.

Acknowledgements

This work was supported by the Russian Science Foundation (Grant No. 20-12-00077).

References

1. A. K. Harding and D. Lai, *Rep. Prog. Phys.*, 2006, **69**, 2631.
2. E. N. Nerush et al., *Phys. Rev. Lett.*, 2011, **106 (3)**, 035001.
3. A. Bashinov et al., *Eur. Phys. J. Spec. Top*. 2014, **223**, 1105.

Retrieval of the wavefront of laser beam based on the analysis of the intensity distribution at the focus using convolutional neural networks

A. V. Kotov[1], **Y. A. Rodimkov**[2] and **A. A. Soloviev**[1]

[1] A.V. Gaponov-Grekhov Institute of Applied Physics of the Russian Academy of Sciences, Nizhny Novgorod, Russia, kotov@ipfran.ru

[2] Lobachevsky State University of Nizhny Novgorod, Nizhny Novgorod, Russia

The paper proposes a method for determining wavefront distortions from the intensity distribution in two planes of laser pulse waist: in focus and out of focus. For the wavefront reconstruction task, we propose to use deep convolutional neural networks. To train the models, we used numerically generated data using Zernike modes. The method makes it possible to reconstruct the shape of the wavefront with an error of less than 20% in the RMS range from 0.075 to 0.75 wavelengths.

The main factor limiting the quality of laser radiation focusing is wavefront distortion. They arise due to the non-ideal shape of the surface of optical elements, adjustment errors, thermal and mechanical effects, and the effect of air flows in the open parts of the laser on the wavefront. To correct the wavefront of the laser pulse, adaptive optical systems (AOS) are used. The AOS consists of a mirror with a controlled surface shape – a deformable mirror (DM), a wavefront sensor (WFS), with the help of which feedback is provided, and a control system.

The presence of unequal wavefront distortions in the focusing channel and in the wavefront measurement channel leads to the fact that even with an ideally flat wavefront on the WFS, the focal spot will differ from the ideal one. Wavefront distortions that arise between the focusing region and the WFS plane are usually called differencial distortions. In the presence of differential distortions in the system, it is necessary to recalibrate the WFS, that is, to find the wavefront corresponding to optimal focusing.

In recent years, wavefront correction methods based on neural networks have been actively developed [1]. Their essence is to reconstruct the wave front from the pattern of intensity distribution in the focal plane. Unlike classical approaches [2, 3], which require a long operating time and the effectiveness of which depends on the correction process and the starting point, neural network methods are able to predict the wavefront required for correction in a small number of iterations, down to one. Therefore, these methods are promising in problems of correcting wavefront distortions.

In this work, a convolutional neural network of the encoder-decoder type was chosen for wavefront reconstruction. The input data for the neural network was images of the focal spot in focus and out of focus, and the output data was shape of wavefront. Data for training the neural network were generated numerically by decomposing the wavefront into Zernike polynomials and Fourier transform.

Using only one in-focus or out-of-focus intensity distribution to reconstruct a wavefront introduces uncertainty in the existence of multiple wavefront shapes that give rise to such a distribution. Therefore, in order to correctly reconstruct the wavefront, unambiguity in the intensity distribution for a given wavefront is required. In this work, we chose the phase diversity method as the simplest and most convenient to implement. In addition to solving the problem of phase ambiguity, the defocusing focal spot pattern highlights the features of the distortions, which should make them easier to identify by the neural network.

Experimental verification of the proposed method was carried out on the PEARL laser facility [4]. The beam diameter was 18 cm, the focusing system had a numerical aperture of F/4. This experimental scheme is used when working with high-power radiation, which shows the practical applicability of the developed method.

Using numerically generated data, the method showed an error in determining the wavefront shape of less than 20% in the wavefront RMS range from 0.075 to 0.75 wavelengths. In real conditions, the error was about 40%.

Acknowledgements. The research was supported financially by the Ministry of Science and Higher Education of the Russian Federation (agreement No. 075-15-2021-1361).

References

1. Guo Youming, et al., *Opto-Electronic Advances*, 5.7 (2022): 200082-1.
2. A. V. Kotov, et al., Adaptive system for correcting optical aberrations of high-power lasers with dynamic determination of the reference wavefront, *Quantum Electronics*, 51.7 (2021): 593.
3. J. V. Sheldakova, T. Y. Cherezova, and A. V. Kudryashov, Genetic and hill-climbing algorithms for high-power laser beam correction, *Topical Problems of Nonlinear Wave Physics.* Vol. 5975. SPIE (2006).
4. V. V. Lozhkarev, et al., Compact 0.56 petawatt laser system based on optical parametric chirped pulse amplification in KD* P crystals, *Laser Physics Letters*, 4.6 (2007): 421.

Bright betatron hard X-ray source developed at SIOM using laser wakefield acceleration

Song Li

Shanghai Institute of Optics and Fine Mechanics, China

With the progressive miniaturization and stabilization of laser wakefield accelerators, table-top X-ray radiation sources based on wakefield accelerators have shown enormous potential. The betatron radiation source, driven by ultrashort laser pulses, features a source size in the micrometer range, pulse duration in the femtosecond range, divergence angles in the milliradian range, and covers a broad spectrum exceeding tens of keV. It is applicable for high-contrast imaging of minute structures and for probing interdisciplinary ultrafast processes. Here we present the achievement of bright betatron hard X-ray radiation sources at Shanghai Institute of Optics and Fine Mechanics (SIOM), Chinese Academy of Sciences, utilizing a 1PW/0.1Hz laser system at Shanghai Superintense Ultrafast Laser Facility (SULF). Such a laser system can produce electron beams with charges above hundred pC and energies exceeding 1 GeV. Meanwhile, electron beams undergo the betatron oscillations in the wakefield, generating high-brightness X-ray radiation sources with critical energies ranging from 15 to 25 keV.

This advancement enables time-resolved imaging and spectroscopy at atomic and molecular scales, suitable for dense materials and biological specimens. The high brightness and energy levels enhance the efficiency and resolution, making these sources competitive with larger synchrotron facilities. The compact nature of table-top betatron X-ray sources offers significant cost and complexity reductions, fostering broader access and innovation across fields such as nuclear photonics, ultrafast chemistry, materials science, and biomedical research, etc. As this technology matures, its transformative impact on scientific and industrial applications is expected to grow.

Development considerations for ultra-intense ultrashort lasers

Zhaoyang Li

Key Laboratory of Ultra-intense Laser Science and TechnologyShanghai Institute of Optics and Fine Mechanics, China, lizy@siom.ac.cn

Current ultra-intense ultrashort lasers have achieved peak powers of 10 petawatt and focused intensities of 10^{23} W/cm^2. What's next for peak power and focused intensity?

In optics, the λ^3 laser or the λ^3 regime named by G. Mourou et al., i.e., compressing all the energy of a laser pulse into a spatiotemporal focal cube edged by the laser center wavelength, is considered as the highest intensity condition of an ultra-intense ultrashort laser [1]. In physics, one recent research shows that the highest intensity in laboratories with a non-ideal vacuum should be 10^{26} W/cm^2, i.e., about a thousandth of the Schwinger limit [2]. Considering a 10^{26} W/cm^2 focused intensity and a single-wavelength focal spot (a ~1 μm center wavelength), the peak power should be at least 1 exawatt (i.e., 1000 petawatt) which is much higher than today's 10 petawatt.

Single-cycle exawatt-class lasers require the lowest energy, which can reduce the size and cost of the project. However, to achieve single-cycle exawatt-class laser pulses, near-octave ultra-broadband high-energy amplification is required. For this purpose, the wide-angle non-collinear optical parametric chirped pulse amplification (WNOPCPA) method was proposed a few years ago [3], and the first experimental demonstration is introduced here. At the same time, a near-octave ultra-broadband grating for pulse stretching and compression of WNOPCPA has been successfully developed [4].

To focus almost all the energy of a single-cycle exawatt-class laser into a single-wavelength focal spot, a two-step focusing method with the combination of a parabola and a hyperbola is introduced here, and the focal spot size can be reduced from several-wavelength to single-wavelength [5].

In conclusion, the exawatt-class λ^3 ultra-intense ultrashort laser with a 10^{26} W/cm^2 focused intensity is viable in the future as technology improves. In addition, as the pulse decreases and the beam increases, the new problem of complex spatiotemporal coupling distortion will become more and more important, which will affect the achievement of the final goal. Related problems and solutions are also discussed here.

References

1. N. M. Naumova, J. A. Nees, I. V. Sokolov, B. Hou, and G. A. Mourou, Relativistic generation of isolated attosecond pulses in a λ^3 focal volume, *Phys. Rev. Lett*., 92(6), 063902 (2004).
2. Y. Wu, L. Ji, and R. Li, On the upper limit of laser intensity attainable in nonideal vacuum, *Photonics Res*., 9(4), 541–547 (2021).
3. Z. Li, Y. Kato, and J. Kawanaka, Simulating an ultra-broadband concept for Exawatt-class lasers, *Sci. Rep*., 11(1), 151 (2021).
4. Y. Han, Z. Li, Y. Zhang, F. Kong, H. Cao, Y. Jin, Y. Leng, R. Li, and J. Shao, 400nmultra-broadband gratings for near-single-cycle 100 Petawatt lasers, *Nat. Commun*., 14(1), 3632 (2023).
5. Z. Li, Y. Liu, X. Guo, Y. Leng, and R. Li, Single-wavelength size focusing of ultra-intenseultrashort lasers with rotational hyperbolic mirrors, *Adv. Photonics Nexus*, 3(3) 036002 (2024).

Backpropagation: Towards fast, intelligent and high-precision adaptive interferometric measurement of optical freeform surfaces

Qi Lu[1,3] and **Shijie Liu**[2,3]

[1] Precision Optical Manufacturing and Testing Center, Shanghai Institute of Optics and Fine Mechanics, Chinese Academy of Sciences, Shanghai, China, luqi@siom.ac.cn
[2] Precision Optical Manufacturing and Testing Center, Shanghai Institute of Optics and Fine Mechanics, Chinese Academy of Sciences, Shanghai, China, shijieliu@siom.ac.cn
[3] China-Russian Belt and Road Joint Laboratory on Laser Science, Shanghai Institute of Optics and Fine Mechanics, Chinese Academy of Sciences, Shanghai, China

Complex surfaces are increasingly pivotal across various disciplines, and the rapid, precise measurement of their surface profile is paramount for these fields' progression. Traditional high-precision interferometric methods, reliant on static "one-to-one" null compensators, are constrained by limited dynamic ranges, rendering them inadequate for the testing requirements in the fabrication of complex surfaces. Consequently, there is continuous exploration among researchers to advance adaptive wavefront interferometry (AWI), utilizing dynamic compensators to broaden the compensation testing methods' dynamic range. Nonetheless, AWI's evolution is impeded by challenges including the laborious optimization process, the absence of mathematical models, and limitations in generalizability and susceptibility to local optima, all of which hinder the enhancement of complex surface measurement efficiency. Hence, the advancement of more efficient and versatile adaptive interferometry techniques and apparatuses holds significant scientific importance in enhancing the efficiency, success rates, and universality of adaptive wavefront interferometric measurement of complex surfaces. To promote the development of AWI, this study presents deterministic adaptive wavefront interferometry (DAWI) based on the backpropagation (BP) theory, and a null test is accomplished in only tens of iterations, which is nearly an order of magnitude lower than the reported number of iterations via the existing AWI methods. The DAWI furnishes robust technical backing and assurance for the production and evaluation of optical complex surfaces in national major scientific research and other cutting-edge programs, offering tangible practical utility.

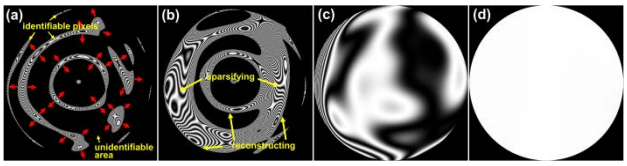

Fig. 1. Four different states of interference fringes in DAWI: (a) initial interference fringes, (b) simultaneous fringe reconstruction and sparsification, (c) fringe reconstruction is completed and the fringes are highly sparse and (d) null test is achieved

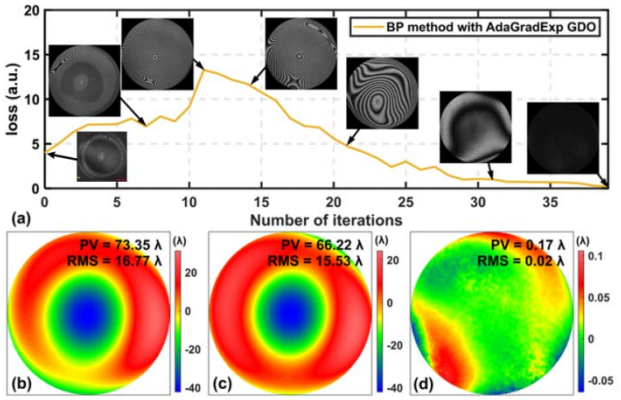

Fig. 2. Measurement result: (a) iterative process, (b) compensation wavefront, (c) the surface profile error of the freeform surface under test, and (d) relative measurement error PV (peak-to-valley) <λ/4

High resolution X-ray imaging of microscale plasma hydrodynamics phenomena with XFEL probe: advantages and limits at modern facilities

S. S. Makarov

Joint Institute of High Temperatures, Russian Academy of Sciences, Moscow, Russia,
seomakarov28@gmail.com

X-ray radiography is a crucial imaging technique in a wide range of High Energy Density (HED) experiments including laboratory astrophysics and inertial confinement fusion research. It makes it possible to obtain the 2D density distribution over the entire volume of the objects and to study the temporal evolution of ultra-fast evolving hydrodynamic phenomena such as laser-induced shock waves or plasma jets, blast waves or hydrodynamic instabilities, which are often opaque to visible light.

The simplest and most widely used probe irradiation is an X-ray source based on laser plasma. The typical resolution achieved today is on the order of 10 μm spatial and ~ ps temporal. It should be emphasised that absorption and phase contrast methods based on an X-ray laser plasma source provide a relative low image contrast, which is often not sufficient to clearly resolve the hydrodynamic phenomena. Since the X-ray image depends on the brightness, monochromaticity and coherence of the illumination source, the images from laser-plasma sources are blurred.

A new opportunity, perhaps even a new era in imaging diagnostics in the field of HED physics was opened with the advent of Free Electron Lasers (FELs). In 2009, at FLASH the first step made to perform Phase Contrast Imaging (PCI) radiography in the soft X-ray spectral range at a photon energy of 155 eV [1]. However, real progress in the development of radiographic methods is associated with hard X-ray FEL.

XFELs create a unique opportunity for decisive advances in the study of extreme hydrodynamic phenomena in plasmas by implementing a coherent phase-contrast radiography approach. Firstly, the femtosecond duration of the XFEL probe pulses provides high temporal resolution, far beyond the usual nanosecond timescale of plasma hydrodynamics. In addition, the extremely narrow spectral bandwidth, the high coherence and the extreme brightness of the source enable high-contrast diffraction-enhanced imaging of objects with low density gradients.

Currently, there are three XFEL facilities (LCLS – USA, SACLA – Japan, EuXFEL – Germany) on which HED stations are operated. Each instrument is capable of simultaneously delivering an X-ray pulse and optical pulses of nanosecond and femtosecond duration into the target chamber.

The combination of an XFEL beam (with probe photons of several keV) with the powerful optical lasers in a laboratory pump-probe experiment opens up enormous possibilities for solving problems in laboratory astrophysics, condensed matter physics, laser nuclear fusion and other fields.

Here we discuss in detail the capabilities and limitations of ultra-high-resolution phase-contrast radiography with XFEL pulse to study fast flow hydrodynamic phenomena in laboratory experiments with laser-plasma [2, 3]. An overview of recent striking studies of laser induced Rayleigh-Taylor instabilities and elastic-plastic shock waves in nanosecond laser plasmas is presented [4–6], taking advantage of X-ray lasers.

This is particularly relevant in the context of the construction of the “mega-science” class facility “SyLa” (Synchrotron and Laser) in the Russian Federation, which includes an accelerator-storage complex with a 4th generation synchrotron source and XFEL. The expected parameters and structure of the complex are described in detail in a recent article [7]. It is important to point out that the project will develop an experimental station at XFEL dedicated to the study of Matter in Extreme States (MEC) generated with high-intensity optical laser radiation of ns-sub/ps duration. Complex investigations of laser plasma performed in such experiments require the development of suitable X-ray diagnostic techniques.

Acknowledgements. The work was carried out within the framework of the Program 10 “Experimental laboratory astrophysics and geophysics of the National Center for Physics and Mathematics”.

References

1. A. Rosenhahn, F. Staier, Th. Nisius et al., Digital In-line Holography with femtosecond VUV radiation provided by the free-electron laser FLASH. *Opt. Expess.* **17**, 2009, 8220.
2. S. S. Makarov, S. A. Pikuz, Possibilities of the Phase-Contrast X-Ray Method in a Laboratory Astrophysical Experiment on the Study of Plasma Instabilities. *Astron. Rep.* **67**, 2023, 61–70.
3. A. Y. Faenov, T.A. Pikuz, P. Mabey et al., Advanced high resolution x-ray diagnostic for HEDP experiments. *Sci Rep* **8**, 2018, 16407.
4. G. Rigon, B. Albertazzi, T. Pikuz et al., Micron-scale phenomena observed in a turbulent laser-produced plasma. *Nat Commun* **12**, 2021, 2679.
5. S. Makarov, S. Dyachkov, T. Pikuz et al., Direct imaging of shock wave splitting in diamond at Mbar pressure. *Matter Radiat. Extrem.* **8**, 2023, 066601.
6. K. Katagiri, T. Pikuz, L. Fang et al., Transonic dislocation propagation in diamond. *Science* **382**, 2023, pp. 69–72.
7. M. V. Kovalchuk, A. E. Blagov, O. S. Naraikin et al., Fourth-Generation Synchrotron Radiation Source with X-ray Free-Electron Laser SILA: Concept of Accelerator–Storage Complex. *Crystallogr. Rep*. **67**, 2022, 676–683.

Enhanced Z-scan technique for cubic and quintic nonlinearity measurement

M. Martyanov, A. Poteomkin, I. Kuzmin and **S. Mironov**

A.V. Gaponov-Grekhov Institute of Applied Physics of the Russian Academy of Sciences, Nizhny Novgorod, Russia,
mmartyan@ipfran.ru

All optical materials exposed to high enough optical intensity exhibit cubic nonlinearity, which in the simplest case of instant Kerr nonlinearity is manifested by the refractive index n dependence of the intensity as $n = n_0 + n_2 I$, where I is the optical intensity, n_0 is the refractive index at vanishing intensity, and n_2 is the cubic nonlinear coefficient. Cubic nonlinearity, even in its simplest form, is responsible for various effects such as beam self-focusing, pulse modulation instability, self-phase modulation and spectral broadening, Kerr lens mode-locking, etc. Proper experimental determination of n_2 is particularly important for applications where cubic nonlinearity is used intentionally and other parameters of the setup directly depend on the magnitude of n_2. The nonlinear post-compression technique is a good example where the dispersion of dedicated chirp mirrors strictly depends on the pulse energy and n_2 of the employed material.

Cubic nonlinearity is a consistent approximation for the intensity roughly below 1 TW/cm^2. At higher intensities, which become readily achievable with modern laser technology, higher order nonlinear terms or other nonlinearity saturation effects should be considered. The quintic nonlinearity term is the most straightforward extension to the refractive index Taylor expansion $n = n_0 + + n_2 I + n_4 I^2$, where n_4 is the quintic nonlinear coefficient. Of course, there could be other effects that would affect the refractive index dependence on the intensity, e.g. finite response time (like the Raman effect), ionization, etc. Currently, debates are ongoing concerning the magnitude and sign of n_4. In [1] for fused silica the following values $n_2 \approx 3.2 \cdot 10^{-4}$ cm^2/TW and $n_4 \approx -4.4 \times \times 10^{-4}$ cm^4/TW^2 were considered. The negative value of n_4 means that for some characteristic intensity $I^* = -n_2 / n_4 = 0.73$ TW/cm^2 the cubic and quantic terms cancel each other out. For instance, this "cancelation" would dramatically change the performance of post-compression or even provide self-compression of high-power laser pulse. Therefore, the correct measurement of the magnitudes and signs of $n_{2,4}$ is very important for practical reasons.

There are several techniques to measure the nonlinear properties of optical materials. Some of them are capable of providing only relative data with respect to a known sample (usually fused silica). Other methods deliver absolute value of n_2 and the Z-scan technique in particular is the most popular one due to its simplicity and robustness.

We proposed an improved Z-scan method with the layout presented in Fig. 1, which, apart from some minor technical improvements, provides factor three better sensitivity with respect to conventional technique. The major improvement is related to a different optical layout, i.e. the image relay of the fixed plain in the vicinity of the focal waist, while the sample is scanning through the entire waist. The sensitivity improvement was easily confirmed theoretically in the model of a Gaussian beam, where the nonlinearity provides only a phase shift in a thin sample plate as:

$$U(t,z,\boldsymbol{r}) = U_0(t,z,\boldsymbol{r}) \cdot \exp(iBI(t,z,\boldsymbol{r})/I_{peak}(z)), \quad (1)$$

where $B = k_0 L n_2 I_{peak}$ is the so-called B-integral, L is the sample length, I_{peak} is the beam peak intensity.

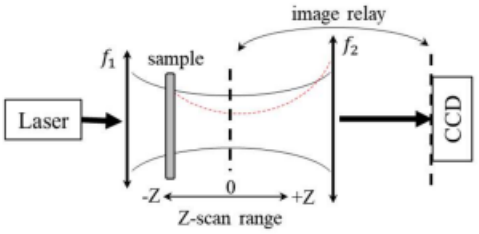

Fig. 1. Z-scan setup layout

The Z-scan signal is the time-integrated peak fluence of the beam detected by the CCD sensor. The typical scan signal is shown in Fig. 2. When the sample is far away from the focal waist from either side, the beam shape and thus the detected peak intensity is the same as in the linear case (the normalized signal is equal to one in Fig. 2). When the thin sample is exactly at the image plain (z=0 in Fig. 2), the normalized signal is also equal to one since the acquired nonlinear phase does not affect the image in this case.

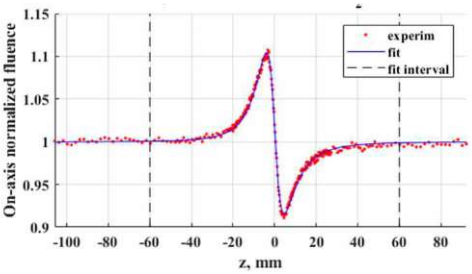

Fig. 2. Typical z-scan raw data and model fit, B=0.22

With this technique, the samples of fused silica, KDP, DKDP crystals, PET films, and others were measured at different intensities ranging from 10 GW/cm^2 to 0.5 TW/cm^2. The measurements were performed for different sample lengths and at different wavelengths (fundamental and second harmonic of Yb:KGW laser). For fused silica, the cubic nonlinear coefficient was measured to be $n_2 = 1.7 \cdot 10^{-4}$ and $2.7 \cdot 10^{-4}$ cm^2/TW at 1030 and 515 nm respectively. No reliable hint of n_4 was detected in the available intensity range.

Acknowledgements. The research was supported by the Ministry of Science and Higher Education of the Russian Federation (Project No. FFUF-2023-0001).

References

1. R. Chen, W. Liang, Y. Xu, X. Shen, P. Wang, J. Liu, R. Li, Self-Compression of Ultrahigh-Peak-Power Lasers. *Laser Photonics Rev.*, 2024, 2301000.

State of the art and future trends in post-compression of high-power laser pulses

S. Yu. Mironov, **V. N. Ginzburg, I. V. Yakovlev, V. V. Lozhkarev, A. A. Shaykin** and **E. A. Khazanov**

A.V. Gaponov-Grekhov Institute of Applied Physics of the Russian Academy of Sciences, Nizhny Novgorod, Russia

Nowadays, the only approach to multiplying the peak power of petawatt laser pulses is the post-compression method, which is implemented directly after the optical compressor. The method relies on the use of thin (~1 mm) plane-parallel transparent dielectric plates for broadening the spectrum and subsequent correction of the spectrum phase due to pulse reflection from the surface of dispersive mirrors.

In experiments with the use of fused silica plates and dispersive mirrors, the pulse duration was reduced from 60–70 fs to 11 fs, which enabled achieving a peak power of ~1.5 PW on the PEARL laser facility [1]. The post-compression method can be applied to laser pulses with high (~1kJ) energy and sub-picosecond pulse duration. Such pulses can be obtained at the output of Nd:glass lasers. The pulse duration limit after pulse shortening is a single oscillation cycle of the optical field. Post-compression is therefore a way of obtaining laser pulses with peak PW power and extremely short duration. The radiation is highly desirable for light-matter and light-vacuum interaction experiments.

The most promising direction for the development of the post-compression method is to combine it with other nonlinear processes, such as SHG (Second Harmonic Generation) and XPW (Cross-Polarized Wave Generation). When the second harmonic is generated under the conditions of cubic nonlinearity, pulse spectrum broadening at doubled frequency occurs directly in a frequency doubler crystal. The use of dispersive mirrors makes it possible to obtain pulses at the doubled frequency with a peak power higher than at the fundamental harmonic. The prospects for this approach are associated with peak power enhancement, improved temporal contrast and, in case of optimal focusing, double reduction of spot size [2]. The combination of these factors will allow improving laser radiation parameters, which is essential for conducting experiments on the extreme light–matter interaction. It should be noted that combination of second harmonic generation and post-compression technique can be also applied to powerful laser pulses with sub-picosecond pulse duration.

At the same time, the post-compression method used in conjunction with SHG implies solution of a number of problems, including those of a technological nature. We propose a method of producing composite nonlinear samples for second harmonic generation by laser beams with a peak intensity of ~TW/cm^2 and demonstrate for the first time second harmonic generation with subsequent time compression of the pulse using dispersive mirrors with anomalous group velocity dispersion.

A proof-of-principle experiments of highly efficient (38%) second harmonic generation was implemented at a ~1 TW/cm^2 intensity of a 45-fs pulse in a composite nonlinear sample – a 1-mm KDP crystal glued onto a 1-mm fused silica substrate. The attenuated replica of second harmonic pulse (455 nm) was compressed down to 28.6 fs by means of dispersive mirrors, with a significant reduction in both the wings and the far temporal contrast. The peak power of the second harmonic was ~74% of the power of the fundamental harmonic, which ensured a three-fold increase in the focal intensity.

The dependence of the duration of the second harmonic pulse ACF on the parameter of the correcting quadratic phase is presented in Fig. 1 (dots – experimental data, solid curve – simulation). Note that without dispersive mirrors the pulse duration at the second harmonic is significantly longer than at the first one (45 fs). With an increase in the modulus of the correcting quadratic phase, the second harmonic pulse compresses.

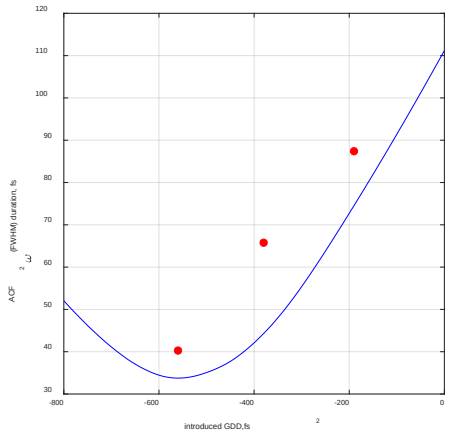

Fig. 1. Second harmonic ACF duration versus correcting quadratic phase parameter: experiment (dots); numerical simulation (solid curve)

The second harmonic post-compression time approach is a very promising way of generating visible, powerful pulses with high quality parameters.

Acknowledgements. The research was supported financially by the Ministry of Science and Higher Education of the Russian Federation (agreement No. 075-15-2021-1361).

References

1. V. Ginzburg, I. Yakovlev, A. Kochetkov, A. Kuzmin, S. Mironov, I. Shaikin, A. Shaykin, and E. Khazanov, *Opt. Express*, 29(18), 28297 (2021).
2. S. Yu. Mironov and E. A. Khazanov, Post-compression of a second harmonic pulse: a way to increase the peak power and temporal contrast of ultrahigh-power laser pulses, *Phys. Usp*., 67(01), 99–103 (2023).

Stimulated emission in HgCdTe-based quantum wells: toward continuous wave and low threshold lasing in THz range

S. V. Morozov

Institute for Physics of Microstructures of RAS, Nizhny Novgorod, Russia, more2009@yandex.ru

Hg(Cd)Te/CdHgTe heterostructures with quantum wells (QW) are an attractive a material for mid infrared (IR) lasers. Due to importance of HgCdTe-based heterostructures for the industry of IR detectors their quality is reaching the quality of A3B5 heterostructures. Hg(Cd)Te/CdHgTe QWs also provide a unique opportunity to change the bandgap from 0 to over 1200 meV, while maintaining the ability to tailor the energy spectrum of the carriers by changing the content of solid solution of the barriers and the QW. In the long-wavelength part of mid Hg(Cd)Te/CdHgTe QWs offer the quasi-relativistic dispersion law of the carriers which suppresses Auger recombination, enabling stimulated emission (SE) up to 31 μm, and laser generation up to 24 μm in the temperature range from 10 to 80 K [1, 2]. The wavelength of emission, which is demonstrated in our experiments, is six times larger than the previous results for HgCdTe lasers [3, 4]. The record wavelength of 31 μm (inaccessible for existing cascade lasers) was achieved by a peculiar design of the structure utilizing the reflection of the waveguide mode from the substrate near the Reststrahlen band of GaAs. Quasi-relativistic dispersion law of the carriers in HgTe/CdHgTe QWs is useful at even longer wavelengths, in terahertz range, where we have recently managed to experimentally demonstrate "Landau emission" (optical transitions between non-equidistant Landau levels formed when quasi-relativistic electron system is placed in magnetic field) between 1 and 3 THz with the frequency adjustable by magnetic field and carrier concentration [5]. These results open up an avenue for a new type of terahertz Landau lasers controlled by magnetic field and gate voltage.

In this work, by carefully optimizing the waveguides and mitigating carrier heating, we achieve stimulated emission at 14–24 μm in HgCdTe QWs under optical pumping in quasi-continious wave regime (pulse duration 20–500 μs). The intensity is as low as 1.5–2 W/cm^2 [6]. The impact of AR happening right after the excitation on the carrier temperature is investigated both theoretically (using the balance equations and calculated AR rates) and experimentally (via PL spectrum analysis). When such "hot" AR is eliminated due to long-wavelength pumping carrier lifetimes are shown to be only slightly limited by Shockley-Read-Hall recombination. Its contribution is also directly investigated via time resolved measurements of the photoconductivity decay and PL spectroscopy of trap states in the bandgap. Finally, we estimate that implementing microdisc cavities would allow continuous-wave operation of HgCdTe lasers in the very long-wavelength infrared range (14–30 μm) and beyond when pumped by last generation quantum cascade lasers.

Fig. 1 presents the emission spectra of studied samples for different wavelengths of excitation. In theory, the photoluminescence (PL) spectrum of a QW should follow a step-like 2D density of states near the edge of the interband transitions. Therefore, the low-energy slope of the PL line reflects the inhomogeneous broadening of the sample by having a finite steepness of W > 2 meV (consider structure #i10_14, for example). At lattice temperature of 9 K, kT energy of 0.8 meV is considerably lower, and the minimal full width at half maximum (FWHM) of the PL line one could expect is 2 W = 4 meV. Instead, the FWHM of the emission line at 10.6 pumping is much less: a line with the FWHM as low as 0.75 meV is observed in structure #i10_14. Dramatic narrowing of the emission line suggests that SE process is taking place, which is further supported by structure #i15_24. In this case, the low-energy slope is much wider, yet the FWHM of the emission line at 10.6-um-pumping conserves at 0.5 meV from 8 K to 19 K, suddenly broadening at 20 K and then disappearing completely at higher temperatures.

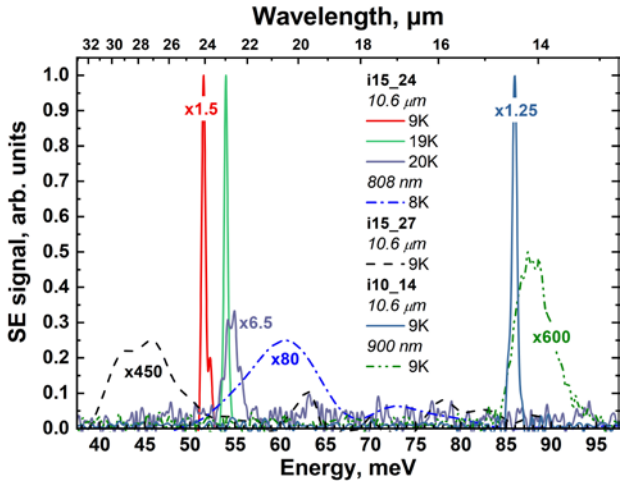

Fig. 1. The emission spectra for structures under study. The labels show the factors by which the curves were multiplied to have the presented amplitude

Acknowledgements. This work was supported by Russian Science Foundation project # 22-12-00310.

References

1. S. V. Morozov et al., ACS Photonics, Vol. 8, No. 12, 3526–3535, 2021.
2. V. V. Rumyantsev et al., Appl. Phys. Lett., Vol. 121, No. 18, 182103, 2022
3. J. M. Arias et al., Semicond. Sci. Technol., Vol. 8, S255–5260, 1993.
4. E. Hadji et al., Appl. Phys. Lett., Vol. 67, 2591, 1995.
5. S. Gebert et al., Nat. Photon., Vol. 17, 244–249, 2023.
6. V. V. Rumyantsev et al., Appl. Phys. Lett. 124, 161111 (2024).

Temporal shaping of narrowband saturately amplified nanosecond pulses

I. B. Mukhin, M. A. Martyanov, S. Yu. Mironov, A. A. Soloviev, I. V. Kuzmin, A. A. Kuzmin, I. A. Samsonov

A.V. Gaponov-Grekhov Institute of Applied Physics of the Russian Academy of Sciences, Nizhny Novgorod, Russia, ivan.mukhin@ipfran.ru

The precise controlling of an envelope of laser pulses is one of topic tasks in high energy lasers. The pulse duration tuning is an advantage in a lot of application from drilling and surface modification to optimization of EUV sources. Temporal pulse shaping is an important feature for improving of such nonlinear processes as second harmonic generation and parametric amplification. Fast electro-optical shutters are usually using for this task, which on the subnanosecond time scale becomes very challenging due to limited bandwidth of electronics. Another approach of spectrally-temporal ns pulse shaping with takin to account its saturated amplification has been investigated in this work.

Lasing with few ns pulses (and longer) is a routine in Q-switched lasers. But, the stretching of a pulse of mode-locked laser is more preferred way in the case of ns pulse and shorter. Additionally this approach allows optically synchronize ns lasers with other laser sources. Note, the spectrum bandwidth of the pulse is usually limited by 1 nm during amplification in Nd or Yb lasing media of high energy amplifiers. An optical layout of a compact pulse shaper for strongly chirped laser pulses of sub- nanosecond time scale exploiting a tilted angle placed chirped volume Bragg grating (CVBG) and a programmable spatial light modulator (SLM) was proposed and investigated (Fig. 1) [1]. A tilted placed CVBG forms not only temporal chirp but a spatial chirp too and SLM controlling the amplitude of the spectral components. Additionally, the pulse is stretched to suitable pulse duration. A feasibility of spectral shaping with a resolution of 0.16 nm, corresponding to the time resolution of 150 ps, and a contrast ratio of 10^2 was demonstrated experimentally. This pulse shaper has been implemented in the frontend of PEARL petawatt laser facility [2] to preshape the seed pulse and obtain Π-shaped pump pulses from Nd:glass amplifier (Fig. 2) during saturated amplification. The pump pulses has been amplified up to 250 J with spectrum bandwidth near 0.5 nm. As authors know, it is the first experimental demonstration of temporal shaping of high energy pulse with near 1 ns pulse duration.

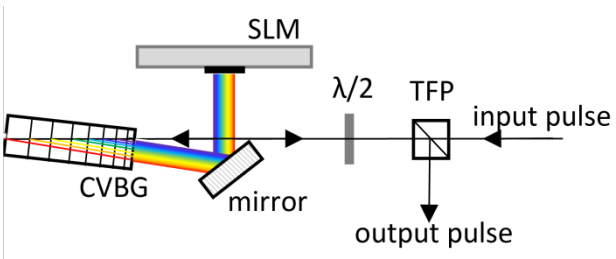

Fig. 1. Optical layout of spectral-temporal pulse shaper. TFP – thin film polarizer, CVBG – chirped volume Bragg grating, SLM – spatial light modulator, SM – scanning spectrometer

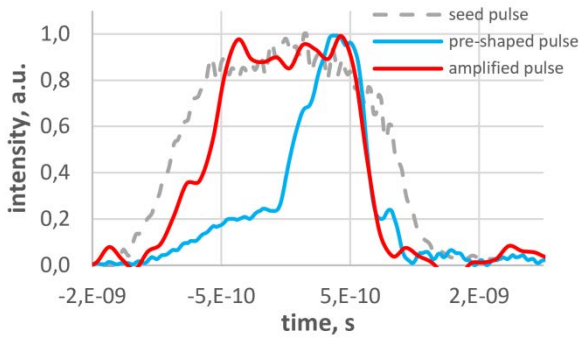

Fig. 2. Envelopes of seed (grey) pre-shaped (blue) and amplified (red) pump pulses of PEARL petawatt laser facility

The saturated amplification in high energy lasers leads to large distortions of temporal profile and the contrast ratio of spectrally-temporal pulse shaping approach may be not enough to its correct preshaping. A saturated amplification of chirped pulses on the wing of emission cross section has been proposed to suppress temporal distortions of the pulse. In this case, compensation for gain saturation occurs due to an increase in the emission cross section at the wavelength on the end of chirped pulse. The absence of chirped pulse temporal distortion has been experimentally observed during saturated amplification in Nd:YLF with output energy range from 0.1 to 1.2 of saturation energy. This method in combination with temporal pulse shaper allows precise tuning the pulse envelope in high gain laser amplifiers.

Some laser media are not sufficient for amplification of chirped pulses because of too narrowband emission cross section (Nd:YAG as an example). This specificity complicates an optical synchronization of Nd:YAG ns laser with other laser sources. The placing of compact pulse shaper into regenerative amplifier gas been proposed to achieve very high dispersion during regenerative amplification. This approach has been experimentally verified and the stretching to ~ 2 ns of 0.05 nm in bandwidth pulses has been demonstrated. The tuning of number of pulse propagation though a regenerative amplifier allowed precise tuning the pulse duration in range of 1.6 to 2.2 ns.

Note, the methods described in this work are suitable not only for ns pulses but for ps pulse duration range too.

Acknowledgements. The research was supported by the State Research Task for the Institute of Applied Physics, Russian Academy of Sciences (Project No. FFUF-2024-0043).

References

1. M. Martyanov, I. Mukhin et al., *Opt. Lett.* 2022, **47**, 557–560.
2. I. Mukhin, K. A. Glushkov et al., *Appl. Opt.* 2023, **62**, 2554–2559.

THz radiation in a nonlinear waveguides

A. S. Nikoghosyan and **V. R. Tadevosyan**

Yerevan State University, 0025 Yerevan, Armenia, nika@ysu.am

Nowadays, optical rectification of femtosecond laser pulses is one of the most promising methods for generation of high-energy THz pulses. A broadband THz pulse was generated in a nonlinear crystal partially filling the cross-section of a rectangular metal waveguide due to the nonlinear frequency conversion of 100 fs Ti Sapphire laser pulses, Fig. 1(a). The thickness of the crystal – t, which ensures the synchronism of the interaction of optical and terahertz pulses, was determined numerically from the transcendental dispersion equation [1, 2]. The generation of a THz pulse was studied in waveguides with cross sections from 23×10 cm^2 to 1.8×0.9 cm^2. Studies of the propagation of a THz pulse in an empty waveguide with a cross-section of 250×125 μm^2, over the frequency band from 0.65 to 3.5 THz, are given in [3].

In this work, the mode composition of a broadband THz pulse, in the frequency band 0.1–3.5 THz (as a linear superposition of coupled propagating modes), in a nonlinear $LiNbO_3$ plate located in the middle of a waveguide parallel metallic plates is investigated. Distribution of the amplitude of the electric field component E_y along the x-axis was determined numerically using the expression obtained from the Helmholtz equations for the TE_{10} mode of the parallel-plate dielectric waveguide, taking into account the boundary conditions (at $-b/2 < y < b/2$) [4]. In Fig. 1(b) $\varepsilon_0 = 1$ is the relative value of the dielectric permittivity of free space and ε_r of the $LiNbO_3$ crystal ($\varepsilon_r = 28$). Distribution of the normalized electric field component E_y of the THz pulse in the "xy" plane of a parallel-plate nonlinear waveguide (PPNW) is shown in Fig. 2, when a = 1.8 mm, b = t = 70 μm (c, d) and t = 270 μm (e, f).

The results of the numerical analysis show that the mode composition of a THz pulse generated in a waveguide partially filled with a nonlinear crystal improves if we move to a waveguide configuration with parallel plates and a thin nonlinear crystal between them (i.e. if two side boundaries are removed), Fig. 1(b). In PPNW, most of the spectral components of broadband THz radiation (0.1–1.2 THz at t = 70 μm and 0.1 = 0.3 THz at t = = 270 μm) propagate as the fundamental mode TE_1. The propagation of the spectral components of the THz pulse in the form of the fundamental mode leads to the suppression of mode dispersion and the undistorted propagation of the THz pulse, as well as to the smoothness of the THz spectrum envelope. The similarity between rectangular waveguide and PPNW lies in the fact that the main energy of the THz pulse propagates inside the crystal and decays outside it the faster, the higher the frequency of the spectral component of the THz pulse. The attenuation of the amplitude of a given frequency outside the crystal is greater in PPNW.

Thus, by using PPNW it is possible to overcome the difficulty of transmitting a wide band of the THz spectrum in the form of a single mode by choosing the size and polarization of the laser beam, the thickness of the nonlinear crystal, and its dielectric susceptibility. The PPNW design allows the use of thinner waveguides, which is desirable for THz integrated circuit applications.

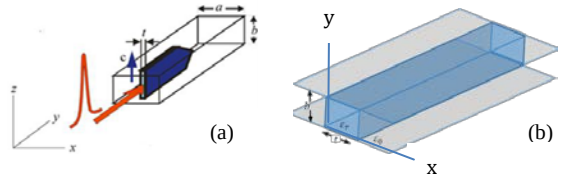

Fig. 1. Nonlinear $LiNbO_3$ crystal partially filling a rectangular waveguide (a) and a waveguide with parallel metal plates (b)

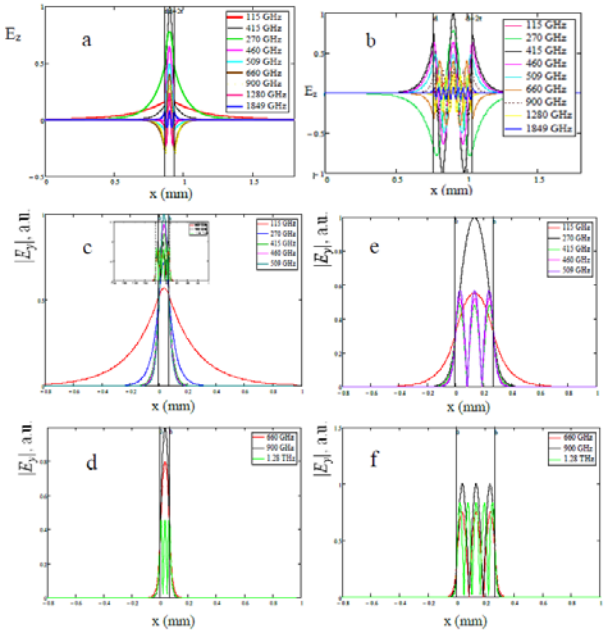

Fig. 2. Distribution of the normalized electric field component E_z of the THz pulse in the "xz" plane of a rectangular waveguide (axb = 1.8×0.9 mm^2) with a $LiNbO_3$ crystal at t = 70 μm (a) and t = 270 μm (b). Distribution of the normalized component of the electric field modulus E_y of the THz pulse in the PPDW "xy" plane at t = 70 μm (c, d) and t = 270 μm (e, f)

Acknowledgements. We thank the Committee of Higher Education and Science of Armenia for the financial support of the scientific work of the YSU Submillimeter Wave Laboratory.

References

1. A. S. Nikoghosyan, *Quantum Electronic*, Moscow, 1988, **15**, 969–971.
2. A. S. Nikoghosyan, R. M. Martirosyan, A. A. Hakhoumian, J. M. Chamberlain, R. A Dudley, N. N. Zinov'ev, *Inter. Journal Electromagnetic Waves and Electronic System*, 2006, 11(4), 47–55.
3. G. Gallot, S. P. Jamison, R. W. McGowan, and D. Grischkowsky, *J. Opt. Soc. Am. B*, 2000, **17**(5), 851–861.
4. Longfang Ye, Ruimin Xu, Zhihui Wang and Weigan Lin, *OPTICS EXPRESS*, 2010, **18** (21), 21725–21731.
5. A. S. Nikoghosyan, V. R. Tadevosyan, G. N. Goltsman and S. V. Antipov. *ICOEO-2022 Journal of Physics*: Conference Series 012013, IOP Publishing 2023, 2548, 1–8.

Laser wave scattering from plasma as a way of bulk material self-organization under the intense femtosecond laser pulse exposure

A. V. Bogatskaya[1,2], E. A. Volkova[3] and A. M. Popov[1,2]

[1] Lebedev Physical Institute, RAS, Moscow, Russia
[2] Faculty of Physics, Moscow State University, Moscow, Russia
[3] Skobeltsyn Institute of Nuclear Physics, Moscow State University, Moscow, Russia

Here we propose new mechanism of plasma self-organization in solid dielectrics exposed to intense laser radiation in the regime of tight focusing which causes the generation of 3D periodic ring structures with subwavelength period both along the laser pulse propagation and in the radial (perpendicular) direction. The basic idea is to form a dense plasma burst in the prefocal region, which provides efficient scattering of the incident wave. The interference of a plane incident laser wave and a divergent scattered one will form the standing wave with local minima and maxima both along the incident wave propagation and perpendicular to it producing the ring patterns of effective ionization regions. We analytically and numerically consider the process of laser wave scattering on a near-spherical plasma object with dimensions both smaller and larger than the wavelength of laser radiation, which will allow us to demonstrate the key relationships of the periodicity formation on the characteristics of prefocal plasma.

In analytics we consider the plasma object with radius a, which is smaller than the radiation wavelength λ in material and the skin layer depth in plasma, as a dipole emitter placed in external linearly polarized field with the amplitude $\vec{E}_0$ (see Fig. 1). The components of the scattered field along the vector $\vec{E}_0$ and perpendicular to it be written as [1]:

$$\begin{Bmatrix} E_s^{\parallel}(\vec{r},t) \\ E_s^{\perp}(\vec{r},t) \end{Bmatrix} = \frac{1}{c^2 r}\omega^2 a^3 \frac{\varepsilon-1}{\varepsilon+2} E_0 \exp\big(i(kr-\omega t)\big) \times \\ \times \cos\theta \times \begin{Bmatrix} -\cos\theta \\ \sin\theta \end{Bmatrix}, \quad (1)$$

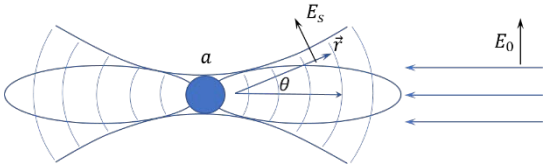

Fig. 1. The schematic picture of plasma dipole scattering

where $\varepsilon = \frac{\varepsilon_p}{\varepsilon_d}$, ε_p is the permittivity of plasma object, ε_d is the permittivity of dielectric. To obtain the interference pattern of the incident and scattered fields we use the following expression of the focused Gaussian laser beam propagating along z-axis [2]:

$$E_i(\rho,z,t) = E_0 \times \exp\left(-\frac{1}{2}\left(\frac{\rho}{\mathcal{R}(z)}\right)^2 - ikz - \frac{ik\rho^2}{2R_c(z)} - \right. \\ \left. -i\mathrm{Arctan}\big(z/z_f\big)\right) \exp(-i\omega t)\, \rho_0/\mathcal{R}(z) \exp\left(-\frac{1}{2}\left(\frac{z}{b}\right)^2\right) \quad (2)$$

where z_f is the Rayleigh length, ρ_0 is beam waist radius, $\mathcal{R}(z)$ is the beam radius, $R_c(z)$ is the radius of front curvature, b is the pulse HWHM. Since interference is possible between waves of the same polarization, for the sought amplitude of the incident and scattered fields we use the component of the scattered field (1) co-directed with the incident laser wave (Fig. 2):

$$E_{int}(\rho,z) = \left|\mathrm{Re}\Big(E_i(\rho,z,t=t_0) + E_s^{\parallel}(\rho,z,t=t_0)\Big)\right|. \quad (3)$$

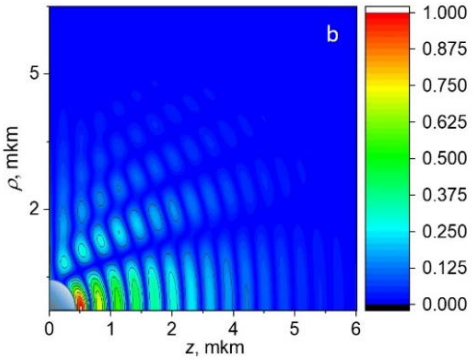

Fig. 2. Normalized distribution of $E_{int}(\rho,z)$ for the plasma object with $n_e = 10^{21}$, $a = 0.5\lambda_0$ The value of focal radius is $\rho_0 = 2.5$ mkm. Area of the spherical plasma object at the origin is indicated by a circular sector

We believe that the formation of such field interference patterns within the discussed mechanism stands as the initial stage of laser microstructuring process and gives rise to a rather complex nonlinear process of laser-plasma interaction leading to the formation of a subwavelength plasma gratings. We would like to stress that the essential point of the proposed mechanism is the extremely sharp dependence of the ionization probability versus electric field strength of the laser pulse. As a result, the set of plasma seeds appears that leads to further self-organization of wave field and plasma structures.

Acknowledgements. The work was supported by the Russian Science Foundation (project no. 22-72-10076).

References

1. L. D. Landau and E. M. Lifshitz, *Electrodynamics of Continuous Media*, 2nd ed., Pergamon Press, Oxford, UK, 1985.
2. R. Herman, J. Pardo, and T. Wiggins, *Appl. Opt.*, 1985, **24**(9), 1346–1354.

Acceleration of particles from targets with controlled preplasm

M. A. Rakitina[1], **A. V. Brantov**[1] and **S. I. Glazyrin**[2]

[1] Lebedev Physical Institute of the Russian Academy of Sciences, Moscow, Russia
[2] Dukhov Research Institute of Automatics (VNIIA), Moscow, Russia

Compact sources of high-energy particles and secondary radiation based on the interaction of high-power laser pulses with plasma targets are of interest due to the possibility of their application in a wide range of practical tasks. One of the ways to optimize such sources is related to the possibility of controlling the plasma of a solid-state target by changing the density gradient of the scattering plasma on the irradiated side [1, 2].

We simulated the expansion of the target under the action of a nanosecond laser pulse and obtained density profiles of the preplasm formed on the irradiated side of the target. The simulation was carried out using the hydrodynamic code FRONT [2], which solved a system of two-temperature hydrodynamics, including the equation of continuity and the equation of motion of plasma density, as well as equations for the internal energy of electrons and ions. The calculations were carried out in three-dimensional (cylindrical) geometry.

During the calculations, laser pulses with an intensity from 10^{10} W/cm^2 to 10^{13} W/cm^2 and a duration from 1 to 5 ns were used. Aluminum was considered as the target material.

The preplasm density profile can be roughly represented as the sum of two exponentials, one of which describes the plasma near the target, and the other describes the sub-critical plasma. The resulting function describing the density profile is written as follows:

$$n(x) = n_1 \exp\left[\frac{-(x-x_0)}{d_1}\right] + n_2 \exp\left[\frac{-(x-x_0)}{d_2}\right] \qquad (1)$$

where d_1 and d_2 are the characteristic gradients of the density profile of the scattering plasma, x_0 is the magnitude of the target shift.

Figure 1 shows the density profile obtained by irradiating a target with a laser pulse with intensity I for different time points, the dotted colored lines on the graph display the n(x) function, which well describes the profiles in the regions of low-density and near-critical plasma.

The calculations compared the results of target expansion for targets with a thickness of 6 microns, 10 microns and 30 microns at different laser pulse intensities. The characteristic gradient of plasma density, close to the critical one, is about 0.2–0.3 microns for the minimum density of the invested energy used in the simulation (about 0.3–0.5 kJ/cm^2). As the energy flow increases for all targets, it increases rapidly. It reaches saturation in the region of ~ 0.4 microns at an energy density above 5 kJ/cm^2.

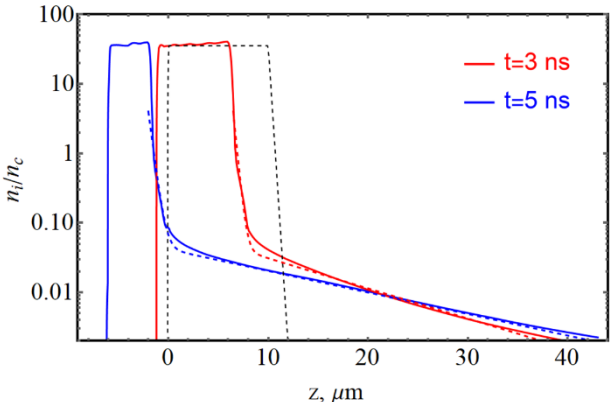

Fig. 1. Density profile obtained during irradiation of a target by a laser pulse with intensity $I = 10^{12}$ W/cm^2

In the low-density plasma region, with increasing energy density, the growth of characteristic gradients slows down somewhat, and the values of the gradients become close to each other and cease to depend on the thickness of the targets. The density gradients of the preplasm in targets with finite and infinite thickness were also compared. According to calculations, in this case, there is also a decrease in the dependence of the gradient value on the thickness of the target as the energy density of the laser pulse increases.

In addition, initially thinner targets are shifted much more strongly. This may need to be taken into account when performing some tasks in which the control of the shear and thickness of the target is important. According to the calculations, a thinner target (6 microns) moves about 2–3 times further than a target of greater thickness (10 microns). Complete burnout (destruction) of a target with a thickness of 6 microns occurs at an energy density of 30 kJ/cm^2, while a target with a thickness of 10 microns is destroyed at an energy density of 100 kJ/cm^2.

The parameters of the characteristic gradients obtained during the calculations will be taken into account in the kinetic code to calculate the optimal density gradient of the plasma during acceleration of charged particles.

The work was carried out with the support of the Russian Science Foundation (Grant No 24-22-00119).

References

1. P. McKenna, D.C. Carroll, O. Lundh et al., Laser and Particle Beams, 2008, **26**(4), 591–596.
2. J. Peebles, M. S. Wei, A. V. Arefiev et al., New J. Phys., 2017, **19**, 023008.
3. S. I. Glazyrin, A. V. Brantov, M. A. Rakitina, V. Yu. Bychenkov, High Energy Density Phys, 2020, **36**, 100824.

Few- and subcycle electromagnetic pulses

N. N. Rosanov

Ioffe Institute, Russia

Recent progress in the generation of short electromagnetic pulses requires theoretical and experimental study of their unusual properties, propagation features and the physics of their interaction with micro-objects. The shortest pulses in a given frequency interval are subcycle and unipolar. In this talk I present the current state of the electrodynamics of such pulses, starting with rigorous Maxwell equations. I also discuss the interaction of few-cycle and unipolar electromagnetic pulses with micro-objects and a number of experiments in this area.

The research is supported by the Russian Science Foundation, grant 23-12-00012.

Twisted high harmonics and attosecond pulses in plasma

S. G. Rykovanov

Skolkovo Institute of Science and Technology, Russia

Angular momentum, encompassing spin-angular momentum (SAM) and orbital angular momentum (OAM), is one of fundamental characteristics of electromagnetic waves. SAM, also known as polarization, and OAM, often referred to as twisted light or vortex light, enable diverse applications from telecommunication multiplexing to the manipulation of macroscopic objects. One can say that generation of light with angular momentum in near infra-red and visible range is currently a routine procedure. High harmonic generation using interaction of intense lasers with gases and plasmas can reach UV region and in this presentation we will discuss the possibilities of generation of UV light with angular momentum. In particular we will explore innovative methods for generating OAM ultraviolet light through the interaction of relativistically intense, short laser pulses with overdense plasma. We will introduce a technique for converting the SAM of a laser driver into the OAM of high-order harmonics generated in plasma. Additionally, we will discuss a new light structure known as “self-torque”, which features dynamically and discretely changing OAM in electromagnetic pulses. Future prospects and experimental approaches will be discussed, highlighting the potential impacts and applications of these advancements.

Electron acceleration with high repetition rate table top lasers

A. B. Savel'ev

Lomonosov Moscow State University, Moscow, Russia

Well collimated electron beams through the interaction of a femtosecond laser pulse of relativistic intensity with subcritical plasma is one of the most actively developing areas at the intersection of laser physics and plasma physics. The most impressive results were obtained using unique laser systems with a peak power from 0.5 to several PW. At the same time, the low pulse repetition rate of such systems determines the low average beam current. In addition, many application areas require not so high electron energies around 10 MeV, but the charge of the electron pulse and the average beam current are important. It is precisely these electron pulses that can be obtained using femtosecond laser complexes with a terawatt peak power level and capable of operating at kilohertz repetition rates.

We present results of computational and experimental studies of several schemes for accelerating electrons with a femtosecond laser pulse with a peak power of 1-2 TW, the possibility of scaling the developed approaches to high powers (tens of TW and PW), as well as the use of these beams for generating secondary radiation in a wide electromagnetic field ranging from terahertz to gamma. In particular, we have obtained electron beams with an energy of up to 15 MeV, a charge of hundreds of picoculombs, and a divergence of about 0.1 rad. Original approaches will be presented that provide effective control of the energy spectrum of the beam at a high repetition rate, generation of quasi-unipolar pulses of terahertz radiation, gamma flares and photonuclear reactions.

2PW OPCPA renewed PEARL facility

A. A. Shaykin, **V. N. Ginzburg, I. V. Yakovlev, A. A. Kuzmin, A. A. Kochetkov, S. Yu. Mironov, I. B. Mukhin, A. A. Soloviev, I. A. Shaikin, S. E. Stukachev, A. I. Pavlikov** and **E. A. Khazanov**

A.V. Gaponov-Grekhov Institute of Applied Physics of the Russian Academy of Sciences, Nizhny Novgorod, Russia, shaykin@ipfran.ru

It was created the most powerful OPCPA laser complex in Russia The laser is the renewed PEARL [1] facility.

The changes affected all parts of laser. In the starting part: the synchronization system, the femtosecond source, the system for generating the temporal and spatial shape of the pump pulse [2]. In the renewed femtosecond chanal pulse duration is 20 fs.

The pump laser of the final parametric amplifier was also updated. The optical amplifiers with the diameters of 20 and 150 mm have been added. And maximum energy at 1 ns @ 1054nm pulse was 400J. A higher gain required the installation of an additional Faraday isolator with an aperture of 60 mm. To reduce polarization distortions, several polarization rotators were used. This made it possible to increase the pulse repetition rate to 1 pulse per 10 min. The use of a quasi-rectangular pulse increased the efficiency of second harmonic generation up to 61% (Fig. 1). Near field of pump beam is shown on Fig. 4(a).

The efficiency of parametric amplification has also increased (Fig. 2). And the signal energy was up to 40 J.

To prevent damage to the compressor gratings, an aberration-free telescope for a broadband signal was developed and manufactured. The increased size of the diffraction gratings makes it possible to compress pulses with an aperture of 200 mm and energy of up to 50 J. Compression efficiency has been increased to 80%. Pulse duration was 34–37 fs (Fig. 3a).

Near field of pump and signal beam is pretty good to (Fig. 4).

CafCA (compression after compressor approach) technology used to increase peak power [3]. Its efficiency is more than 97%. This made it possible to reduce the pulse duration to 14–17 fs (Fig. 3b). All of the above (40J before compressor; 80% compressor efficiency; 97% CafCA efficiency; 15fs pulse duration) allowed us to obtain pulses with a power of more than 2 PWt.

Acknowledgements. The research was supported by the Ministry of Science and Higher Education of the Russian Federation (Project No. FFUF-2023-0001).

References

1. V. Lozhkarev et al., *Laser Physics Letters*, 2007, **4**(6), 421–427.
2. I. Mukhin et al., *Applied Optics*, 2023, **62**(10), 2554.
3. E.Khazanov, S. Mironov and G. Mourou, *Physics-Uspekhi*, 2019, **62**(11), 1096.

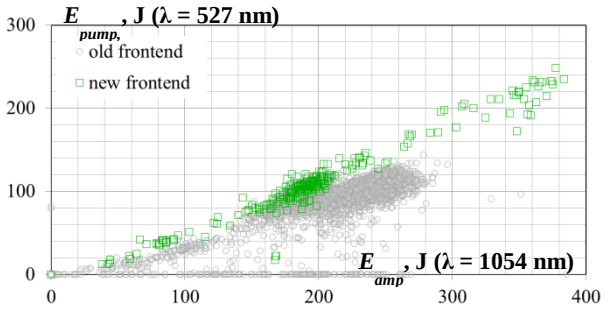

Fig. 1. SHG efficiency

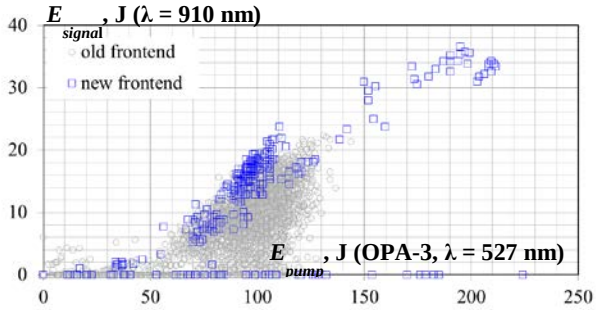

Fig. 2. Optical parametrical amplifying efficiency

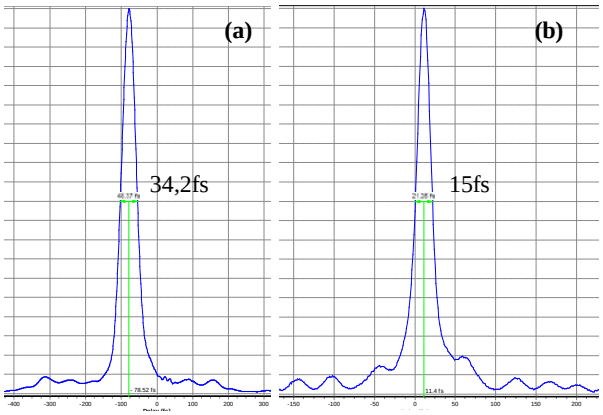

Fig. 3. Autocorrelation functions before (a) and after (b) CafCA

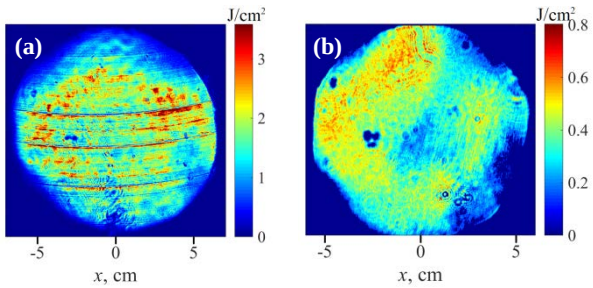

Fig. 4. Near field of pump (a) and signal (b) beam

Multi-beam focusing features of XCELS exawatt laser facility

A. A. Sidnev[1], **A. A. Soloviev**[2], **O. E. Vais**[3] and **A. M. Pukhov**[4]

[1] N. I. Lobachevsky State University, Nizhny Novgorod, Russia
[2] A.V. Gaponov-Grekhov Institute of Applied Physics of the Russian Academy of Sciences, Nizhny Novgorod, Russia
[3] P. N. Lebedev Physics Institute of the Russian Academy of Science, Moscow, Russia
[4] Heinrich-Heine-Universität Düsseldorf, Düsseldorf, Northrhine-Westphalia, Germany

The pursuit of extreme optical field magnitudes represents a pressing challenge for ambitious laser system projects at various stages of global implementation. A significant milestone for such systems involves the exploration of Schwinger fields and the consequent generation of particle cascades emerging from the physical vacuum. Amidst this context, the Russian XCELS project stands out by employing the concept of dipole focusing, realized through the utilization of 12 laser pulses with a combined power reaching up to 600 PW. The field configuration in dipole focusing mimics that of a time-reversed elementary vibrator, comprising 12 tightly focused pulses converging from all directions towards a shared focal point. By coherently combining these laser pulses, the energy density of the electromagnetic field at the focal point increases by over 20 times compared to a single laser pulse of equivalent total power. Consequently, this intense focusing substantially lowers the power threshold for radiation and quantum electrodynamics (QED) effects, facilitating the attainment of the Schwinger limit and quantum plasma degeneracy. Therefore, the implementation of dipole focusing in experiments holds the potential for significant advancements in fundamental physics, astrophysics, and the prospective utilization of such field geometry in practical applications. Alongside laser technologies and nonlinear optics methodologies, a critical element for achieving the project's objectives is the technology of coherent addition of tightly focused high-power laser pulses. The XCELS project entails the development of an exceptionally intricate optical system for the coherent integration of tightly focused laser pulses with an initial aperture of up to 65 cm.

Acknowledgements. The research was supported by the Ministry of Science and Higher Education of the Russian Federation (Project No. FFUF-2023-0001).

Laser plasma interaction at the petawatt laser complex PEARL

A. A. Soloviev, K. F. Burdonov, V. N. Ginzburg, M. Yu. Glyavin, R. S. Zemskov, A. V. Kotov, A. A. Kochetkov, A. A. Kuzmin, A. A. Murzanev, I. B. Mukhin, S. E. Perevalov, M. V. Starodubtsev, A. N. Stepanov, I. A. Shaykin, A. A. Shaykin, A. A. Sidnev, I. V. Yakovlev and **E. A. Khazanov**

A.V. Gaponov-Grekhov Institute of Applied Physics of the Russian Academy of Sciences, Nizhny Novgorod, Russia, so_lo@ipfran.ru

The PEARL laser facility was developed at the Institute of Applied Physics RAS in 2007 [1] based on optical parametric chirped pulse amplification (OPCPA) technology. At that time, the laser became the most powerful parametric system in the world, and even now, almost two decades later, it remains a popular scientific instrument [2] for conducting, first and foremost, basic scientific research.

The exeptional paremeters of the PEARL laser facility made it is possible to obtain record efficiency of interaction of femtosecond laser radiation with matter, in the interaction with both gas and solid targets [3–5], and the results are in good agreement with similar studies at other laser facilities around the world with similar laser parameters.

Recently, the PEARL system underwent additional upgrades [6, 7], with the result that the jitter between the signal and the pump was reduced down to subpicosecond values by switching to optical synchronization. The technological difficulties overcome at the design stage became the key advantage of the laser system at the stage of applied research in laboratory astrophysics. The high precision synchronization of the nanosecond laser driver and femtosecond radiation allow pump-probe experiments with a probe pulse of exceptional optical quality, enabling for clear interferometric shadow and polarization images, as well as the most accurate investigation of time dynamics due to low jitter. To implement the pump-probe technique, an original scheme for extracting a nanosecond pulse from the pump laser was developed [8], which makes it possible to have a nanosecond pulse with an energy of up to 250 J perfectly synchronized with the signal without energy loss of the femtosecond pulse. In concert with the original pulsed magnetic system [9], the facility offers a unique combination of conditions for scaled modeling of plasma astrophysical processes like matter accretion [10], jet collimation [11], and the experimental study of magnetohydrodynamic [12] and kinetic instabilities [13] in plasmas.

The technologies employed in the laser system have proven themselves well and laid the basis for the XCELS exawatt project [14, 15]. The recently emerged CafCA technology for increasing the peak power [16], together with the approaches developed for wavefront correction [17, 18], in particular of nonlinear phase distortions [19], have made it possible not only to significantly increase the power of the laser system [20] but also to almost proportionally increase the peak focal intensity [21], which further expanded the range of possible laser parameters on the target towards higher intensities. The use of CafCA technology for a probing pulse, among other things, makes it possible to increase, when necessary, the time resolution of optical diagnostics of relativistic objects, for example, to study the BISER radiating singularity [22].

The talk presents potential experimental scenarios for utilizing the laser and describes experiments already conducted with the laser across a diverse spectrum of fields.

Acknowledgements. The research was supported financially by the Ministry of Science and Higher Education of the Russian Federation (agreement No. 075-15-2021-1361).

References

1. Lozhkarev V. V. et al. Laser Phys. Lett. 4 421 (2007).
2. Soloviev A. et al. G Phys. Usp. 67 293(2024); Usp. Fiz. Nauk 194 313(2024).
3. Soloviev A. et al. Sci. Rep. 7 12144 (2017).
4. Soloviev A. A. et al. Nucl. Instrum. Meth. Phys. Res. A 653 35 (2011).
5. Perevalov S. E. et al. Plasma Phys. Control. Fusion 62 094004 (2020).
6. Mukhin I. B. et al. Quantum Electron. 51 759 (2021); Kvantovaya Elektron. 51 759 (2021).
7. Mukhin I. B. et al. Appl. Opt. 62 2554 (2023).
8. Andreev N. E. et al. Quantum Electron. 51 1019 (2021); Kvantovaya Elektron. 51 1019 (2021).
9. Luchinin A. G. et al. Rev. Sci. Instrum. 92 123506 (2021).
10. Burdonov K. et al. Astron. Astrophys. 648 A81 (2021).
11. Soloviev A. A. et al. Radiophys. Quantum Electron. 63 876 (2021); Izv.Vysh. Uchebn. Zaved. Radiofiz. 63 973 (2020).
12. Burdonov K. et al. Astron. Astrophys. 657 A112 (2022).
13. Weibel E. S. Phys. Rev. Lett. 2 83 (1959).
14. Kostyukov I. Yu. et al. Bull. Lebedev Phys. Inst. 50 (Suppl. 6) S635(2023); Kvantovaya Elektron. 51 95 (2023).
15. Khazanov E. et al. High Power Laser Sci. Eng. 11 e78 (2023).
16. Khazanov E. A., Mironov S. Yu., Mourou. G. Phys. Usp. 62 1096 (2019); Usp. Fiz. Nauk 189 1173 (2019).
17. Kotov A. V. et al. Quantum Electron. 51 593 (2021); Kvantovaya Elektron. 51 593 (2021).
18. Soloviev A. A. et al. Quantum Electron. 50 1115 (2020); Kvantovaya Elektron. 50 1115 (2020).
19. Martyanov M. et al. J. Opt. Soc. Am. B 39 1936 (2022).
20. Ginzburg V. et al. Opt. Express 29 28297 (2021).
21. Soloviev A. et al. Opt. Express 30 40584 (2022).
22. Kotov A. V. et al. JINST 17 P07035 (2022).

Rare earth ions doped glass materials in fiber lasers and amplifiers

Y. Sun[1], X. Wang[1], L. L. Hu[1,2], S. B. Chen[1] and C. L. Yu[1,2]

[1] Shanghai Institute of Optics and Fine Mechanics, Chinese Academy of Sciences, Shanghai, China
[2] University of Chinese Academy of Sciences, Hangzhou, China

With the development of Internet of Things and cloud computing, the next generation of optical communication places great demand for the dense wavelength division multiplexing (DWDM). L-band (1565–1625 nm) Er doped fiber amplifier (EDFA) in the fiber communication system is the next generation of commercial EDFA. However, the Er-doped fiber lasers at wavelengths longer than 1600 nm face challenges of excited-state absorption (ESA) and low gain coefficient. Co-doping phosphorous in Er-doped silica fiber is a good way to enhance the L-band amplification. Unfortunately, the strong volatilization of phosphorus in heavy concentration during the high-temperature (near 2000 °C) fiber drawing process has degraded the repeatability and vertical uniformity of Er-doped silica fibers. In this work, we have developed the L-band spectral shaping methodology of Er doped functional glasses through manipulating the glass network formers, glass modifiers, oxygen to phosphorous atom ratios and Er concentrations in multicomponent glasses.

In phosphate glasses, adjusting oxygen to phosphorous atom ratios in the glass composition can broadening the emission band of Er^{3+} ions by manipulating the local structures around Er^{3+} ions in glass structure. More than 260 nm band width (1420–1680 nm) has been achieved in self-developed Er doped phosphate fiber. The laser wavelength of Er-phosphate fiber was extended to 1630 nm. The maximum output powers and slope efficiencies of the lasers at 1627 nm and 1630 nm reached up to 44 mW/12.5% and 16.5 mW/5.6%, respectively, in a 30-cm phosphate fiber. These are the highest output powers and slope efficiencies at 1627 nm and 1630 nm from an Er^{3+}-doped all-fiber laser configuration.

In silicate glass system, the emission spectroscopic properties of Er^{3+} ions are influenced by glass modifiers. Increasing the content of glass modifiers with high field strength will enhance the emission cross sections especially in the L-band wavelength. A L-band Er doped functional glass with excellent performance was fabricated into fibers with the propagation loss of <0.5 dB/m at 1.2 μm through a modified rod-in-tube method. More than 1.2×10^{-21} cm^2 of emission cross section at 1625 nm has been achieved in Er doped silicate fiber. The gain coefficient at 1625 nm wavelength of Er-silicate fiber was increased to 4.7 dB/m. The gain flatness in a 1-m silicate fiber was achieved to be 0.8 dB. We obtained >10 dB net gain at L-band region in a 1-m long silicate fiber from an all-fiber configuration. Our approach provides a new solution for the next generation of EDFA and provides new glass materials support for the development of optical fiber communication.

Acknowledgements. This work was supported by National Natural Science Foundation of China (62205355, 51972317, 61875052); National Key Research and Development Program of China (2020YFB1805900).

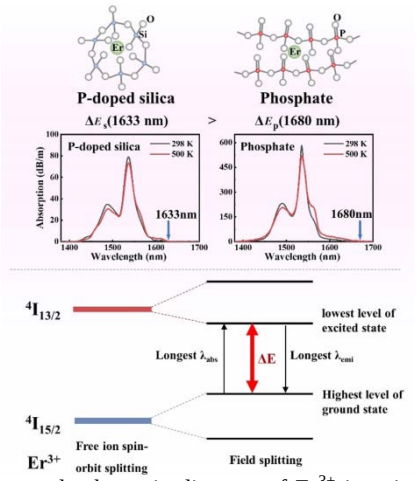

Fig. 1. Structural schematic diagram of Er^{3+} ions in silica and phosphate glasses, the absorption spectra of Er/Al/P-silica and Er phosphate glasses measured at 298 K and 500 K, and the splitting of Er^{3+}: $^4I_{13/2}$ and $^4I_{15/2}$ states

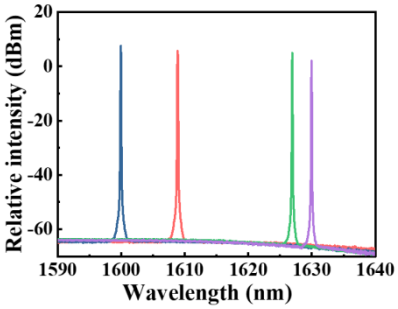

Fig. 2. Optical spectra of a 15-cm Er^{3+}-doped phosphate fiber laser operating at 1600, 1609, 1627 and 1630 nm

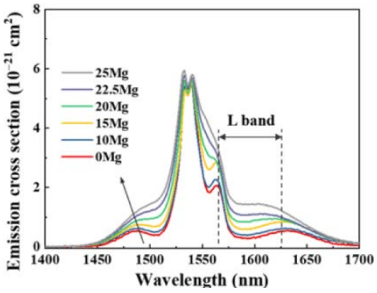

Fig. 3. Emission cross sections of Er^{3+} ions doped in silicate glasses with molar compositions of $60SiO_2$-(40–x)Na_2O-xMgO, x=0, 10, 15, 20, 22.5 and 25

References

1. V. Kapitanov and Y. Ponomarev, *Appl. Phys. B*, 2008, **90**, 235–241.
2. X. Shen, S. Chen, Y. Sun, *et al.*, *IEEE Photonics J.*, 2021, 13(6), 2200506.
3. G. Lin, J. Chang, Y. Liao, *et al.*, *Opt. Express*. 2006, **14**(21), 9743–9749.

DBR lasing by integrating FBGs into germanium-free photosensitive highly Yb^{3+}-doped silica fiber

Y. F. Wang, **C. L. Yu** and **L. L. Hu**

Shanghai Institute of Optics and Fine Mechanics, Shanghai, China, wangyafei@siom.ac.cn

Over the past decades, single frequency fiber lasers (SFFLs) opened widespread applications in high-precision spectroscopy, coherent beam combining and lidar because of their compact all-fiber configuration, narrow spectral linewidth and ultra-low noise [1]. Among these schemes of SFFLs, monolithic distributed Bragg reflector (DBR) cavity which directly integrates fiber Bragg gratings (FBGs) into the photosensitive RE-doped fibers is a promising configuration in constructing compact and efficient SFFLs [2]. Yet, the doping level of rare-earth (RE) ions has generally to be sacrificed in the classical Ge-photosensitized RE-doped silica fibers because of the dramatic refractive index increase caused by the introduction of Ge.

Here, we demonstrate an approach to realize the trade-off between photosensitivity and RE doping concentration. We validate that the addition of a small amount of cerium (0.37wt.%) instead of Ge could photosensitize Yb^{3+}-doped silica fiber (YDF), while maintaining fiber numerical aperture (NA) at 0.12 under a high 2.5-wt.% Yb doping level. The photosensitivity mechanism of Ce is as follow:

$$\begin{aligned} Ce^{3+} &\xrightarrow{UV} Ce^{4+} + e^{-} \\ h^{+} + e^{-} &\longrightarrow 0 \end{aligned} \quad . \qquad (1)$$

Under the exposure of UV light, e.g., 248 nm, the Ce^{3+} ions are inclined to lose one electron (e-) and transform into Ce^{4+}. At the same time, the hole (h^{+}) centers in the glass matrix would trap these released electrons. This mechanism enables FBGs formation in Ce photosensitized fibers when combined with UV laser phase mask technique. Especially, different to the Ge-photosensitized fibers, hydrogen loading process could be avoid which simplifies the FBG inscription process to a large extent. The influence of Ce concentration on photosensitivity is researched. As shown in Fig. 1(a) and (b), the 0.37wt% Ce doping enables FBGs inscription with over 95% reflectivity and $0.8*10^{-4}$ refractive index modulation. As mentioned above, a single-mode highly Yb doped silica fiber is further developed with 0.37wt% Ce doping. As shown in Fig. 1(c) and (d), the 1064 nm FBG could be successfully inscribed into this YDF without any prominent thermal degradation after annealing.

This excellent photosensitivity allows us integrating FBGs pair into this YDF to form a monolithic short DBR cavity [3]. The experimental setup is shown in Fig. 2(a). a short 3-cm long YDF was used to build the monolithic cavity, where the HR-FBG and LR-FBG were written to its ends with a 1-cm interval. The center wavelengths of HR-FBG and LR-FBG were well matched (Fig. 2(b)). The output power characteristics is shown in Fig. 2(c). The maximum laser output power of 210 mW was achieved at the launched pump power of 457 mW, corresponding to a laser efficiency of 48.6%. The linear

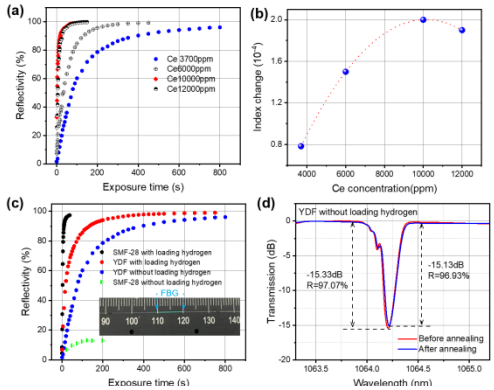

Fig. 1. (a) Reflectivity evolution of FBGs under different Ce concentrations. (b) Derived UV-induced refractive index modulation amplitude. (c) Reflectivity evolution of FBGs by commercial Ge-doped fiber and YDF with loading hydrogen and without loading hydrogen. Inset in a photograph of FBG written in YDF. (d) Transmission spectra of FBGs in YDF before and after annealing treatment

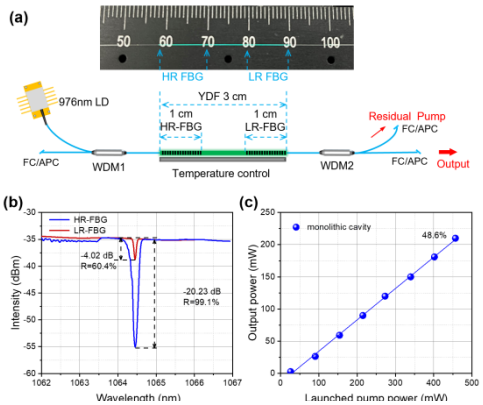

Fig. 2. (a) Experimental setup of the monolithic efficient DBR laser by this photosensitive YDF. Inset is the photograph of the constructed monolithic cavity. (b) Transmission spectra of HR-FBG and LR-FBG written in YDF. (c) The laser output power versus the launched pump power

increase tendency shows the output power could be further elevated by higher pump power.

Acknowledgements. The authors thank the financial support from National Natural Science Foundation of China (6220535, 61975216) and the Strategic Priority Research Program of the Chinese Academy of Sciences (XDB0650000).

References

1. S. J. Fu, W. Shi, and Y. Feng et al., *J. Opt. Soc. Am. B.*, 2017, **34**(3), A49–A62.
2. Y. Lai, A. Martinez, I. Khrushchev, I. Bennion. *Opt. Lett.*, 2006, **31**(11), 1672–167.
3. Y. Wang, Q. Yang, and F. Wang et al., *Opt. Express*, 2024, **32**(10), 1757–17580.

Time-domain electric field analysis of ultra-broadband chirped mirrors

Tianze Xu[1,2,3], **Yanzhi Wang**[1,2], **Yu Chen**[1,2] and **Jianda Shao**[2]

[1] Key Laboratory of Material for High Power Laser, Shanghai Institute of Optics and Fine Mechanics, Shanghai, China
[2] Laboratory of Thin Film Optics, Shanghai Institute of Optics and Fine Mechanics, Shanghai, China
[3] Center of Materials Science and Optoelectronics Engineering, Shanghai Institute of Optics and Fine Mechanics, Shanghai, China

The laser-induced damage threshold resistance performance of ultra-broadband chirped mirrors (UBCMs) is a key factor influencing the generation of high peak intensity laser pulses in post-compression techniques. Two different UBCMs were designed and fabricated for a comparative study of their laser-induced damage under a 7fs pulse irradiation. Because the electric field distribution in UBCMs is not standing wave field in femtosecond regime, we established a time-domain electric field model to analyze the damage behavior. The model successfully elucidated the origin of the damage and discrepancy between the two UBCMs in terms of damage thresholds, showcasing its potential applications in designing high-threshold UBCMs for high-power laser systems.

Damage morphology and time-domain electric field distribution of UBCMs

For a comparative study, we obtained two different UBCMs by setting different GDD targets. The bandwidth of both mirrors meets the spectral range of the 7fs pulse. The design work was completed by Optilayer [1]. Both mirrors were fabricated using dual-ion beam sputtering and deposited on fused silica substrates. A 1-on-1 test was conducted on both mirrors. The laser-induced damage threshold (LIDT) of the two mirrors are 0.094 and 0.136 J/cm^2, respectively, and the initially damaged layer is both located at the fourth layer, as shown in Fig. 1.

To elucidate the reasons for the initial damage in the fourth layer of both mirrors and the discrepancies in their LIDTs, we calculated the time-domain electric field distribution. The specific process involves solving the wave equation, which can be accomplished by the finite element method or the finite-difference time-domain method. The key task is to obtain the time-domain electric field waveform of the incident pulse, which can be completed by performing an inverse Fourier transform on the complex spectrum amplitude of the 7 fs pulse. The spectrum and phase information of the pulse was obtained using D-scan technique [2, 3]. Fig. 2 illustrate the calculated results for the time-domain electric field distribution of the two mirrors.

A peak electric field intensity (EFI) can be observed at 8024 nm and 8320 nm in UBCM1 and UBCM2, respectively. The position of the peak EFI corresponds to the fourth layer of both mirrors, which aligns with the observed position of the initially damaged layer, as previously mentioned. A strong EFI within the initially damaged layer can be identified as the cause of the damage. Additionally, the peak EFI value of the initially damaged layer in UBCM1 is 1.32, whereas that in UBCM2 is 0.93. The value of UBCM1 was approximately 41.9% higher than that of UBCM2, and the LIDT of UBCM2 was approximately 44.7% higher than that of UBCM1. Considering the system errors in testing laser-induced damage, this result may suggest an inverse relationship between the peak EFI and LIDT. The specific functional relationship between the EFI and LIDT requires additional experimental data.

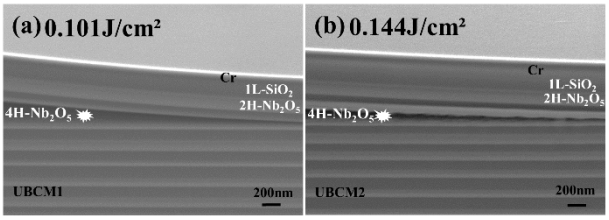

Fig. 1. The initially damaged layer of (a) UBCM1 and (b) UBCM2

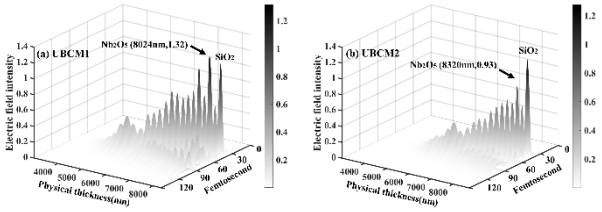

Fig. 2. Time-domain electric field distribution of (a) UBCM1 and (b) UBCM2. The black arrow indicates the peak EFI inside the mirror. The physical thickness is calculated from the substrate, with a physical thickness of 0 nm at the substrate

Acknowledgements. This work was supported by the attosecond laser station in the Synergetic Extreme Condition User Facility (SECUF).

References

1. A. V. Tikhonravov and M. K. Trubetskov, *Optilayer software*.
2. M. Miranda, T. Fordell, C. Arnold, A. L'Huillier and H. Crespo, *Opt. Express*, 2012, **20**(1), 688–697.
3. D. Fabris, W. Holgado, F. Silva, T. Witting, J. W. G Tisch and H. Crespo, *Opt. Express*, 2015, **23**(25), 32803–32808.

Laboratory modeling of YSO jets collimation by a large-scale divergent interstellar magnetic field

R. S. Zemskov[1], **K. F. Burdonov**[1], **A. A. Soloviev**[1], **A. D. Sladkov**[1], **A. V. Korzhimanov**[1], **J. Fuchs**[2] and **M. V. Starodubtsev**[1]

[1] A.V. Gaponov-Grekhov Institute of Applied Physics of the Russian Academy of Sciences, Nizhny Novgorod, Russia, zemskov@ipfran.ru

[2] CNRS, CEA, Sorbonne Université, École Polytechnique, Institut Polytechnique de Paris, France

Introduction

Jets are commonly observed in accreting young stellar objects (YSO). Such collimated supersonic outflows are usually observed along the rotation axis of a star-accretion disk system [1], and they are believed to play a key role in the evolution of YSO's [2]. The mechanisms of the generation of outflows and their collimation into jets are still not fully understood and are being actively discussed.

Numerical studies as well as scaled laboratory experiments suggest that bipolar outflows arising from young stellar objects (YSOs) could be collimated into narrow and stable jets as a result of their interaction with a poloidal magnetic field [3]. However, this magnetic collimation mechanism was demonstrated in the laboratory only for the simplified topology of the uniform poloidal magnetic field [4].

We have extended the experimental studies to the case of a plasma outflow expanding in a region of strong poloidal magnetic field and then propagating through divergent magnetic field lines. In this case the magnetic field distribution is closer to the hourglass magnetic field distribution expected near YSOs. Our aim was to find out whether (and under what conditions) magnetic collimation is possible in such a strongly nonuniform B-field configuration.

Experimental approach and results

The experiments [5] were carried out on the PEARL high-power laser facility [6]. The laser produced plasma outflow was embedded in a strong (~10 T) magnetic field generated by the unique magnetic system. The morphology and dynamics of the plasma were diagnosed with a Mach-Zehnder interferometer.

Laboratory experiments and 3D numerical modeling allow us to reveal the various stages of plasma jet formation in a divergent poloidal magnetic field. The results show that there is a fundamental possibility for magnetic collimation of a plasma outflow in a divergent magnetic field. Also there is good scalability of astrophysical and laboratory flows. Conditions for the formation of a magnetic nozzle, hence collimation by poloidal magnetic field, have been discovered and the propagation of the jet proceeds unimpeded through the region of weak and strongly divergent magnetic fields, maintaining a high aspect ratio was demonstrated. We observed that a strong poloidal magnetic field region can lead to the generation of a plasma cavity with a magnetic nozzle tip and, as a result, it can collimate the outflow into a narrow jet. We studied experimentally and numerically how the collimation process depends on the scale of a region where a strong poloidal magnetic field is present, and found that the minimum scale-length of this region has to be on the order of $2R_b$ to collimate the flow.

Laboratory studies, such as the one presented here, are of particular importance as they allow us to address extreme flow conditions that are only accessible to simulations, and thus can help validate the theoretical and numerical models of jet collimation.

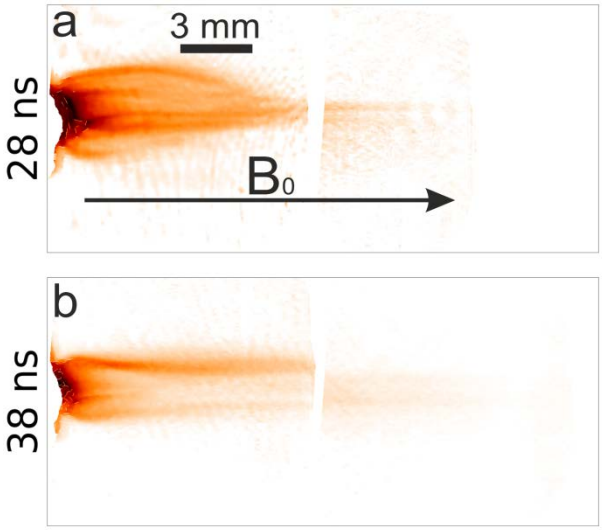

Fig. 1. Two-dimensional density profiles of the plasma stream propagating along a quasi-uniform magnetic field at 28 ns (a), 38 ns (b) after the laser irradiation of the target

Acknowledgements. The research was supported financially by the Ministry of Science and Higher Education of the Russian Federation (agreement No. 075-15-2021-1361).

References

1. F. Kamali, C. Henkel, S. Koyama, et al. *Astronomy & Astrophysics*., 2019, 624, A42.
2. R. E. Pudritz, R. Ouyed, C. Fendt, et al. *Protostars and Planets V*., University of Arizona Press, 2007.
3. S. Ustamujic., S. Orlando, R. Bonito, et al. *Astronomy & Astrophysics*, 2018, 615, A124.
4. B. Albertazzi, A. Ciardi, M. Nakatsutsumi, et al. *Science*, 2014, **346**(6207), 325–328.
5. R. Zemskov, K. Burdonov, A. Soloviev, et al. *Astronomy & Astrophysics*, 2024, 681, A37.
6. V. V. Lozhkarev, G. I. Freidman, V. N. Ginzburg, et al. *Laser Physics Letters*, 2007, **4**(6), 421.

Spatio-temporal dynamics of femtosecond laser pulses during apodization by a serrated diaphragm

M. A. Zolotavin[1] and **A. A. Soloviev**[2]

[1] N. I. Lobachevsky State University, Nizhny Novgorod, Russia, mihailzolotavin@gmail.com
[2] A.V. Gaponov-Grekhov Institute of Applied Physics of the Russian Academy of Sciences, Nizhny Novgorod, Russia

Aperture separation of high-power laser radiation can only be realized using rigid diaphragms, the use of which leads to a significant influence of diffraction effects on the spatial distribution of intensity, expressed in the occurrence of local maximums, in some cases leading to breakdown of optical elements. The reduction of diffraction inhomogeneities in intensity profile is facilitated by the use of special serrated diaphragms in combination with a spatial filter (Fig. 1) [1, 2]. The issue of using serrated diaphragms has been studied in some detail for narrowband radiateon, in particular high-power nanosecond pulses. At the same time, the issue of aperture separation of femtosecond pulses has not been studied previously in the literature, although it is relevant for pump-probe experiments [3, 4] and large multichannel femtosecond installations such as XCELS [5]. In contrast to monochromatic radiation, diffraction of broadband femtosecond pulses leads to local modulations of the spectrum and spectral phase. In this research, using numerical modeling, we study the spatio-temporal dynamics of femtosecond laser pulses after aperture separation on a serrated diaphragm and subsequent spatial filtering. The results of the research can be useful in realization aperture separation of femtosecond radiation in laser systems of terawatt [6] and higher power levels [5].

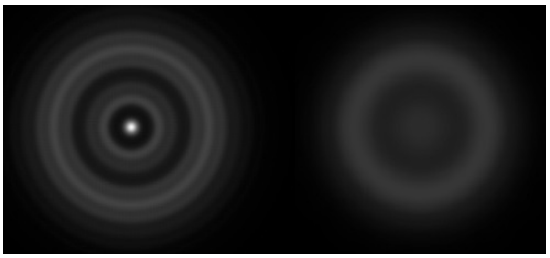

Fig. 1. View of the intensity distribution in the cross section of the laser beam at some distance from the diaphragm when using a classic circular diaphragm (left) and serrated diaphragm in combination with a spatial filter (right)

Acknowledgements. The research was supported by the Ministry of Science and Higher Education of the Russian Federation (Project No. FFUF-2023-0001).

References

1. Peter M. Celliers, Kent G. Estabrook, Russell J. Wallace, James E. Murray, Luiz B. Da Silva, Brian J. MacGowan, Bruno M. Van Wonterghem, and Kenneth R. Manes, Spatial filter pinhole for high-energy pulsed lasers, *Appl. Opt.* 37, 2371–2378 (1998).
2. Burdonov K. F. et al. Short spatial filters with spherical lenses for high-power pulsed lasers, *Quantum Electronics*. 2013. V. 43, no. 11. P. 1082–1087.
3. Soloviev A. A., Burdonov K. F., Ginzburg V. N., Glyavin M. Yu., Zemskov R. S., Kotov A. V., Kochetkov A. A., Kuzmin A. A., Murzanev A. A., Mukhin I. B., Perevalov S. E., Pikuz S. A., Starodubtsev M. V., Stepanov A. N., Fuks Zh., Shaykin I. A., Shaykin A. A., Yakovlev I. V., Khazanov E. A. Research in plasma physics and particle acceleration using the PEARL petawatt laser, *UFN*, 194, 313–335 (2024).
4. Kotov A. V. et al. Enhanced diagnostics of radiating relativistic singularities and BISER by nonlinear post-compression of optical probe pulse, *Journal of Instrumentation*. 2022. V. 17, no. 07. P. P07035.
5. Bashinov A. V. et al. New horizons for extreme light physics with mega-science project XCELS, *The European Physical Journal Special Topics*. 2014. V. 223. P. 1105–1112.
6. Vais O. E. et al. Efficient Acceleration of Electrons by Moderate-Power Femtosecond Laser Pulses, *JETP Letters*. 2023. V. 118, no. 12. P. 875–880.

Two-photon resonant interaction of few-cycle terahertz waves with optical media vibrational bond

M. S. Guselnikov and **S. A. Kozlov**

ITMO University, St. Petersburg, Russia, msguselnikov@itmo.ru

Introduction

Recently discovered vibrational nature giant and low-inertia nonlinearity of refractive index in THz spectral range [1] promises great prospects for ultrafast radiation control [2]. Particularly, it is expected a strong increase of nonlinear refractive index coefficient near two-photon resonance area which can cause significant amplifying of nonlinear effects as well as appearance of new ones. In this paper features of few-cycle THz pulses two-photon resonant interaction with optical media is analyzed for the first time.

Results

In the present study a system of dynamic equations for few-cycle terahertz pulses spectrum has been derived. It considers linear refractive index dispersion, non-resonant and two-photon vibrational nature resonant dispersion of the optical medium nonlinear refractive index. It is shown that the perturbation parameter of the system, which characterizes nonlinear change of refractive index, is determined by the square of the matter thermal expansion coefficient, the fourth power of the resonant vibrational bond central frequency, and the radiation intensity.

It has been revealed that the efficiency of nonlinear effects generation is maximal when the ratio of the input spectrum HWHM to the vibrational bond two-photon absorption profile HWHM tends to unity, and the difference between the input pulse spectrum central frequency and two-photon absorption profile central frequency tends to zero. In this case, nonlinear effects generation efficiency can increase by an order of magnitude to compare with the case of non-resonant interaction.

It has been discovered that when the central frequency of the input pulse spectrum exceeds the central frequency of the two-photon absorption profile, a low-frequency sub-pulse generation in the pulse spectrum at the output of the nonlinear medium can be observed. This effect is caused by the inertia of the resonant nonlinear response.

To illustrate obtained results we modeled dynamic of few-cycle THz pulse propagating along optical axis of lithium niobate crystal near two-photon resonance of $LiNbO_3$ THz valence bond with pulse spectrum central frequency. At Fig. 1 one can see appearance of low-frequency sub-pulse in the spectrum of THz pulse of 3 field oscillations and central frequency equaled 64% of resonant valence bond central frequency.

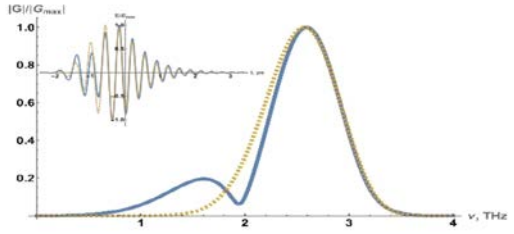

Fig. 1. Normalized spectrum of THz pulse at the output of nonlinear medium considering (blue solid curve) and not considering (yellow dashed curve) nonlinear effects. In the inset one can see normalized fields corresponding to plotted spectra.

At Fig. 2 one can observe dependence on the pulse field oscillations number p of squared modulus of difference between the pulse spectrum at the output of a nonlinear medium considering and not considering nonlinear effects to squared modulus of input pulse spectrum (S_{res}) divided by this ratio in non-resonant case (S_{nr}) for a pulse with central frequency equaled one half of resonant valence bond central frequency. It is seen that this ratio arises in one order for p~9.5.

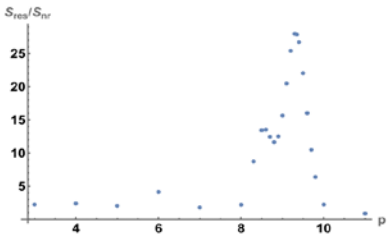

Fig. 2. Dependence of squared modulus of difference between the pulse spectrum at the output of a nonlinear medium considering and not considering nonlinear effects to squared modulus of input pulse spectrum S_{res} divided by this ratio in non-resonant case S_{nr} for pulse with central frequency equaled one half of resonant valence bond central frequency on pulse field oscilla- tions number p .

Acknowledgements. All authors acknowledge support from the Russian Science Foundation (Grant No. 24-22-00084).

References

1. A. Tcypkin et al. *Phys. Rev. Appl.*, 2021, **15**(5), 054009.

2. A. Nabilkova et al. Opt. Lett., 2023. **48**(5), 1312–1314.

Generation of ultrashort deep UV pulses at the third harmonic of the optical field by Na atoms in the two-photon Rabi-flopping regime

I. R. Khairulin[*], **A. A. Romanov**, **V. A. Antonov** and **A. A. Silaev**

A.V. Gaponov-Grekhov Institute of Applied Physics of the Russian Academy of Sciences,
Nizhny Novgorod, Russia, *khairulinir@ipfran.ru

Harmonic generation is a fundamental nonlinear optical process in which n photons with the same frequency interact with a nonlinear medium and are converted into a new photon with a frequency n times the frequency of the original photons. Typically, the pulse duration of the generated harmonic is less than pulse duration of the driving field. For example, the pulse duration of the 3rd harmonic generated by a Gaussian laser pulse in a medium with cubic nonlinearity is the root of three times less than the pulse duration of the fundamental frequency field.

In the present work, we propose a method that makes it possible to generate harmonics with pulse duration shorter than in the case of standard cubic nonlinearity. The method is based on the coherent population transfer between different energy states of alkali metal atoms [1, 2]. As an example, we consider the 3rd harmonic generation in Na atoms irradiated with a strong femtosecond laser pulse with a frequency resonant to the $|3s\rangle$-$|3p\rangle$ transition of the active electron. In this case, the active electron in Na is resonantly transferred from the initial $|3s\rangle$ state to the excited $|5s\rangle$ and $|4d\rangle$ states due to the two-photon cascade transition through the intermediate $|3p\rangle$ state. If the femtosecond pulse is strong enough, then the populations of all states $|3s\rangle$, $|3p\rangle$, $|5s\rangle$ and $|4d\rangle$ are significant, and the two-photon Rabi-flopping regime occurs.

Recently, the two-photon Rabi-flopping regime was theoretically studied in [2] for Li atom. It was shown that in this case a resonant behavior of the electronic population is reflected in complex oscillatory structures of the harmonic peaks in the frequency domain. Moreover, as was also shown in [2], such oscillatory structure of a harmonic spectral profile corresponds to the complex modulation pattern of the harmonic signal in the time domain.

Here, based on both numerical and analytical solutions of the time-dependent Schrödinger equation with the effective potential obtained by solving the Kohn-Sham equations for Na atom, we show that for optimal laser pulse intensity and duration in the two-photon Rabi-flopping regime, the temporal modulation of the 3rd harmonic leads to the formation of a single intense pulse with a duration approximately two times shorter than in the nonresonant case. In particular, a single short pulse of the 3rd harmonic in deep ultraviolet (at wavelength in the vicinity of 200 nm) with a duration of 4.7 fs (Fig. 1, solid curve) is generated by a Na atom irradiated by a laser pulse with a duration of 20 fs and a peak intensity of 6.3×10^{11} W/cm^2 (Fig. 1, dotted curve). For comparison, in the case of the nonresonant regime corresponding to cubic nonlinearity, the 3rd harmonic pulse duration is about 11.5 fs (Fig. 1, dashed curve), and its peak intensity is more than 50 times less than in the two-photon Rabi-flopping regime.

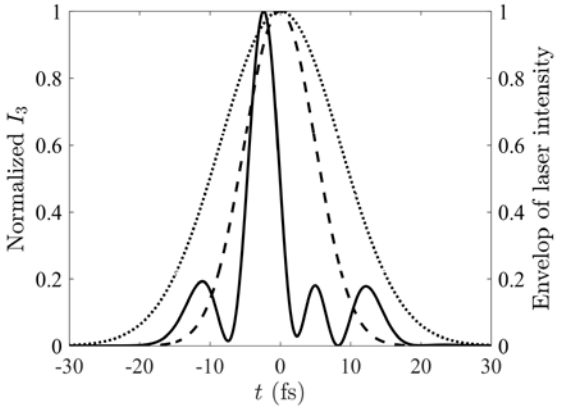

Fig. 1. Envelope of the 3rd harmonic generated by Na atom (solid and dashed curves, left axis) and the laser field envelop (dotted curve, right axis), which is Gaussian pulse with FWHM 20 fs. The solid curve corresponds to the two-photon Rabi-flopping regime; the dashed curve corresponds to the nonresonant regime. The laser field intensity is 6.3×10^{11} W/cm^2

Acknowledgements. This work was supported by the Russian Science Foundation (grant No. 22-12-00389).

References

1. M. F. Ciappina, J. A. Perez-Hernandez, A. S. Landsman, T. Zimmermann, M. Lewenstein, L. Roso, and F. Krausz, *Phys. Rev. Lett.*, 2015, **114**(14), 143902.
2. K. N. Avanaki, D. A. Telnov, and S.-I Chu, *Phys. Rev. A*, 2016, **94**(5), 053410.

Simple method for creating ultraviolet radiation with orbital angular momentum through laser-plasma interactions

K. Kolupaev[1], **Jingwei Wang**[2] and **S. Rykovanov**[1]

[1] Skolkovo Institute of Science and Technology, Moscow, Russia, K.Kolupaev@skoltech.ru
[2] Shanghai Institute of Optics and Fine Mechanics, Shanghai, China

Modern advances in laser physics and nonlinear optics are opening up new possibilities for understanding and controlling the interaction between high-intensity laser pulses and materials. One promising area of research is the high order harmonic generation (HOHG), which occurs when a powerful laser pulse interacts with a plasma. This process produces radiation in the ultraviolet (UV) spectrum with unique properties, such as the presence of orbital angular momentum (OAM).

UV radiation with OAM has significant potential for various applications, including spectroscopy, microscopy, and the creation of novel quantum materials and information transmission technologies. Its unique properties make it a valuable tool for studying and manipulating matter at the atomic and molecular level.

This article discusses the theoretical and numerical modeling of the process of creating high-frequency radiation in the interaction between a powerful laser beam and plasma. Special attention is paid to the characteristics of the laser beam and the plasma with some assumptions, which influence the efficiency of ultraviolet radiation generation using OAM. A modeling technique is introduced that is based on solving Maxwell's equations and the equations of motion for charged particles, which allows predicting the conditions for the most efficient production of HOHG.

Theoretical background

One of the processes responsible for HOHG is called the Relativistic Oscillating Mirror (ROM) [1, 2]. In this process the laser pulse with linear polarization while interacting with overdense plasma creates an oscillating surface and gets reflected for this self-generated oscillating mirror. Every time the surface moves towards the laser pulse an XUV attosecond pulse is generated. In order to simulate the precise electromagnetic field generated by the laser pulse in the process of its interaction with plasma, it is necessary to solve the system of nonlinear partial differential equations – self-consistent Vlasov-Maxwell system.

Numerical method that is commonly used for that is called the Particle-in-Cell [3] method and it typically requires a large amount of high performance computing (HPC) resources for the multidimensional cases.

However, for qualitative research it is not always obligatory to compute precise models for various types of matter interaction with the pulses. In 1905 A. Einstein proposed a model of relativistic mirror motion [4]. In many cases this model is appropriate to describe qualitatively the interaction between the laser pulse and the overdense plasma, substituting the real complicated behavior of the matter with the ideal relativistic moving mirror. This approach is much simpler, does not require large HPC resources, and, if one assumes no correlation between mirror motion at different transverse locations, can be used to model 3D cases.

Methodology

To simulate laser pulse reflections from a relativistic mirror, we used the following approximations:

The laser pulse is modeled using Laguerre-Gaussian polynomials, with the simplest case being a Gaussian pulse.The target is treated as a moving mirror following relativistic motion laws input into the code.The reflected field assumes perfect reflection with no energy loss.

This paper aims to introduce a lightweight 3D numerical tool for modeling high-order harmonic generation (HOHG) from overdense plasma and to demonstrate the generation of harmonics with orbital angular momentum (OAM).

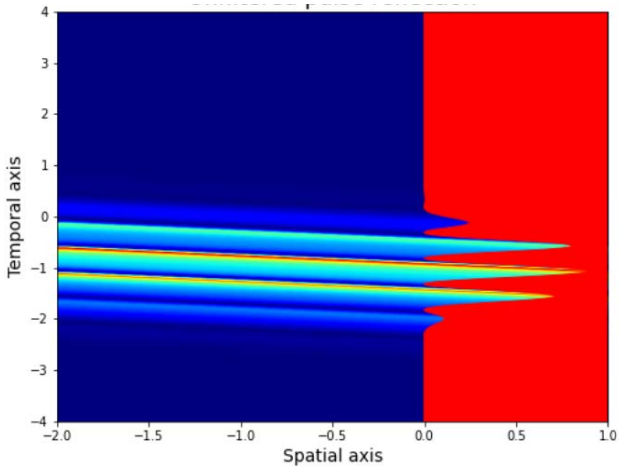

Fig. 1. Reflected field generation and mirror motion visualization (red graph)

The workflow of the paper is organized as follows. Firstly, we introduce the ROM model for 1 dimensional and 3 dimensional cases. Secondly, the concept of retarded time (1) is obtained with respect to the problem. Thirdly, the calculations for 1-d (Fig. 1) and 3-d are provided and results are discussed.

$$t' = t - X_m(t')/c \qquad (1)$$

References

1. S. Bulanov, N. Naumova, and F.Pegoraro, *Phys. Plasmas*, 1994, **1**, 745.
2. R. Lichters, J. Meyer-ter-Vehn, and A. Pukhov. *Physics of Plasmas*. 1996. **3. 3425. 10.1063/1.871619.**
3. C. Birdsall, and A. Langdon. *Plasma Physics Via Computer Simulation*. New York: McGraw-Hill, 1985.
A. Einstein, *Ann. Phys*. Leipzig. **17**. 1905. 891–921.

SECTION 3

SOURCES AND APPLICATIONS OF STRONG MICROWAVES, MODERN TRENDS IN NUCLEAR FUSION

Preliminary experiments on a demountable prototype of a MW level 230 GHz gyrotron

A. A. Ananichev[1], A. V. Chirkov[1], G. G. Denisov[1], A. P. Fokin[1], Yu. M. Guznov[1], A. N. Kuftin[1], A. N. Leontyev[1], V. N. Manuilov[1], L. G. Popov[2], E. A. Soluyanova[1,2], E. M. Tai[1,2]

[1] A.V. Gaponov-Grekhov Institute of Applied Physics of the Russian Academy of Sciences, Nizhny Novgorod, Russia,
[2] Closed Joint-Stock Company Scientific Production Enterprise «GYCOM», Nizhniy Novgorod, Russia
a0810@ipfran.ru

The gyrotron is a powerful source of microwave radiation in the millimeter and submillimeter wavelength ranges with a large number of applications. One of the most important is electron cyclotron resonance plasma heating in tokamaks and stellarators [1]. The development of such machines goes in the direction of the increase of plasma density, magnetic field and, therefore, the increase of the heating frequency. However, for megawatt-class gyrotrons such increase is complicated by the competition between different modes of the cylindrical waveguide.

Also, practically all facilities use several identical radiation sources to increase the total heating power. While not so important for heating itself, the incoherence of the radiation of several gyrotrons reduces the efficiency of suppressing the instability of the plasma and creates difficulties in creating highly gradient particle accelerators [2, 3].

The solution to these problems has been known for a long time [4, 5], but it was experimentally demonstrated last year on a pulsed megawatt gyrotron developed for ITER at a frequency of 170 GHz [6]. The solution to the problem is to use an external control signal for phase and frequency synchronization of gyrotrons. The input of the external control signal into the device became possible after the development of a mode converter capable of both entering and withdrawing high-power radiation through the same window.

This paper presents the development of the next generation of megawatt gyrotrons developed for future fusion power plants such as DEMO at a frequency of 230 GHz. A unique cryomagnet with a maximum field value of 10 Tesla and a warm bore with a diameter of 150 mm was used for the design and experiment.

A distinctive feature of this gyrotron is the use of two different windows: for the input of a synchronizing signal and the output of high-power radiation. This design is more convenient in terms of further applications. For this gyrotron, the input of the external signal should suppress the excitation of the parasitic modes and advance into the optimal range of parameters for the megawatt operation.

The gyrotron has a demountable design and operates in pulse mode with a pulse length of up to 100 microseconds. The operating magnitude of the magnetic field is 9.2 Tesla, the accelerating voltage is 80 kV at a beam current of 35 A, which corresponds to the working mode $TE_{33,13}$. The first experiments demonstrated the successful excitation of the operating mode with the output power up to 400 kW at a frequency of 229,8 GHz.

The experiments were carried out without an external synchronizing signal, but in the future, it is planned to conduct an experiment with frequency stabilization using a medium-power gyrotron (approximately 100 kW) and a frequency stabilization system.

Fig. 1. Photo of a megawatt gyrotron with a frequency of 230 GHz

This work was supported by the IAP RAS project FFUF-2022-0007 within the framework of the program "Development of engineering, technology and scientific research in the field of atomic energy until 2024".

References

1. M. K. A. Thumm, G. G. Denisov, K. Sakamoto and M. Q. Tran, "High-power gyrotrons for electron cyclotron heating and current drive", Nucl. Fusion, vol. 59, no. 7, Jul. 2019.
2. M. Fukunari, K. Komurasaki, Y. Nakamura, Y. Oda and K. Sakamoto, "Rocket propulsion powered using a gyrotron", J. Energy Power Eng., vol. 11, no. 6, pp. 1–10, Jun. 2017.
3. L. J. Wong, A. Fallahi and F. X. Kartner, "Compact electron acceleration and bunch compression in THz waveguides", Opt. Exp., vol. 21, no. 8, pp. 9792–9806, 2013.
4. V. S. Ergakov and M. A. Moiseev, "Theory of synchronization of oscillations in a cyclotron-resonance maser monotron by an external signal", Radiophys. Quantum Electron., vol. 18, no. 1, pp. 89–97, Jan. 1975.
5. V. L. Bakunin, G. G. Denisov and Y. V. Novozhilova, "Frequency and phase stabilization of a multimode gyrotron with megawatt power by an external signal", Tech. Phys. Lett., vol. 40, no. 5, pp. 382–385, May 2014.
6. Andrey N. Kuftin; Gregory G. Denisov; Alexey V. Chirkov; Mikhail Yu. Shmelev; Vladimir I. Belousov; Andrey A. Ananichev; Boris Z. Movshevich; Irina V. Zotova; Mikhail Yu. Glyavin "First Demonstration of Frequency-Locked Operation of a 170 GHz/ 1 MW Gyrotron", IEEE Electron Device Letters. Volume: 44, Issue: 9, September 2023. doi.org/ 10.1109/LED. 2023.3294755.

Nonlinear processes in beam-plasma system at pumping plasma waves by high-current REB

A. V. Arzhannikov[1,2]

[1] Budker Institute of Nuclear Physics SB RAS, Novosibirsk, Russia, press@inp.nsk.su
[2] Novosibirsk state university, Novosibirsk, Russia, press@nsu.ru

The necessity to study pumping plasma electron waves in by a high current (≥ 10 kA) relativistic electron beam (REB) is associated with a wide range of its results applications. For example, the absorption of these waves by plasma electrons allows heating plasma up to thermonuclear parameters and the transformation of the plasma waves into electromagnetic ones gives possibility to generate radiation fluxes in various frequency ranges. This report provides an overview of research conducted in these two areas of using the beam-plasma interaction process over the past fifty years.

For the first time, the process of beam-plasma interaction was considered to explain radiation fluxes coming from cosmic objects. The authors of [1, 2] did start of systematical theoretical study on the problem of pumping plasma waves. In [1] this research was done for the case of homogeneous plasma at the hydrodynamic and the kinetic stages of the two-stream instability. The kinetic stage of the instability was investigated in [2] in more detail with paying principal attention to that, the inhomogeneity of the plasma limits the amplitude of the plasma wave pumped by a beam. In the case of a homogeneous plasma, at the ratio of beam electrons concentration to the plasma one lower then 10^{-4}, the amplitude of Langmuir waves is limited by nonlinearity in the weakly turbulent regime [3]. At these conditions, the waves, scattered by ion-acoustic oscillations, are transformed into electromagnetic radiation at the plasma frequency [3]. At the ratio of beam electrons concentration to the plasma one above 10^{-3} the plasma oscillations achieve so high level amplitude, when strong Langmuir turbulence develops [4, 5] and a rapid transfer of Langmuir waves across the spectrum to the region of large wave numbers is realized. Under these conditions, electromagnetic radiation near harmonics of the plasma frequency can arise due to the processes of scattering of Langmuir oscillations on forced fluctuations of the plasma density associated with the development of modulation instability. The radiation with frequency near these harmonics escape from the plasma due to the merging of high-frequency oscillations of the wave turbulent spectrum not locked into caverns [6] and as result of highly nonlinear processes inside collapsing caverns [5].

In the presence of a strong magnetic field in the plasma, when the electron cyclotron frequency approaches the Langmuir frequency, the magnetic addition to the dispersion of plasma oscillations becomes significant. In this case, beam-plasma interaction should be considered based on pumping plasma oscillations of the upper hybrid branch, and when calculating the probabilities of various nonlinear processes involving these oscillations, it is necessary to take into account the influence of the magnetic field [7, 8]. Experiments at the ratio of beam electrons concentration to the plasma one above 10^{-3} were started at the INAR device when injection beam electrons had angular spread on a level 0.5 rad and energy transfer from the beam to the plasma was low [9]. Decrease in the angular spread of beam electrons propagating in plasma down to 0.1 rad gave establishing conditions for achieving high amplitudes of upper-hybrid plasma waves and realization of strong Langmuir turbulence regime in time of beam propagation in plasma column [10, 11]. Beam energy lost due to deceleration of the beam electrons on resonant plasma waves has achieved 35% in these experiments. Mentioned experiments were carried out at beam pulse duration about 100 ns. The next series of experiments on E-beam heating the magnetized plasma, that was accompanied strong nonlinear phenomena, were conducted at the GOL-3 facility for the beam pulse duration 10 μs [12].

It was on this GOL-3 installation that the first series of experiments on the generation of radiation fluxes at harmonic frequencies of plasma oscillations was carried out [13, 14], since the parameters of the REB and the plasma column were suitable for the generation of electromagnetic radiation (see [7–9]). Detail research of the generation of radiation fluxes in a beam-plasma system for frequency range 0.1–0.5 THz has been conducted at the GOL-PET facility [15, 16]. The spectral composition of the generated radiation fluxes, as well as the evolution of beam electrons energy distribution function due to the beam relaxation in the plasma have been measured for various parameters of these experiments.

References

1. Ya. B. Fainberg et al., *JETP*, 57, 966 (1969).
2. B. N. Brelzman and D. D. Ryutov, ibid. 57, 1401 (1969).
3. V. N. Tsytovich, Theory of turbulent plasma, M.: Atomizdat, 1971 (in Russian).
4. L. I. Rudakov, *JETP*. 1970. T. 59. P. 2091.
5. V. E. Zakharov, Fundamentals of plasma physics. M.: Atomizdat, 1984. T. 2 (in Russian).
6. E. N. Kruchina et al., *JETP Let.*, 1980. T. 32, no. 6. p. 443.
7. A. V. Arzhannikov, I. V. Timofeev, *Plasma Phys. Controlled Fusion*,. 2012. Vol. 54, № 10. P. 105004.
8. I. V. Timofeev, V. V. Annenkov, A. V. Arzhannikov, *Physics of Plasmas*. 2015. T. 22. № 11.
9. Yu. I. Abdrashitov et al., *JETP*, 1974, vol. 66, p. 1324–1337.
10. A. V. Arzhannikov et al., *Physica Scripta*, 1982, V. T2'2, pp. 303–310.
11. L. N. Vyacheslavov et al., *JETP Letters*, 75:1 (2002), 44.
12. A. V. Arzhannikov et al., *Fusion Tech*. 1999. **35**. T. 1. P. 146.
13. A. V. Arzhannikov et al., *Vestnik Novosibirsk State University. Series: Physics* **5,** 44 (2010).
14. A. V. Arzhannikov et al., *Physics of Plasmas*. **21**, 082106, 2014.
15. A.V. Arzhannikov et al. *Plasma Physics and Control. Fusion*, 2020, PPCF-102698.
16. A. V. Arzhannikov et al., *Plasma Physics Reports*. 2024. T. 50, № 3, pp. 331–341.

The effect of accumulation of non-uniformity of the electric field and initiation of the L-H transition during the development of the Geodetic Acoustic Mode in a tokamak

L. G. Askinazi, G. I. Abdullina, A. A. Belokurov, V. A. Kornev, S. V. Lebedev, D. V. Razumenko, A. S. Tukachinsky and **N. A. Zhubr**

Ioffe Institute, St Petersburg, Russia, Leonid.Askinazi@mail.ioffe.ru

In this presentation, the issue of non-linear interplay between an oscillating radial electric field and turbulent transport in a tokamak is addressed. The framework adopted in this work uses transport equations with transport coefficients depending on inhomogeneity of the rotational velocity ω^{eff}_{ExB}, i.e. for particle diffusion in a form

$$D_{eff}(r,t) = D_{ANO}(r)\cdot\left(k(r)+\frac{1}{1+\left(\omega^{eff}_{E\times B}(r,t)/\gamma\right)^2}\right). \quad (1)$$

A model for switching the plasma confinement mode under the influence of oscillating radial electric field in the presence of the geodetic acoustic mode (GAM) is proposed and compared with observations made at several tokamaks.

This type of oscillations in the toroidal plasma is observed in many devices, both the tokamaks and stellarators. The source of free energy that feeds the GAM is thought to be a non-linear interaction of relatively high-frequency (~100–500 kHz) components in the spectrum of drift turbulence. The GAM itself does not drive radial flows of particles and energy in a toroidal fusion device, but it can affect the transport coefficients, since it acts as a regulator of the intensity of fluctuations that cause anomalous transport. The influence of the GAM on the level of anomalous transport is due to the high value of shear ω^{eff}_{ExB} (radial inhomogeneity of the *ExB* poloidal rotation velocity) in the GAM localization region.

In the TUMAN-3M tokamak, GAM manifests itself as a spatially localized oscillation of the radial electric field with a relatively low frequency of $\sim(1/R)(T_e/m_i)^{0.5} \sim$ 20–30 kHz, together with the associated weak perturbation to the plasma density [1]. Earlier, in experiments on the TUMAN-3M tokamak it was found [1] that a burst of intense GAM usually occurs immediately before the transition to the improved confinement mode, the so-called L-H transition. Using gyrokinetic calculations, the influence of GAM oscillations on the turbulence level and anomalous flux was confirmed [1]. The model proposed in [2] accounts for the GAM influence of the turbulence level, the modification of the transport due to the change in turbulence level, and effect of pressure gradient on steady state radial electric field and total (mean plus oscillating) E_r shear. Despite the fact that the magnitude of the electric field non-uniformity fluctuates with the GAM frequency, the effect of confinement improvement can accumulate on average over time and eventually lead to a transition to the self-sustaining H-mode.

To make modeling as close to the real experiment as possible, some important parameters of the GAM burst were taken from HIBP measurements (i.e., frequency and duration of the burst, and the amplitude of plasma potential perturbation), others, such as spatial localization, were provided by doppler reflectometry.

The conditions under which this occurs have been analyzed, and the role of not only the shear of the poloidal rotation, but also the intensity of the ionization source of particles has been revealed [4].

Whether the L-H transition is initiated by a GAM burst or not, depends on a combination of amplitude, frequency and other parameters of the GAM and the background plasma [3]. It was found, that the transition to the self-sustained high confinement mode in the TUMAN-3M tokamak may be triggered by a burst of GAM with parameters close to the observed in the experiment. If the GAM frequency is too high, or the amplitude is too low, the improvement in the confinement is only transient, and plasma goes back to the ordinary (low) confinement regime after the end of the GAM burst. On the other hand, even this “under threshold” GAM bursts may trigger the L-H transition if they go in a series, as it frequently observed on the TUMAN-3M.

The developed model, with some modifications, has been used to describe the L-H transition in other operating modes of the TUMAN-3M tokamak (mode with injection of a cryogenic macroparticle) [5] and to simulate the mode of good confinement in deuterium plasma at another FTI tokamak, FT-2 [5, 6]. Recently, a modified version of the model was used for the analysis of the L-H transition triggered by a Limit Cycle Oscillations in the Globus-M tokamak [8].

Acknowledgements

The experimental studies were supported by the Contract between the Ioffe Institute and the RF Ministry of Science and Education (0040-2024-0028). The investigation of the role of the oscillating ra-dial electric field was performed with the support of the RSCF grant 22-12-00062.

References

1. L. G. Askinazi et al., Plasma Phys. Control. Fusion (2017) 59 014037.
2. G. Abdullina, L. Askinazi, A. Belokurov et al., AIP Conference Proceedings 2179, 020002 (2019).
3. A. A. Belokurov, G. I. Abdullina, L. G. Askinazi et al., Tech. Phys. Lett., v. 45, 8, 2019, p. 783–785.
4. Bakharev, et al., Nucl. Fusion 59 112022 (2019).
5. A A Belokurov et al, Phys. Scr. 95 115604, (2020).
6. Denis V. Kouprienko et al., Nucl. Fusion, v. 62, 6, 2022.
7. A. A. Belokurov, L. G. Askinazi, V. K. Gusev, et al., *accept- ed for publication in* Fusion Science and Technology, 2024, DOI: 10.1080/15361055.2024.2362530.

Concept of a compact EUV FEL with a micro-undulator

I. V. Bandurkin, **A. E. Fedotov, P. V. Loginov, N. Yu. Peskov** and **A. V. Savilov**

A.V. Gaponov-Grekhov Institute of Applied Physics of the Russian Academy of Sciences,
Nizhny Novgorod, Russia, iluy@ipfran.ru

Recently, a design of a pulsed micro-undulator was proposed and experimentally tested [1], allowing the achievement of an undulator parameter of about 1 with a period as short as 1 mm. Such a micro-undulator, combined with compact sources of high-density accelerated electron beams like plasma wakefield accelerators, opens up the possibility to create compact extreme ultraviolet (EUV) free-electron lasers (FELs). The short undulator period allows to significantly reduce the wavelength of the generated radiation:

$$\lambda = \frac{\lambda_u}{2\gamma^2}(1 + K_{rms}^2),$$

where γ is the relativistic factor of electrons, K_{rms} is the undulator parameter, and λ_u is the undulator period. At the same time, the large undulator parameter leads to a high Pierce parameter ρ and, consequently, to a large FEL spatial increment in the SASE regime [2]:

$$\Gamma = \frac{4\pi\sqrt{3}\rho}{\lambda_u}.$$

This allows efficient lasing even with electron beams having an energy spread of several percent, comparable to the Pierce parameter.

Micro-Undulator Design and Testing

The primary challenge in designing a micro-undulator is ensuring the required undulator parameter. Since the undulator parameter is proportional to the amplitude of the synchronous spatial harmonic of the vector potential, $K = eA/mc^2$, the necessary amplitude of the magnetic field increases inversely with the period,

$$B_{rms} = \frac{2\pi}{\lambda_u} A_{rms},$$

and for $\lambda_u = 1$ mm and $K_{rms} \approx 1$ reaches the value of about 10 T. Such magnetic field values cannot be achieved with permanent or induced magnet systems, as the saturation field of all ferromagnetic materials is limited to about 2 T, and the induction of magnetic materials does not exceed a few Tesla. Calculations of periodic conductive structures creating the undulator field by inducing eddy currents in a rapidly changing strong uniform magnetic field also show that the achievable field amplitudes are much lower than required.

Fig. 1. Photo of the micro-undulator plate with a period of 1 mm used for the electric and mechanical durability tests

The proposed in [1] pulsed micro-undulator consists of two thin copper plates with periodic counter-cuts, creating a curved path for the undulator current flowing along the plates (Fig. 1). The design ensures high mechanical and thermal stability, allowing the operation at a frequency of up to 10 Hz. For the undulator period of 1 mm, the undulator parameter of about 1 is achieved with a current of approximately 8 kA. The capability of the design to withstand such a high current during pulses of several microseconds was demonstrated experimentally.

EUV Laser Simulation

Simulation of an EUV laser with such an undulator was conducted using the specialized code Genesis 1.3 [3]. It showed (Fig. 2) that electron bunches with particle energy around 100 MeV, a current of 10 kA, and a transverse size of several microns, obtained in a wakefield accelerator, can provide significant amplification even with an energy spread of a few percent.

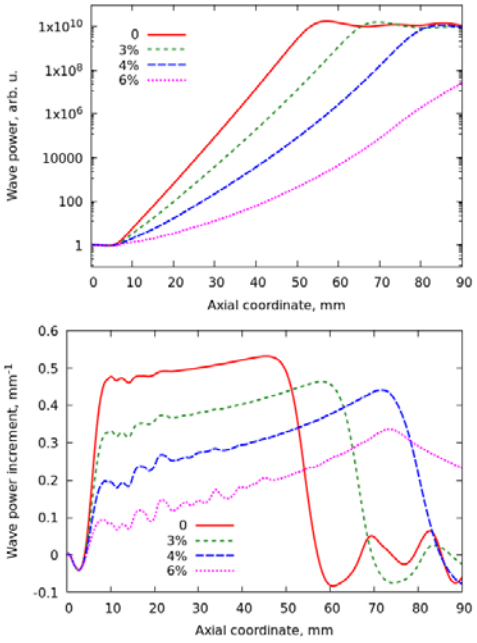

Fig. 2. Simulation results. Wave power (top panel) and wave power increment (bottom) for various electrons energy spread

Acknowledgements

The work is supported by the Russian Science Foundation, project No. 21-72-30027.

References

1. Bandurkin I. V. et al. *Radiophys. Quantum Electron*, 2024. doi: 10.1007/s11141-024-10313-y.
2. Freund H. P., Antonsen T. M. "Principles of Free-Electron Lasers." 2nd ed. London: Chapman and Hall, 1996.
3. https://genesis.web.psi.ch/

Intense ion beams of rare enriched isotopes for SHE synthesis

S. L. Bogomolov, V. E. Mironov, A. G. Popeko and **D. K. Pugachev**

Joint Institute for Nuclear Research, Dubna, Russia, sbogomolov@jinr.ru

The discovery of new superheavy elements (SHE) with Z = 114÷118 was one of the most bright scientific results of the last decade [1]. The synthesis was performed in complete fusion reactions of a double-magic-number ^{48}Ca nucleus with neutron-excess actinide nuclei such as ^{242,244} Pu, ^{243}Am, ^{249}Cm, ^{249}Bk, and ^{249}Cf.

The direct synthesis of the elements with Z > 118 in fusion reactions involves the transition to bombarding nuclei heavier than Ca, since the capabilities of producing target materials in nuclear reactors are limited by the production of Cf isotopes. The cross sections of the formation of nuclei with Z = 119 and with Z = 120 are expected to be about 10–20 times lower than the cross section of the formation of SHE isotopes in experiments with ^{48}Ca. To study the nuclear-physical and chemical properties of the SHEs more thoroughly, the efficiency of the experiments has to be increased significantly.

To solve this problem a new cyclotron DC-280 was put into operation at the G.N. Flerov Laboratory of Nuclear Reactions [2] with planned beam intensities of up to 10 pμA of ions with average masses (A ~ 50) that is one order of magnitude higher than those produced at the U-400 cyclotron up to now.

Presently, the DC-280 is equipped with the permanent magnet DECRIS-PM ECR ion source with operating frequency of 14 GHz [3], capable to provide the intense ion beams in the medium mass range, more than 20 pμA of ^{48}Ca for example.

As mentioned above beams of rare isotopes (^{48}Ca, ^{50}Ti, ^{54}Cr etc.) are mainly used for the synthesis of SHE. As all these isotopes usually are available as a solid material in the form of oxides or metals, their neutrals feed into the source plasma is the prior condition to ionization. The use of new isotopes for the production of accelerated beams calls for searching for ways of optimization of the ECR source operation mode and the development of a material feeding technique. In case of rare isotopes, the crucial point is the efficiency. The long-term beam stability is also very important due to the fact, that experiments on the synthesis of SHEs are quite lengthy.

For production of ^{48}Ca ion beam the combination of microoven with “hot screen” is used at the FLNR for over 25 years [4]. This method also used with the DECRIS-PM source. For the moment, the maximum intensity of $^{48}Ca^{10+}$ achieved before the physical target reached 84 eμA with the intensity of 230 eμA extracted from the source. The data of material consumption are presented at different intensities of ^{48}Ca ion beam.

For production of ^{50}Ti and ^{54}Cr ion beams presently, we use MIVOC technique [5], which was successfully used at the U-400 cyclotron. At the DC-280 cyclotron the long term (about 2 months) experiment was performed with $^{54}Cr^{10+}$ beam, produced from the $^{54}Cr(C_5H_5)_2$ compound. The average intensity on the target was kept at the level of 2 pμA according to requirements of experiment with rather good stability.

For production of ^{50}Ti ion beams the same method was used with $(CH_3)_5C_5Ti(CH_3)_3$ compound. For the moment with the injected Ti beam of 5 pμA the accelerated beam reached up to 2 pμA.

Also, the test experiments on production of Ti ion beam using SF_6 plasma with titanium foil were performed. Up to 60 eμA of $^{48}Ti^{11+}$ were produced from the source for tuning, and then accelerated beam of $^{48}Ti^{10+}$ was produced with the intensity of 30 eμA and good stability.

Except the MIVOC technique for production of ions of solids we are also developing the inductive oven for DECRIS-PM source. The preliminary results of the off-line tests will be presented.

To extend desired mass and energy ranges and the beam intensity in the DC-280 cyclotron 28 GHz ECR ion source is under construction at FLNR JINR [6]. According to working diagram of the DC-280 cyclotron (Fig. 1), the mass range of the cyclotron can be extended up to U with the energies suitable for SHE synthesis.

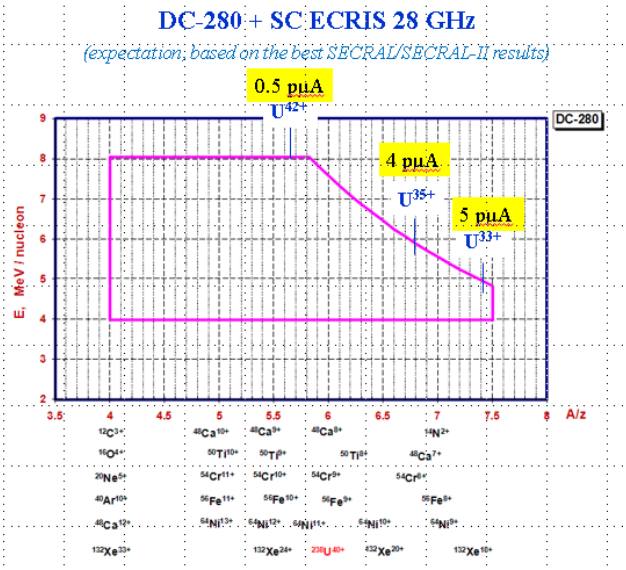

Fig. 1. Working diagram of the DC-280 cyclotron

Brief overview of the source subsystems and status of the construction will be given in the report.

References

1. Yu. Ts. Oganessian and V. K. Utyonkov, *Nucl. Phys. A* **944**, 62–98 (2015).
2. G. G. Gulbekian et al., *Physics of Particles and Nuclei Letters.* 2019. Vol. 16, No. 6, pp. 866–8753.
3. S.L. Bogomolov et al., *Physics of Particles and Nuclei Letters.* 2018, Vol. 15, No. 7, pp. 878–881.
4. V. B. Kutner et al. *Review of Scientific Instruments.* V. 71, N. 2 FEBRUARY 2000, pp. 860 – 862.
5. S.L. Bogomolov et al. *Physics of Particles and Nuclei Letters.* 2015. Vol. 12, No. 7, pp. 824–830.
6. V. Amoskov et al. *27th Russian Particle Acc. Conf. RuPAC2021, Alushta, Russia* doi:10.18429/JACoW-RuPAC2021-TUPSB35.

Microwave discharge in powder mixtures of mineralogical samples for plasma-dust cloud modelling

V. D. Borzosekov[1,2], N. S. Akhmadullina[3], N. N. Skvortsova[1]

[1] Prokhorov General Physics Institute of the Russian Academy of Sciences, Moscow, Russia, borzosekov@fpl.gpi.ru
[2] RUDN University, Moscow, Russia
[3] Baikov Institute of Metallurgy and Materials Science of the Russian Academy of Sciences, Moscow, Russia

When a mixture of dielectric and metal (or semiconductor) fine powders is exposed to microwave radiation of a gyrotron the microwave discharge can be initiated in the mixture [1]. Breakdown for this type of discharge is a rapid process that happens that happens within ~100 μs from the microwave pulse start with plasma filling the whole gaussian beam cross section in ~1 ms. Wave intensity necessary for the breakdown depends on the material of particles, fraction and size of conducting particles.

Microwave discharge in powder mixtures has been actively used for material science and chemical applications [2]. However, in [3] it was found that plasma-dust cloud forming during the microwave discharge in powder mixtures is suitable for laboratory modelling of various plasma-dust occurrence in nature. Such examples of occurrence are micrometeroid high-velocity impact on lunar surface, meteoroid hyper-velocity motion in planetary atmosphere, protoplanetary disks, cometary plasma, or even lightning in a volcanic ash cloud.

For more precise modelling it is necessary to use as a target not just mixture of industry produced powders of oxides but minerals or actual matter of cosmic origin (e.g. meteorites). And in the present work we summarize our recent experiments with microwave discharge in mineralogical powder samples during their exposure to radiation of a gyrotron: 1) ilmenite concentrate; 2) lunar mare dust simulant LMS-1D; 3) Tsarev meteorite.

A gaussian beam with linearly polarized microwave radiation was used in the experiments. The beam diameter was ~6 cm at the location of the target, and typically used power was 300-400 kW. Gyrotron's frequency is 75 GHz. Microwave pulse duration somewhat differs for various targets: routinely a 6–8 ms single pulse is used, but some targets are exposed to the pulse train of 3 pulses (1–2 ms pulse duration, 6–10 ms pause). The idea behind the pulse train exposure mode is to implement a "dynamical" regime when during limited number of repetitions, the sample experiences more stages of fast heating and cooling down. To omit unnecessary details let's say that powder samples were located horizontally on the surface of the quartz disk at the bottom of the quartz cylinder. Radiation of the gyrotron was introduced to the cylinder vertically from the cylinder bottom and a plasma-dust cloud is created above the sample. Various gases at atmospheric or lower pressures can be used in the experiments.

Parameters of the discharge (plasma density, electron and gas temperatures) and its dynamics were studied with optical emission spectrometry, microwave absorption measurements and high-speed camera recording.

The ilmenite concentrate (ilmenite 95 %, rutile 3 %, zircon 0.4 %), and specifically ilmenite, was chosen as a sample for its widespread presence in planetary regoliths and meteoroids. Also, ilmenite has decent electrical conductivity when exposed to microwave radiation. The main goal of the experiment was to achieve the breakdown and further development of the discharge in the pure ilmenite concentrate without artificial addition of the metal powder. Such a breakdown will be reassuring in use of ilmenite (or mineral with similar electrical conductivity) in complex samples instead of artificial addition of metal powder. The experiment was carried out at air atmosphere.

The LMS-1D simulant copies the mineral composition (pyroxene, glass-rich basalt, anorthosite, olivine, ilmenite) of an actual lunar regolith from maria. For the goal of modelling a plasma-dust cloud after micrometeoroid impact on the lunar surface the metallic Mg powder was added to the LMS-1D simulant to achieve the breakdown. Argon at atmospheric pressure was used in the experiment. A study of prebiological synthesis is another goal for which the set of experiments was done. The goal was to create a plasma-dust cloud from matter with composition close to the meteoroids, for which the lunar regolith simulant is suitable as a first approach, in the medium of gases supposed for Earth's early atmosphere. Appropriate gas composition was achieved by addition of ammonium carbonate powder and its presumable decomposition at the first stages of the discharge onto CO_2, H_2O, NH_3. The experiment was carried out at starting argon atmosphere.

Even if the Tsarev meteorite called "stony" its class (L5 chondrite) supposes presence of iron, nickel and their alloys. Thus, beside obtaining a plasma-dust cloud from the actual cosmic sample it was crucial to achieve the microwave breakdown of the sample without artificial addition of the metal powder confirming sufficiency of the conducting phase.

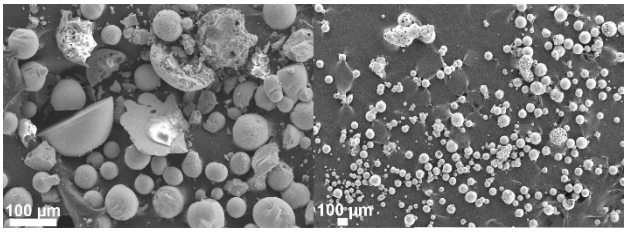

Fig. 1. SEM images of ilmenite and Tsarev samples

Scanning electron microscopy (SEM) and energy dispersive X-ray analysis (EDX) was done to find any morphological or phase transformations for most of the samples after the experiments. Spheroidization of particles is routinely observed (Fig. 1).

References

1. G. M. Batanov and I. A. Kossyi, *Plasma Phys. Rep.*, 2015, **41**, 847–857.
2. N. N. Skvortsova et al., *Ceram. Int.*, 2021, **47,** 3978–3987.
3. N. N. Skvortsova et al., *JETP Lett.*, 2019, **109**, 441–448.

Permanent micro-undulators from magnetized helices

V. L. Bratman[1], **N. Balal**[1] and **E. Magory**[2]

[1] Department of Electrical and Electronic Engineering, and the Schlesinger Family Center for Compact Accelerators, Radiation Sources and Applications (FEL), Ariel University, Ariel, Israel, v_bratman@yahoo.com
[2] Department of Electrical and Electronic Engineering, Jerusalem College of Technology, Jerusalem, Israel

All the existing X-ray Free Electron Lasers are gigantic and very expensive facilities based on the use of electron beams with energies of 5–18 GeV, accessible to a relatively small number of researchers. Many authors propose smaller, more affordable versions of XFELs with lower electron energies and smaller setup sizes. One of the key elements in all such projects is high-field micro-undulators. For example, in the concepts based both on advanced linear [1] and plasma wakefield [2] accelerators, these are permanent NdFeB micro-undulators with a period of down to 3 mm and a field of 1 T. To do this, it is proposed to use a planar structure of Halbach gratings [3], assembled not from individual magnets (Fig. 1 a), but from solid combs consisting of equally magnetized elements. In contrast to [1, 2], the article [4] and the present work consider helical Halbach-type undulators with sections assembled from helices, each of which, like the combs, is made of a single piece of ferromagnetic material. Compared to a planar system with the same gap for electron transport, a helical undulator provides a significantly larger root-mean-square electron oscillatory velocity. Due to this such undulators can provide higher radiation efficiency of compact XFELs.

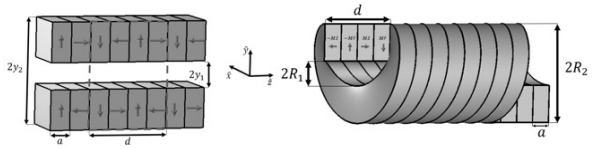

Fig. 1. a) Planar Halbach undulator consisting of eight identical rods for a period with alternating vertical and horizontal magnetizations [3]; b) Helical Halbach undulator comprising four identical helices with alternating axial and radial magnetizations [4]

Our proposed helical Halbach-type undulators [4], formed by four alternately axially and radially magnetized rare-earth helices (Fig. 2), could produce a stronger field than two planar Halbach undulators with perpendicular polarization. Hybrid undulators of two longitudinally premagnetized rare-earth helices and two initially unmagnetized steel (or vanadium permendur) helices produce an equal or higher field and are easier to implement.

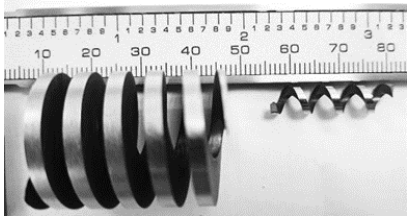

Fig. 2. NdFeB helices with a period of 6 mm and half (*left*) and quarter (*right*) period wide, manufactured by WEDM

High-quality NdFeB helices without internal holes and with a period of down to 1 mm, intended for other purposes, have been produced by Wire Electric Discharge Machining (WEDM) [5]. Together with us at Viteris Technologies LLC, Salt Lake City, Utah, USA, the same method was used to produce hollow helices for undulators [6]. We magnetized, assembled, and experimentally studied a short prototype undulator consisting of two such helices with a period of 20 mm, magnetized oppositely in the axial direction. We have recently also started working with micro-undulators having periods of 6 and 3 mm (Fig. 2). In addition, we demonstrated the operation of helical hybrid undulators on a simplified model formed by four quasi-helices consisting of helically arranged alternating sets of axially and radially magnetized ring sectors.

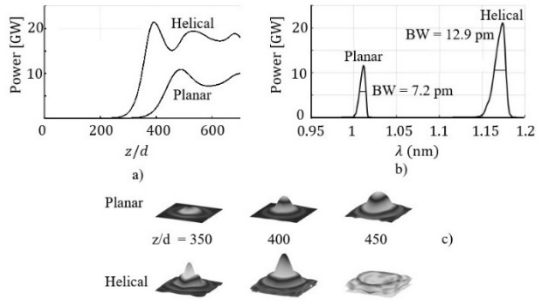

Fig. 3. Comparison of radiation power (a), spectra at maxima (b), and evolution of radiation intensity distribution (c) in a soft X-ray XFEL for helical and planar micro-undulators with field amplitudes of 1 T and a period of 6.5 mm and an 1-GeV electron bunch, focused by a periodic quadrupole FODO array

According to the simulations based on stationary version of Genesis [7], when using identical electron bunches with moderate initial spreads in energy and angles, the gain in power from replacing planar micro-undulators in XFELs with electron energy of 1 and 1.6 GeV and undulator period of 6.5 and 3 mm, respectively, designed in [1], with the helical micro-undulators can reach 1.8 (Fig. 3), which is significantly greater than predicted by the simplest 1D theory with a cold electron beam. This makes such micro-undulators promising for creating compact XFELs of various types.

References

1. J. B. Rosenzweig, N. Majernik, R. R. Robles, et al., *New J. Phys.*, 2020, **22**(9), 093067.
2. F. Habib, G. G. Manahan, P. Scherkl, et al., *Nat. Commun*, 2023, **14 (1)**, 1054.
3. K. Halbach, *NIMA*, 1981, **187(**1), 109–117.
4. E. Magory, N. Balal, and V. L. Bratman, *IEEE Trans. Electron Devices*, 2022, **69(**2**)**, 798–801.
5. J. Greer, A. J. Petruska, A. W. Mahoney, M. Nambi, E. Bamberg, and J. J. Abbott, *J. Mater. Eng. Perform.*, 2014, **23**(4), 1392–1401.
6. N. Balal, E. Bamberg, V. L. Bratman, and E. Magory, *IEEE Trans. Electron Devices*, 2023, **70** (11), 5911–5915. S. Reiche, *NIMA* A **429**(6), 243–248.

Mode conversion in electron cyclotron resonance region

P. A. Chuvakin, **E. D. Gospodchikov** and **A. G. Shalashov**

A.V. Gaponov-Grekhov Institute of Applied Physics of the Russian Academy of Sciences, Nizhny Novgorod, Russia,
p.chuvakin@ipfran.ru

Electron cyclotron resonance (ECR) plasma heating using microwave radiation is one of the most widely used methods for heating plasma in toroidal and axially symmetric magnetic traps. Theoretical approaches to studying this process typically exploit a significant difference in spatial scales, with wavelengths being much smaller than scales of inhomogeneities in plasma density, temperature, and external magnetic fields. This allows the use of geometric optics (ray tracing) or its extensions (beam tracing) for numerical modeling of ECR heating scenarios in fusion devices. However, these approximations break down near the resonance region due to the intrinsic nature of electromagnetic waves and their interactions with the plasma where non-geometric-optics effects such as mode coupling and spatial dispersion play a role in wave propagation and absorption.

The problem of the propagation of electromagnetic waves through the ECR region of in an inhomogeneous plasma is characterized by the combined effects of spatial dispersion (non-locality) and inhomogeneity, leading to complex interactions between electromagnetic: ordinary (O), extraordinary (X) and quasi-electrostatic Bernstein (B) waves [1]. As finite aperture microwave beam field distribution contains Fourier harmonics that propagate not strictly perpendicular an external magnetic field, the problem of oblique incidence of plane waves must be considered. In this case the ordinary and extraordinary mode coupling may be also important [2].

In this paper, we analyze the results of a full-wave numerical simulation of the X-polarized beam propagation through ECR region at the second harmonic in a weakly relativistic plasma. These results are applicable to large magnetic traps such as tokamaks and stellarators, where the scale of magnetic field inhomogeneity is significantly larger than the size of the resonance region. Under these conditions, it is possible to assume that the electron density and temperature and external magnetic field direction are all homogeneous, with the absolute value of the magnetic field growing linearly along the perpendicular axis in resonance region.

To solve Maxwell equations in anisotropic gyrotropic media with spatial dispersion, and to correctly take account for boundary conditions, we use the ‘impedance techique’ [3]. The boundary conditions are as follows: an X-wave with the unit amplitude enters the resonance region from the low magnetic field side ($2\omega_c < \omega$) and after the resonance region, at the high magnetic field side ($2\omega_c > \omega$) only the transmitted electromagnetic and exponentially decaying B-waves can exist. So, the mistake in boundary condtions may cause exponentially increasing error, and this is the very reason it’s required to accurately take into account the boundary conditions.

Figure 1 shows two examples of the calculated distributions of the electric field components inside the interaction region calculated at the same electron density and temperature for normal incidence [4]. In case (b) the magnetic field changes in space approximately three times faster than in case (a). The linear transformation of the waves can be seen in the appearance of the short-wave modulation of the longitudinal component of the electric field.

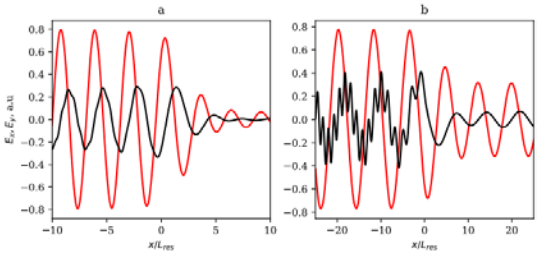

Fig. 1. Spatial distributions of the E_x (black curves) and E_y (red curves) components of the electric field

It may be shown that in case of normal incidence conversion efficiency depends only on normalized density $\upsilon = \omega_p^2/\omega^2$ and the dimensionless parameter $\kappa = \omega L_{res} / c$, where L_{res} – characteristic size of resonance region. Figure 2 shows the dependencies of the reflection coefficient R_X and conversion coefficient in Bernstein waves R_B on κ at several consecutively increasing values of υ. As one can see conversion efficiency is about 10% in dense enough plasma. This effect can change significantly absorption efficiency.

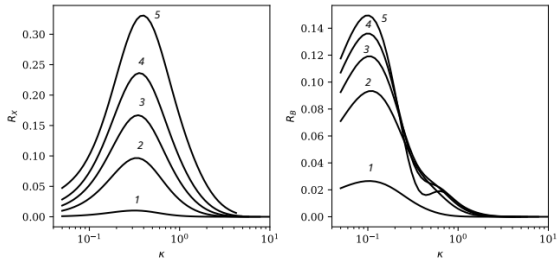

Fig. 2. Reflection coefficients into the extraordinary mode (*left*) and conversion coefficients into Bernstein wave (*right*)

Acknowledgments

The work was supported by the Russian Science Foundation (grant No. 19-12-00377).

References

1. A. V. Zvonkov, Sov. J. Plasma Phys., 1983, 9, 319.
2. M. Tereshchenko, Phys. Rev. E., 2023, **107**, 055209.
3. A. G. Shalashov and E. D. Gospodchikov, Phys.-Usp., 2011, 54, 145.
4. E. D. Gospodchikov, P. A. Chuvakin and A. G. Shalashov, Plasma Phys. Rep., 2023, **49**(10), 1151–1161.

Progress of antenna type miniaturized permanent magnet 2.45 GHz ECR ion source at Peking University

Bujian Cui, Shixiang Peng, Tenghao Ma, Wenbin Wu, Yicheng Dong, Zhiyu Guo and **Jiaer Chen**

State Key Laboratory of Nuclear Physics and Technology & Institute of Heavy Ion Physics, School of Physics, Peking University, Beijing, China, bjcuig@pku.edu.cn

2.45 GHz electron cyclotron resonance ion source has the advantages of intense current, low emittance, high stability, simple structure, low cost and long life. It is the primary choice for generating hydrogen ion beams. Many compact applications such as the compact neutron tube, ion thruster, EUVL cleaner and medical accelerator, require the miniaturization of hydrogen plasma sources. Therefore, the miniaturization of the 2.45 GHz ECR ion source is of great significance for its wide applications. Unfortunately, the miniaturization of ECR ion sources is limited by its RF transportation and microwave coupling. To miniaturize it, a new method for microwave coupling beyond ridge waveguide or microwave window is urgently needed. At Peking University (PKU), an antenna coupling type miniaturized 2.45 GHz ECR ion source with an inner diameter of 13 mm was developed. A photograph of the antenna type source body is shown in Fig. 1. Primary testing was done on PKU ion source test bench and an 8.5 mA hydrogen beam at 40 W microwave power was obtained. The fraction of proton is about 50 %. A 5 hours operation was done at 40 W, the high voltage load keeps at 8.5 mA, as shown in Fig. 2.

Fig. 1. Photograph of the 2.45 GHz ion source

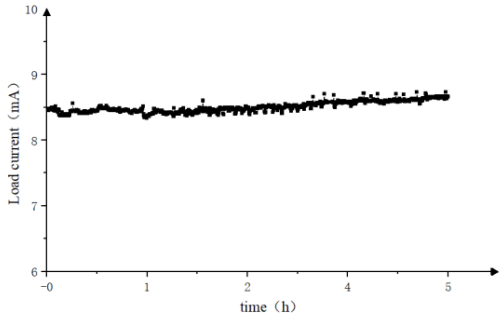

Fig. 2. Results of longtime running

Acknowledgements

This work was supported by the NSFC (Grant Nos.11975036, 11775007). The authors would like to thank the colleagues who participated in fruitful discussions, and all the component manufacturer.

References

1. Cui, B., Peng, S., Wu, W., Ma, T., Jiang, Y., Guo, Z., & Chen, J. (2023). Improvement of miniaturized 2.45 GHz ECR plasma flood gun at PKU. Journal of Instrumentation, 18(10), P10038.
2. Peng, S. X., Ma, T. H., Wu, W. B., Cui, B. J., Zhang, A. L., Jiang, Y. X., ... & Chen, J. E. (2023). New progress of the miniaturized microwave ion source at Peking University. Radiation Detection Technology and Methods, 7(4), 545–549.

Basic research with Electron String Ion Sources (ESIS)

E. E. Donets, **A. Yu. Ramsdorf** and **D. N. Rassadov**

Laboratory of High Energy Physics, Joint Institute for Nuclear Research,
Dubna Moscow reagion, 141980, Russia, edonets@jinr.ru

The electron string ion source (ESIS) "Krion-6T" is the main operational device for producing multicharged heavy ions for the NICA injector (ion collider based on a Nuclotron). This type of ion sources was first proposed and created at the JINR Laboratory of High Energy Physics [1, 2] as a new approach in the development of the electron beam ionization method, previously successfully implemented in electron beam ion sources (EBIS) [3].

Recently, $^{124}Xe^{28+}$ ion beams, produced with «Krion-6T» ESIS were accelerated in the HILAC (Heavy Ion Linac)-Booster (booster synchrotron)-Nuclotron (synchrotron) complex in framework of the 4-th stage of commissioning of the NICA injector. Further development of the ion source requires the production of $^{176}Yb^{30+\div32+}$, $^{197}Au^{31+\div32+}$, $^{209}Bi^{35+\div37+}$ … up to $^{238}U^{40+\div42+}$ ion beams and their multiple injection through RFQ-HILAC into Booster and Nuclotron. Some aspects of possible technologies for injecting vapors of these heavy elements (or their corresponding chemical compounds) into a cryogenic ion trap of an ion source will be briefly considered.

Despite the successful practical use of ESIS-type ion sources in injection complexes of synchrotrons, the basic physical processes underlying their operation remain the subject of fundamental research. Indeed, the key physics ingredient was discovered in a reflex mode of EBIS operation – a stable state of hot magnetized pure electron plasma, which was called electron string [4]. The interest to the reflex mode of EBIS operation studies was motivated first by an attractive possibility to decrease the power of electron beam by a hundred times while simultaneously preserving ion yield. It was found that under certain conditions one component pure electron plasma, which consists of the multiply reflected electrons, confined in a strong solenoidal magnetic field, exhibits properties similar to a phase transition. This transition to the electron string state leads to a stepwise increase of the confined electron plasma density, as well as an increase of a total number of an accumulated electrons. Thus, electron strings provide considerable electron trap capacities and effective electron current densities in order to get intense beam of highly charged ions.

Electron string formation, frames of it's stability, frames of their capacity and effective current density will be discussed with use of the obtained experimental data and several model considerations.

One of the most interesting features is the conversion of a pure electrical circuit into an electronic string filled with ions. This task will be considered in more detail, since it is directly related to the limitations of ion yield.

Additional self-compression of the electron string when it is filled with ions was observed experimentally under various conditions. Thus, natural questions arise about the upper limit of the effective current density of an electron string filled with ions, and whether it is possible to approach a corresponding Brillouin limit in this way.

Finally, the design of an ion trap for studying nuclear fusion reactions between fully ionized bare nuclei will be described [5].This tubular type Electron Strung Ion ion trap is under construction now.

References

1. A. Yu. Boytsov, D. E. Donets, E. D. Donets, E. E. Donets, K. Katagiri, K. Noda, D. O. Ponkin, A. Yu. Ramsdorf, V. V. Salnikov and V. B. Shutov, *Rev. Sci. Instrum.*, 2015, **86**, 083308-1–083308-5.
2. E. D. Donets, *Rev. Sci. Instrum.*, 1998, **69(2)**, 614–619.
3. E. D. Donets, *IEEE Trans. Nucl. Sci.*, 1976, **23,** p. 897.
4. D. E. Donets, E. D. Donets, E. E. Donets, V. V. Salnikov and V. B. Shutov, J. of Instrumentation (Conference Series), 2010, **5(09)**; DOI: 10.1088/1748-0221/5/09/C09001.
5. T. Itahashi, N. Kudomi, E. D. Donets and E. E. Donets, *Rev. Sci.Instrum.*, 2002, **73(2)**, 667–669.

Development of compact low-voltage medium-power millimeter-wave gyrotron and transmission line

Wenjie Fu[1], **Mikhail Glyavin**[2], **Dun Lu**[1], **Alexey Fedotov**[2], **Tao Zhu**[1], **Mikhail Proyavin**[2] and **Yang Yan**[1]

[1] Terahertz Science and Technology Key Laboratory of Sichuan Province, School of Electronic Science and Engineering, University of Electronic Science and Technology of China, Chengdu, China, fuwenjie@uestc.edu.cn

[2] A.V. Gaponov-Grekhov Institute of Applied Physics of the Russian Academy of Sciences, Nizhny Novgorod, Russia

With the development of millimeter-wave technology, the millimeter-wave power applications attract researchers' highlight attention. The higher frequency of millimeter waves compared to microwaves results in different physical processes in the processed materials, which opens new opportunities for applications. Gyrotrons are the most competitive millimeter-wave power sources that provide up to megawatts of radiation in the continuous-wave mode and are extensively used for plasma heating. For industrial millimeter-wave power applications, such as material processing, the demand typically revolves around medium power levels ranging from kilowatts to hundreds of watts and, in some cases, even at the watt level. Therefore, gyrotron could operate at low voltage, that could sufficiently reduce size and cost of both the tube and power supply unit. Meanwhile, its safety would be improved.

To develop the compact low-voltage medium-power millimeter-wave gyrotron, University of Electronic Science and Technology of China (UESTC) and Institute of Applied Physics of the Russian Academy of Sciences (IAP-RAS) conducted collaborative studies. A 30 GHz compact low-voltage TE_{01} mode gyrotron is developed and which is operated using a 4.2 kV microwave oven magnetron transformer as a high-voltage power supply unit. A recorded output power of 140 W with an interaction efficiency of 11.9 % at a frequency of 30.192 GHz was achieved with a beam voltage below 5 kV. Remarkably, even at an extra-low voltage of 1.9 kV, a power output of 5.0 W was observed.

In power application, the compact and economic transmission line is also need. Then, the TE_{01} mode compact cylindrical waveguide is investigated to be the transmission line for applications. To measure the transmission power and reflection power in the transmission line, a Ka-band compact circular waveguide directional coupler for TE_{01} mode is proposed and developed. In this design, the main waveguide is cylindrical waveguide, the secondary waveguide is rectangular waveguide, and an orthogonal connection between the main and secondary waveguides is adopted. To improve its performance, three metal stubs is loaded on the isolating port of the coupler. Both the simulation and experimental results show, through adjusting the metal stubs on the isolating port, the performance of the directional coupler can be improved, meanwhile, the TE_{01}° mode maintains good transmission efficiency.

To further reduce the system size, a non-superconducting magnet for millimeter wave gyrotron is designed and under developing.

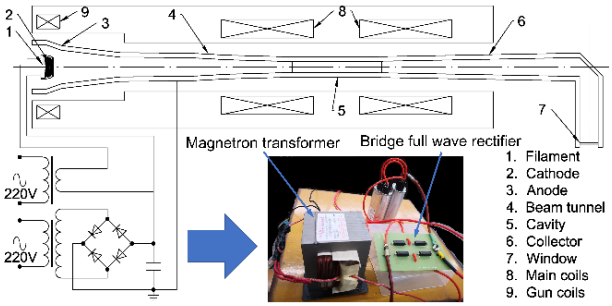

Fig. 1. Scheme of the compact low-voltage gyrotron with power supply

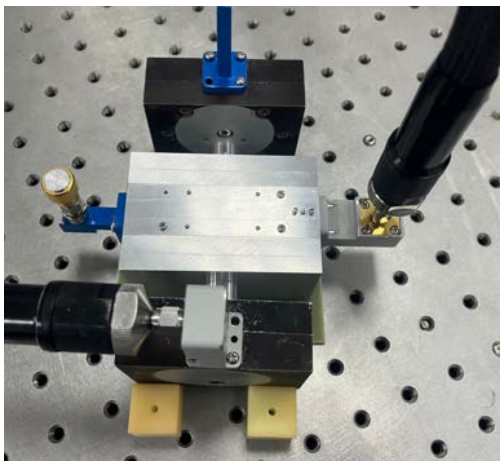

Fig. 2. The photo of the measurement of the fabricated sample

References

1. D. Lu, W. Wenjie, M. Glyavin, A. Fedotov, M. Proyavin, Y. Yan, Ultimate transverse power of pulsed low-voltage gyrotron beam, *Physics of Plasmas*, 2022, 29(9), 093107.
2. D. Lu, W. Wenjie, M. Glyavin, A. Fedotov, Q. Zeng, Y. Pan, Y. Yan, Demonstration of a Low-Voltage High-Efficiency Continuous-Wave Millimeter-Wave Gyrotron, *IEEE Transactions on Electron Devices*, 2024, 71(5), 3228–3231.
3. T. Zhu, W. Fu, D. Lu, Y. Pan, C. Li, L. He, H. Sun, Y. Yan, A Compact Circular Waveguide Directional Coupler for High-Order Mode Vacuum Electronic Devices, *Electronics*, 2024, 13(3), 633.

Optimization of synthesis processes in plasma-chemical chain reactions in Ti-(c)BN/(h)BN and Ti-B powder mixtures initiated by gyrotron radiation

T. E. Gayanova[1], E. A. Obraztsova[1,2], A. S. Sokolov[1], I. R. Nugaev[1], N. N. Skvortsova[1]

[1] Prokhorov General Physics Institute of the Russian Academy of Sciences, Moscow, Russia, tatyanagayanova97@gmail.com
[2] Moscow Institute of Physics and Technology (National Research University) Dolgoprudny, Moscow oblast, Russia

In experiments to optimize the synthesis of boron nitride microstructures using a powerful gyrotron in chain plasma-chemical reactions in air, it was shown that hydrogen-containing additives to metal-dielectric powder mixtures contribute to the development of exothermic processes (the main stage of the chain synthesis process) in the reactor with an increase in synthesis products [1].

It has been shown that synthesis in chain processes with maximum yield of substances is possible using the $B_{10}H_{10}C_2H_2$ additive with (c)BN. In the process of chain synthesis under certain modes of exothermic processes (the main phase of the process), depending on the chemical composition of the powder mixtures ((c)BN + 20%Ti + + 0.026g $B_{10}H_{10}(Et_3NH)_2$, (c)BN + 20% Cu), a transition occurred cubic phase of boron nitride into the hexagonal phase (Figure 2) [2]. The process was initiated at a microwave power of 400 kW and a pulse duration of 4 ms.

The different types of particle surfaces observed in the after samples cannot be obtained by melting or oxidizing the original particles in Ti/B/N systems. This indicates that the evaporation and subsequent condensation of materials occurs during the synthesis process in plasma-chemical reactions.

Together with data on the formation of hexagonal BN particles from a cubic form in a precursor powder, these results confirm that new materials are synthesized in chain plasma-chemical oscillating reactions initiated by a gyrotron discharge (synthesis example in Figure 1).

Table 1

Change in the mass of some substances after the experiment

Compound	Mass before synthesis, g	Mass after synthesis, g	Mass increase, g
cBN+20%Ti+ $B_{10}H_{10}C_2H_2$	1,52	1,698	1,117105
hBN+20%Ti+$B_{10}H_{10}$	1,512	1,571	1,039021
hBN+20%Ti+$B_{12}H_{12}$	1,543	1,643	1,064809

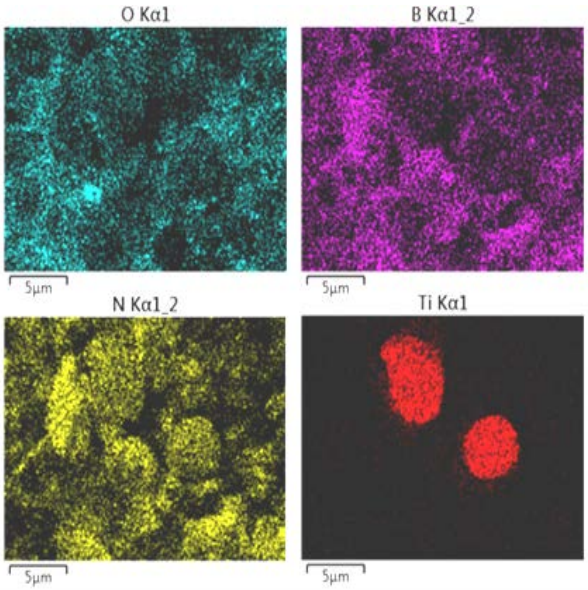

Fig. 1. Elemental composition of Ti-cBN powder after synthesis

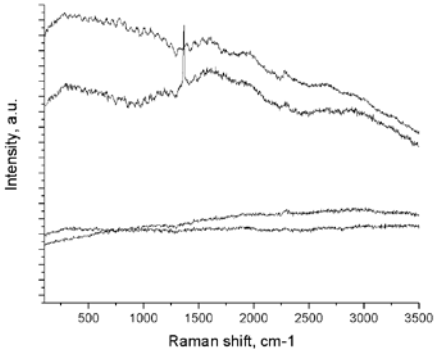

Fig. 2. Spectra of (h)BN after synthesis of the powder mixture (c)BN+20%Ti + 0.026g $B_{10}H_{10}(Et_3NH)_2$

References

1. G. M. Batanov and I. A. Kossyi, *Plasma Phys. Rep.*, 2015, **41**, 847–857.
2. T. E. Gayanova et al., *High Energy Chemistry*, 2023, Vol. 57, Suppl. 1, pp. S53–S56.

Progress in development of high power relativistic sources of coherent millimeter and sub-millimeter radiation

N. S. Ginzburg

A.V. Gaponov-Grekhov Institute of Applied Physics of the Russian Academy of Sciences, Nizhny Novgorod, Russia, ginzburg@ipfran.ru

Sources of coherent radiation based on stimulated emission of high-current relativistic beams have achieved record (gigawatt) values of pulse power in the centimeter and long-wavelength parts of the millimeter range [1–4]. Recently, there has been significant progress in the development of such sources in the short-wavelength part of the millimeter range with the prospect of moving into the submillimeter range. This report reviews recent advances in this area.

Three main types of promising sources can be distinguished. First of all, these are relativistic Cherenkov surface wave oscillators with traditional single-periodic and recently proposed two-dimensional periodic slow-wave structures [5]. On the basis of such oscillators, 150 GHz pulses with a peak power of up to 100 MW have already been experimentally obtained [6].

Simulations and the preliminary experiments show that the development of relativistic high-current gyrotrons, where power from 30 to 100 MW can be obtained at frequencies from 90 to 300 GHz, has significant prospects [7].

Apparently, free electron lasers (FELs), where electrons move in a periodic undulator field, should be considered as the shortest wavelength sources. Due to the Doppler effect, the radiation frequency can significantly exceed the frequency of electron oscillations in the specified field. At relatively moderate particle energies of up to 1–1.5 MeV typical for high-current beams, the possibility of generating multimegawatt radiation in the range up to 1 THz opens up the use of microundulators, recently implemented at the Institute of Applied Physics RAS [8]. In the case of traditional undulators with a period of 5–10 cm, it is worth noting the project of long-pulse FELs based on linear induction accelerators, developed jointly by the Institute of Nuclear Physics of RAS and the Institute of Applied Physic [9]. The implementation of long-pulse FELs will ensure the generation of sub-gigawatt pulses in the terahertz and sub-terahertz ranges.

Acknowledgements

This work was supported by the RSF project by the IAP RAS project FFUF-2022-0007.

References

1. N. F. Kovalev, *JETF*, 1973, **18**(4), 232–235.
2. A. N. Vlasov, A. G. Shkvarunets, J. S. Rodgers et al., *IEEE Trans. Plasma Sci*., 2000, **28**(3). 550–560.
3. S. P. Bugaev, V. A., Cherepenin, V. I. Kanavets et al., *IEEE Trans. Plasma Sci*., 1990,**18**(3), 525–536.
4. V. V. Rostov et al., *IEEE Electron Device Letters.* 2021. **42**. 935–937.
5. N. S. Ginzburg, A. M. Malkin, A. S. Sergeev, V. Yu. Zaslasky, *Appl. Phys. Lett.*, 2012, **100**, 143510.
6. N. Yu. Peskov, V. Yu. Zaslavsky et al., *Proc. of PIERS Chengdu*, China, 2024.
7. Y. Y Danilov, A. N. Leontyev, N. V. Leontiev et al., *IEEE Trans. Electron Devices*, 2021, **68**(4), 2130–2132.
8. I. V. Bandurkin, P. V. Loginov, N. Yu. Peskov et al., *Radiophys. Quantum Electron*., 2023, **66**, 529–537.
9. A. V. Arzhannikov, P. A. Bak, V. I. Belousov et al., *Radiophys. Quantum Electron.* 2020, **64**, 814–824.

High power cyclotron-resonance rectenna: “Inverted-gyrotron”

G. G. Denisov[1], I. V. Zotova[1], I. V. Zheleznov[1], R. M. Rozental[1,2], A. S. Sergeev[1], S. V. Samsonov[1], V. N. Manuilov[1,2] and **M. Yu. Glyavin[1]**

[1] A.V. Gaponov-Grekhov Institute of Applied Physics of the Russian Academy of Sciences, Nizhny Novgorod, Russia, glyavin@ipfran.ru
[2] Nizhny Novgorod State University, Nizhny Novgorod, Russia

Development of Wireless Power Transmission (WPT) is one of the important tasks of modern physics referring to remote power supply for different applications. One of the current trends in this area is associated with the use of directive beams of microwave radiation which allows significantly increasing the transmitted power. The key elements of microwave WPT systems are rectifiers that convert free-space radiation power into DC power. Currently, the most common type of microwave rectifiers are Schottky-diode rectennas, which, however, cannot withstand high levels of microwave power and have low output voltages (several volts).

An alternative concept of microwave rectennas is the use of the interaction of microwave radiation with a rectilinear electron beam under electron cyclotron resonance (ECR) conditions. To date, centimeter-wave ECR rectenna with operating frequency of 2.45 GHz and near-axis (“single-jet”) electron beams can provide high conversion efficiency (up to 80%) with a microwave input power of 10 kW and an output voltage of 15–20 kV [1]. At the same time, it is desirable to significantly increase the frequency and power of the received radiation. In particular, advancement into the millimeter wave range will makes it possible to significantly reduce the size of the transmitting and receiving antennas, improve the directivity of the microwave beams, and reduce transmission losses when using the atmospheric transparency windows.

At present, the most powerful (megawatt) continuous-wave millimeter-range radiation is generated by gyrotrons [2]. Recent theoretical and experimental studies on the gyrotron locking by an external signal [3] opens up an opportunity for creating complexes of a large number coherently operating MW-level gyrotron and antenna-phase arrays for transmitting extremely high power over long distances. To convert high-power high-frequency signals into DC current, we are considering the possibility of implementing ECR rectifiers with significantly increased frequency and power based on the proven principles of development of MW-level gyrotrons for plasma heating, which are based on the near-cutoff interaction of electron beams of large (on a wavelength scale) radius with high-order transverse modes of oversized cylindrical waveguides. The main difference from gyrotrons is the interaction with rectilinear (rather than rotating) electron beams to absorb radiation . Thus, the proposed design can be interpreted as an “inverted gyrotron” with a “multi-jet” rectilinear electron beam. The general view of such “inverted gyrotron” is presented in Fig. 1. In this report we present the principal design of a ECR rectenna for several frequency bands. In particular, for W-band (90 GHz) the tube with an operating mode $TE_{12.5}$ and received power of 1 MW has been discussed. According to simulations, the maximum efficiency of the rectenna can be more than 80% with output voltage of 150 kV (Fig. 2).

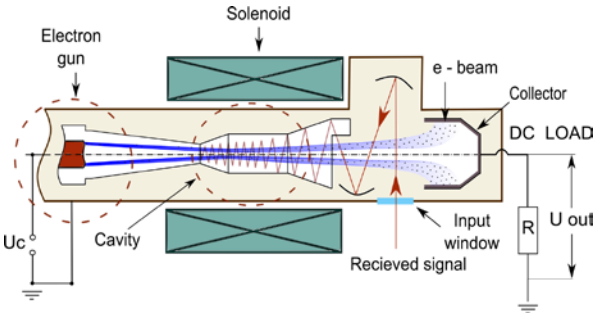

Fig. 1. The principal design of a ECR rectenna

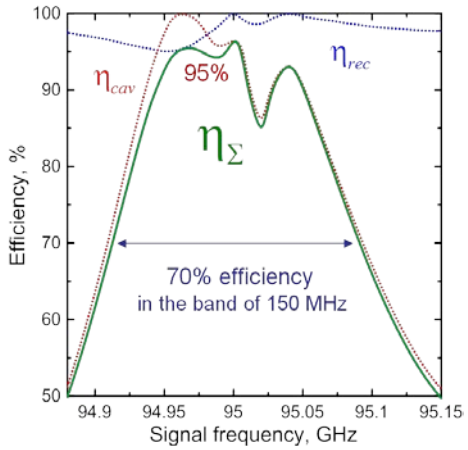

Fig. 2. Results of numerical simulations of rectenna efficiency. Here $\eta_\Sigma = \eta_{res}*\eta_{conv}*\eta_{rec}$; η_{res} – efficiency of conversion of microwave signal energy into electron rotation energy, η_{conv} – efficiency of converting the rotation energy of electrons into the energy of longitudinal motion, η_{rec} – efficiency of converting the energy of longitudinal motion of electrons into DC on the collector

Acknowledgements

This work was supported by the RSF project №19-79-30071 (prolongation).

References

1. Biao Hu et al., “A long-distance high-power microwave wireless power transmission system based on asymmetrical resonant magnetron and cyclotron-wave rectifier”, *Energy Reports* 7, 1154 (2021).
2. M. K. A. Thumm, G. G. Denisov, K. Sakamoto, M. Q. Tran, “High-power gyrotrons for electron cyclotron heating and current drive”, *Nucl. Fusion* 59, 073001 (2019).
3. A. N. Kuftin, G. G. Denisov, A. V. Chirkov, et al. “First Demonstration of Frequency-Locked Operation of a 170 GHz / 1 MW Gyrotron”, *IEEE Electron Device Letters*, 44(9), 1563–1566 (2023).

Studies of physical basis of jet propulsion using strongly nonequilibrium plasma of electron cyclotron resonance discharge

A. Abramov, S. Golubev, E. Gospodchikov, S. Vybin, I. Izotov, E. Kiseleva, V. Skalyga, A. Shalashov

A.V. Gaponov-Grekhov Institute of Applied Physics of the Russian Academy of Sciences, Nizhny Novgorod, Russia, ivizot@ipfran.ru

Currently, the movement and adjustment of Earth's artificial satellites' orbits is mainly provided by plasma ion engines, in which accelerated ions are used to generate reactive force. The principle of action of such engines is based on the ionization of the working gas, the extracting of ions from the plasma and formation of reactive force by their acceleration by electrostatic fields. One way of improving plasma engines is the development of electrode-free engines based on plasma magnetohydrodynamics, because they can provide the highest flow rate of the working substance, which allows to significantly increase the efficiency of its use and consequently extend the life of the satellites. An example of the most advanced and brightest engine development based on plasma magnetohydrodynamics is the most powerful VASIMR engine to date. In this engine, the plasma is created and heated in an open magnetic trap using the electromagnetic radiation of the RF-band, then when plasma flows through the magnetic nozzle its energy is converted into the energy of the directional movement of ions, providing reactive force.

This paper discusses one of the ways of improving modern plasma engines in which, unlike most existing schemes, using various methods of transfer of energy directly to ions (electrostatic acceleration of ions, heating of ions by RF fields under conditions of ion-cyclotron resonance with subsequent accelerations of ions in magnetic nozzle), it is proposed to use electron heating under conditions of electron cyclotron resonance (ECR) in collisionless mode [1]. In the ECR heating of transparent plasma, the energy of the microwave radiation is transferred mainly to the transverse energy component of the electrons in relation to the direction of the magnetic field until electrons are expelled from the resonance due to relativistic mass increase. Thus, the electron distribution function has a boundary energy (this energy can reach values at the level of hundreds of keV), and then drops sharply [2, 3], i.e. substantially non-maxwellian distribution function is realized. Then with adiabatic expansion of such plasma in a magnetic nozzle, there is transformation of the transverse energy of electrons into longitudinal, and due to the charge separation field there is acceleration of ions.

With continuous microwave heating, the stationary mode may be realized, in which electrons and ions have the same velocity at the magnetic nozzle, forming a quasi-neutral flow. At the same time, a potential gap is formed between the ECR zone and the magnetic nozzle, providing the deceleration of electrons and acceleration of ions. In this mode, the magnitude of the established potential gap is determined by the boundary energy of the electrons. As a result, the most part of electron energy is transferred to the kinetic energy of ions, thus forming a flow of plasma with ions accelerated to record energies at the level of hundreds of keV.

References

1. A. Abramov, S. Golubev, E. Gospodchikov, S. Vybin, I. Izotov, E. Kiseleva, V. Skalyga, A. Shalashov. Patent #2791084, “A plasma jet engine that uses plasma heated by powerful electromagnetic radiation flowing through a magnetic nozzle to create thrust, and a method for creating jet thrust”, 22.07.2022.
2. S. V. Golubev, I. V. Izotov, D. A. Mansfeld, and V. E. Semenov, Experimental electron energy distribution function investigation at initial stage of electron cyclotron resonance discharge Rev. Sci. Instrum. 83, 02B504; 2012, doi: 10.1063/1.3673012.
3. I. V Izotov, A G Shalashov, V A Skalyga, E D Gospodchikov, O Tarvainen, V E Mironov, H Koivisto, R Kronholm, V Toivanen, B Bhaskar The role of radio frequency scattering in high-energy electron losses from minimum-B ECR ion source Plasma Physics and Controlled Fusion Plasma Phys. Control. Fusion, 63 045007 (13pp), 2021, doi.org/10.1088/1361-6587/abddf0].

Nonlinear wave phenomena in the magnetic fusion ECRH experiments

E. Z. Gusakov and **A. Yu. Popov**

Ioffe Institute, St. Petersburg, Russia, Evgeniy.Gusakov@mail.ioffe.ru

Electron cyclotron resonance heating (ECRH) and current drive is widely used in toroidal plasmas and is considered for application in ITER for heating and neoclassical tearing mode control. Nowadays an abrupt increase of the ECRH power from 20 MW up to 67 MW is under discussion by the ITER team. Following the predictions of the theory developed in late 80s [1–3] nonlinear effects and first of all parametric decay instabilities (PDIs), which can accompany the ECRH experiments, were believed to be deeply suppressed by huge energy loss of daughter waves from the decay region. However, during the last 15 years many experiments have demonstrated excitation of the anomalous nonlinear phenomena at the less than 1 MW level ECRH experiments. The clearest evidence of the nonlinear effects onset was obtained first at TEXTOR [4] and then at ASDEX-UG and W7-X [5, 6], where a strong microwave emission down–shifted in frequency was observed. At ASDEX-UG and TCV [7, 8] emission at the pump wave half frequency has recently been observed. A convincing demonstration of the anomalous ion acceleration during the ECRH pulse under conditions when the energy exchange between ion and electron components is negligible was obtained at TCV and TJ-II [9, 10]. Besides this in the second harmonic ECRH experiments a substantial broadening of the power deposition profile (T-10, L2-M, DIII-D [11–13]) and the missing power effect (TEXTOR, T-10, TJ-II [14, 15]) were reported.

In this talk we present a review of experimental observations and of the theory progress taking into account, as distinct from the standard approach, trapping of the decay waves due to non-monotonic features of the density profile, which always exist on the discharge axis or may be present due to a magnetic island, density pump-out effect, or ELM filaments and blobs. We interpret the anomalous microwave emission and the ion heating, as a result of secondary nonlinear processes that accompany the primary low-threshold PDI leading to excitation of trapped waves. The primary PDI growth is saturated in our model due to both the secondary decays of daughter waves and the pump wave depletion. The coupling of different daughter waves and the pump is responsible in the model for the strong microwave emission, which is a spurious signal for a tokamak microwave diagnostics. This mechanism appears capable of reproducing the fine details of the frequency spectrum and the absolute value of the emitted radiation. It also predicts substantial anomalous absorption in the range of 10–70% in the electron channel, which could be responsible for the broadening of the ECRH power deposition profile, and explain the anomalous ion heating by the generation of the secondary ion modes, which directly transfer the pump power to ions. Results of theoretical analysis of anomalous emission at TEXTOR and W7-X as well as anomalous absorption reported by L-2M, DIII-D, TEXTOR, TJ-II and T-10, where broadening of the power deposition profile and the missing power effect were observed in the case of monotonic plasma density profile will be presented. The possibility of induced side-scattering instability in the ITER edge transport barrier driven by ordinary mode in the first harmonic ECRH experiment will be discussed including the instability saturation due to the stochastic damping effect. Ways to reduce the influence of anomalous absorption and scattering effects will be indicated.

Acknowledgements

The analytical treatment of emission signal is supported under the RSF 22-12-00010 grant, the numerical modelling – by the Ioffe Institute contract 0040-2024-0028 whereas the code for the PDI saturation modeling was developed under the Ioffe Institute contract 0034-2021-0003.

References

1. M. Porkolab, B. I. Cohen *Nucl. Fusion* 1988, **28**, 239.
2. B. I. Cohen, R. H. Cohen, W. M. Nevins, T. D. Rognlien. *Rev. Mod. Phys.* 1991, **63**, 949.
3. A. G. Litvak, A. M. Sergeev, E. V. Suvorov et al. *Phys. Fluids* 1993, **B 5**, 4347.
4. E. Westerhof, S. Nielsen, J. W. Oosterbeek et al. *Phys. Rev. Lett.* 2009, **103**, 125001.
5. S. K. Hansen, S. K. Nielsen, J. Stober et al. *Nucl. Fusion* 2020, **60**, 106008.
6. A. Tancetti, S. K. Nielsen, J. Rasmussen et al. *Nucl. Fusion* 2022, **62**, 074003.
7. S. K. Hansen, A. S. Jacobsen, M. Willensdorfer et al. *Plasma Phys. Control. Fusion* 2021, **63**, 095002.
8. A. Clod, M. G. Senstius, A. H. Nielsen et al. *Phys. Rev. Let.* 2024, **132**, 135101.
9. S. Coda for the TCV Team, *Nuclear Fusion* 2015, **55**, 104004.
10. B. Zurro, A. Baciero, V. Tribaldos et al. *Nucl. Fusion* 2013, **53**, 083017.
11. V. F. Andreev, Yu. N. Dnestrovskij, M. V. Ossipenko et al. *Plasma Phys. Control. Fusion* 2004, **46**, 319–335.
12. E. Z. Gusakov, A. Yu. Popov, A. I. Meshcheryakov et al. *Phys. Plasmas* 2023, **30**, 122112.
13. J. H. Slief, R. J. R. van Kampen, M. W. Brookman et al. *Nucl. Fusion* 2023, **63**, 026029.
14. M. Yu. Kantor, G. Bertschinger, P. Bohm et al. *36th EPS Conference on Plasma Phys. Sofia,* 2009 ECA **33E**, P-1.184.
15. Yu. N. Dnestrovskij, A. V. Melnikov, D. Lopez-Bruna et al. *Plasma Phys. Control. Fusion* 2023 **65**, 015011.

Development the 50-MW S-band klystron

V. Ya. Ivanov

Budker Institute of Nuclear Physics, Novosibirsk, Russian Federation

The paper provides an overview of mathematical models, algorithms and computer codes for calculations and design of high-power klystrons. A study was carried out of a 50 MW S-band klystron developed at the Institute of Nuclear Physics SB RAS. A comparison of numerical results with experimental data is given.

Klystrons with a power of 50–100 megawatts are the main source of high-frequency power for modern charged particle accelerators. Klystrons of such power have not previously been produced in Russia. Currently, the BINP SB RAS is participating in the construction of the 4th generation synchrotron “SKIF” and the Super C-tau factory. The need for klystrons for these projects is in the tens, which necessitated the development of our own klystron.

The full cycle of klystron design consists of many stages, among which the following can be distinguished:

1. Analytical methods are used for the preliminary design. At this stage, based on the technical specifications containing the specified parameters – operating frequency, input power of the RF power supply of the grouper, output power of the klystron – the main characteristics of the device are determined – the number of resonators, klystron dimensions, current, diameter and initial energy of the beam, dimensions of drift tubes, the magnitude of the accompanying magnetic field, device efficiency.

2. Optimization of the design solution obtained during preliminary design. At this stage, the detuning of the grouper resonators, the length and diameter of the drift tubes, the operating frequency band, the gain, the design of the power input and output, as well as the tolerances for the main variable parameters are determined. At this stage, simplified numerical models are used that take into account the longitudinal and transverse dynamics of grouped clumps.

3. Detailed calculation, which includes calculations of electromagnetic fields, optics of charged particles taking into account their own fields, thermal calculations and calculations of elastic deformations, both when setting up resonators and under the influence of thermal loads. These calculations must include such physical processes as multipactor and dark currents, which include the mechanisms of field emission and secondary electron emission from the surfaces of the device.

4. Information obtained at each design stage can then be used for new design cycles with refined input data until the desired results are obtained or information is obtained about the limits of permissible variation in the input data.

The variety of software tools for calculating individual klystron units gives rise to the problem of exchanging calculation results between different programs. Some results presented in Fig.1.

References

1. V. Ivanov. Design algorithms and computer codes for computing multicavity klystrons // Preprint 2023-03, BINP SB RAS, Novosibirsk, 2023.
2. V. Ivanov. Method for solving multidimensional problems of optimizing the parameters of high-power klystrons // submitted to the IEEE Trans of Electron Devices, 2023.

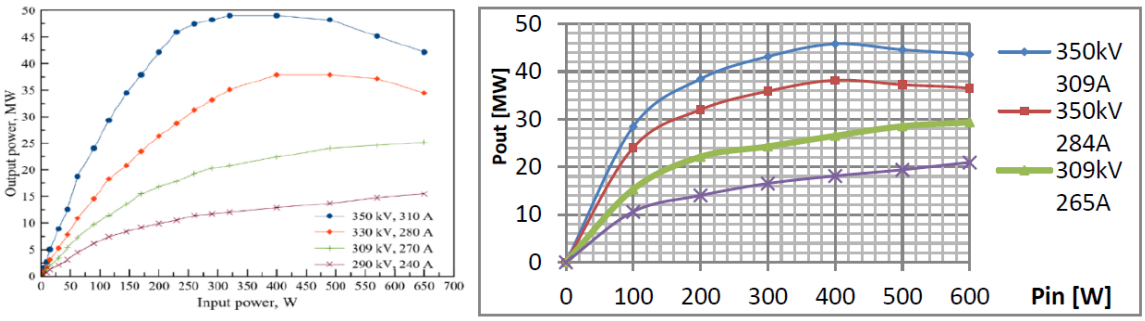

Fig. 1. Output pulsed RF power of klystron vs. input power at different beam currents and accelerating potentials. Experimental data – *left*, numerical calculations – *right*

Proton beam formation at the injector prototype for DARIA accelerator-based neutron source

S. S. Vybin, A. F. Bokhanov, I. V. Izotov, A. V. Polyakov, V. A. Skalyga and **D. M. Smagin**

A.V. Gaponov-Grekhov Institute of Applied Physics of the Russian Academy of Sciences, Nizhny Novgorod, Russia,
vybinss@ipfran.ru

Light ion (H^+, D^+, H^-, D^-, etc.) beams with high current density (above 100 mA cm^{-2}) obtaining is an important problem. Sources of such beams are used as neutral beam injectors at nuclear fusion facilities [1], serve as charged particles injectors for accelerators [2] and are applied for ion implantation [3].

Ion sources based on electron cyclotron resonance (ECR) discharge are frequently used as positively charged particles injectors for accelerators [4]. It is caused by high stability of operation, reliability of facility, electrodeless way of plasma maintenance and possibility of ion beam creation from a wide range of particle species. 2.45 GHz ECR sources of light ions are quite common. It tend to have moderate current density of extracted ion beam (100–200 mA cm^{-2}). Therefore, plasma electrodes with aperture about 1 cm are used in order to obtain beams with total current above 100 mA. The current density increase can help to gain the beam quality. It can be achieved by plasma density increase. Its growth is limited to cutoff density at fixed microwave frequency but there are studies of overdense plasma heating [5]. Another way to gain plasma density is the microwave frequency increase.

ECR ion source GISMO [6] (Gasdynamic Ion Source for Multipurpose Operation) was created in accordance with the last paradigm. The plasma of the source is sustained by microwave radiation of gyrotron [7] with frequency of 28 GHz and power up to 10 kW. High volumetric energy input level (up to 250 W cm^{-3}) is achieved because of relatively small plasma volume (about 40 cm^3). The extracted beam current density is above 1 A cm^{-2} [8] due to high density (close to 10^{13} cm^{-3}) and electron temperature (above 30 eV) of plasma [9].

An overview of experimental activities with proton beam at GISMO facility over the past few years is given in this work. Several experimental sessions were conducted during this time. The total beam current was the main parameter to measure. The content of the beam was measured using magnet analyzer. The space charge compensation of the beam was estimated through beam profile images processing. Also, the beam formation at different extraction system configurations was studied. The beam emittance was measured using pepper-pot method. Experiments were accompanied with numerical calculations of plasma processes kinetics and the ion beam formation from plasma.

Also, the way towards modernization which leads to gain of the facility effectiveness is discussed in this work.

Acknowledgements

The work was supported by the Ministry of Science and Higher Education of the Russian Federation within the framework of scientific project no. 075-15-2022-830.

"Development of Compact Sources of Photons and Neu-trons Based on New Technologies of Linear Accelerators: The Main Elements of a Free Electron Laser and Pulsed Neutron Sources."

References

1. R. S. Hemsworth, D. Boilson, P. Blatchford, M. D. Palma, G. Chitarin, H. P. L. de Esch, F. Geli, M. Dremel, J. Graceffa, D. Marcuzzi, G. Serianni, D. Shah, M. Singh, M. Urbani, P. Zaccaria, New Journal of Physics, 2017, **19**(2), 025005.
2. D. A. Fink, T. Kalvas, J. Lettry, Ø. Midttun, D. Noll, Nuclear Instruments and Methods in Physics Research Section A: Accelerators, Spectrometers, Detectors and Associated Equipment, 2018, **904**, 179–187.
3. R. Swaroop, N. Kumar, G. Rodrigues, D. Kanjilal, I. Banerjee, S. K. Mahapatra, Review of Scientific Instruments, 2021, **92**(5), 053306.
4. T. Akagi, L. Bellan, B. Bolzon, P. Cara, Y. Carin, N. Chauvin, M. Comunian, H. Dzitko, E. Fagotti, F. Harrault, A. Kasugai, K. Kondo, K. Sakamoto, M. Sugimoto, Review of Scientific Instruments, 2020, **91**(2), 023321.
5. W. Wu, S. Peng, A. Zhang, T. Ma, Y. Jiang, K. Li, B. Cui, Z. Guo, J. Chen, Journal of Applied Physics, 2022, **132**(8), 083305.
6. V. A. Skalyga, A. F. Bokhanov, S. V. Golubev, I. V. Izotov, M. Yu. Kazakov, E. M. Kiseleva, R. L. Lapin, S. V. Razin, R. A. Shaposhnikov, S. S. Vybin, Review of Scientific Instruments, 2019, **90**(12), 123308.
7. Y. Bykov, G. Denisov, A. Eremeev, V. Gorbatushkov, V. Kurkin, G. Kalynova, V. Kholoptsev, A. Luchinin, I. Plotnikov, Review of Scientific Instruments, 2004, **75**(5), 1437–1439.
8. V. A. Skalyga, I. V. Izotov, S. S. Vybin, T. V. Kulevoy, G. N. Kropachev, A. L. Sitnikov, S. V. Grigoriev, Journal of Physics: Conference Series, 2022, **2244**(1), 012092.
9. A. V. Polyakov, I. V. Izotov, V. A. Skalyga, S. S. Vybin, E. M. Kiseleva, A. F. Bokhanov, Physics of Plasmas, 2023, **30**(4), 043519.

Effect of electromagnetic field on densification, grain growth and phase transformations during rapid microwave sintering

S. V. Egorov, A. G. Eremeev, V. V. Kholoptsev, K. I. Rybakov, A. A. Sorokin

A.V. Gaponov-Grekhov Institute of Applied Physics of the Russian Academy of Sciences, Nizhny Novgorod, Russia, rybakov@ipfran.ru

High-temperature processing of materials is a promising application of microwave radiation. Over the recent years, the authors have been investigating the processes of rapid microwave sintering of ceramic and composite materials. With heating rates of up to 300 °C/min and zero hold time at the maximum temperature, the overall duration of such processes is reduced by orders of magnitude compared to conventional sintering that normally takes hours or even days.

The implementation of rapid heating requires a significant volumetric energy input in the materials undergoing processing, with an absorbed microwave power density $p = \sigma E^2$ (where σ is the high-frequency conductivity of the material and E is the effective microwave electric field strength inside the sample) on the order of about 30...100 W/cm^3. This intense microwave impact apparently results in unusual changes in the microstructure of the materials.

The rapid microwave sintering experiments were carried out in the workchamber of a gyrotron system operating at a frequency of 24 GHz with a maximum output power of 6 kW [1]. The microwave power supplied to the workchamber was regulated automatically in accordance with the predefined temperature-time schedule. The shrinkage of the samples was monitored using optical dilatometry. In addition to comparing different heating rates, the intensity of the electromagnetic field acting on the samples was varied by using heat insulation assemblies containing different microwave absorbing elements (susceptors).

The results of rapid microwave sintering experiments with oxide ceramics are summarized in Table 1.

Table 1

Summary of rapid microwave sintering experiments with oxide ceramics: maximum temperature (T_{max}), relative sintered density (ρ/ρ_{th}) and the absorbed microwave power per unit volume (p)

Material	T_{max}, °C	ρ/ρ_{th}, %	p, W/cm^3	Ref.
Yb:$(La_{0.1}Y_{0.9})_2O_3$	1350…1500	98.6	20...160	2
Y_2O_3	1500…1700	98.3	40...43	3
ZrO_2 (+ 3%Y_2O_3)	1400	99.4	60...120	4
$MgAl_2O_4$	1500…1700	99.2	27...80	5, 6
TiO_2	1100	94.8	–	7
Al_2O_3	1400…1550	99	15...100	8
Al_2O_3 + CNT	1550…1600	95.0	–	9
ZnO + Bi_2O_3 + Sb_2O_3	1150…1300	95…96	≥ 20	10
$BaTiO_3$	1150…1300	95…96	40	11
$Ba_{0.75}Sr_{0.25}TiO_3$	1250	94.2…95.6	19…93	12
ZnO + Bi_2O_3	1200	≤ 98.3	14…23	13
Gd:CeO_2	1450…1580	≤ 96	40	14

It has been observed in these studies that the onset temperature of densification decreases with increasing electromagnetic field intensity. The enhanced densification coincides with the development of a thermal instability, which suggests that a highly absorptive grain-boundary phase with enhanced transport properties is formed.

The microstructural studies have revealed abnormal grain growth in the samples exposed to intense microwave irradiation. According to impedance spectroscopy measurements, the properties of grain boundaries, such as the effective width, dielectric permittivity, and/or ionic conductivity, may be influenced by the electromagnetic field.

In recent experiments with alumina – zirconia ceramic composites obtained from nanopowders by rapid microwave sintering it has been found that the temperature of phase transformation from metastable alumina phases to the stable α-phase decreases with increasing electromagnetic field intensity. The shift in the phase transformation temperature reached 200 °C compared to conventional sintering. A similar microwave influence on a sequence of phase transformations has been observed in the experiments on rapid microwave sintering of luminescent Al_2O_3 – Ce:Y_2O_3 composites.

Acknowledgement

This research was supported in part by Russian Science Foundation, grant No. 23-19-00363.

References

1. S. Egorov et al., *Rev. Sci. Instrum.* 2022, **93**, 064708.
2. Yu. Bykov et al., *J. Am. Ceram. Soc*., 2015, **98**, 3518–3524.
3. Yu. Bykov et al., *Ceram. Trans*., 2016, **259**, 233–242.
4. Yu. Bykov et al., *IOP Conf. Ser. Mater. Sci. Eng.*, 2017, **218**, 012001.
5. Yu. Bykov et al., *J. Am. Ceram. Soc*., 2019, **102**, 559–568.
6. S. Egorov et al., *J. Infrared Millim. Terahertz Waves*, 2019, **40**, 447–455.
7. K. Rybakov et al., *J. Mater. Res*., 2019, **34**, 2620–2634.
8. S. Egorov et al., *Scripta Mater*., 2020, **174**, 68–71.
9. S. Egorov et al., *Ceram. Int*., 2021, **47**, 4604–4610.
10. S. Egorov et al., *J. Eur. Ceram. Soc*., 2021, **41**, 6508–6515.
11. S. Egorov et al., *Materialia*, 2022, **24**, 101513.
12. S. Egorov et al., *Radiophys. Quantum Electron.*, 2022, **65**, 219–228.
13. S. Egorov et al., *J. Am. Ceram. Soc*., 2023, **106**, 878–887.
14. S. Egorov et al., *Materialia*, 2024, **33**, 101980.

Project of powerful long-pulse THz-band FEL with Talbot-type cavity: design and optimization

D. D. Krygina and **A. V. Savilov, Yu. S. Oparina, N. Yu. Peskov**

A.V. Gaponov-Grekhov Institute of Applied Physics of the Russian Academy of Sciences, Nizhny Novgorod, Russia, mkd@ipfran.ru

Currently, active work is being carried out at the Institute of Applied Physics of the Russian Academy of Sciences to create a terahertz free-electron maser with a high-current beam in collaboration with the Budker Institute of Nuclear Physics of the Siberian Branch of the Russian Academy of Sciences [1]. Here we describe designs of FELs on the basis of a long-pulse (hundreds nanoseconds) 10 MeV / 1–2 kA electron beam and a pulsed undulator with a period of several centimeters. At a ~ 5% efficiency of the electron-wave interaction, a close-to-GW level of the power of the output wave signal at frequencies of several THz can be provided.

An important problem is the design of a cavity which must inevitably be oversized (hundreds of wavelengths in the transverse directions and tens of thousands of wavelengths in the longitudinal direction) and, at the same time, provide stable narrow-band generation of a given operating mode. Previously, a system based on the Talbot effect was proposed as an oversized microwave system [2]. In this work, we develop a simplified model of a FEL with a Talbot-type cavity (Fig. 1), and describe structures of super-modes (formed by partial eigenmodes of the cavity) with various oversizing factors (Fig. 2 and Fig. 3). An optimization of the system from the point of view of the intensity of the electron-wave interaction is also carried out (Fig. 4).

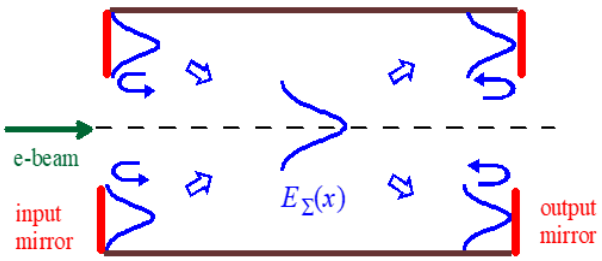

Fig. 1. Super-mode of a Talbot-type cavity

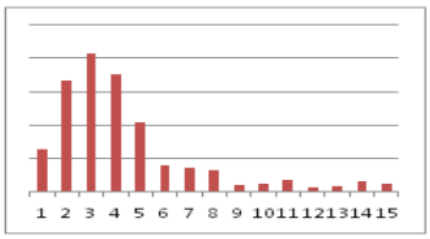

Fig. 2. Typical spectrum of partial modes forming the operating supermode of the cavity

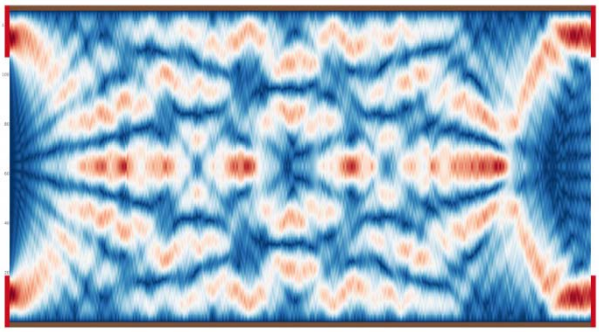

Fig. 3. 2D field structure of the operating supermode

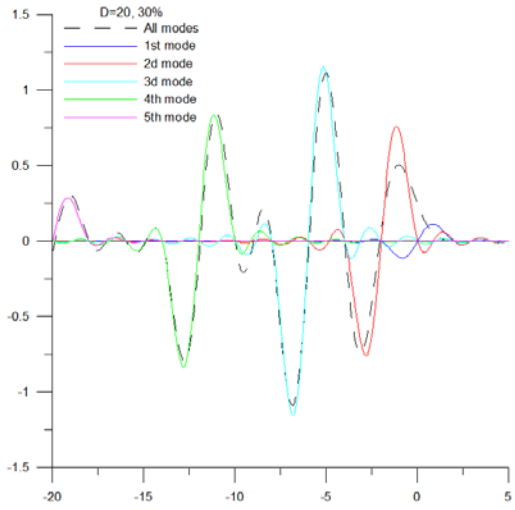

Fig. 4. Normalized starting current versus the mismatch of the electron-wave resonance

Acknowledgements

This work was supported by RSF grant № 21-72-30027.

References

1. N. Yu. Peskov, A. V. Arzhannikov, V. I. Belousov, e.a. “Electrodynamic system of a powerful THz band free electron laser based on the LIU linear induction accelerator: modelling and cold tests”, Bulletin of the Russian Academy of Sciences: Physics, 2023, vol. 87, p. 669.
2. Yu. S. Oparina, N. Yu. Peskov, A. V. Savilov/ “Electron rf oscillator based on self-excitation of a Talbot-type supermode in an oversized cavity”, Physical Review Applied, 2019, vol. 12, art.no.044070.

A fast path to the ion temperatures required for magnetically confined nuclear fusion

G. S. Kurskiev[1], V. B. Minaev[1], N. V. Sakharov[1], V. K. Gusev[1], Yu. V. Petrov[1], E. Z. Gusakov[1], I. V. Miroshnikov[1], N. N. Bakharev[1], I. M. Balachenkov[1], F. V. Chernyshev[1], V. V. Dyachenko[1], V. Yu. Goryainov[1], E. M. Khilkevich[1], N. A. Khromov[1], E. O. Kiselev[1], S. V. Krikunov[1], A. D. Melnik[1], A. N. Novokhatskii[1], M. I. Patrov[1], A. Yu. Popov[1], P. B. Shchegolev[1], A. E. Shevelev[1], K. D. Shulyatiev[1], O. M. Skrekel[1], V. V. Solokha[1], A. Yu. Telnova[1], E. E. Tkachenko[1], V. A. Tokarev[1], S. Yu. Tolstyakov[1], E. A. Tukhmeneva[1], V. I. Varfolomeev[1], A. V. Voronin[1], N. S. Zhiltsov[1], E. N. Bondarchuk[2], A. A. Kavin[2], A. B. Mineev[2,3], V. N. Tanchuk[2], A. A. Voronova[2], P. A. Bagryansky[4], S. V. Ivanenko[4], I. V. Shikhovtsev[4], A. L. Solomakhin[4], A. M. Ponomarenko[5], I. Yu. Senichenkov[5], A. Yu. Yashin[5], E. G. Zhilin[6] and **V. A. Solovey[7]**

[1] Ioffe Institute, St. Petersburg, Russia, gleb.kurskiev@mail.ioffe.ru
[2] JSC "NIIEFA", St. Petersburg, Russia
[3] Saint Petersburg State University, Saint Petersburg, Russia
[4] BINP SB RAS, Novosibirsk, Russia
[5] Peter the Great Polytechnic University,St. Petersburg, Russia
[6] Ioffe Fusion Technology Ltd., St. Petersburg, Russia
[7] Petersburg Nuclear Physics Institute named by B.P. Konstantinov of NRC, 'Kurchatov Institute',St. Petersburg, Russia

The spherical tokamak (ST) is known as an effective magnetic trap for a fusion plasma confinement. Experiments carried out on first-generation spherical tokamaks (STs operating at B_T < 0.55 T) confirmed the theoretically predicted high MHD stability of the plasma, allowing operation at high values of β_T (the ratio of the gaskinetic pressure of the plasma to the pressure of the toroidal magnetic field) of up to 40%. Moreover, it was found that the phenomenological picture of thermal energy confinement in STs differs significantly from high aspect ratio tokamaks. The extrapolation of the experiments on STs predicted that a further increase in the toroidal magnetic field up to 1 T and higher will significantly improve the efficiency of plasma thermal insulation (primarily electrons) and significantly expand the range of achievable electron and ion temperatures in a compact small tokamak. This became the basis for the preparation of experiments on plasma confinement and heating in 2nd generation STs (STs operating at B_T > 0.7 T) at an increased value of B_T. Globus- M2 [1] became the first in the new generation ST family presenting systematic results of experimental studies on heating and thermal insulation of plasma, which confirmed the favorable dependence of the energy confinement time on the magnetic field and collisionality.

The toroidal magnetic field is a key parameter that determines the efficiency of plasma heating and thermal energy confinement in a spherical tokamak. One of the most important results of recent campaigns is the pioneering achievement of a hot ion mode with $T_i \geq 4$ keV in a compact spherical tokamak having a small radius of 0.24 m and a magnetic field of 0.9 T [2]. The ion temperature in Globus-M2 experiments approaches the thermonuclear values due to the good plasma thermal insulation. In Globus-M2, ions demonstrated predominantly neoclassical behavior with linear dependence of χ_i on ν_i*, in accordance with neoclassical theory for the collisionless "banana" regime. At the same time ν_i* reaches the values typical for the plasma of large tokamaks such as DIII-D, ASDEX-U and JET.

The favorable τ_E dependence on the toroidal magnetic field and plasma current (so-called ST scaling, previously found on STs with $B_T \leq 0.55$ T) $\tau_E \sim I_p^{0,4} B_T^{1,2}$ is confirmed for $B_T \leq 0.8$ T [3]. The value of $n_e \cdot \tau_E \cdot T_{i0} \approx$ $\approx 5 \cdot 10^{18}$ m^{-3} s·keV ($n_e \cdot \tau_E \sim 10^{18}$ m^{-3}s) for the Globus-M2 plasma was achieved. The increase in the fusion triple product compared to the Globus-M plasma at B_T = 0.4 T was by a factor of 50.

These breakthrough results achieved on Globus-M2 raised the concept design of a next-generation compact spherical tokamak (Project Globus-3). The main features of the Globus-3 are a long pulse and a strong B_T at a low aspect ratio. For the basic tokamak operational parameters, the plasma current as high as 0.8 MA and B_T as high as 1.5 T, direct losses during neutral injection do not exceed 15% for energies of 50–150 keV that provides favorable conditions for plasma heating. Being half the size of the T15MD and with a plasma volume ~5 times smaller, Globus-3 will facilitate the rapid development of fusion energy technologies, such as plasma heating using NBI and radio frequency waves. Long pulse duration with a high bootstrap current fraction approaching will also provide unique capabilities to embed advanced control regimes for plasma profile optimization. Globus-3 also can be considered as a full-scale hydrogen prototype of a fusion neutron source, providing the necessary physical and technological basis for further development of the compact tokamak operating with D-T mixture enebling high neutron yield.

Acknowledgements. The work was financially supported by the Ministry of Science and Higher Education of the Russian Federation. Experiments on plasma heating using NBI were supported by the contract no. 0034-2021-0001. Measurements of T_e and n_e profiles were supported by the contract no. 0040-2024-0028.

References

1. V. B. Minaev, V. K. Gusev, N. V. Sakharov et. al., *Nucl. Fusion*, (2017) 57 066047.
2. G. S. Kurskiev, I. V. Miroshnikov, N. V. Sakharov et. al., *Nucl. Fusion*, (2022) 62 104002.
3. G. S. Kurskiev, V. K. Gusev, N. V. Sakharov et. al., *Nucl. Fusion*, (2022) 62 016011.

Whistler waves in the ohmically heated plasmas in the TUMAN-3M tokamak

S. V. Lebedev, G. I. Abdullina, L. G. Askinazi, A. A. Belokurov, V. A. Kornev, D. V. Razumenko, A. S. Tukachinsky and **N. A. Zhubr**

Ioffe Institute, St Petersburg, Russian Federation, Sergei.Lebedev@mail.ioffe.ru

Three types of high frequency magnetic oscillations have been observed in the experiments with low-density ohmically heated plasma in the TUMAN-3M tokamak. Range of the frequencies described in this report lies between ω_{ci} and ω_{ce}. The experiments were performed in hydrogen plasma with an averaged density $\overline{n}_e \leq 1.5\times$ $\times 10^{19}$ m^{-3}, toroidal magnetic field $B_t \leq 1$ T, plasma current $I_p \leq 160$ kA, plasma major and minor radii $R_0 =$ $= 0.53$ m and $a_l = 0.22$ m, respectively. The measurements were performed using array of 16 magnetic probes sited at the inner wall of the vacuum vessel.

Oscillations of the first type had relatively long duration (0.1–1 ms) and existed in a frequency range from 120 to 290 MHz which corresponds to (10–20)ω_{ci} and is lower than $\omega_{LH}/2$. The oscillations appeared as several spectral lines separated by frequency gaps of 18 to 60 MHz, see figure 1. Frequency variation during the train lifetime allowed to conclude whistler character of the oscillations.

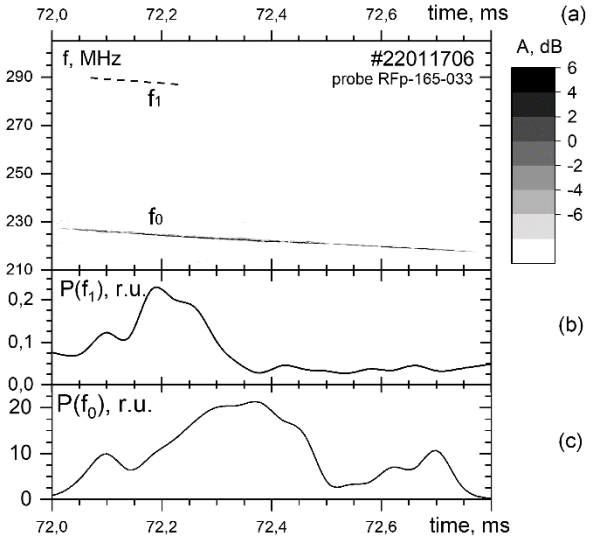

Fig. 1. Temporal evolution of whistlers' frequencies – (a), time variation of the emission power, f_1 – (b), f_0 – (c). Note, the amplitude scale in frame (a) is valid for f_0 only

Oscillations of the second type appeared as short bursts with duration of 10–20 μs and characterized by a clear harmonic structure with up to 7 observable harmonics. Their fundamental harmonic frequencies, 18–40 MHz, are much lower compared to that of oscillations of the first type, but are higher than ω_{ci}. With increased electron density from 0.87 to 1.18·10^{19} m^{-3} a splitting of the harmonics was found with a spacing of ~ 4.2 MHz, see figure 2. Amount of the subharmonics can come up to 6 instead of the sole peak. Due to short duration of the bursts of this type oscillations it is difficult to establish an underlining mechanism of their generation. Further experiments are planned to clarify role of runaway electrons in the triggering of this emission.

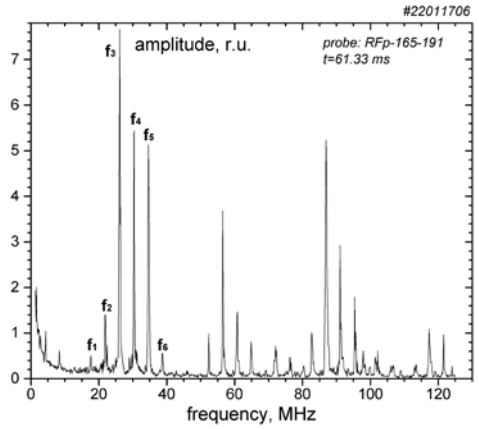

Fig. 2. Spectrum of second type oscillations measured by the magnetic probe located at the poloidal angle of 11° below the inward mid-plane

Oscillations of the third type were discovered in the discharges with density being lower than in the two previous cases – 0.5·10^{19}m^{-3}. Spectrum of a magnetic probe signal recorded using the ADC with sampling rate 2.5 GHz is shown in figure 3. In the spectrum the above-mentioned oscillations of the first and second types are concentrated in the range of frequencies below 300 MHz. In vicinity of 300 MHz a well in spectral peak amplitude was observed. In remaining part of the spectrum two ranges can be distinguished: (1) $300 < f < 650$ MHz and (2) $f > 650$ MHz. Frequency 650 MHz roughly corresponds to f_{LH}. Average spacing in lower-f range (1) is 18.1 MHz and 23.9 MHz in higher-f range (2).

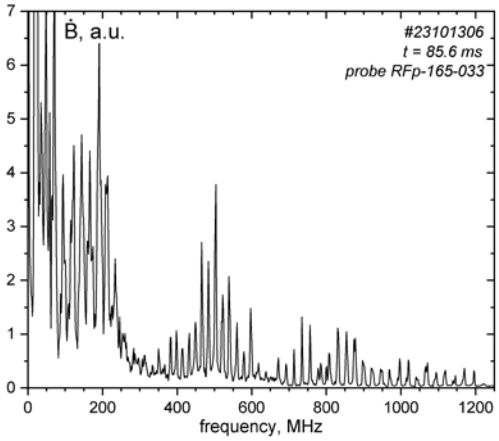

Fig. 3. Magnetic oscillations spectrum measured using ADC with sampling rate 2.5 GHz

Although the frequencies of the third type oscillations fall into the range of whistler waves a further analysis is planned to conclude the underlining mechanism of the observed phenomenon.

Acknowledgements. The study was performed within a framework of the Contract between the Ioffe Institute and the RF Ministry of Science and Education (FFUG-2024-0028).

Microwave discharge in liquids: physics and some aspects of applications

T. S. Batukaev[1], I. V. Bilera[1], G. V. Krashevskaya[1,2], Yu. A. Lebedev[1]

[1] Institute of Petrochemical Synthesis, RAS. Moscow, Russia
[2] National Research Nuclear University "MEPhI", Moscow, Russia

Electric discharges in the presence of a liquid phase are now one of the most important areas of research in plasma physics and its applications. Microwave discharge in liquids has been least studied. Microwave plasma is created in a gas bubble inside a liquid, which ensures a high rate of formation of high concentrations of active particles in a mini-reactor, which is a plasma bubble.

A microwave discharge is created at the end of a metal antenna immersed in a liquid (a wide range of liquid hydrocarbons, water and aqueous solutions of ethanol) at powers up to 2.5 kW [1–6]. The discharge was studied using gas chromatography, emission spectroscopy, high-speed photo recording, schlieren and shadow photography.

It has been shown [2, 3] that a discharge is a sequence of solitary discharges randomly distributed in time. The formation of a solitary discharge is accompanied by a shock wave, which causes damped sound vibrations in the discharge volume. The growth rate and maximum size of a gas bubble were obtained for various types of electrodes. The results of calculations on the role of ionization by electron impact at the initial stage of the occurrence of a discharge were also experimentally confirmed.

A study was carried out on the possibilities of using a discharge to decompose CO_2 and produce hydrogen [4–6]. The results obtained show the promise of using microwave discharges to solve applied tasks.

Acknowledgments. The work was carried out within the framework of the State Plan of the A.V.Topchiev Institute of Petrochemical Synthesis, RAS.

References

1. Yu. A. Lebedev, *Polymers* **13, 11** (2021), 1678.
2. Yu. A. Lebedev, G. V. Krashevskaya, T. S. Batukaev, I. L. Epstein, *Plasma Processes and Polymers* **18, 10** (2021), e2100051.
3. Yu. A. Lebedev, G. V. Krashevskaya, T. S. Batukaev, A. V. Mikhaylyuk, *Plasma Process and Polymers* **19, 5** (2022), e2100215.
4. T. S. Batukaev, I. V. Bilera, G. V. Krashevskaya, Yu. A. Lebedev, N. A. Nazarov, *Plasma* ***6*** (2023), 115–126.
5. T. S. Batukaev, I. V. Bilera, G. V. Krashevskaya, Yu. A. Lebedev, I. L. Epstein, *Plasma Process and Polymers* ***20, 6*** (2023), e2300015.
6. T. S. Batukaev, I. V. Bilera, G. V. Krashevskaya, Yu. A. Lebedev, *Processes* **11, 8** (2023), 2292.

Millimeter-wave plasmatron based on gyrotron and transmission line

Dun Lu, **Wenjie Fu** and **Yang Yan**

University of Electronic Science and Technology of China, Chengdu, China, ludun@uestc.edu.cn

Microwave plasma has been well-known in material surface modification, etching, clean, wound treatment, and sterilization [1]. Microwave plasma provides several advantages as compared to other plasma technology, including higher ionization efficiency than radio frequency discharge, and has a lower chance of contamination and damage of sensitive components than the dielectric barriers discharge (DBD) and gliding arc plasma (GAP) as microwave discharge does not involve electrodes for its discharge [2]. Millimeter-wave plasma allows to significantly increase the specific energy input and plasma density compared to the 2.45 GHz or 915 MHz microwave plasma [3].

This abstract presents a millimeter-wave plasmatron (MWP) based on gyrotron and transmission line. A typical microwave plasma reactor usually involves three major components, which are microwave generator (microwave source magnetron), microwave plasma sources (MPS), and a plasma cavity equipped with a dielectric tube (usually quartz) [4]. The system of this MWP is shown in Fig. 1. A 30 GHz low-voltage CW gyrotron is used to generate millimeter wave, the output mode is TE01 [5]. Then, the mode converter changes the operating mode to the main mode of the rectangular waveguide (WR-28). The transmission line consists of a 60 dB directional coupler, a three-pin tuner and an adjustable short road surface consist. A Φ6.1 mm quartz tube is inserted from the top of the rectangular waveguide as a reaction chamber.

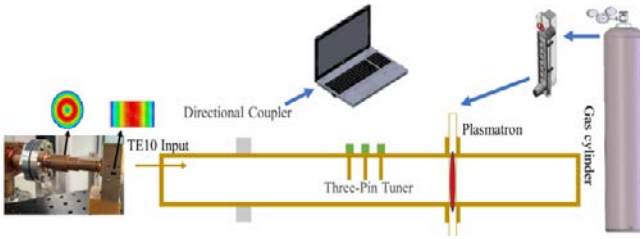

Fig. 1. Schematic diagram of the millimeter-wave plasmatron based on gyrotron and transmission line

When the flow rate of 1 SLM of Ar, the photographs of plasma under radiation 100 W is shown in Fig. 2. The waveguide stub tuner is a compact section of waveguide strategically inserted into the main waveguide. By adjusting its position and length, the tuner can manipulate the overall impedance characteristics of the combined structure. This allows for fine tuning to achieve an optimal impedance match. Changes in operating frequency or other system parameters can potentially disrupt the initial impedance match. The stub tuner provides the flexibility to rectify these disruptions, ensuring the waveguide continues to operate at maximum efficiency and reduce reflection to protect the gyrotron continuous operation. Fig. 3 shows the typical spectral of MWP produced by the continuous millimeter wave, the fiber optic probe is fixed at the middle of the plasma filament, and the integration time is 5ms. As can been seen, owing to the gas shielding, three spectra lines occurred, namely Ar I (4p-4s), Ar II and OH lines. The Ar II line could be observed due to the high ionization rate of Ar.

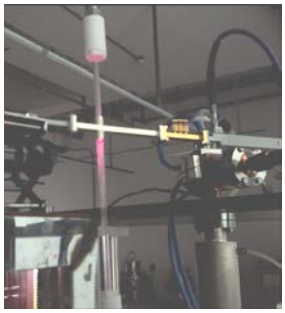

Fig. 2. Photo of the Ar plasma under 100W@30GHz radiation

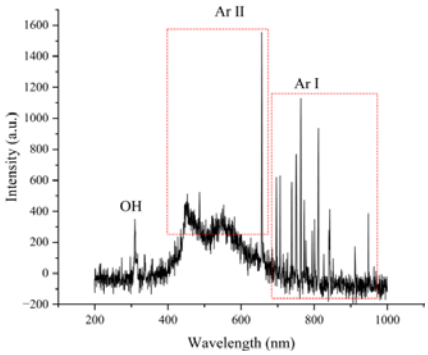

Fig. 3. Emission spectra of plasma

Acknowledgements. This work was supported in part by the National Natural Science Foundation of China under Grant 62371105 and Grant 61971097.

References

1. C. Chaichumporn, P. Ngamsirijit and N. Boonklin et al., Design and Construction of 2.45GHz Microwave Plasma Source at Atmospheric Pressure. Procedia Engineering 8, 94–100 (2011).
2. Yue Qin, Guanghui Niu and Xu Wang et al. Status of CO2 conversion using microwave plasma. J CO2 UTIL 28, 283–291 (2018).
3. Dmitry Mansfeld, Sergey Sintsov and Nikita Chekmarev et al. Conversion of carbon dioxide in microwave plasma torch sustained by gyrotron radiation at frequency of 24 GHz at atmospheric pressure. J CO2 UTIL 40, 101197 (2020).
4. M. Y. Ong, S. Nomanbhay and F. Kusumo et al. Application of microwave plasma technology to convert carbon dioxide (CO2) into high value products: A review. J CLEAN PROD 336, 130447 (2022).
5. L. Dun, F. Wenjie, M. Glyavin, et al. Demonstration of a Low-Voltage High-Efficiency Continuous-Wave Millimeter-Wave Gyrotron. IEEE Trans. Electron Devices, vol. 71, no. 5, pp. 3228–3231, 2024.

A 45 GHz gasdynamic ECR ion source developed at IMP

Y. T. Lu[1,2], **J. D. Ma**[1], **P. Zhang**[1], **J. J. Zhang**[1,2], **L. B. Li**[1], **Y. G. Liu**[1], **H. Y. Zhao**[1,2] and **L. T. Sun**[1,2]

[1] Institute of Modern Physics, Chinese Academy of Sciences, Lanzhou, P. R. China
[2] School of Nuclear Science and Technology, University of Chinese Academy of Sciences, Beijing, P. R. China

The HIAF, High Intensity heavy ion Accelerator Facility, requires its pre-injector to deliver over 1 emA U^{35+} beam [1], which is far beyond the capability of state-of-the-art high charge state ion sources. As an alternative solution, it was proposed to pre-accelerate tens of emA ion beams with low-to-medium charge states produced by a gasdynamic ECR ion source, the capability of which to produce very intensive low charge state ion beams had been confirmed [2], and then to strip them to the required charge states. As the first step to investigate this scheme, a 45 GHz gasdynamic ion source operating in pulsed mode is being developed at the Institute of Modern Physics, IMP.

The layout of the test facility is shown in Fig. 1. The 45 GHz microwave radiation with a power up to 20 kW is converted into TE_{01} mode of a circular waveguide, and then transmitted into a plasma chamber with an inner radius of 45 mm. A microwave launcher with an embedded gas injection system is installed between the waveguide and the plasma chamber. The launcher is designed to prevent the plasma flow from damaging the microwave window while ensuring a high microwave power transmission efficiency.

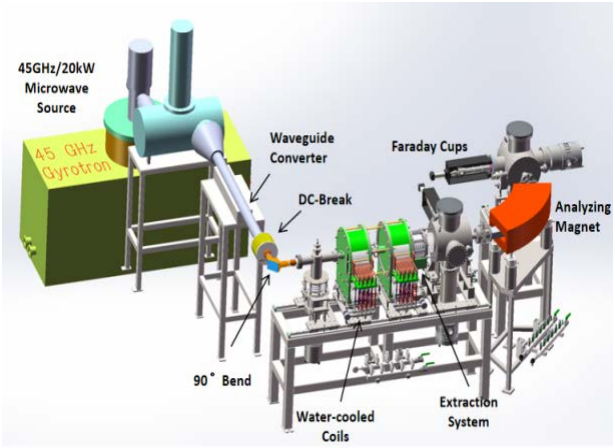

Fig. 1. Layout of the gasdynamic ion source

The magnetic field configuration is a simple mirror trap produced by two water-cooled coils (Fig. 2). The trap length can be adjusted between 20 and 40 cm and the mirror ratio between 1.5 and 3.5, correspondingly. The maximum magnetic field strength on the axis is 3.6 Tesla and the pulse width varies between 10 and 15 ms with a repetition rate up to 1 Hz.

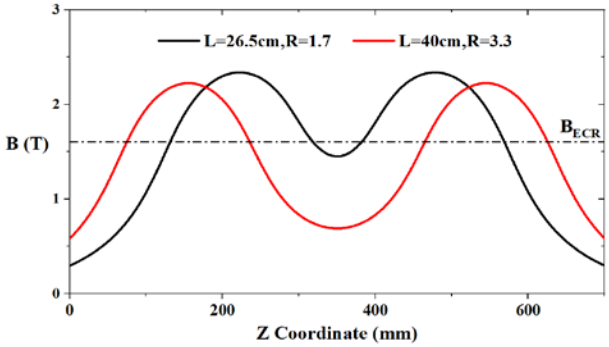

Fig. 2. The magnetic field distribution along the trap axis with 70% of the maximum current. The field stability during the microwave pulse is better than 1%

For beam extraction, a two-electrode system is used with extraction voltage up to 50 kV. A 90° bending magnet is installed in the beam line to analyze the extracted beam spectrum.

The first experiments with light elements (H, N, etc.) have been carried out at this facility. Preliminary results will be presented in the full paper.

Acknowledgements. This research was supported by the National Natural Science Foundation of China (Grant Nos. 12025506) and by the Key Research Program of Frontier Sciences, CAS, (Grant No. 2023YFA1606800).

References

1. X. H. Zhou, J. C. Yang, and the HIAF project team, AAPPS Bulletin, 2022, 32:35.
2. V. Skalyga, I. Izotov, S. Golubev, A. Sidorov, S. Razin, A. Vodopyanov, O. Tarvainen, H. Koivisto, and T. Kalvas, Rev. Sci. Instrum., 2016, 87, 02A716.

Using quasi-optical approach for synthesis of complex periodic structures for relativistic surface-wave oscillators and amplifiers

A. M. Malkin, **N. S. Ginzburg**, **V. Yu. Zaslavsky**, **A. E. Fedotov**, **E. D. Egorova** and **A. S. Sergeev**

A.V. Gaponov-Grekhov Institute of Applied Physics of the Russian Academy of Sciences, Nizhny Novgorod, Russia, malkin@ipfran.ru

Currently, relativistic surface-wave oscillators (SWOs) are among the most prominent radiation sources operating in short millimeter and submillimeter bands. [1, 2]. These devices feature a periodically corrugated planar or cylindrical metal slow-wave structure which supports an evanescent mode (surface wave) confined at this structure. Surface waves are slow so they can be used for synchronous interaction with a rectilinear electron beam; shallow corrugations provide small deceleration of the wave, so they are compatible with relativistic electron beams.

As shown in [3], in the case of shallow corrugation formation of surface mode can be associated with coupling of counter-propagating quasi-optical wavebeams. Such an approach, along with theoretical description of operation of SWO with conventional single-periodic slow-wave structures [1, 2] provides a reliable method for synthesizing novel schemes of surface-wave devices aimed at solving their intrinsic problems, which hamper high-power operation in shorter-wavelength bands. Some examples of such schemes are presented in Fig. 1.

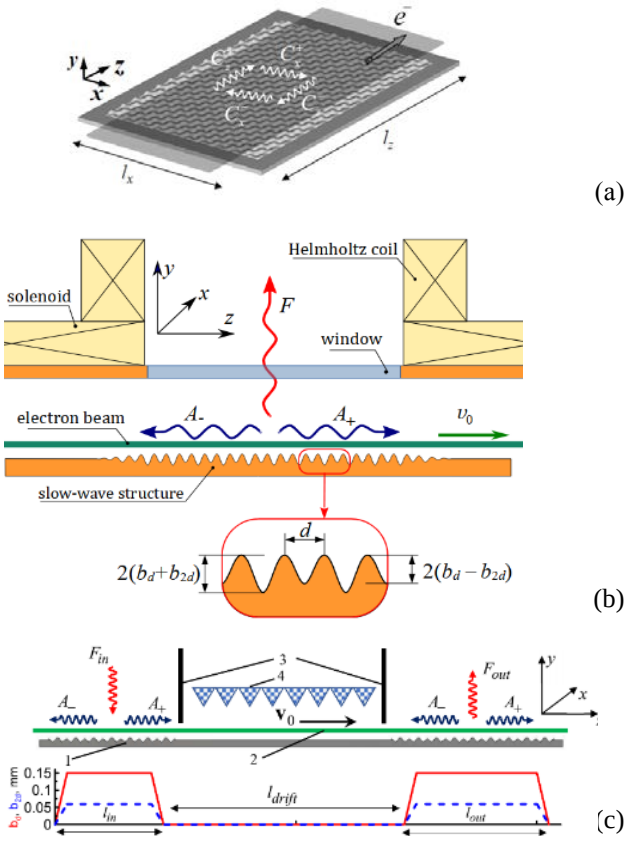

Fig. 1. Schemes of an SWO with 2D SWS (a), an SWO with transverse energy output (b) and a surface-wave amplifier with transverse energy input and output (c). Wavy arrows indicate coupled wavebeams

First of all, two-dimensional periodic corrugation must be mentioned (Fig. 1a), which provides coupling of four longitudinally and transversely propagating wavebeams and thus ensures mode selection over both transverse coordinates. This concept can be applied to both planar [4] and cylindrical [5] SWO configurations.

In the planar configuration, additional sub-harmonic (i.e. with a period larger than the fundamental one) corrugation facilitates the transverse output in the direction normal to the corrugated surface. The output emission in the form of Gaussian-type beam appears to be an attractive solution for outcoupling of radiation from the interaction space (Fig. 1b) [6]. Besides, this sub-harmonic corrugation can also be used for radiation input in a klystron-type amplifier device (Fig. 1c) [7]. Lastly, the above configurations can be combined to propose an SWO with 2D slow-wave structure and transverse radiation output.

To conclude, we emphasize that the first successful experimental realizations of strongly oversized SWOs with 2D slow-wave structures of both cylindrical and planar geometry [8, 9] have demonstrated the fruitfulness of the quasi-optical approach for development of new schemes of surface-wave oscillators and amplifiers.

Acknowledgement

The research was supported by IAP RAS program No. FFUF-2022-0007.

References

1. J. Wang, G. Wang, D. Wang, S. Li, and P. Zeng, Sci. Rep., 2018, **8**, (1), 6978.
2. H. Xi, J. Wang, Z. He, G. Zhu, H. Wang, R. Li, and L. Liu, Sci Rep, 2018, **8,** 348.
3. N. Ginzburg, A. Malkin, A. Sergeev, V. Zaslavsky, *Appl. Phys. Lett*., 2011, **99**(12), 121505.
4. N. Ginzburg, A. Malkin, A. Sergeev, V. Zaslavsky, *Appl. Phys. Lett*., 2012, **100**(14), 143510.
5. N. Ginzburg, A. Malkin, A. Sergeev, V. Zaslavsky, *J. Appl. Phys.*, 2013, **100**(10), 104504.
6. A. Malkin, A. Fedotov, V. Zaslavsky, S. Fil'chenkov, A. Sergeev, E. Egorova, N. Ginzburg, *IEEE Electron Device Letters*, 2021, **42**(5), 751–754.
7. N. Ginzburg, A. Malkin, V. Zaslavsky, A. Fedotov, A. Sergeev, *IEEE Transactions on Electron Devices*, 2022, **69**(2), 759–762.
8. N. Peskov, V. Zaslavsky, A. Denisenko, E. Abubakirov, A. Malkin, M. Proyavin, A. Sergeev, N. Ginzburg, IEEE Electron Dev. Lett., 2023, **44** (10),1766–1759.
9. V. Zaslavsky, I. Zheleznov, A. Sergeev, A. Palitsin, Yu. Rodin, M. Goykhman, A. Gromov, Proceedings of PIERS 2024.

Dynamics of accumulation of electrons reflected from a magnetic mirror in adiabatic and nonadiabatic helical electron beams formation systems

V. N. Manuilov

A.V. Gaponov-Grekhov Institute of Applied Physics of the Russian Academy of Sciences, Nizhny Novgorod, Russia,
v.manuilov@ipfran.ru

Helical electron beams (HEBs) play the role of an active medium (source of radiation energy) in gyrotrons - the most powerful at the moment generators in the millimeter and submillimeter wavelength ranges. The formation of HEBs can be carried out both by adiabatic (the scale of the electron trajectory step h and the radius of rotation $r_\perp$ is much smaller than the characteristic scales of inhomogeneity of the electric L_E and magnetic L_B fields) and nonadiabatic (h, $r_\perp >> L_E, L_B$) fields.

In the first case, the primary formation of the rotational velocity of electrons occurs immediately after the particle start from the cathode surface into crossed weakly inhomogeneous electric and magnetic fields; in the second, a rectilinear beam is formed first, and then the particles enter the region of non-adiabatic electric or magnetic fields. Further, in both cases, electrons are injected into the region of a smoothly increasing (adiabatic) magnetic field, where, in accordance with the law of conservation of the transverse adiabatic invariant, their rotational speed increases to the required value.

Since in both adiabatic and non-adiabatic HEB formation systems, the formed beam, due to some reasons, has a spread of rotational velocities, at large pitch factors, some electrons are reflected from the magnetic mirror and then begin to perform longitudinal oscillations between the region of primary formation (the cathode-anode gap, where an electrostatic mirror for returning particles is formed) and a magnetic mirror.

During the oscillation process, the captured charge increases and can cause a number of negative phenomena, which primarily include bombardment of the cathode and the occurrence of secondary emission from its surface, as well as loss of the beam stability. The development of these phenomena obviously depends on the specific features of distribution of the electric field in the region of the electrostatic mirror.

Therefore, it is of interest to compare the described processes in the most widely used HEB formation systems. Among nonadiabatic systems, systems with cusp magnetic field [1] (Fig. 1), widely used in large-orbit gyrotrons, and systems with nonadiabatic beam injection at an angle to the magnetic field [2] (Fig. 2) are currently being most intensively studied. The class of adiabatic systems obviously includes magnetron-injection gyrotron guns (MIGs [3], see Fig. 3).

The report presents a comparative analysis of the systems listed above from the point of view of the magnitude of the trapped charge, and the possibility of developing low-frequency oscillations of the space charge in the HEBs at large pitch factors. The features of bombardment of the cathode by reflected particles and the process of interception of reflected particles by the gun electrodes, as well as the time dependence of the potential in different sections of the beam, were studied. The beam current passing into the working space of the device was found. The analysis was performed on the basis of the large particle method within the framework of a quasi-static electric field approximation.

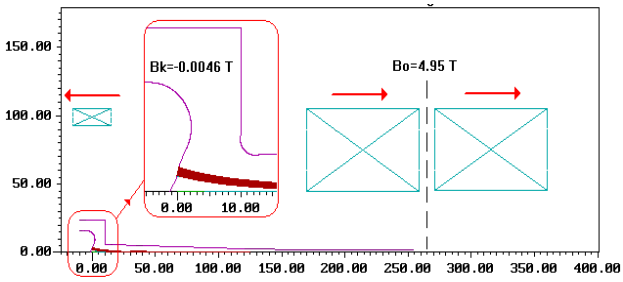

Fig. 1. HEB formation system with cusp magnetic field

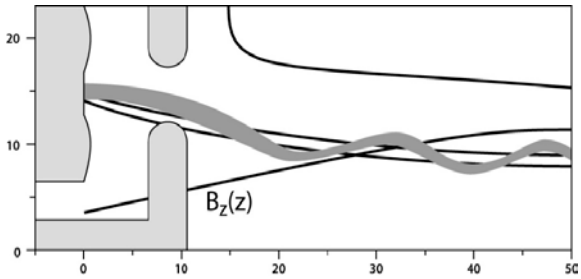

Fig. 2. Diode region of the non-adiabatic formation system with injection of the rectilinear beam through an annular slit

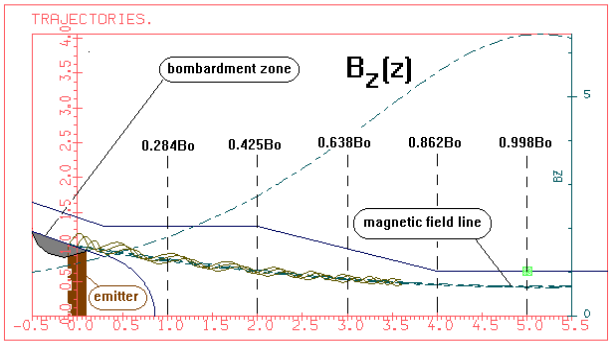

Fig. 3. Example of the adiabatic magnetron-injection gun

Acknowledgements

This work was supported by the IAP RAS project FFUF-2022-0007.

References

1. V. L. Bratman, Yu. K. Kalynov, V. N. Manuilov. *J. Commun. Technol.* El. **56**(4), 500–507 (2011).
2. A. L.Goldenberg, M. Yu. Glyavin, K. A. Leshcheva, et al. *Radiophys Quantum El* **60**, 395–400 (2017).
3. A. L. Goldenberg, M. I. Petelin. *Radiophysics and Quantum Electronics*, **16**(6), 141–149 (1973).

Analysis of the experiments with neon puffing under ECRH/ECCD in T-10 tokamak plasmas with tungsten and carbon limiter

S. V. Neudatchin, A. A. Borschegovskiy, A. R. Nemets, I. S. Pimenov, I. A. Zemtsov

NRC «Kurchatov Institute», RF, 123182 Moscow, Kurchatov sq. 1, sneudat@yandex.ru

A new type of L-H transitions, called semiglobal, was found in plasma with a tungsten limiter. Spontaneous transitions (including quasi-periodical one) are observed only with simultaneous co+contr ECCD with 1.5 MW power [1, 2]. The electron heat and density fluxes drop abruptly in almost the entire volume of the plasma at the moment of transition. Such transitions were not previously known in tokamaks with a circular cross-section and a limiter.

At the moment of global L-H transitions reported on JET and JT-60U tokamaks earlier (see [3] and references therein), the electron, ion temperature $T_{e,i}$ and density n_e start to rise simultaneously in almost the entire plasma volume. A typical abrupt increase in the value of the energy confinements time τ_E is 30–50%. The evolution of the EAST tokamak discharge parameters at L-H transition reported in [4] shows that the value of τ_E is abruptly doubled.

In T-10, the growth of T_e occurs only in the central part of the plasmas and ITB is formed on T_e. The accumulation of tungsten is absent. An analysis of experiments [5, 6] showed that similar semiglobal transitions in plasma with a tungsten limiter are also caused by neon puffing at different EC power. An example of ITB formation after a transition caused by neon puffing is shown in Fig. 1. In a series of pulses [5, 6], the edge density was also measured. The diffusion coefficient drops abruptly in almost the entire plasma volume, and the density at the edge increases 1.5 times faster than inside. The formation of a weak external transport barrier begins. It is this fact that allows us to call the new type of transitions L-H transitions.

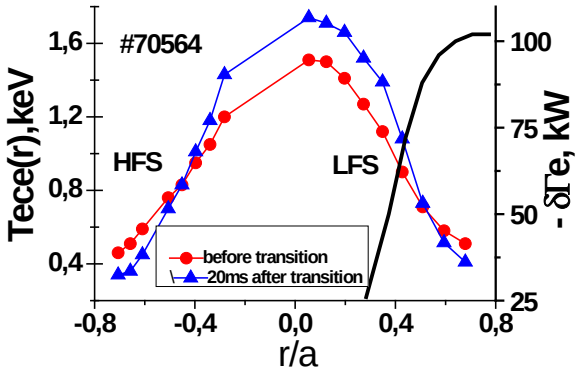

Fig. 1. T_e profiles before and 20 ms after the L-H transition induced by neon puffing and profile of the electron heat flux jump $\delta\Gamma_{Te}$ at the moment of the L-H transition at P_{ECRH} = = 0.85 MW

The profile of the jump in the electron heat flux $\delta\Gamma_{Te}$ at the moment of transition (P_{ECRH} = 0.85 MW) is shown in Fig. 1. A typical abrupt increase in the value of τ_E is about 15%, which is noticeably less than with global L-H transitions on JET and JT-60U tokamaks. This is not surprising, since at L-H transitions on all tokamaks with a circular cross section, the value of τ_E increases insignificantly. It is shown that the energy content of plasma W is almost linearly dependent on density, and the role of ITB is not significant in the stationary phase of the discharge in all studied cases. In the pulse shown in Fig. 1, the value of W and the central line averaged density increase by 30% in 20 ms after the moment of transition. Radiation losses only begin to increase at the moment of transition, rising from 90 to 150 kW in 20 ms.

Transitions similar to those described above were not detected at neon puffing into a plasma with a carbon limiter. There is no growth of T_e, and a smooth small increase of τ_E begins after peaking of the density profile, resembling a typical picture of the transition to the RI mode at various tokamaks (the Z_{eff} value increases after the neon puffing, ITG instability is suppressed, density is peaked, leading to further suppression of instability). The edge density increases slightly after short neon puffing and returns to its previous level later. The final growth of W is proportional to the growth of the central line averaged density.

The report also provides new examples of semiglobal transitions triggered by spontaneous drop of lithium-containing flakes at a various EC power lower than in the pulse described in [7] (simultaneous co+contr ECCD with 1.5 MW power).

The work was carried out with the support of the NRC Kurchatov Institute.

References

1. A. Borschegovskiy, S. Neudatchin, I. Pimenov et al., *EPJ Web of Conf.* 2019, 203 02004.
2. S. Neudatchin, A. Borschegovskiy, I. Pimenov, I. Zemtsov *Proc. 28-th Fusion Energy Conference* 2021 EX/P4-26.
3. S. Neudatchin, T. Takizuka, H. Shirai et al., *Pl. Phys.* Control. Fusion 2002, 44 A383-389.
4. G. Xu et al., *Nucl. Fusion* 2014 54 103002 (21pp).
5. N. Kasyanova, K. Rasumova et al, *45th EPS Conf. on Pl. Phys., Prague, ECA*, 2018, Vol. 42A, P4. 1106.
6. N. Kirneva et al., *45th EPS Conf. on Pl. Phys., Prague, ECA*, 2018, Vol. 42A, P4. 1081.
7. S. Neudatchin, I. Pimenov, A. Borschegovskiy, et al., *J. of Phys.: Conf. Ser.* 2019, 1383 012005.

Quasi-analytical models of the gyro-BWO with zigzag quasi-optical microwave system: one-wave and two-wave implementations

E. M. Novak[1, 2], **A. V. Savilov**[1,2] and **S. V. Samsonov**[2]

[1] National Research Lobachevsky State University, Nizhny Novgorod, Russia
[2] A.V. Gaponov-Grekhov Institute of Applied Physics of the Russian Academy of Sciences, Nizhny Novgorod, Russia

Intensive work is currently being carried out by a number of scientific groups aimed at developing alternative schemes of sub-terahertz gyro-oscillators possessing relatively broad bands of continuous (or quasi-continuous) frequency tuning. In particular, a microwave system in the form of a quasi-optical transmission line was proposed recently as an interaction circuit for certain varieties of the cyclotron resonance maser, including the gyrotron Backward-Wave Oscillator (gyro-BWO) [1]. The circuit consists of focusing mirrors, which are periodically spaced along the longitudinal z-axis and provide transport of the Gaussian wave beam along a zigzag path (Fig. 1). A beam of electrons is guided by a static magnetic field along the z -axis so that the e-beam periodically crosses the wave beam. The electron-wave interaction occurs in regions where the wave, as in a gyrotron, propagates strictly across the e-beam resulting in the interaction with minimal sensitivity to particle velocity spread. 3D PIC simulations demonstrate the attractiveness of this "zigzag" cyclotron-resonance maser for the implementation of gyro-BWOs operating in the sub-THz frequency range with unique frequency tunability [1].

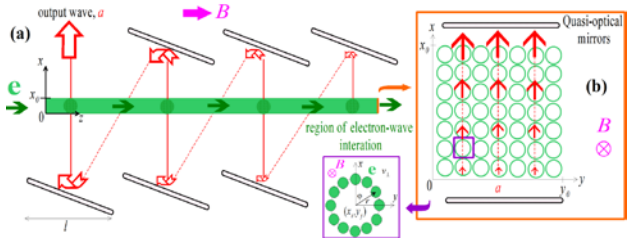

Fig. 1. (a) A 2D scheme of the gyro-BWO with a zigzag path of the operating wave, consisting of $N = 4$ sections of electron-wave interaction. (b) A cross section of an electron beam

In our work [2, 3], we proposed a quasi-analytical 2D model of the zigzag-type gyro-BWO to describe the small-signal (linear) stage of excitation of this auto-oscillator in the stationary single-frequency approximation. In fact, the zigzag-type gyro-BWO represents a system that is principally different from "more classical" versions of electron RF oscillators. The main purpose of this paper is not so much the development of a non-stationary spatio-temporal theory of the zigzag gyro-BWO, as the description of the rich possibilities of a fairly simple approach that allows the development of such a theory. Actually, a simple quasi-analytical 2-D model describes a large number of effects specific to this device, including (i) a discrete piecewise character of the dependence of the generation frequency on the magnetic field $f(B_0)$, (ii) establishment of stationary generation modes in the process of competition of various modes, (iii) switching to self-modulation modes with increasing operating current (normalized length of the system), (iv) the possibility of implementing the super-radiant regimes of formation of short powerful wave pulses in this device, (v) an increase in the generation power when using external feedback in the system and (vi) the phenomenon of hysteresis with a smoothly changing synchronism mismatch in continuous generation mode.

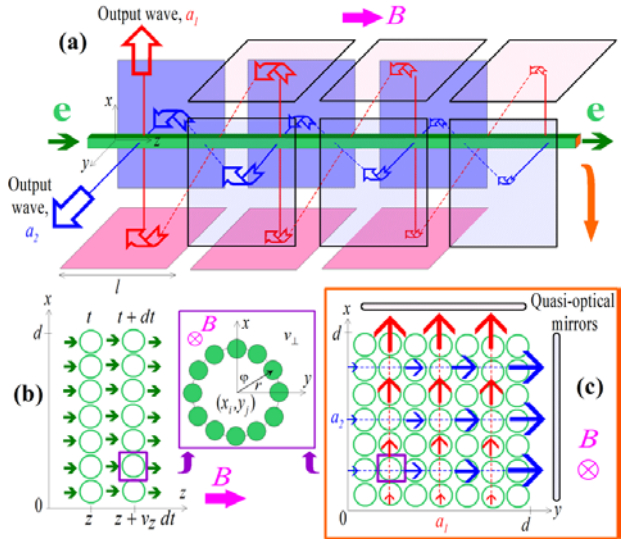

Fig. 2. (a) A 3D model of a zigzag gyro-BWO with two orthogonal wave beams. (b) An electron beam in the form of a set of micro-ensembles (c) A cross section of an electron beam. The scheme of electron-wave interaction

In addition, the spatio-temporal theory of a 3D zigzag gyro-BWO circuit consisting also of 4 amplification sections of electron wave interaction, but in which two orthogonal waves propagating in some perpendicular directions (along x- and y- axes) are investigated (Fig. 2). The important issue of the competition of these two waves in the system has been resolved, during which stable single-frequency generation of one of these waves is ensured.

Acknowledgements

This work is supported by the State Assignment of the Institute of Applied Physics RAS, project No. FFUF-2022-0007.

References

1. S. V. Samsonov, G. G. Denisov, A. A. Bogdashov, and I. G. Gachev, *Photonics & Electromagnetics Research Symposium (PIERS)*, 2021, pp. 2790–2799.
2. E. M. Novak, S. V. Samsonov and A. V. Savilov, *IEEE Trans. Electron Devices*, 2022, 69, 5199.
3. E. M. Novak, S. V. Samsonov and A. V. Savilov, *Phys. Plasmas*, 2023, 30, 043101.

Enhancement of megawatt power gyrotron operation using injection locking

Yu. V. Novozhilova, A. N. Kuftin, A. P. Fokin, G. G. Denisov, M. Yu. Glyavin, A. S. Zuev

A.V. Gaponov-Grekhov Institute of Applied Physics of the Russian Academy of Sciences, Nizhny Novgorod, Russia,
julia.novozhilova2009@yandex.ru

Introduction

Gyrotrons are the most powerful sources of continuous-wave radiation in millimeter and submillimeter wavelength ranges [1]. The most prominent application of gyrotrons is the plasma heating and current drive, as well as plasma diagnostics in controlled fusion facilities. the operation of powerful gyrotrons at high-order modes of the cylindrical cavity brings the problem of mode competition, which limits the maximum power and efficiency [2]. The use of the frequency locking by an external low-power narrowband signal [2] can simultaneously provide the frequency stabilization, increase of output power and mode selection. Such approach is well investigated theoretically [2–4], but only recently was verified in experiment at 170GHz/1MW gyrotron [5]. Such experiment became possible after the development of the mode converter for the modes of cylindrical waveguide with different rotation directions [6] and gyrotron frequency stabilization technique by the means of phase-lock loop [7, 8].

Experimental results

The operations regimes are different under the influence of the external signal: there is a zone of frequency-locked operation, where the frequency of the generation is equal to the frequency of the external signal at all magnetic fields, and the zone of beating of frequency and field amplitude. The position of the locking zone relative to the operation zone is determined by the frequency of the external signal. The exit of the operating zone is accompanied, as in a free-running gyrotron, by the excitation of the parasitic modes.

The possibility of significant (up to 2.5 times) increase of the operating zone of the desired mode under the influence of the external signal was demonstrated in the experiment [5]. The locking zone shifted over the operating zone of the $TE_{28,12}$ mode with the increase of the external signal frequency. At low solenoid currents the boundary of the operating zone was shifted by a small amount due to the suppression of the parasitic $TE_{27,12}$ mode. At the same time the maximum output power was also increased by 11% due to advance to optimal operating parameters. At high solenoid currents (112–113 A) the operating zone was significantly enlarged due to suppression of $TE_{29,12}$ mode.

Theoretical results and discussion

The numerical simulations of the system were performed in the self-consistent model with the fixed axial field structure. The frequency of the external signal is close to the eigenfrequency of the operating mode and differs significantly from the eigenfrequencies of other interacting modes (compared to the bandwidth of each mode, while all the interacting modes lie within the cyclotron resonance band. We also assume that the external signal has the same transverse structure as the operating mode $TE_{28,12}$. The energy of all electrons at the entrance to the interaction space is the same, but a spread in transverse and longitudinal velocities.

As in experiment, the output power and efficiency are increased when the locking zone is at the low magnetic fields, the calculated power increase of 11% corresponds to one observed in experiment. The tuning band can be extended about 2 times at high magnetic fields, which also matches with the experimental results.

The calculated dependencies of the field amplitude outside of the locking zone present the beating at the frequency close to the difference between the frequencies of the free-running gyrotron and the external signal in the case of big frequency mismatch. Closer to the locking zone the beating frequency is decreased, in conformity with [9].

Conclusion

Demonstrated agreement of the theoretical calculations with the experimental observations confirm the accuracy of the developed theoretical model and allow to use such rather simple and non-demanding of computer resources approach to simulation of complex multi-mode dynamics of modern gyrotrons.

Acknowledgements

This work was supported by the RSF project № 19-79-30071.

References

1. M. Thumm. Karlsruhe: KIT Scientific Publishing (2024).
2. V. L. Bakunin, G. G. Denisov, Y. V. Novozhilova, and A. P. Fokin, *Radiophys. Quantum Electron.*, 2017, **59** (8–9), 638–647.
3. I. V. Zotova, N. S. Ginzburg, G. G. Denisov, et al. *Radiophys. Quantum Electron.*, 2016, **58** (9), 684–693.
4. P. Brucker, K. A. Avramidis, A. Marek, M. Thumm, and J. Jelonnek, *46th Int Conf Infrared, Millim and Terahertz Waves (IRMMW-THz)*, 2021, 1–2.
5. A. N. Kuftin, G. G. Denisov, A. V. Chirkov, et al. *IEEE Electron Device Lett.*, 2023, **44**(9), 1563–1566.
6. A. V. Chirkov, G. G. Denisov, and A. N. Kuftin, *Appl. Phys. Lett.*, 2015 , **106** (26), 263501.
7. A. Fokin, M. Glyavin, G. Golubiatnikov, et al. *Sci. Rep.*, 2018, **8**(1), 4317.
8. G. G. Denisov, A. N. Kuftin, V. N. Manuilov, et al. *Microw. Opt. Technol. Lett.*, 2020, **62**(6), 2137–2143.
9. M. I. Rabinovich and D. I. Trubetskov, *Oscillations and Waves in Linear and Nonlinear Systems*. Dordrecht: Springer Netherlands, 1989.

High intensity compact 2.45 GHz PMECR ion source and its fundamental physics

Shixiang Peng, Bujian Cui, Tenghao Ma, Wenbin Wu, Kai Li, Yicheng Dong, Zhiyu Guo and **Jiaer Chen**

State Key Laboratory of Nuclear Physics and Technology & Institute of Heavy Ion Physics,
School of Physics, Peking University, No.201, Chengfu Road, Haidian District, Beijing, China, sxpeng@pku.edu.cn

2.45 GHz Electron Cyclotron Resonace (ECR) ion source has been widely used in particle accelerators, materials science, astrophysics and atomic physics because of its plentiful advantages, such as intense current, low emittance, simple structure, convenient maintenance, low cost, high stability and long life. In recent years, the miniaturization of 2.45 GHz ECR ion source has become significant for its wide application. Meanwhile, imperious demands have been placed on the intensity of $H^+/H_2^+/H_3^+$ ion beams with the development of numerous fields. Although a multitude of breakthroughs have been made in the experimental research of the ECR hydrogen ion source, the related mechanism research is still in process, which badly limits the improvement of ion source performance. At Peking University (PKU), the research of compact microwave ion source has been launched since the last century. Attentions are paid both on experimental research as well as the fundamental physics study. A series of 2.45 GHz permanent magnet ECR ion sources with dielectric RF matching have been built at PKU. The dimension of a water-cooling three-electrode ion source is about 160 mm × ϕ180 mm, a homemade high-voltage breakup was developed to limited the high voltage region within a 180 mm × ϕ220 mm and a 50 kV @ 130 mA proton beam already be extracted with this course. It can also easily produce tens mA $H_2^+/H_3^+/O^+/N^+/Ar^+/He^+$ beam with beam density over 400 mA/cm^2. The photograph of PKU-type 2.45 GHz ECR ion source is shown in Fig. 1. A continuous operation more than 300 hours has been recorded, and neither sparks nor plasma instability occurred during that running period, displayed in Fig. 2. Several copies of that ion source have been used to deliver beams for accelerator facilities like DWA, C-RFQ, PKUNIFTY, Proton-therapy and BNCT machines since 2006. In the meantime, some physical models are established, including global model, hybrid discharge heating model and antenna coupling mechanism, to provide guidance for the design and operation of high current compact ion sources to provide guidance for the design and operation of high current compact ion sources.

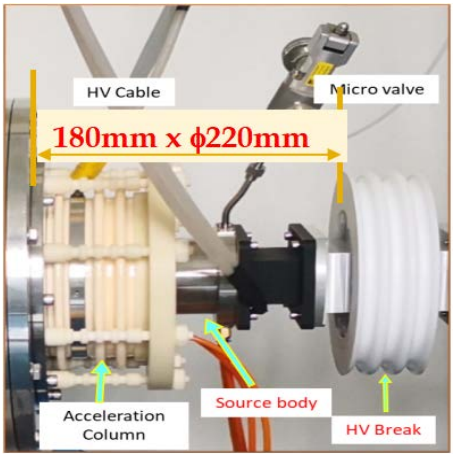

Fig. 1. Photograph of a PKU-type 2.45 GHz ECR ion source

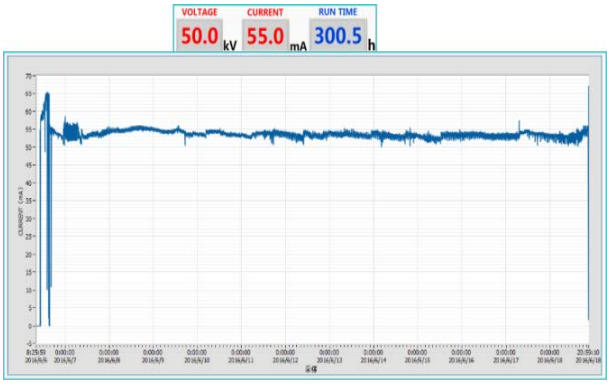

Fig. 2. (color online) Screenshot of the monitor computer at the end of longevity test. Top: extraction voltage, instantaneous current, and counting hours. Bottom: beam current versus elapsed time

Acknowledgements. This work was supported by the NNSF of China (Grant Nos.11975036, 11775007). The authors would like to thank the colleagues who participated in fruitful discussions, and all the component manufacturer.

References

1. Peng, S. X., Zhang, A. L., Ren, H. T., Xu, Y., Zhang, T., Zhang, J. F., ... & Chen, J. E. (2017). New progress on beam availability and reliability of PKU high intensity CW proton ECR ion source. Chinese Physics B, 26(2), 025206.
2. Wu, W., Peng, S., Zhang, A., Ma, T., Jiang, Y., Li, K., ... & Chen, J. (2022). Theoretical and experimental study of the over-dense plasma generation in a miniaturized microwave ion source. Journal of Applied Physics, 132(8).
3. Wu, W., Zhang, A., Peng, S., Ma, T., Jiang, Y., Li, K., ... & Chen, J. (2020). A global model of 2.45 GHz ECR ion sources for high intensity H+, H2+ and H3+ beams. Vacuum, 182, 109744.
4. Wu, W., Peng, S., Ma, T., Ren, H., Zhang, J., Zhang, T., ... & Chen, J. (2019). Status of high current H2+ and H3+ ion sources. Review of Scientific Instruments, 90(10).
5. Peng, S.X., Ma, T.H., Wu, W.B. et al. new progress of the miniaturized microwave ion source at Peking University. Radiat Detect Technol Methods 7, 545–549 (2023).

Sub-GW / sub-THz Cherenkov masers with 2D-periodic slow-wave structures

N. Yu. Peskov[1,2], V. Yu. Zaslavsky[1,2], A. N. Denisenko[1], N. S. Ginzburg[1], E. B. Abubakirov[1], A. V. Palitsin[1], A. N. Panin[1], M. D. Proyavin[1], Yu. V. Rodin[1], A. V. Arzhannikov[2], P. V. Kalinin[2], E. S. Sandalov[2], S. L. Sinitsky[2] and **V. D. Stepanov[2]**

[1] A.V. Gaponov-Grekhov Institute of Applied Physics of the Russian Academy of Sciences, Nizhny Novgorod, Russia, peskov@ipfran.ru

[2] Budker Institute of Nuclear Physics of the Russian Academy of Sciences, Novosibirsk, Russia

Introduction

Relativistic Cherenkov-type generators based on high-current electron beams provide a record level of pulsed power in the centimeter and long-part of the millimeter wavelength ranges. However, further increase in the output power and the advance to shorter radiation wavelength bands inevitably leads to the need to increase the oversize of the interaction space, and, correspondingly, to the problem of provision of mode selection with respect to the transverse index.

The most effective method for solving this problem in high-power oversized Cherenkov masers is the use of 2D distributed feedback (DFB), which is implemented in 2D-periodic slow-wave structures (SWS) by means of additional transverse wave-fluxes arising on such a corrugation [1]. Conducted studies have demonstrated high potential of using the 2D DFB mechanism to obtain powerful narrow-band radiation in relativistic masers of various types, whose transverse dimensions exceed the radiation wavelength by an order of magnitude or more [2, 3].

SWO with 2D SWS of cylindrical geometry

Spatially-extended Cherenkov Surface-Wave Oscillator (SWO) operating at the W-band (operating frequency ~ 73 GHz) was constructed based on the "Sinus-6" accelerator 0.5 MeV / 5 kA / 25 ns (IAP RAS) forming annular electron beam with a diameter of ~ 40 mm. Oscillators of such type are preferable among the relativistic Cherenkov masers due to the larger values of the electron-wave coupling impedance. For this SWO, the 2D SWS was designed with oversize factor $Ø/\lambda \sim 10$, number of azimuthal variations of 32, and a total length of 11 cm.

Simulations of the 2D SWO were carried out using PIC-code CST Studio Suite. Results of simulations demonstrated establishment of narrow-band oscillation with the output power of ~ 175 MW under the design parameters. Mode pattern of the synchronous slow-wave demonstrates azimuthally symmetric distribution and contains the $TM_{0,n}$ – type waveguide modes.

In the conducted experiments, a stable narrow-band generation was observed under the design parameters. The radiation frequency, according to the heterodyne technique used, was measured as ~ 73 GHz with a spectrum width close to its theoretical limit at the detected pulse duration up to 10 ns, which corresponded to the excitation of the fundamental mode of the 2D SWS. Output radiation directional diagram demonstrated a pronounced minimum on the axis and coincided with the excitation of the designed pattern of $TM_{0.n}$ – type modes, thus, proved the azimuthally-symmetric structure of the output radiation. The maximum output power was observed at a guide magnetic field of ~ 1.2 T and, according to calorimetric measurements, reached 150 MW, which is in good agreement with the simulations.

Currently, experimental studies of cylindrical SWO with 2D SWS have been started at the G-band (frequency ~ 150 GHz), where the oversize factor of the generator is $Ø \sim 20\lambda$ while maintaining the transverse size of the beam. For this project, 2D SWS was constructed with 64 azimuthal variations (turns) and 7.5 cm long.

Simulations under experimental conditions demonstrated stable selective excitation of the fundamental "azimuthally-symmetric" mode of the 2D SWS, the radiation power reached 70–90 MW.

In the initial experiments, a powerful narrow-band generation was obtained at optimal parameters. Heterodyne measurements demonstrated the excitation of the operating surface wave of the 2D SWS having an azimuthally-symmetric structure of the output radiation. The measured radiation power was ~ 30–50 MW. The SWO parameters are currently being optimized in order to increase electron efficiency and output power.

Project of super-power planar SWO with 2D DFB

Projects of super-power Cherenkov masers of planar geometry are under development within the framework of the BINP - IAP collaboration based on the ELMI accelerator 1 MeV / 10 kA / 3 μs, forming sheet electron beams with a transverse size up to 20 cm (BINP RAS). Simulations showed that in such generators, a GW-power level in the W-band (operating frequency ~ 75 GHz) and up to ~ 0.6 GW in the G-band (frequency ~ 150 GHz) can be achieved. Herewith, the use of planar 2D-periodic SWS implementing the 2D DFB mechanism makes it possible to ensure a stable coherent oscillation regime with transverse size (width) of the system amounting to 50 and 100 radiation wavelengths, respectively.

Currently, all components of the W-band SWO have been manufactured. The assembly of the generator was completed and its high power testing was started.

Acknowledgements

Creation of SWO with cylindrical 2D SWS is supported by the IAP RAS Program (# FFUF-2022-0007). Development of planar schemes of SWO with 2D DFB is carried out with the support of the Russian Science Foundation (grant # 23-19-00370).

References

1. N. S. Ginzburg, V. Yu. Zaslavsky, A. M. Malkin, et al., *Tech. Phys. Lett*., 2010, **36**(1), 83–87.
2. A. V. Arzhannikov, N. S. Ginzburg, V. Yu. Zaslavsky, et al., *Tech. Phys. Lett*., 2013, **39**(9), 801–804.
3. N. Yu. Peskov, V. Yu. Zaslavsky, A. N. Denisenko, et al., *IEEE Electr. Dev. Lett.*, 2023, **44**(10), 1756–1759.

Gyrotrons and applications in Ariel

Moritz Pilossof, Sergey Shevchenko, Yarden Shay and **Moshe Einat**

Ariel University, Ariel, Israel, moritzp@ariel.ac.il

Research on gyrotrons and applications is conducted at Ariel University, Israel. Advance in gyrotron developments during the recent years of is presented. W-band long and short pulse gyrotrons as well as Ka-band short pulse gyrotrons were developed [1], built and tested experimentally. Long pulse gyrotron at W-band with room temperature electromagnets were developed for almost a decade.

The first gyrotron demonstrating the concept of room temperature electromagnet for W-band gyrotron at second harmonic was presented at 2016 [2, 3]. It produced few kilowatts peak power with pulse duration of 50 μs and 5% duty cycle for a few seconds.

Following, a long pulse gyrotron with room temperature magnet was made with internal mode converter and cooled collector [4]. The output power for a long pulse operation was about 10 kW limited by the high voltage power supply. For short pulses the gyrotron output was more than 30 kW with efficiency above 20%.

The third gyrotron in this series is with improved efficiency after some modification of the magnetic profile and depressed collector, see Fig 1. Its output power is ~ 30 kW with efficiency of ~ 30%. This gyrotron experimental results will be presented.

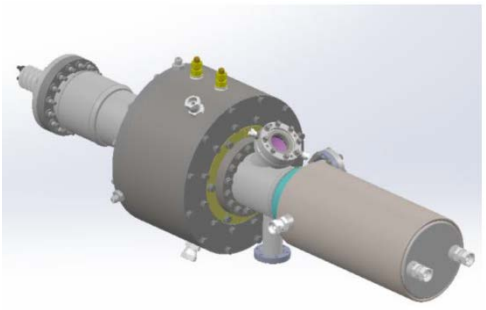

Fig. 1. Model of the W-band room temperature gyrotron with depressed collector

These long pulse gyrotrons are millimeter wave sources for applicator that is used for collaborations with scientists in the fields of chemistry, biology [5] and materials engineering within Ariel University and worldwide. Hard rock melting and initial results of drilling with this gyrotron will be present. Development of 100 kW W-band second harmonic gyrotron for deep drilling of hard rock is an ongoing research. Some preliminary work of this gyrotron will be presented too.

A Ka-band MW short pulse gyrotron is also in the initial stage of development, it is intended for integration in particle accelerator.

Acknowledgements

This work is supported by the Israeli Ministry of Energy and Infrastructure, the grant number 222-11-011.

References

1. M. Witman, E. Avraham, R. Ben-Moshe, M. Pilossof and M. Einat, "Long-Pulse Uncooled Copper Magnet for Gyrotron," in IEEE Transactions on Electron Devices, vol. 66, no. 11, pp. 4928–4931, Nov. 2019.
2. D. Borodin and M. Einat, "Copper Solenoid Design for the Continuous Operation of a Second Harmonic 95-GHz Gyrotron," in IEEE Transactions on Electron Devices, vol. 61, no. 9, pp. 3309–3316, Sept. 2014.
3. M. Pilossof and M. Einat, "Initial results of 95 GHz gyrotron with water cooled magnet," 2016 41st International Conference on Infrared, Millimeter, and Terahertz waves (IRMMW-THz), Copenhagen, Denmark, 2016, pp. 1–2.
4. M. Pilossof and M. Einat, "High-Average-Power Second Harmonic W-Band Gyrotron with Room-Temperature Solenoid," in IEEE Transactions on Electron Devices, vol. 67, no. 4, pp. 1804–1807, April 2020.
5. L. S. Kaczmarczyk, K. S. Marsay, S. Shevchenko, M. Pilossof, N. Levi, M. Einat, M. Oren, & G. Gerlitz. Corona and polio viruses are sensitive to short pulses of W-band gyrotron radiation. Environmental chemistry letters, 19(6), 3967–3972. 2021.

On saturation of induced scattering low-threshold instability in the tokamak edge transport barrier at O1 ECRH

E. Z. Gusakov and **A. Yu. Popov**

Ioffe Institute, St.-Petersburg, Russia, a.popov@mail.ioffe.ru

Parametric decay instability (PDI) is a nonlinear phenomenon often encountered in various plasmas. The threshold of PDI excitation in inhomogeneous plasmas is usually determined by the efficiency of nonlinear coupling of a pump wave with daughter waves leaving the finite interaction region, where the wave decay conditions for the numbers of interacting waves are fulfilled. Theoretical analysis of the behavior of microwaves used for electron cyclotron resonance heating (ECRH) of plasma in toroidal fusion devices had been carried out three decades ago and had resulted in fairly high values of excitation thresholds and optimistic predictions on the role of nonlinear phenomena in ECRH experiments [1]. However, recent observations of anomalous scattering of microwaves [2], plasma emission at half-integer harmonics of the gyrotron frequency [3], fast ion group generation during ECRH [4], broadening of the power deposition profile (PDP) of EC waves [5–7] and missing power effect [8,9] evidence a nonlinear behavior of strong microwaves in toroidal devices.

To explain and describe the anomalous phenomena that accompany microwave propagation, the model of low-threshold PDI was proposed [10]. It predicts the decay of a pump wave, when it passes any local maximum of the density profile, into daughter waves, at least one of which is localized in the decay region. This model allows a detailed quantitative explanation of anomalous phenomena during ECRH (see, e.g., [11, 12]).

It deserves to be mentioned that the broadening of the PDP at ECRH and the missing power effect was observed also in the case of a monotonic plasma density profile [6, 8, 9]. In this report, we propose the model describing a significant decrease in the PDI threshold at a monotonic density profile and allowing us to qualitatively explain the broadening of the PDP. Quite unexpectedly the pump microwave parametric decay can occur in the steepest region of the density profile, *i.e.* in the edge transport barrier, which usually exists in high performance discharges, and where, at first sight, the convective losses of daughter waves should be maximum and the conclusions of the theoretical analysis [1] should be justified. Nevertheless, the specific transparency domains [13] for intermediate frequency range electron plasma waves (EPWs) within the transport barrier result in their easy parametric excitation [14]. As it was shown, these daughter EPWs can be trapped both in the direction of plasma inhomogeneity due to the edge transport barrier and along the magnetic field in its ripples associated with a finite number of the toroidal magnetic field coils. Since the threshold of the PDI leading to the excitation of localized EPWs [14] turn out to be much lower than those predicted for the generation of non-localized daughter EPWs [1], absolute PDI of megawatt microwave beams seems possible in future O1-mode ECRH experiments at ITER. This can lead to a broadening of the PDP at ECRH. The characteristics of this broadening are determined by the saturation level of this instability.

We show that the saturation of this low-threshold PDI in current toroidal devices is due to the amplitude-dependent "stochastic" damping of the daughter localized EPWs [15]. The balance between the "stochastic" damping of the daughter EPWs and their nonlinear pumping leads to equilibrium in this nonlinear system and, eventually, to the instability transition to the saturation regime [15]. However, in the case the pumping provided by several microwave beams acting in the same tokamak port exceeds the EPW maximal stochastic damping the instability develops further. This “second” PDI power threshold in the case of ITER edge transport barrier is estimated as 4 MW. In the case the “second” threshold is exceeded a substantial pump depletion can be expected.

Acknowledgements

The work was supported by the Russian Science Foundation (project no. 22-12-00010, analytical study) and by the Ministry of Science and Higher Education of the Russian Federation (state contract №0040-2024-0028, numerical simulation, and state contract no. 0034-2021-0003, the development of a code for the PDI simulation).

References

1. A. G. Litvak, A. M. Sergeev, E. V. Suvorov, et al., *Phys. Fluids*, 1993, B **5**, 4347.
2. A. Tancetti, S. K. Nielsen, J. Rasmussen, et al., *Nucl. Fusion*, 2022, **62**, 074003.
3. S. K. Hansen, S. K. Nielsen, J. Stober, et al., *Nucl. Fusion*, 2020, **60**, 106008.
4. M. Martinez, B. Zurro, A. Baciero, et al., *Plasma Phys. Control. Fusion*, 2018, **60**, 025024.
5. E. Z. Gusakov, A. Yu. Popov, A. I. Meshcheryakov, et al., *Phys. Plasmas*, 2023, **30**, 122112.
6. J. H. Slief, R. J. R. van Kampen, M. W. Brookman, et al., 2023, *Nucl. Fusion* **63**, 026029.
7. J. Cazabonne, S. Coda, J. Decker, et al., 2024, *Nucl. Fusion*, **64**, 026019.
8. M. Yu. Kantor, G. Bertschinger, P. Bohm, et al., 2009, *Proc. of 36th EPS Conference on Plasma Phys.*, Sofia, ECA Vol. 33E, P-1.184.
9. Yu. N. Dnestrovskij, A. V. Melnikov, D. Lopez-Bruna, et al., *Plasma Phys. Control. Fusion*, 2023, **65**, 015011.
10. E. Z. Gusakov, A. Yu. Popov, *Phys. Usp.*, 2020, **63**, 365.
11. E. Z. Gusakov, A. Yu. Popov, P. V. Tretinnikov, *Nucl. Fusion*, 2019, **59**, 106040.
12. E. Z. Gusakov, A. Yu. Popov, *Plasma Phys. Rep.*, 2023, **49**, 949.
13. E. Z. Gusakov, M. A. Irzak, A. D. Piliya, 1997, *JETP Lett.*, **65**, 25.
14. E. Z. Gusakov, A. Yu. Popov, *Phys. Rev. Lett.*, 2022, **128**, 065001.
15. E. Z. Gusakov, A. Yu. Popov, *JETP Letters*, 2024, **119**, 505.

Gyrotron-based setups for low temperature plasma physics

M. D. Proyavin[1], **M. V. Morozkin**[1], **D. I. Sobolev**[1], **I. V. Izotov**[1], **A. A. Orlovskiy**[1], **M. V. Kamenskiy**[1], **E. A. Soluyanova**[2], **E. M. Tai**[2] and **M. Yu. Glyavin**[1]

[1] A.V. Gaponov-Grekhov Institute of Applied Physics of the Russian Academy of Sciences, Nizhny Novgorod, Russia, pmd@ipfran.ru

[2] GYCOM, Nizhny Novgorod, Russia

Microwave complexes are currently actively used as ECR heating of low-temperature plasma in various installations. The most striking examples of such applications are compact sources of high-current ion beams and heavy ions. The areas of application of such systems are varied: from the production of new elements to ion and boron-neutron capture therapy [1, 2]. Low-temperature plasma physics technologies also include growing diamond films and disks using the CVD method. In all such installations, complexes based on gyrotrons are increasingly used as a source of ECR plasma heating. Unlike other vacuum microwave generators, these devices are capable of providing radiation in large frequency ranges (from several GHz to the THz range) and powers (from several watts to megawatts). The overwhelming number of existing gyrotron complexes operate at the second harmonic of cyclotron resonance, which allows one to significantly reduce the consumption of an electromagnet, which provides a magnetic field for electron-wave interaction. The development of the such technologies increases the requirements for frequency, power and long-term (months) stability of microwave radiation, which is becoming increasingly difficult to achieve in existing systems.

Therefore, the development of a new generation of technological gyrotron complexes is currently underway, some of which have already been successfully implemented. The basis of such systems is a magnetically shielded system (MSS), which makes it possible to obtain twice the magnetic field while maintaining the same level of power consumption. On the one hand, this makes it possible to operate at the main cyclotron resonance. In this way, it is possible to achieve greater efficiency, power and stability of single-mode excitation in the process, for example, of power adjustment over a wide range. On the other hand, the concentration of the magnetic field in the cavity region leads to a complication of the problem of electron optics - the formation and deposition of an electron beam. In the process of developing such a gyrotron complex, the following tasks were self-consistently solved: optimization of the MSS and the profile of its ferromagnetic screens, electron optics, electron-wave interaction, synthesis of the radiation output system.

As the first prototype, a 28 GHz / 25 kW / CW gyrotron complex (fig. 1) was created [3]. The experimental results showed the possibility of achieving large ($g \approx 2$) values of the beam pitch factor while maintaining a small spread of electron transverse velocities. This is evidenced by both the low anode current (about 20 mA) and the obtained generation efficiency (up to 55%) without a residual energy recovery system. The development of this complex was primarily carried out in order to upgrade the existing complex for growing diamonds using the CVD method at the IAP RAS [4]. To integrate the new generator into the existing microwave path, a unique converter of complex shape was synthesized and produced.

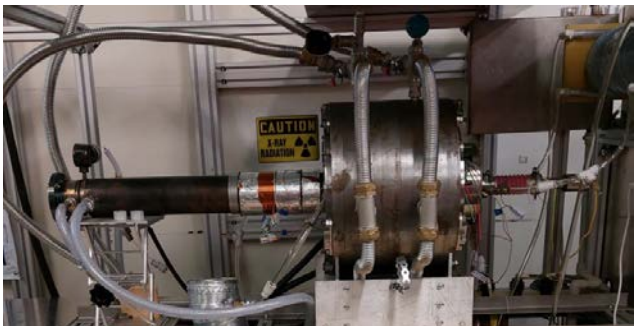

Fig. 1. Photograph of the 28 GHz/25 kW first harmonic gyrotron setup based on MSS

Currently, similar complexes are being developed in the frequency range of 14-28 GHz and powers of 2–10 kW for projects on the synthesis of new elements at the Joint Institute for Nuclear Research [5]. As part of the first stage, the PRISMA 28 GHz / 10 kW complex (fig. 2) with a new control system was successfully implemented.

Fig. 2. Photograph of the 28 GHz /10 kW-based complex for ion sources in JINR

Acknowledgements. This work was supported by the IAP RAS project FFUF-2022-0007.

References

1. Lu, L. et al., High power test of an injector linac for heavy ion cancer therapy facilities. Physical Review Special Topics - Accelerators and Beams, 18(11). doi:10.1103/physrevstab.18.111002.
2. V. A. Skalyga et al., Gasdynamic electron cyclotron ion sources: Basic physics, applications, and diagnostic techniques. Rev. Sci. Instrum. 1 March 2022; 93 (3): 033502. https://doi.org/10.1063/5.0075486.
3. M. D. Proyavin et al., "Results of the Study of a New Generation Technological Gyrotron System With High Power and Efficiency," Electron Device Letters, vol. 44, no. 1, pp. 148–151, Jan.2023, doi:10.1109/LED.2022.3222169.
4. A. L. Vikharev et al., "Diamond films grown by millimeter wave plasma-assisted CVD reactor", Diamond Rel. Mater., vol. 15, no. 4, pp. 502–507, Apr. 2006.
5. A. Efremov, S. Bogomolov, V. Mironov; The role of ion sources in synthesis of the super-heavy elements. Rev. Sci. Instrum. 1 January 2020; 91 (1): 013314. https://doi.org/10.1063/1.5128172.

Preliminary tests of the DECRIS-5M ion source

D. K. Pugachev, S. L. Bogomolov, A. E. Bondarchenko, K. I. Berestov, K. I. Kuzmenkov, V. N. Loginov, A. N. Lebedev, V. E. Mironov, D. S. Podoinikov

Joint Institute for Nuclear Research (JINR), Dubna, Russia, pugachev@jinr.ru

The new ECR ion source DECRIS-5M has been developed to meet the needs of the DC-140 accelerator complex. The planned experiments are primarily intended to solve applied problems across a variety of fields. For successful experiments, the ion source must produce a wide range of metallic ion beams and gases ($Ne^{4+} \div Bi^{38+}$).

The source is a modification of the source developed in 2010 for the DC-110 accelerator complex project [1]. Most of the changes are related to the modernization of axial and radial magnetic systems to increase magnetic fields in terms of injection (2.5 T) and extraction (1.4 T) of the ECR source. The assembly of the ion source was completed in early 2024.

The source design

For applied experiments, ion beams in the A/Z range 5÷8 are required (O^{3+}, Ne^{4+}, Ar^{8+}, Fe^{11+}, Kr^{16+}, Xe^{24+}, Au^{36+} и Bi^{38+}). To achieve the desired charge level, it is necessary to create sufficient plasma density and ion confinement time. A sufficient level can be achieved using a frequency of 18 GHz and a power of up to 2 kW. At this frequency, the value of the resonance magnetic field of the ECR zone corresponds to a value of 0.64 T. The magnetic fields of the source were selected in accordance with the established ratios for ion sources of this type, relative to the field of the ECR zone and amounted to B_r = 1.3 T, B_{inj} = 2.5 T (using a soft iron plug), B_{extr} = 1.4 T.

The magnetic system of the DECRIS-5M include 5 coils with the sizes: D_{inner}/D_{outer} = 88/343 mm for the injection and extraction coil, the middle coil has D_{inner}/D_{outer} = = 230/406 mm. The coils are cooled with water with an operating pressure of 15 atm. The winding is made of an 8×8 mm copper conductor, with an inner diameter of 5 mm for cooling.

Figure 1 shows the distribution of the magnetic field at operating currents of I_{inj} = 1150 A (injection current), I_{mid} = 700 (current on the middle coil) and I_{ext} = 1050 (current on the extraction coil).

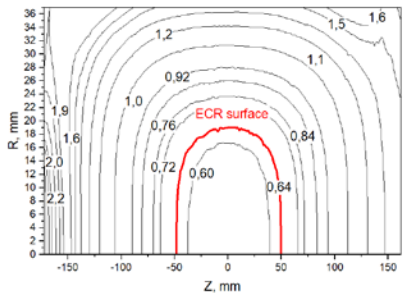

Fig. 1. The distribution of the magnetic field in the plasma chamber of the DECRIS-5M ion source

To create a radial distribution of the magnetic field, a hexapole magnet with an inner diameter of 80 mm and an outer diameter of 210 mm, the length of the hexapole is 300 mm. This system consists of 24 sectors, the material is NdFeB.

The injection plug in the form of cone-shaped soft iron insert is used to enhance the local magnetic field. It includes a standard 16×8 mm waveguide for injecting 18 GHz microwaves, a biased electrode, and two identical stainless-steel tubes with a 10 mm inner diameter. These tubes serve the purpose of gas injection and installing the micro-oven, both positioned off-axis. The plug's design also allows for the integration of equipment to generate solid element ions through MIVOC and sputtering techniques.

The DECRIS-5M accel-decel extraction system comprises of three electrodes. The electrodes, one negatively biased and the other grounded, are mechanically connected to each other using ceramic insulators. They are assembled together and mounted on a driven carriage capable of remote positioning. The extraction gap can be adjusted up to a distance of 13 mm in both directions along the extraction axis. The plasma electrode has an aperture of 10 mm. The extraction voltage ranges from 15 to 20 kV. The negatively biased puller electrode can receive a voltage of up to 5 kV. Unlike the prototype, this electrode is not equipped with a water-cooling system in order to simplify the design.

The first results

Magnetic measurements were taken for each of the source systems, and the cooling system for the solenoids and plasma chamber were tested. Enhancements were made to the design of multiple injection components to improve the vacuum seal and facilitate system assembly. Initial results were obtained using an argon beam in the ECR source test bench. At the UHF power 92 W, 330 μA of Ar^{8+} ions were produced, and 200 μA of Ar^{11+} ions at 300 W (fig. 2). Further tests will be aimed at obtaining beams of Krypton, Xenon and Bismuth of the required charges.

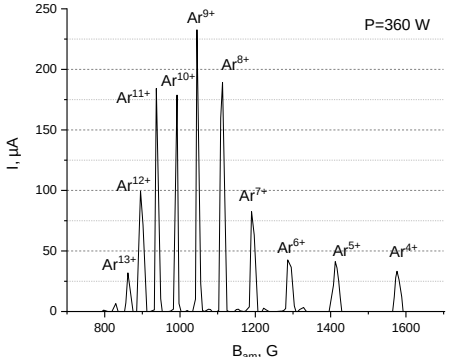

Fig. 2. The ion spectrum of ^{40}Ar tunned on 11+ charge. The value of the UHF power is 360 W

References

1. Gikal, B. N., Dmitriev, S. N., Gul'bekyan, G. G. *et al. Phys. Part. Nuclei Lett.* 11, 137–150 (2014).

Measurements of characteristics of an electron beam – driver for FEL based on the linear induction accelerator

E. S. Sandalov, S. L. Sinitsky, D. I. Skovorodin, A. V. Arzhannikov, P. V. Logachev, P. A. Bak, D. A. Nikiforov, K. I. Zhivankov, A. V. Petrenko, E. K. Kendjebulatov, D. F. Reshetov, N. Yu. Peskov, N. S. Ginzburg

Budker Institute of Nuclear Physics of SB RAS, Novosibirsk, Russia, E.S.Sandalov@inp.nsk.su

Currently, despite the availability of various sources of electromagnetic radiation of low and medium power in a wide range of wavelengths [1], the development and creation of long-pulse (0.1–1 μs) sources of coherent electromagnetic radiation of subGW power in the millimeter and submillimeter ranges is of great interest for various scientific research and technical applications. The need for such radiation sources is relevant in the development of new chemical compounds, drugs and energy materials, in particular for the implementation of the mechanism of vibration pumping processes in the crystal structures of materials [2]. In this regard, various promising schemes for generating radiation pulses with such parameters are being developed and studied at the Institute of Nuclear Physics (BINP) together with the Institute of Applied Physics (IAP) [3–5]. Based on one of these schemes, we have proposed and are currently implementing a project for a subTHz free electron laser (FEL) [4, 5], based on the electron beam (E_e = 5–10 MeV, I_b = 1–2 kA, normalized emittance ~500–1000 π mm mrad), generated on the new linear induction accelerator "LIU". The report provides a description of individual systems and the overall technical design of the FEL-generator (see Fig. 1).

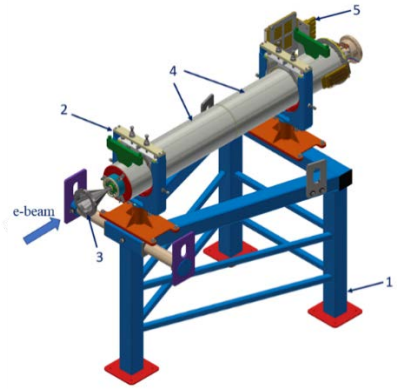

Fig. 1. 1 – stand, 2 – FEL section positioning system, 3 – input section of the FEL vacuum chamber, 4 – magnetic compression system (two solenoids) located inside the magnetic shield, 5 – helical undulator, 6 – platforms for mounting current leads from power supplies

Despite the presence of a large number of beam instabilities in a multi-module linear induction accelerator, we managed to select the necessary geometry of the accelerating modules and the location of electromagnetic absorbers in them, which made it possible to obtain the beam at the "LIU" exit with the amplitude of the beam oscillations acceptable for the FEL operation. As an example of measurement result Fig. 2 demonstrates the dependence of the logarithm of the oscillation amplitude of the beam centroid on the number of the accelerating module. The slope of this curve characterizes the increment of the strongest BBU-instability of the electron beam along the accelerator which value (Γ = 0.1 ± 0.02) coincides within the error bars with the result of our computer simulations. So, based on the modeling results and data from the first experiments on compression and transport in stable equilibrium of an electron beam with a diameter of ~10 mm, a current of 1 kA and an energy of 5 MeV in the FEL channel close in diameter to its electrodynamic system, we can conclude that the compressed beam from the "LIU" applicable as a driver for FEL in the THz range [5].

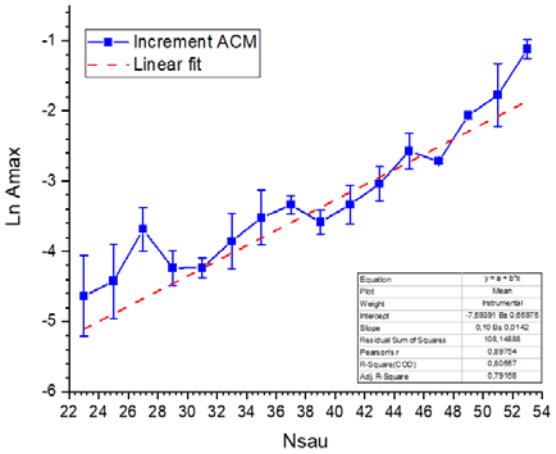

Fig. 2. The dependence of the logarithm of the maximal oscillation amplitude of the beam centroid on the number of the accelerating module in the "LIU", obtained from the signals of fast current transformers in these modules

References

1. Lee Y. Principles of Terahertz Science and Technology (Lecture Notes in Physics). New York: Springer, 2009. 352 p.
2. Michalchuk A. A. L. et al. Predicting the impact sensitivities of energetic materials through zone-center phonon uppumping. J Chem Phys. 2021 Feb 14;154(6):064105.
3. Сандалов Е. С., Синицкий С. Л., Сковородин Д. И. и др. Исследование инкремента поперечной неустойчивости килоамперного электронного пучка в ЛИУ для его применения в терагерцовом ЛСЭ. Сибирский физический журнал. 2022;17(2):16–29.
4. Nikiforov D. A. et al. Investigation of high current electron beam dynamics in linear induction accelerator for creation of a high-power THz radiation source // Journal of Instrumentation, 2021, vol. 16. P. 11024.
5. Sandalov E. S. et al. Magnetic System of a Sub-Gigawatt Free-Electron Laser of the Terahertz Range Based on a Kiloampere Beam of Relativistic Electrons // Radiophysics and Quantum Electronics. 2024. С. 1–15.

Broadband gyrotron-type devices with zigzag quasi-optical transmission line

S. V. Samsonov, G. G. Denisov, A. A. Bogdashov, I. G. Gachev, M. V. Kamenskiy, K. A. Leshcheva, A. V. Savilov, E. M. Novak, M. Yu. Glyavin, S. Yu. Kornishin and **E. M. Tai**

A.V. Gaponov-Grekhov Institute of Applied Physics of RAS, Nizhny Novgorod, Russia, samsonov@ipfran.ru

Introduction

Gyrotron travelling-wave tubes (gyro-TWTs) and gyrotron backward-wave oscillators (gyro-BWOs) are types of cyclotron resonance masers (CRMs), which differ from gyro-klystrons and gyrotrons (the most developed versions of CRM) by the potential for a much wider amplification band or band of smooth oscillation frequency tuning (see e.g. [1, 2]). In conventional gyro-BWOs using a section of a smooth waveguide, the frequency tuning is, as a rule, piecewise with strong variations in the power and spatial structure of the output radiation [3].

In [4] we proposed a concept of a CRM, based on the use of an open quasi-optical (QO) mirror transmission line, in which a Gaussian wave beam is guided by mirrors along a zigzag trajectory, so that it periodically intersects with the electron beam (Fig. 1). The CRM instability and thus resonant beam-wave interaction occurs at the regions of perpendicular beam-wave intersections inside which an electromagnetic wave with the Bz-component propagates across the e-beam yielding in the cyclotron phase bunching and energy exchange with minor sensitivity to the particle velocity spread similar to a gyrotron.

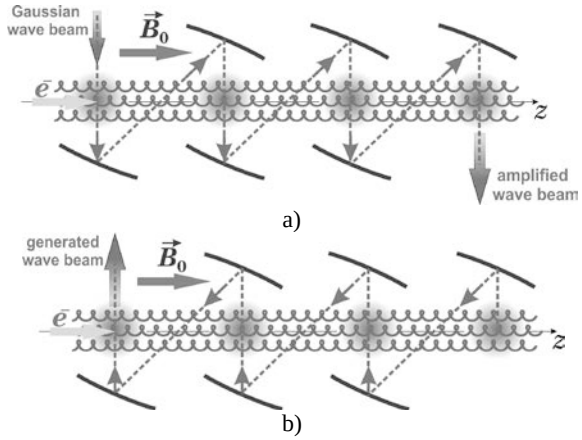

Fig. 1. Schematic layout of a gyro-TWT (*a*) and a gyro-BWO with 3-period zigzag QO transmission line

Results

The developed simplified theory and 3D PIC simulations shows prospects of this "zigzag" CRM in realization of frequency tunable amplifiers and oscillators capable of high power and unique (octave frequency band) tuning in the short-millimeter wavelength range [4–9].

In the first experiments on a zigzag gyro-BWO [10], it has been proven that the device can ensure the operating bandwidth as wide as one octave (more than 70%), within which there are a number of sufficiently wide bands (3–5%) with smooth and continuous tuning (Fig. 2). At all operating frequencies, it generates a nearly Gaussian wave beam at the output. Despite rather low interaction efficiency (around 3%), the net efficiency can be enhanced to 10–12% using a single-stage depressed collector. As the theoretical analysis shows, the gaps between the bands of continuous frequency tuning can be significantly narrowed (or even eliminated) using the specific hysteresis [8, 9].

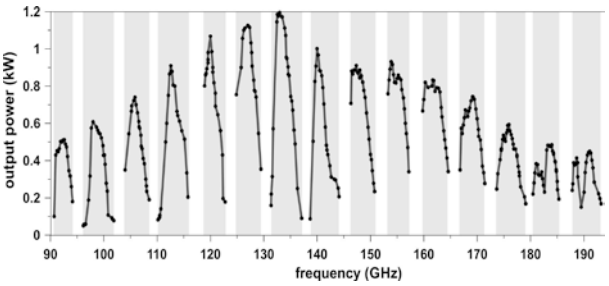

Fig. 2. Measured bands of continuous frequency tuning for a zigzag gyro-BWO powered by DC power supplies with a total power of 10 kW

Acknowledgements. This work was supported by the Russian Science Foundation under Grant 21-19-00443 and Institute of Applied Physics of the Russian Academy of Sciences, Project FFUF-2022-0007.

References

1. M. Thumm, *J. Infr., Millim., THz Waves*, 2020, **41**(1), 1–140, doi: 10.1007/s10762-019-00631-y.
2. G. S. Nusinovich, *Introduction to the Physics of Gyrotrons.* Johns Hopkins Univ. Press, Baltimore, MD, USA, 2004.
3. C.-H. Tsai et al., *IEEE Trans. Electr. Dev.*, 2021, **68**(1), 324–329, doi: 10.1109/TED.2020.3036323.
4. S. V. Samsonov, G. G. Denisov, A. A. Bogdashov and I. G. Gachev, *IEEE Trans. Electr. Dev.*, **68**(11), 5846–5850, doi: 10.1109/ted.2021.3114141.
5. S. V. Samsonov, G. G. Denisov, A. A. Bogdashov, and I. G. Gachev, *Proc. 2021 Photonics & Electromagnetics Research Symp.(PIERS)*, 2021, Hangzhou, China, 2790–2799, doi: 10.1109/PIERS53385.2021.9695051.
6. S. V. Samsonov, G. G. Denisov, A. A. Bogdashov, I. G. Gachev, M. V. Kamenskiy, K. A. Leshcheva, *Proc.8th Int. Congr. Energy Fluxes and Radiation Effects (EFRE)*, 2022, Tomsk, Russia, 248–253, doi: 10.56761/EFRE2022.S3-O-034602.
7. S. V. Samsonov, G. G. Denisov, A. A. Bogdashov, I. G. Gachev, M. V. Kamenskiy and K. A. Leshcheva, *Proc. 24th Int. Vacuum Electronics Conf. (IVEC)*, 2023, Chengdu, China, doi: 10.1109/IVEC56627.2023.10156909.
8. E. M. Novak, S. V. Samsonov, A. V. Savilov, *Phys. Plasmas*, 2023, **30**(4), p. 043101, doi: 10.1063/5.0140591.
9. E. M. Novak, S. V. Samsonov, A. V. Savilov, *IEEE Trans. on Elect. Dev.*, 2023, **70**(12), 6579–6586, doi: 10.1109/ted.2023.3326114.
10. S. V. Samsonov, G. G. Denisov, A. A. Bogdashov, I. G. Gachev, M. V. Kamenskiy and K. A. Leshcheva, *IEEE Elect. Dev. Letters*, 2024, Early Access. doi: 10.1109/LED.2024.3400976.

Upgrade of plasma creation system of GOL-PET facility to increase frequency of the radiation generated in beam-plasma system

D. A. Samtsov[1], A. V. Arzhannikov[1,2], S. L. Sinitsky[1,2], E. S. Sandalov[1,2], M. A. Makarov[1], P. V. Kalinin[1,2], K. N. Kuklin[1]

[1] Budker Institute of Nuclear Physics SB RAS, Novosibirsk, Russia, press@inp.nsk.su
[2] Novosibirsk state university, Novosibirsk, Russia, , press@nsu.ru

Generation of powerful electromagnetic radiation in frequency range 0.1–10 THz is one of the important tasks of modern physical research. One of the approaches for solving this problem is to apply processes of radiation emission from plasmas due to pumping electron plasma wave by a high-current relativistic electron beam (REB). Experimental research in this frame was started in Budker institute of nuclear physics at the GOL-3 facility in 2010 year [1]. Further these studies aimed at generation of multi-megawatt radiation fluxes in frequency range 0.1–1 THz were continued at GOL-PET facility [2, 3]. There are several physical mechanisms to generate such radiation fluxes in the beam-plasma system. In particularly, among of them is a plasma waves conversion into electromagnetic ones on plasma density gradients [3] and a merging of two upper-hybrid waves into electromagnetic one [4].

To the current moment, the experimental studies at the GOL-PET facility have shown that the spectrum of the flux generated in magnetized plasma column covers frequency range 0.1–0.5 THz and the maximum of the spectral power density localizes near the upper-hybrid frequency 0.15–0.25 THz [5]. Pulse duration is up to 4 us, total energy in pulse up to 10 J [6]. Flux outgoing from vacuum into atmosphere has angular divergence less than 10° and propagates at distance of several meters [7].

The purpose of the further experiments is to in-crease main frequency of the radiation flux outgoing into the atmosphere. As it was mention above one of the methods to control radiation frequency is varying of plasma density. In order to create preliminary plasma with higher density, a plasma creation system is now upgraded. Scheme of plasma section before and after upgrade presented in fig. 1. Previous configuration was described in [8]. Three main changes were made during the upgrade. Higher plasma density requires higher density of the neutral gas. In order to ensure sufficient density level of neutral hydrogen, a gas puffing system was reconstructed to provide gas puffing in cross-section of the REB transportation. Configuration of discharge electrodes was modified to ensure preliminary plasma discharge developing inside quartz tube. That's why two half-ring electrodes located in a center cross-section of a quartz tube and powered by the same voltage was removed.

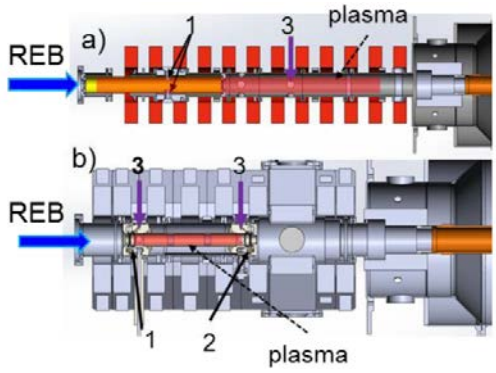

Fig. 1. The scheme of plasma creation system before (a) and after (b) upgrade. 1 – high-voltage electrode; 2 – ground electrode; 3 – hydrogen puffing

Two ring electrodes was installed at ends of the quartz tube. High voltage applied only to one of these electrodes and the second is grounded. Also to de- crease time of plasma discharge developing a system to form high-voltage pulse was reconstructed. In given report changes of plasma creation system will be described. Parameters of preliminary plasma and REB-plasma system measured in experiments with new plasma creation system will be presented. Ac- cordance of the properties of the upgraded plasma creation system to general requirements of the THz radiation flux generation in the GOL-PET facility has been tested in a series of experiments.

References

1. Arzhannikov V., Burdakov A. V., Kalinin P. V., et al. // Vestnik Novosibirsk State University. Series: Physics. 2010. Vol. 5, nr 4. P. 44–49.
2. Arzhannikov A. V., Burdakov A. V., Burmasov V.S., et al. // IEEE Transactions on terahertz science and technology. 2016. T. 6, № 2. C. 245–252.
3. Timofeev I. V., Annenkov V. V., Arzhannikov A. V. // Physics of Plasmas. 2015. T. 22, № 11.
4. Arzhannikov A. V., Timofeev I. V. // Plasma Physics and Controlled Fusion. 2012. T. 54, № 10. C. 105004.
5. Arzhannikov A. V., Sinitsky S. L., Samtsov D. A., et al. // Plasma Physics Reports. 2024. T. 50, № 3. C. 331–341.
6. Arzhannikov A. V., Sinitsky S. L., Popov S.S. et al. // IEEE Transactions on Plasma Science. 2022. T. 50, № 8. C. 2348–2363.
7. Samtsov D. A., Arzhannikov A. V., Sinitsky S. L. et al. // IEEE Transactions on Plasma Science. 2021. T. 49, № 11. C. 3371–3376.
8. Arzhannikov A. V. Ivanov I. A., Kalinin P. V., et al. // Journal of Physics: Conference Series. – IOP Publishing, 2020. T. 1647, № 1. C. 012011.

Prospects of creation of pulsed 1 THz high-harmonic gyrotrons of the kilowatt power level

A. V. Savilov, **I. V. Bandurkin, G. I. Kalynova, Yu. K. Kalynov** and **I. V. Osharin**

A.V. Gaponov-Grekhov Institute of Applied Physics of the Russian Academy of Sciences,
Nizhny Novgorod, Russia, savilov@ipfran.ru

Currently, the possibility of creating gyrotrons operating at the frequency of 1 THz with the output wave power at the level of several kilowatts is being investigated at the IAP RAS [1]. Such gyrotrons should be used to provide a gas-discharge plasma; this is a way to create a stable point-like source of extreme UV radiation.

To ensure 1 THz radiation, it is attractive to work at higher harmonics of the cyclotron frequency using the large-orbit-gyrotron configuration (based on axis-encircling electron beams) providing an improved mode selectivity. In 2008, a pulsed gyrotron was successfully implemented, in which, when operating on the 3rd cyclotron harmonic at the mode TE 3,7 at an accelerating voltage of 80 kV in a magnetic field of 13.7 T, radiation at a frequency of 1 THz with a power of 0.4 kW was obtained [2]. Work is underway to modify this gyrotron in order to increase the radiation power at a frequency of 1 THz to a level of several kW [1]. At the first stage of the modification in the 80 kV / 0.7 A/10 μs version, a cavity with a short selective irregularity (Fig. 1) was used in a new experiment. This modification allowed to expand the range of parameters of the selective excitation of the operating high-harmonic wave, as well as to increase the output radiation power up to 1.3 kW due to a significant reduction of Ohmic losses [3]. According to CST simulations (Fig. 1), this became possible due to the transition to operation on the two-variation axial mode having a reduced diffraction Q-factor.

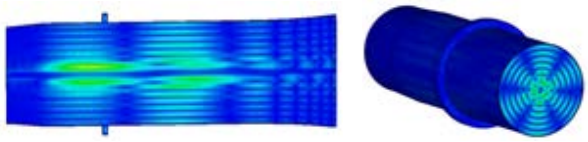

Fig. 1. CST simulations of the gyrotron based on the cavity with a short azimuthal selective irregularity

In the experiment [3], the characteristic duration of the output wave power was ~ 10 μs (Fig. 2 a). Recently, in a new series of experiments the duration of the output wave pulse has been increased up to ~ 30 μs (Fig. 2 b) at practically the same level of the output power. In addition, in the long-pulse experiment we observed a regime of competitions of two axial mode, where the lowest axial mode was exited at the edges of the electron beam pulse, whereas in the center of the pulse the second axial mode (having lower ohmic losses and, therefore, higher power) was generated (Fig. 2 c). Two-peak pulses of the output power were also observed (Fig. 2 d).

As a way for the further increase in the output power, we consider transition from 80 kV / 0.7 A to 100 kV / 1.2 A electron beam. SCT simulations predict the possibility for achieving the output power of 4 kW in this case due to (i) doubling the electron beam power was doubled, (ii) increase in the electron-wave coupling in the case of the higher electron energy, and (iii) decrease in Ohmic losses [1]. However, a special cavity providing selective excitation of the third cyclotron harmonic should be used.

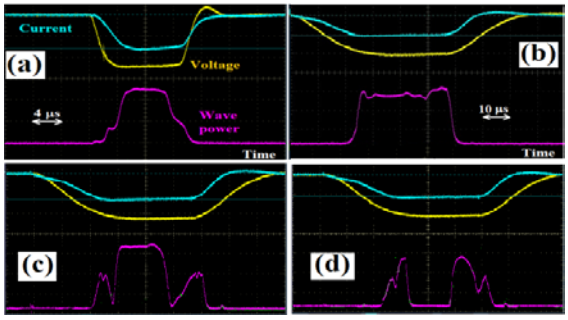

Fig. 2. Typical oscilloscope traces. Voltage, current, and the detected output power versus the time in regimes of (a) 10 μs and (b) 30 μs operation, as well as (c) in the regime of competition of two axial modes and (d) in the two-pulse regime

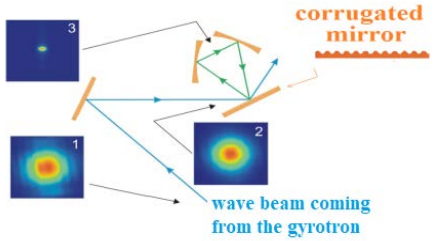

Fig. 3. Scheme of the gyrotron radiation input into a quasi-optical cavity with a traveling wave. The stages of correction and the result of focusing the wave beam are shown

One more way to increase the wave power used to provide the plasma discharge is to use a quasi-optical cavity three-mirror cavity consisting of two focusing mirrors and one flat corrugated Bragg-type photonic structure providing coupling between the gyrotron wave pulse and the operating wave of the cavity (Fig. 3). Despite the high pumping frequency (1 THz) and, therefore, a huge oversize factor (the ratio between typical sized to the wavelength) of the operating cavity, as well as despite the pulsed character of the output wave signal of the gyrotron, it is possible to propose a cavity that ensures both effective accumulation of the wave signal in time and focusing of the wave in space simultaneously [4].

Acknowledgements. This work is supported by the State Assignment of the Institute of Applied Physics RAS, project No. FFUF-2022-0007.

References

1. Y. K. Kalynov et al., 2020, Radiophys. Quantum Electron, 2020, **43**(5/6), 354–362.
2. V. L. Bratman et al, Phys. Rev. Lett., 2009, **102**(24), 245101.
3. Y. K. Kalynov et al., IEEE Electron Device Letters, 2023, 44(10), 1740–1743.
4. G. Kalynova et al., Photonics, 2023, **10**, 440.

The code ANGEL as a universal tool for gyrodevices modeling

E. S. Semenov, A. S. Zuev, O. P. Plankin and **A. P. Gashturi**

A.V. Gaponov-Grekhov Institute of Applied Physics of the Russian Academy of Sciences, Nizhny Novgorod, Russia,
semes@ipfran.ru

Introduction

Gyrodevices make it possible to obtain high power in the mm wavelength range. In particular, gyrotrons are used for microwave generation [1]. To achieve maximum efficiency, optimization is carried out according to a variety of parameters, which requires multiple calculations of various device components.

This paper lists the possibilities implemented in the ANGEL software package created at the IAP RAS, designed for the development and optimization of gyrotrons. This complex contains numerous tools for trajectory analysis, modeling of electron-wave interaction, analysis and synthesis of output transducers and windows for gyrodevices. The entire software package is enclosed in an integrated development environment that makes it possible to carry out the primary design of the device, select regimes and configure parameters, analyze the processed calculation results in tabular and graphical form.

Trajectory analysis

For the design and optimization of the electron gun and collector, a trajectory analysis is performed. This allows calculating the trajectories of electrons from the emitter to the collector. It is assumed that the gun operates in the regime of temperature limitation of emission. An initial velocity spread can be added to the position velocity spread, which simulates the roughness of the cathode. The calculation can be performed both without and with taking into account the static spatial charge of the beam. The algorithm implemented in the code consists in an iterative solution of the Poisson equation by the method of discrete sources together with the method of current tubes [2, 3]. Basically, an azimuthally symmetric (2D) magnetic system and an electrode system are used. Therefore, it allows to quickly obtain a result by performing a calculation. It is also possible to set azimuthally asymmetric electron emission and form electron-optical systems (EOS) with misalignment of the electrode and magnetic subsystems. In addition to the static calculation model, modeling of dynamic processes has been implemented, including reflected electrons.

Electron-Wave interaction

The possibility of mode excitation in the first approximation is proportional to the structure factor. The calculation of starting currents $I_{st}(B_0)$ is an additional tool for analyzing the conditions of self-excitation of the operating mode and estimating the probability of excitation of competing modes [4]. The efficiency of the electron-wave interaction and the power of the output radiation of gyrotrons with a hollow or coaxial resonator can be found within the framework of a stationary self-consistent model that takes into account the heterogeneity of the static magnetic field, and the spread of oscillatory electron velocities [5]. Non-stationary models with both fixed and self-consistent field structure are used to analyze the start up scenarios and modes competition [6].

Radiation output system

The radiation output system includes a wave beam transportation system with the possibility of converting the transverse structure and an output window. To optimize the transportation system, the following tools are integrated into the ANGEL complex: synthesis of a wave converter with a gyrotron $TE_{m,p}$ mode into a Gaussian wave beam, convenient for further transportation [7]; analysis of RF-fields in the entire output path consisting of a converter and a set of cylindrical, parabolic and flat reflectors [8]; preparation of geometric parameters and visualization of fields. The tools implemented in the ANGEL software package allow to optimize the output window consisting of a set of flat layers.

Conclusion

Mathematical models implemented in the ANGEL software package make it possible to perform preliminary optimization of gyrotron parameters using minimal computational and time resources. The results of calculations based on these models have been repeatedly verified both in comparison with calculations in other programs and with experimental gyrotron data. Currently, the ANGEL software package is actively used in the IAP RAS and GYCOM Ltd. in the development of gyrotrons with various frequency ranges and powers.

Acknowledgements

The authors are grateful to A.S. Sergeev, M.Yu. Glyavin, V.E. Zapevalov, A.P. Fokin and A.S. Sedov.

The work supported by State Agreement #H.4a.241.19.24.1024 from 20.03.2024, Contract #1770641334824000019O/37-24/01/45-416 from 22.05. 2024.

References

1. G. S. Nusinovich, M. K. A. Thumm, M. I. Petelin, *J. Infrared Millim. THz Waves*, 2014, **35**(4), 325–381.
2. V. K. Lygin, V. E. Manuilov, Sh. E. Tsimring, *Elektronnaya tekhnica. Ser.1. Elektronica SVCh*, 1987. *7*(401), 36–38.
3. E. S. Semenov, O. P. Plankin, R. M. Rosenthal. *Izvestiya VUZ Applied Nonlinear Dynamics.*, 2015, **23** (3), 94–105.
4. E. S. Semenov, A. S. Zuev, A. P. Fokin, Information and mathematical technologies in science and management, 2022, № 1 (25), 35–47.
5. E. S. Semenov, M. D. Proyavin, M. V. Morozkin, et al., *Radiophys. Quantum Electron*., 2023, **66**(7/8).
6. E. S. Semenov, V. E. Zapevalov, A. S. Zuev, Communic. in Computer and Information Science, 2021, **1413**, 49–62.
7. D. I. Sobolev and G. G. Denisov, *IEEE Trans. Plasma Sci.*, 2010, **38**(10), 2825–2830.
8. A. P. Gashturi and D. I. Sobolev, *Radiophys. Quantum Electron.*, 2022, **65**(5), 442–450.

Kinetic instabilities of a mirror confined plasma driven by strong electron-cyclotron heating

A. G. Shalashov, E. D. Gospodchikov, I. V. Izotov, V. A. Skalyga, M. E. Viktorov

A.V. Gaponov-Grekhov Institute of Applied Physics of the Russian Academy of Sciences, Nizhny Novgorod, Russia, ags@ipfran.ru

In this paper, we focus on electron-cyclotron interaction of electromagnetic waves and plasma confined in laboratory mirror traps. Such studies are usually associated with electron-cyclotron resonance plasma heating used to achieve a high electron temperature in open magnetic configurations of various scales, from compact technological ion sources to large-scale magnetic traps used in fusion researches. These applications have a long history but still remain topical, mostly due to a progress in the development of high-power sources of microwave radiation, especially gyrotrons, followed by essential increasing the rf-power load and thereby by increasing the population of non-equilibrium resonant electrons.

The interaction of rf waves with resonant electrons leads to a specific transport of electrons in a momentum space that ends with their falling into the loss-cone and precipitation from a trap. Such electrons may result in the development of electromagnetic electron-cyclotron instabilities in a wider frequency range then those used for the resonant plasma heating. If this occurs, suprathermal electrons act as an amplifying medium for its own electromagnetic noise while bulk plasma and vacuum chamber serve as a cavity providing positive feedback for unstable modes. In many cases this mechanism determines the losses of excess energy stored in accelerated electrons, thereby limiting the achievement of peak plasma parameters in applications [1]. Recent advance in the basic theory suggests approaches for the control of unwanted plasma turbulence caused by the strong ECR heating. We review these new ideas aimed at fundamental understanding of various dynamic regimes of cyclotron maser emission in laboratory traps [2–4], discuss its experimental verification available at present [5–7] and achievement of a better plasma performance in applications [8].

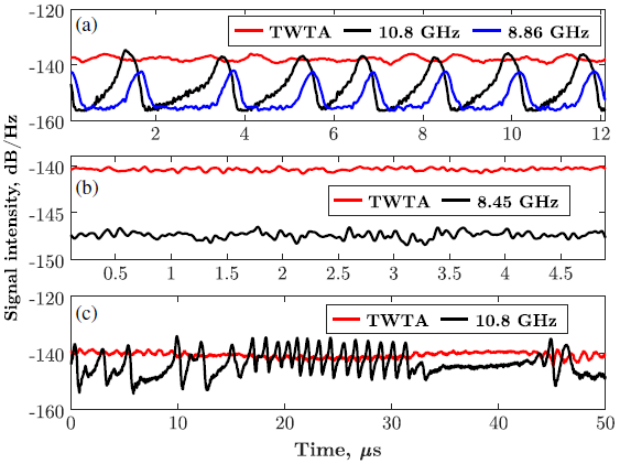

Fig. 1. Example of bifurcation of electron cyclotron instability regimes found in ECR ion source at the JYFL accelerator laboratory. Intensity of microwave emission in 8–12 GHz band referred to the generation of (a) periodic bursts, (b) cw emission, and (c) spontaneous transition from quasiperiodic bursts to cw and back. Stray radiation of the heating TWT amplifier at 11.8 GHz is shown with a red line. Three regimes differ only by the value of the minimum magnetic field in the trap: B_{min}/B_{ECR} = = 0.935 for the burst, 0.947 for the cw, and 0.98 for the transient regimes, correspondingly. First published in [5]

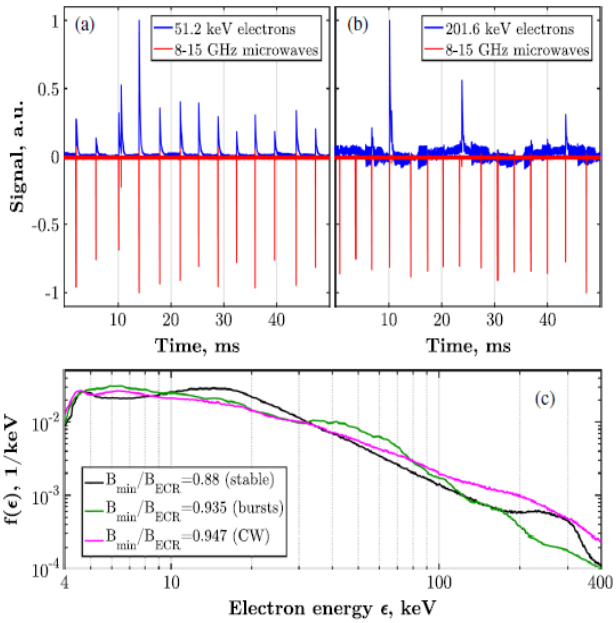

Fig. 2. Example of electron precipitations through the axial mirror with energies of (a) 51.2±0.25 keV and (b) 201.6± ±0.25 keV measured at JYFL ECR ion source; the microwave emission in the 8–15 GHz range is denoted with red lines. (c) Energy distributions of escaping electrons averaged over 100 s in the stable, burst, and cw regimes First published in [5]

Acknowledgements

This work was supported by the Russian Science Foundation (project No. 19-72-20139).

References

1. V. Skalyga et al., *Phys. Plasmas*, 2015, **22**, 083509.
2. A. G. Shalashov et al., *EPL*, 2018, 124, 35001.
3. A. G. Shalashov et al., *Plasma Phys. Control. Fusion*, 2020, 62 065005.
4. A. G. Shalashov, E. D. Gospodchikov, *Phys. Plasmas*, 2023, **30**, 112107.
5. A. G. Shalashov et al., *Phys. Rev. Lett.*, 2018, **120**, 155001.
6. I. V. Izotov et al., *Plasma Phys. Control. Fusion*, 2021, **63**, 045007.
7. A. G. Shalashov, E. D. Gospodchikov, *Phys. Rev. E*, 2023, **108**, 025207.
8. V. A. Skalyga et al., *J. Phys. D: Appl. Phys.*, 2021, **54**, 385201.

Pumping waves in vacuum and plasma with a high-current electron beam for generation of a multi-megawatt flux of mm/submm-radiation

S. L. Sinitsky, A. V. Arzhannikov

Budker Institute of Nuclear Physics of SB RAS, Novosibirsk, Russia, S.L.Sinitsky@inp.nsk.su

Today, the problem of creating sources of high-power pulses of electromagnetic radiation in the mm/submm range is of great interest for scientific research and technical applications. In this regard, the research activities on the creation of such sources based on various generation schemes are being successfully developed by the BINP (Novosibirsk) together with the IAP (Nizhnii Novgorod). Among them are the experiments with beam-plasma generator of intense fluxes of THz radiation in the range 0.1–0.5 THz with a power level of ~10 MW, a duration of ~1 μs at the GOL-PET device (BINP) [1]. In these experiments, plasma waves are pumped by a high-current electron beam (0.6–1 MeV/20 kA/8 μs) in a plasma with a density of 10^{14}–10^{15} cm^{-3}, confined in a multi-mirror trap with the magnetic field of 4 T. Another high-power source of mm-radiation is a planar free electron maser (FEM) with two-dimensional feedback at the ELMI-device (BINP). In this maser a sheet electron beam (0.7–0.9 MeV/3 kA/5 μs) pumps EM-oscillations in a hybrid Bragg resonator and produces 20–40 MW narrow-band radiation pulses at a frequency of 75 GHz with a duration of 100 ns [2]. In addition, two projects of high-power THz-radiation sources are being constructed now by the BINP together with the IAP. The first is a new FEL-generator based on an electron beam formed by the linear induction accelerator LIU (5 MeV/2 kA/100 ns). It will advance long-pulse FELs into subTHz/THz ranges with subgigawatt power level and energy content in a radiation pulse of ~10–100 J [3, 4]. Another one is a high-power short-wavelength Cherenkov maser of planar geometry [5] based on a sheet electron beam (0.7–0.9 MeV/2–3 kA/5 μs), which pumps the surface wave in the area adjacent to the two-dimensional Bragg structures. According to calculations, it will allow generating intense flows of coherent radiation in the frequency range up to 300 GHz with a subgigawatt power level.

All of these sources of mm/submm radiation use high- intensity relativistic electron beams (REB) with small energy and angular spreads of their particles as a driver. The values of these spreads determine the level of the beam-wave interaction and, ultimately, the electron efficiency of the interaction. To generate such beams of microsecond duration, we use a magnetically insulated diode of ribbon geometry [6]. For this type of diode, we analyzed the contributions of the main sources of angular divergence of the beam electrons: noncollinearity of the electric and magnetic fields near the cathode surface, cathode roughness, anode lens effect, and nonadiabaticity of the beam compression by the magnetic field. Based on these results, the necessary conditions for achieving maximum beam current density at minimum angular divergence of beam electrons are discussed. To generate a hundred nanosecond beam in the linear induction accelerator, we use an axially symmetric diode with Pierce geometry in the absence of a magnetic field. For this type of diode, we studied the contribution of the cathode temperature, residual magnetic field, and cathode roughness to the value of the normalized beam emittance [7]. Various aspects of ensuring the transportation of such beams in slit and round channels under stable equilibrium conditions are considered.

In relation to the beam-plasma generator, the problem of transforming the ribbon cross-section of an intense electron beam into a round one without loss of current and subsequent compression of the beam cross-section by a magnetic field has been solved [8]. The conditions for achieving synchronism between the motion of the beam electrons and plasma waves [9] and the possibility of transforming plasma waves into a well-directed flux of EM radiation [10, 11] are discussed.

The presented analytical estimates, as well as the results of modeling the processes of the beam generation, transport and transformation of its cross section are confirmed by data obtained in experiments on both mentioned devices.

Acknowledgements. The research was partially supported by Russian science foundation, grants: #19-12-00212, 19-12-00250, 23-19-00370.

References

1. A. V. Arzhannikov , A. V. Burdakov , V. S. Burmasov, et al. // IEEE Transactions on terahertz science and technology. 2016. T. 6, № 2. C. 245–252.
2. A. V. Arzhannikov, N. S. Ginzburg, P. V. Kalinin, et al. // Phys. Rev. Lett., 117, 114801 (2016).
3. A. V. Arzhannikov, N. S. Ginzburg, A. M. Malkin, et al. // Proceedings of the 44th International Conference on Infrared, Millimeter, and Terahertz Waves, Paris, France, 2019, pp. 1–2. DOI: 10.1109/IRMMW-THz.2019.8874573.
4. E. S. Sandalov, S. L. Sinitsky, A. V. Arzhannikov, et al. // Bulletin of the Russian Academy of Sciences: Physics. 2023. T. 87, № 5. C. 573–579.
5. A. V. Arzhannikov, N. S. Ginzburg, P. V. Kalinin, et al. // IEEE Transactions of Electron Devices, V. 69, № 5, pp. 2662–2667. DOI: 10.1109/TED.2022.3161899.
6. S. L. Sinitsky. Generation and transport of microsecond ribbon REBs with energy content up to 50 kJ // Ph.D. Thesis, Novosibirsk, 1992.
7. D. A. Nikiforov, A. V. Petrenko, S. L. Sinitsky, et al. // Journal of Instrumentation, vol. 16, P11024, 2021. https://doi.org/10.1088/1748-0221/16/11/P11024.
8. V. T. Astrelin, A. V. Arzhannikov, V. B. Bobylev, et al. // Proc. of 15th Intern. Symp. on High Current Electronics: Tomsk: Publishing house of IAO SB RAS, 2008, p. 69–72.
9. I. V. Timofeev, V. V. Annenkov, A. V. Arzhannikov, et al. // Physics of Plasmas. 2015. T. 22, № 11.
10. A. V. Arzhannikov, S. L. Sinitsky, S. S. Popov, et al. // IEEE Transactions on Plasma Science. 2022. T. 50, № 8. C. 2348–2363.
11. D. A. Samtsov, A. V. Arzhannikov, S. L. Sinitsky, et al. // IEEE Transactions on Plasma Science. 2021. T. 49, № 11. C. 3371–3376.

Prospects of multicharged ions formation in a dense ECR plasma sustained by powerful millimeter waves

V. A. Skalyga[1], I. V. Izotov[1], S. V. Golubev[1], A. V. Polyakov[1], S. V. Razin[1], D. M. Smagin[1], A. V. Vodopyanov[1], S. S. Vybin[1], L. T. Sun[2], H. Y. Zhao[2], Y. T. Lu[2], J. J. Zhang[2], B. Zhang[2], J. B. Li[2], J. D. Ma[2]

[1] A.V. Gaponov-Grekhov Institute of Applied Physics of the Russian Academy of Sciences, Nizhny Novgorod, Russia, skalyga@ipfran.ru

[2] Institute of Modern Physics of the Chinese Academy of Sciences, Lanzhou, China

The research in the field of heavy ion physics and the synthesis of superheavy elements, the improvement of methods and technologies for accelerating charged particle beams, and new horizons in nuclear and quantum physics continuously pose ambitious tasks in the development of ion sources with previously inaccessible characteristics. Among the most striking current projects are the Superheavy Element Factory at the Joint Institute for Nuclear Research (JINR) in Russia and the Heavy Ion Accelerator Facility at the Institute of Modern Physics of the Chinese Academy of Sciences (IMP CAS) in China. Depending on the specific experiment, generation of beams of multiply charged ions up to uranium with a charge of up to +40 and a current of up to 1 mA is required. Existing ion sources are not able to satisfy all the requirements and provide such a high current of ions with a similar charge. Solutions to the problems of further increasing the current and particle charge while maintaining high beam quality are critical in a number of experiments.

One of the most promising types of multiply charged ion beam injectors are systems based on electron cyclotron resonance (ECR) discharge plasma confined in open magnetic traps, or ECR ion sources (ECRIS). The main direction of ECRIS development is an increase of frequency and power of radiation used to heat the plasma. All ECRISs operating at frequencies above 24 GHz use modern gyrotrons as a radiation source. IMP CAS is the present leader in the ECRIS development in the world. In Russia, the greatest experience in this field has been accumulated at JINR, Dubna. IMP CAS is currently creating a source using a classical design with a record plasma heating frequency of 45 GHz and a power of up to 20 kW. But even this flagship system will not be able to satisfy all the requirements of the most modern projects. The task has been set to search for new principles for constructing high-current sources of ultra-highly charged ions.

Another approach to creating (improving) the required sources is associated with the use of a high-current quasi-gasdynamic source of multiply charged ions. Such a source was proposed at IAP RAS and it is based on studies of ECR discharge in simple magnetic traps sustained by gyrotron microwave radiation with a frequency of up to 75 GHz and a power of hundreds of kW. The use of powerful millimeter-wave radiation made it possible to obtain plasma with a density of up to 10^{14} cm^{-3}, which ensured the transition to a quasi-gasdynamic regime of plasma confinement with a short lifetime (several tens of microseconds) and, accordingly, to obtain plasma flows with an equivalent density of up to 10 A/cm^2. The possibility of using this mode to obtain ion beams with high current and low emittance was demonstrated. In the pulsed operating mode of the source, experiments performed to date have demonstrated the possibility of obtaining beams of multiply charged nitrogen and argon ions with a total current of more than 150 mA and a normalized emittance of 0.9 π·mm·mrad [1], beams of hydrogen ions with a current of 450 mA and 0.07 π·mm·mrad emittance [2]. This combination of parameters is a record to date. Thus, the use of a quasi-gasdynamic ion source with powerful microwave gyrotron heating makes it possible to obtain ion beams with record currents and a moderate average charge.

A new concept for generating high-current multicharged beams is to use a quasi-gasdynamic ion source in combination with a linear pre-acceleration system (up to energies of the order of 1 MeV) and an additional solid-state "stripping" system (foil stripper). Estimates show that a current of 1 mA of heavy ions with a charge of +40 can be achieved with additional "stripping" of the beam with a charge from +10 to +20 and a current of 10 mA. This paper is devoted to discussion of possible ways and prospects of an ion source development for the implementation of such a scheme.

To carry out experimental research at the Institute of Applied Physics of the Russian Academy of Sciences, it is planned to use the SMIS 37/75 facility after its significant modernization. The modernization involves the launch of new power systems for gyrotron complexes and new magnetic systems (including those based on permanent magnets), which will allow experiments with high pulse repetition rates (up to 5 Hz), a record level of specific energy input into plasma (up to 1 kW/cm^3) and a sufficient level of the magnetic field of the trap (up to 3 T). During the experiments the limiting capabilities of high-current ECR sources of multiply charged ions with plasma heating will be investigated.

Acknowledgements

The work was supported by Russian Science Foundation grant # 24-19-00263.

References

1. A. Sidorov, M. Dorf, A. Bokhanov, I. Izotov, S. Razin, V. Skalyga, V. Zorin, A. Balabaev, P Spädtke, J. Roßbach, *Rev. Sci. Inst.*, 2008, **79**, 02A317.
2. V. Skalyga, I. Izotov, A. Sidorov, S. Razin, V. Zorin, O. Tarvainen, H. Koivisto, T. Kalvas, *JINST*, 2012, **7**, 10010.

Synthesis of micro- and nanostructured materials via chain plasma-chemical reactions initiated by high-power microwave pulses

N. N. Skvortsova[1,5], N. S. Akhmadullina[1,2], V. D. Borzosekov[1,3], N. G. Gusein-zade[1], E. M. Konchekov[1], D. V. Malakhov[1], E. A. Obraztsova[1,4], O. N. Shishilov[1,5], V. D. Stepakhin[1]

[1] Prokhorov General Physics Institute of the Russian Academy of Sciences, Moscow, Russia, mukudori@mail.ru
[2] A.A. Baikov Institute of Metallurgy and Material Science of Russian Academy of Sciences, Moscow, Russia
[3] RUDN University, Moscow, Russia
[4] Moscow Institute of Physics and Technology, Dolgoprudny, Moscow Region, Russia
[5] MIREA – Russian Technological University, Institute of Fine Chemical Technologies, Moscow, Russia

An original plasma-chemical facility has been developed at the GPI RAS, based on the powerful pulsed gyrotron (power up to 0.8 MW, pulse duration up to 12 ms, 75 GHz [1]). The description of the experiment, diagnostics, the conditions for the development of a microwave discharge, and the evolution of process parameters in the reactor are described in detail in [2]. Chain plasma-chemical synthesis reaction was initiated when absorbed microwave energy in the powders mixture were reached 1–3 kJ [3]. The synthesis phase duration of the chain process was as long as several seconds. The first stage of the chain reaction is accompanied by the expansion of charged particles according to the Coulomb mechanism from the surface of the powder mixture into the reactor volume. These particles serve as additional centers of condensation of synthesized secondary materials. The addition of catalysts to the mixture of powders makes it possible to lengthen the second stage of the chain process and transfer the reactions to a self-oscillatory mode. Various types of particle observed in our samples cannot be obtained by melting or oxidizing the initial particles of metals and dielectrics. This indicates that the evaporation and subsequent condensation of materials occur during the plasma synthesis. Together with the data on the formation of hexagonal BN particles from the cubic form in the precursor powder [3], these results confirm that new materials are synthetized in reactions.

To date, the synthesis of materials has been carried out in many experiments for various applied problems. In this report we will focus on two tasks. 1. The synthesis of heterogeneous catalysts in the form of microparticles from various dielectrics with nanoparticles of platinum, palladium, copper, silver, etc. deposited on them (Figure 1). With the examples of their use in the reactions of methylcyclohexane dehydrogenation and olefin oxidation. 2. The synthesis of oxide, nitride and oxonitride ceramic materials with the introduction of doping additives (rare earth metals) to impart luminescent properties in Al/Al_2O_3/melamine mixtures with the addition of europium acetylacetonates ($Eu(acac)_3$) and cerium ($Ce(acac)_3$). Intense bands are observed in the cathodoluminescence emission spectra (Figure 2).

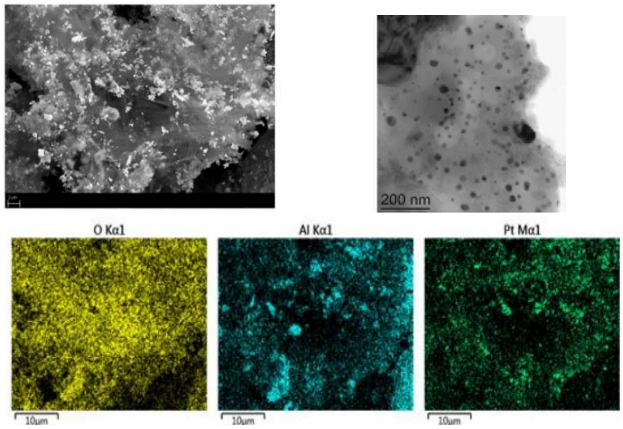

Fig. 1. Top row SEM (right) and TEM (left) images of the sample with platinum. Bottom row EDX cards

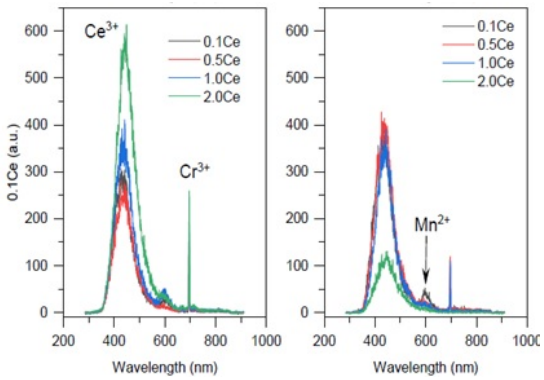

Fig. 2. Cathodoluminescence emission spectra of materials syntheses in the mixtures Al/Al_2O_3/melamine/$Ce(acac)_3$ (*left* – 1:2:1, *right* – 2:2:1), poured on top of the powder AlN

References

1. N. S. Akhmadullina, N. N. Skvortsova, E. A. Obraztsova, et al. *Chem. Phys.*, 2019, **516**, 63–70.
2. A. S. Sokolov, N. S. Akhmadullina, V. D. Borzosekov, et al. *Radiophysics and Quantum Electronics*, 2023, **65**(11). 840–854.
3. N. N. Skvortsova, O. N. Shishilov, N. S. Akhmadullina, et al. *Ceram. Int.* 2021, **47**(3), 3978–3987.
4. T. E. Gayanova, E. V. Voronova, S. V. Kuznetsov, et al. *High Energy Chemistry (Supp. 1)*, 2023, 57, S53.

Frequency-tunable gyrotrons of the sub-terahertz bandwidth with multi-mirror confocal-type resonators

D. I. Sobolev, **V. Yu. Zaslavsky** and **M. Yu. Glyavin**

A.V. Gaponov-Grekhov Institute of Applied Physics of the Russian Academy of Sciences,
Nizhny Novgorod, Russia, zaslav@ipfran.ru

High-power gyrotrons at the sub-terahertz and terahertz frequency range are currently in demand in a number of modern scientific applications, such as technological complexes for sintering composite materials, spectroscopy and diagnostics of various media, development of communication systems, environmental monitoring, and security systems. A number of the above applications require radiation sources with moderate power level (from tens of watts to several kilowatts), operating in long-pulse or continuous-wave (CW) regimes. In addition, a smooth-tunable of a generation frequency within a few percent is required.

At the same time, in the submillimeter wavelength range, at the moment, the power of gyrotrons, even in record-breaking devices, does not exceed several kilowatts in CW regime and several hundred kilowatts in pulsed regime even at a wavelength of about 1 mm. Moreover, in the vast majority of experiments, the radiation power dropped quite quickly as the wavelength shortened. The main problem in the implementation of short-wave gyrotrons is the selective excitation of an operating mode.

One of the methods of a radical increase in the output power and improvement of selective properties of short-wave gyrotrons compared to existing analogues can be achieved by developing modified circuits that differ in the configuration of the interaction space. For example, in article [1] gyrotron based on confocal 2-mirror resonator was investigated. Such circuit configuration allows to provide smooth frequency tuning by changing a gap between mirrors. However, the efficiency of electron-wave interaction for this oscillator powered by a tubular polyhelical electron beam (HEB) is rather low due to non-optimal operating mode transverse structure. Double-confocal configuration proposed in [2] partially solves this problem, but does not provide the optimal efficiency value due to the standing structure of the operating mode, as in the previous case.

To solve these problems, we propose gyrotron scheme with triple confocal resonator consisting of 6 mirrors, the distance between which is much larger than a radiation wavelength [3]. In addition to the standing mode formed by 3 confocal resonators, such a system has a high-quality rotating mode formed by a pair of three-mirror resonators. With optimally selected parameters, the specified electrodynamic system is capable of providing selective excitation of the operating mode. Such a system can be driven by a tubular HEB formed in a conventional magnetron-injection gun. Note that this scheme ensures frequency tuning by mechanical variation of the distance between mirrors. Another important advantage of the proposed electrodynamic system configuration is the bility to operate at harmonics of the cyclotron frequency. This report is devoted to modeling the electrodynamic characteristics of a 6-mirror gyrotron-type resonator, as well as PIC simulations of the electron-wave interaction in the gyrotron with a such resonator type. A comparison of the three resonator schemes described above was carried out.

Figure 1 demonstrates modeling results of the steady-state single-frequency oscillations establishment for the gyrotron with 6-mirror cavity in the cases of rotating mode excitation. Simulations were performed by 3D PIC (particle-in-cell) method based on CST STUDIO SUITE software. The gyrotron was powered by the HEB with electron's energy of 30 keV, total current of 5 A and pitch-factor of 1.2. The electrons rotated in a homogeneous magnetic field with the intensity of 7.5 T corresponding to a resonance with an operating mode at the fundamental cyclotron harmonic. The operating frequency was chosen near 200 GHz to provide parameters required for potential applications. The spatial distributions of the radiation fields are close to the cavity eigenmode. The maximum radiation power reaches 10 kW which corresponds to total efficiency of ~ 7%. Further increasing of the efficiency can be achieved by using of an energy recovery system [4].

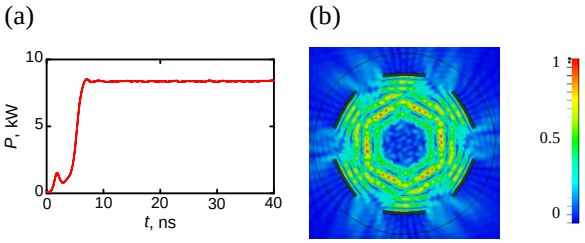

Fig. 1. Results of 3D PIC simulations: (a) scenario of establishment of steady-state regime, (b) H_z structure at an operating frequency

Acknowledgements

This work is supported by the IAP RAS Program No FFUF-2022-0007.

References

1. Temkin R. J., Abe D. K., Barker R. J., et al., IEEE Press, WileyInterscience, Chap. 11, 2005.
2. Wenjie Fu, Xiaotong Guan, and Yang Yana, Physics of Plasmas, 2019, 26, 043109.
3. Zaslavsky V. Yu., Glyavin M. Yu., and Zotova I. V., Proceedings of PIERS 2024, 21–25 April.
4. Glyavin M. Yu., Kuftin A. N., Venediktov N. P., and Zapevalov V. E., Int J Infrared Milli Waves, 1997, 18, 21292136.

Features of plasma confinement in gas-dynamic magnetic mirror trap

E. I. Soldatkina, P. A. Bagryansky, A. A. Lizunov, A. K. Meyster, E. I. Pinzhenin, V. V. Prikhodko, E. A. Shmigelsky, A. L. Solomakhin

Budker Institute of Nuclear Physics of SB RAS, Novosibirsk, Russia, E.I.Soldatkina@inp.nsk.su

Magnetic mirror systems for plasma confinement (mirror traps) hold potential for controlled nuclear fusion applications. A mirror cell of simple design could serve as a D-T nuclear fusion neutron source, generating a neutron flux with power density of several megawatts per square meter [1]. This is essential for research on the first wall of future fusion reactors and controlling subcritical fission reactors, including the disposal of long-lived radioactive waste [2]. Advanced magnetic mirror traps with improved longitudinal particle confinement can serve as the basis for fusion reactors with a high power amplification factor ($Q >> 1$) that can use alternative, non-radioactive fuels. Since 1986, the Budker Institute of Nuclear Physics has studied the principles of mirror trap physics at the Gas Dynamic Trap (GDT) facility. Recent unique results from the GDT hold promise for ambitious future projects based on open traps [3]. Achievements include successful hot plasma confinement with a high relative pressure (ratio of plasma pressure to magnetic field pressure) $\beta = 0.6$ [4], a fast deuterium ion density of $n_{fast} \sim 5\times10^{19}$ m^{-3} with an average energy of 10 keV, and electron temperatures $T_e \sim 1$ keV with additional electron cyclotron resonance (ECR) heating of moderate power [5].

The current research program at the GDT focuses on several key plasma confinement issues in mirror traps.

High β Regimes

Achieving maximum relative plasma pressure β is crucial for developing future fusion reactors based on mirror traps, since the thermonuclear power gain coefficient depends on the relative pressure as $Q_{\mathrm{DT}} \propto \frac{\beta}{\sqrt{1-\beta}}$. High β regimes approaching $\beta \to 1$, known as "diamagnetic confinement" [6], are of particular interest. Fast ions, generated through charge exchange of powerful neutral atom beams with the target plasma, are the prime contributors to the plasma pressure. These ions oscillate between the so-called turning points, where they exert peak pressure. Previous experiments achieved a hot ion β of 0.6 at the turning points. In the new experiments, by reducing the distance between turning points at a constant beam heating power, we have achieved $\beta \approx 0.45$ at the GDT central plane, suggesting that in this configuration β could approach unity at the turning points.

Kinetic Instabilities

High anisotropy in the fast ion distribution can trigger kinetic instabilities that scatter ions into the loss cone, reducing neutron flux efficiency. In mirror traps, Drift-Cyclotron Loss-Cone instability often arises [7], but it can be stabilized by partially filling the loss cone with warm ions, which has been experimentally demonstrated at the GDT.

When β exceeds a certain threshold, Alfven Ion Cyclotron instability occurs [8], slightly widening the fast ion peak at the turning points; however, the related power loss is less than 0.5% of total captured neutral beam power.

Electron Cyclotron Heating

The confinement time of fast ions in a plasma with relatively cold electrons is determined by Coulomb collisions as $\propto T_e^{3/2}$. Electron temperature, therefore, limits the confinement time and power efficiency of a beam-driven magnetic mirror fusion reactor. Typical electron temperatures in GDT are around 250 eV. In 2014 experiments, an on-axis electron temperature of 660 ± 50 eV (with plasma density of 0.7×10^{19} m^{-3}) was achieved, occasionally exceeding 900 eV in several plasma discharges. To obtain these temperatures a 0.7 MW/54.5 GHz ECR heating system was used in addition to standard 5 MW neutral beam heating.

To achieve a wide heating profile, ECR heating at the second harmonic of an extraordinary wave was proposed, utilizing a new gyrotron with 800 kW output at 54.5 GHz. Initial experiments showed a 25% increase in electron temperature across the entire profile with 300 kW injected ECR power (fig. 1), as well as increasing in plasma diamagnetic flux and neutron yield.

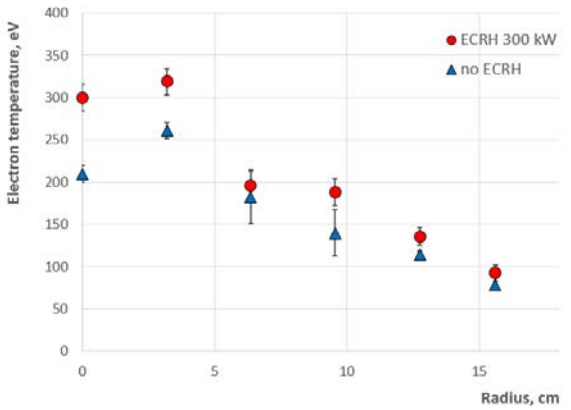

Fig. 1. Profiles of electron temperature with ECR heating and without it measured by Thomson scattering diagnostic system

References

1. Bagryansky P. A. et al. *Fusion Eng. Des.*, 2004, **70**, 13.
2. Simonen T. C. et al. *Nucl. Fusion*, 2013, **53**, 063002.
3. Skovorodin D. I. et al. *Plas. Phys. Reports*, 2023, **49**(9), 1039.
4. Ivanov A. A. et al. *Trans. Fus. Technol.*, 2001, **39**, 127.
5. Bagryansky P. A. et al. *Phys. Rev. Lett.*, 2015, **114**, 205001.
6. Beklemishev A. D. *Phys. Plasmas*, 2016, **23**, 082506.
7. Kotelnikov I. A. et al. *Phys. Plasmas*, 2017, **24**, 122512.
8. Chernoshtanov I. S. and Tsidulko Y. A. *Fus. Sci. Tech.*, 2013, **63**(1T), 319–321.

Development of field emitters electron-optical systems for sub-terahertz gyrotron with an annular electron beam

G. G. Sominskii[1], V. E. Sezonov[1], T. A. Tumareva[1], E. P. Taradaev[1], S. P. Taradaev[1], M. Yu. Glyavin[2], A. S. Zuev[2]

[1] Peter the Great St. Petersburg Polytechnic University, 195251, Russia, St. Petersburg, 29 Polytechnicheskaya st.
[2] A.V. Gaponov-Grekhov Institute of Applied Physics of the Russian Academy of Sciences, Nizhny Novgorod, 46 Ul'yanov st.

Subterahertz gyrotrons devices are used for plasma heating, for diagnostic of various media and other applications [1, 2]. Traditionally, to form electron flows in such devices magnetron injection guns (MIG) with thermal cathodes are used. MIG forms polyhelical electron flow with velocity spread and transverse energy reasonable for effective electron beam – microwave interaction. The use of thermal cathodes with continuous filament complicates the design of compact cathode units and made impossible inertia-free operation. The last one looks promising for some goals. It seems tempting to replace thermionic cathodes with non-heated field emitters in subterahertz tubes to solve both problems.

Using numerical modeling methods and experimentally, the patterns of formation of electron flows by electron optical systems (EOS) with field emitters of a new type developed by the authors were studied [3, 4]. The influence of inhomogeneous magnetic and electric fields on the formation of flows has been studied. The limiting currents of the studied EOS are determined, and the electron velocity distribution functions are found. It is shown that the generation powers achievable with such parameters of electron beams are sufficient for most of the applications under consideration. Optimized EOS provide electron currents up to 50–100 mA and give a possibility to realized stable operation at typical technical pressures of ~ 10^{-7}–10^{-8} Torr.

The main focus of the study was on examining the operation of EOS and gyrotron development based on the most attractive and reliable multi-tip emitters with a special metal-fullerene coating [3] on a silicon substrate and multilayer emitters made of hafnium and platinum nanolayers brought into contact. Since the experimentally observed pitch factor values are somewhat lower than in thermionic cathodes, to achieve stable single-mode lasing, a larger length of the interaction space is required than in traditional gyrotrons.

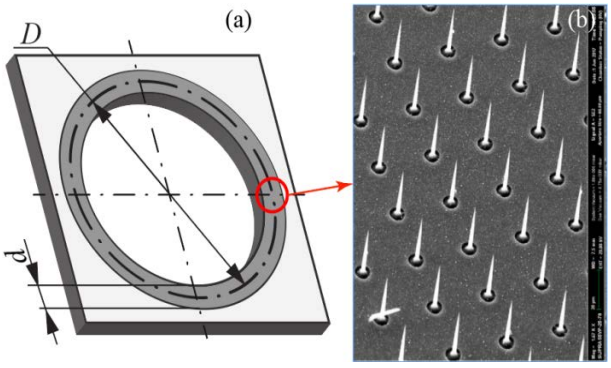

Fig. 1. Multi-tip cathode. *a* – emitting cathode belt, *b* – optimized tip structure: tip height and spacing between them is 30 micrometers. Cathodes with diameters *D* = 14 mm and 18 mm were investigated with a belt width *d* of 0.65 mm

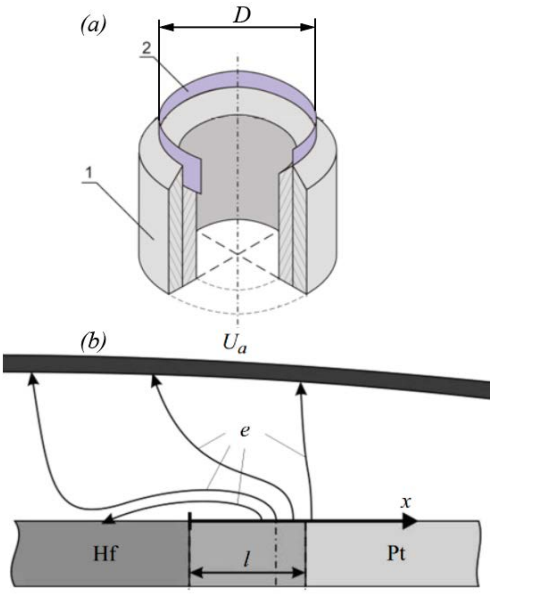

Fig. 2. Schematic representation of a multilayer hafnium platinum cathode on a thin substrate: 1 – multilayer cathode holder, 2 – emitting tape (*a*); emitting cathode structure. Cathodes with diameters *D* = 14 mm were investigated (*b*)

Results of numerical simulations demonstrate that under the specified parameters, an electron beam in a subterahertz gyrotron with a operating frequency of 140 GHz can achieve an output microwave power of about 50 W.

Acknowledgements

The work was carried out with the financial support of the Russian Science Foundation grant No. 23-29-00224.

References

1. M. Thumm. *State-of-the-Art of High-Power Gyro-Devices: Update of Experimental Results 2023*, KIT Scientific Publishing, 2024, 164.
2. M. Glyavin, S. Sabchevski, T. Idehara and S. Mitsudo, *Journal of Infrared, Millimeter, and Terahertz Waves*, 2020, **41**, 1022–1037.
3. E. Taradaev, G. Sominskii, *IEEE Transactions on Electron Devices*, 2022, **69**(5), 2675–2679.
4. G. G Sominskii, V. E. Sezonov, E. P. Taradaev, T. A. Tumareva, S. P. Taradaev, A. A. Rukavitsyna, A. A. Givargizov, A. N. Stepanova, *Radiophysics & Quantum Electronics*, 2019, **62**(7), 539–546.

Formation of high-beta plasma equilibria in magnetic traps

I. V. Timofeev[1,2], **E. A. Berendeev**[1,2] and **V. A. Kurshakov**[1,2]

[1] Budker Institute of Nuclear Physics SB RAS, Novosibirsk, Russia, I.V.Timofeev@inp.nsk.su
[2] Novosibirsk State University, Novosibirsk, Russia

Achieving extremely high relative plasma pressure (β~1) has been a long-standing dream of the fusion community, since it allows to realize the idea of magnetic confinement as efficiently as possible. Today such regimes are considered as the most promising for achieving reactor parameters in cusp [1] and mirror [2] open traps. In the prototype of a fusion reactor, based on the GDMT mirror trap, it is supposed to create an equilibrium in which the magnetic field will be completely displaced from the plasma (diamagnetic bubble [3]) due to high-power neutral injection. Since all losses of particles and energy through the open ends of the system will be dictated by a narrow transition layer with a size smaller than the radius of the bubble (λ<<a), the plasma lifetime should increase by a/λ times compared to time of gas-dynamic outflow. Thus, the size of the transition layer is an important parameter that affects not only the rate of losses, but also the maximum pressure of the confined plasma. Indeed, if the layer turns out to be comparable or even smaller than the ion gyroradius, ion trajectories can no longer be considered circular, so the plasma pressure inside it becomes non-gyrotropic (the azimuthal momentum flux $\Pi_{\varphi\varphi}$ does not coincide with the radial one Π_{rr}). Under these conditions, the MHD limit β=1 for the central region of the confined plasma can be markedly exceeded.

At the moment, however, there is no consensus regarding the size of current sheet. In Kotelnikov's theory [4], which neglects charge separation fields and assumes the dominance of the diamagnetic current of ions, this size is several ion gyroradii ρ_i. In 2D PIC simulations of a multicusp trap [5], a jump in the electric potential (T_i/e) is formed in the transition layer, so the current is created by the electron E×B-drift, and the size of the sheet decreases to $4\rho_e$. At the same time, 2D PIC simulations [6, 7] with the resolution of the particle drift direction show that the electric field transverse to the layer is also formed, but the current sheet turns out to be unstable against drift ion-cyclotron instabilities, which lead to its broadening to a size of the order of ρ_i.

To understand which estimate for the transition layer size is more adequate in equilibria with a completely displaced magnetic field and how strongly the MHD pressure limit can be exceeded in such equilibria, we perform three-dimensional particle-in-cell simulations of plasma injection into various magnetic configurations (uniform, mirror and cusp) using a semi-implicit 3D3V PIC code with precise energy and charge conservation [8]. For a cylindrical plasma column in a uniform field, the size of the current sheet is found to be independent of ion mass, and the growth of plasma pressure is stabilized at β=1.15 due to the development of MHD instability (Fig. 1).

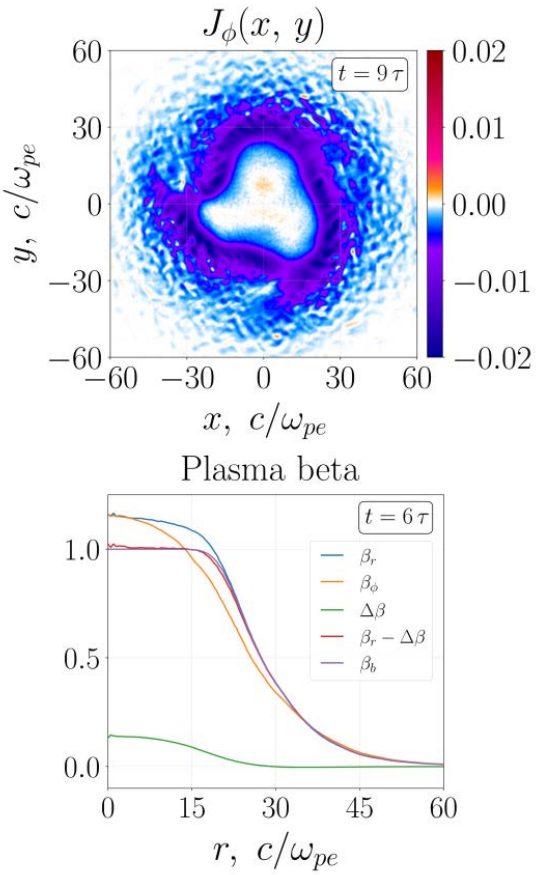

Fig. 1. Azimuthal current at the plasma cross section during the development of MHD instability (top) and radial profiles of β calculated from Π_{rr}, $\Pi_{\varphi\varphi}$, non-gyrotropic addition $\Delta\Pi$ and the pressure of displaced magnetic field $1\text{-}B^2/B_v^2$

Acknowledgements. The work is supported by the Russian Science Foundation (grant 24-12-00309).

References

1. J. Park, N. A. Krall, P. E. Sieck et al. // Phys. Rev. X, 2015, **5,** 021024.
2. D. I. Skovorodin, I. S. Chernoshtanov, V. Kh. Amirov et al. // Plasma Phys. Rep., 2023, **49**(9), 1039.
3. A. D. Beklemishev // Phys. Plasmas, 2016, **23**, 082506.
4. I. Kotelnikov // Plasma Phys. Control. Fusion, 2020, **62**, 075002.
5. J. Park, G. Lapenta, D. Gonzalez-Herrero and N. A. Krall // Front. Astron. Space Sci., 2019, **6**, 74.
6. J. Berchem and H. Okuda // J. Geophys. Res., 1990, **95**(6), 8133.
7. V. A. Kurshakov, I. V. Timofeev // Phys. Plasmas, 2023, **30**, 092513.
8. E. A. Berendeev, I. V. Timofeev, V. A. Kurshakov // Comput. Phys. Comm., 2024, **295**, 109020.

Development of the electron cyclotron system for ITER project

G. G. Denisov[1], A. G. Eremeev[1], A. V. Krasilnikov[2], L. G. Popov[3], E. M. Tai[3], A. P. Fokin[1], A. L. Ustinov[2]

[1] A.V. Gaponov-Grekhov Institute of Applied Physics of the Russian Academy of Sciences, Nizhny Novgorod, Russia, aeremeev@ipfran.ru
[2] Institution "Project CENTER ITER", Moscow, Russia, a.ustinov@iterrf.ru
[3] NPP GYCOM, Nizhny Novgorod, Russia, tai@gycom-nn.ru

The electron cyclotron system, along with ion cyclotron and neutral beams, is one of the additional heating systems of the ITER project. As the baseline, the project planned to use 24 gyrotrons with an output power of about 1 MW each, two 20 MW ion-cyclotron heating units and two 16 MW neutral beam sources with particle energy up to 1 MeV. All systems were considered promising not only for heating plasma components, but also for generating or maintaining a toroidal current. For the electron cyclotron system (EC), additional functions were planned: the breakdown and initial formation of plasma and the suppression of MHD instabilities, which involved the use of gyrotrons in a pulse-periodical regime with modulation frequency of up to 5 kHz. It should be noted that the mentioned prospects were associated with expectations of the successful development of technology samples for all three methods and the possibility of their use for thermonuclear plasma purposes. However, to date, of all the methods, only gyrotrons have achieved the planned parameters. Therefore, and also in connection with the change in the material of the first wall of the reactor to tungsten, it is planned to increase the power of the gyrotron complex by 2 times by the first stage of ITER operation (Augmented First Plasma) and then by the next phase (DT1) to increase the total number of gyrotrons to 72. Meanwhile, the prospects of other methods need to be explored.

The EC system functionally consists of high-voltage sources (HVPS), control systems and gyrotrons located at a distance from tokamak of more than 100 m in the region of weak scattered field of the tokamak, transmission lines (TL) and radiation shapers (Equatorial and Upper Launchers) located in the ports of the tokamak. High-voltage sources and gyrotron complexes with a control system are located in building B15, transmission lines pass through building 13 (assembly hall), adjacent to the tokamak building B11. High-voltage sources, each for 2 gyrotrons (with an output power of up to 6 MW), are the responsibility of Europe and India in equal shares. The supply of gyrotrons, which includes installation and configuration of equipment, is distributed between Japan – 8 pcs., Russia – 8 pcs., Europe – 6 pcs. and India – 2 pcs. The transmission line in the assembly elements is being prepared by the USA. Equatorial Launcher (located in Port 14) is the responsibility of Japan, 4 Upper Launchers located in upper ports 12, 13, 15, 16 in development of Europe. The entire infrastructure of the complex is the responsibility of Europe. In 2024, it is planned to begin the installation of the main gyrotron equipment already manufactured and partially delivered in ITER. At the time of the launchers are in design phase.

The production phase of the gyrotrons provided by Russia was finished un may of 2024. All 8 gyrotron successfully passed tests. Here are the main technical characteristics of gyrotrons produced by NPP GYCOM: output power at the diamond window is at least 1 MW, frequency 170 GHz, efficiency. not less than 50% (actually up to 57%), the HE11 mode content at the input to the transmission line is not less than 95%, the pulse duration is not less than 1000 s with a reliability of more than 95%, etc.

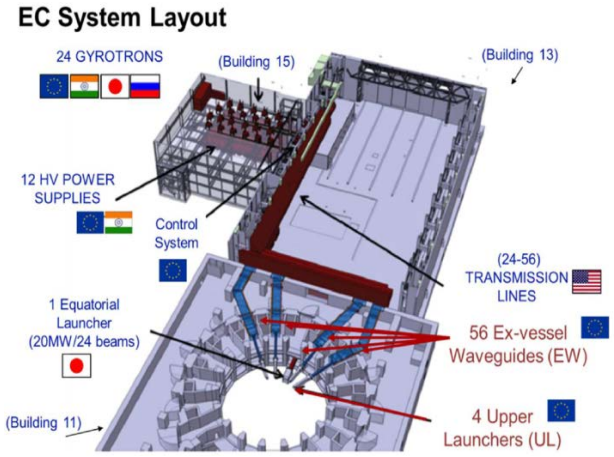

Fig. 1. The ITER EC system layout as presented in baseline

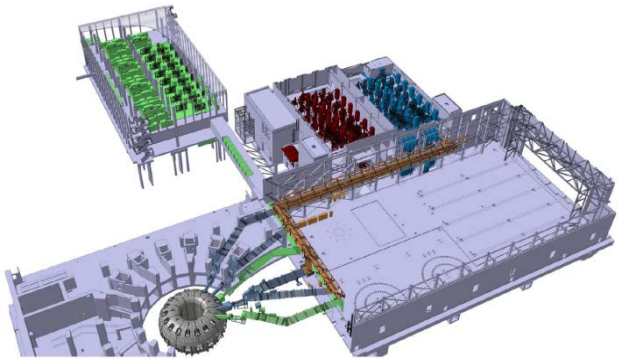

Fig. 2. The 3D representation of the proposed EC system layout for DT1 phase with 72 gyrotrons

The work was carried out within the State Contracts of the State Corporation Rosatom.

Peculiarities of nonthermal electromagnetic emission spectrum of a dense mirror-confined ECR discharge plasma

M. E. Viktorov, I. V. Izotov, A. G. Shalashov, E. D. Gospodchikov, V. A. Skalyga

A.V. Gaponov-Grekhov Institute of Applied Physics of the Russian Academy of Sciences, Nizhny Novgorod, Russia,
mikhail.viktorov@ipfran.ru

Under natural conditions in the Earth's magnetosphere, processes often occur that involve several types of plasma emissions and a coupling between the plasma modes is observed. Observations from spacecrafts have shown that the whistler mode chorus waves are often modulated by low-frequency waves (ULF radiation) [6]. ULF waves periodically change the second derivative of the background magnetic field, which, in turn, changes the threshold for nonlinear excitation of chorus waves and, therefore, contributes to the excitation of chorus in the vicinity of the maximum amplitude of ULF waves. The study of such nonlinear processes in space plasma is associated with difficulties in their detection and the irregularity of their occurrence, therefore, studies of nonlinear processes of interaction of various plasma waves in nonequilibrium laboratory plasma under repeatable and controlled conditions are extremely important.

We study the stationary stage of plasma turbulence arising in a dense nonequilibrium plasma of an electron cyclotron resonant (ECR) discharge sustained in an open magnetic trap by the microwave radiation. The use of high-power millimeter radiation of modern gyrotrons allows one to create in the laboratory a nonequilibrium two-component plasma characteristic of space conditions and to simulate the physical mechanisms of instabilities developing in space magnetic traps.

We present results obtained at two experimental facilities, where plasma is created by pulsed microwave radiation (SMIS37, 100 kW at 37.5 GHz) and continuous radiation (GISMO, 10 kW at 28 GHz).

At both facilities we observe the development of cyclotron instability, which leads to the generation of whistler waves, which are accompanied by the development of low-frequency plasma turbulence in lower hybrid frequency range [2, 3]. This leads to amplitude modulation of higher-frequency whistler oscillations at the frequency of plasma oscillations and the formation of a zebra-like structure of emission spectra.

In the plasma created by pulsed gyrotron radiation at a frequency of 37.5 GHz under ECR conditions in a mirror magnetic trap at the SMIS37 setup, nonthermal electromagnetic radiation at higher frequencies, corresponding to 2–5 electron cyclotron harmonics of the ambient magnetic field, was detected [4]. The plasma emission is attributed to the excitation of electrostatic plasma waves such as electron Bernstein waves. During these experiments we found experimental evidence of two different mechanisms of plasma wave transformation into electromagnetic modes.

At both facilities with plasma created in pulsed and continuous mode we found common features in electron cyclotron instabilities development. In the pulsed ECR discharge whistler waves and electron Bernstein waves are excited at the same time independently. We discuss the self-consistent model of plasma turbulence in these experiments, responsible for the excitation of different plasma modes by multi-component ECR discharge plasma.

Acknowledgements

The work was supported by the Ministry of Science and Higher Education of the Russian Federation within the framework of scientific project no. 075-15-2021-1361.

References

1. L. Li et al., *JGR: Space Phys.*, 2023, **128**, e2022JA031127.
2. M. Viktorov et al., *Phys. Plasmas*, 2020, **27**, 062104.
3. M. Viktorov et al., *Phys. Plasmas*, 2023, **30**, 022101.
4. B. Eliasson et al., *Phys. Rev. Research*, 2020, **2**, 043272.

Energy conservation equations of motion

N. A. Vinokurov

Budker Institute of Nuclear Physics, Siberian Branch of the Russian Academy of Sciences, Novosibirsk, Russia,
vinokurov@inp.nsk.su

A development of generalized Lagrange's and Hamilton's equations without the use of variational principles is proposed. The use of new technique is applied to derivation of some equations.

Introduction

For a wide class of mechanical systems and fields, equations of motion can be derived from variational principles (see, e. g., [1–4]). On the one hand, this fact may reflect some specific properties of related differential equations and can be considered as a more compact writing of these equations. On the other hand, these specific properties and variation principles are important since they form the background of quantum mechanics. In these approaches, conservation of energy is a consequence of no explicit dependence of the Lagrangian on time. This paper suggests an alternative approach. Based on conservation of energy, we derive equations of motion that are a generalization of Lagrange's equations. The important fact, that the energy is defined as the function on the tangent bundle (of coordinates and velocities), is used explicitly for the derivation.

Motion equations

Let $E(\mathbf{q},\mathbf{v}) = const$ be the energy of the system, which depends on the generalized coordinates q^i, $i = 1, \ldots N$ and generalized velocities $v^i = dq^i/dt$, the bold letters denoting a set of variables: $\mathbf{q} = (q^1, \ldots, q^N)$. The state of the system is described with a point with the coordinates $(\mathbf{q}, \mathbf{v})$ on the tangent bundle **TQ** of N-dimension manifold $\mathbf{Q} = \{\mathbf{q}\}$ [4]. It means that the motion equations have to be the second order differential equations. Conservation of energy along the motion trajectory can be written as

$$0 = \frac{dE(\mathbf{q},\mathbf{v})}{dt} = \frac{\partial E}{\partial q^i} v^i + \frac{\partial E}{\partial v^i} \dot{v}^i . \qquad (1)$$

Now we will try to find equations of motion that conserve the energy. Eq. (1) is true for any coordinate **q** and velocity **v**. One scalar equality $v^i f_i(\mathbf{q},\mathbf{v},\dot{\mathbf{v}},t) = 0$, which is true for any **q** and **v** in the tangent bundle **TQ** is equivalent to N equalities $f_i(\mathbf{q},\mathbf{v},\dot{\mathbf{v}},t) = C_{ij}(\mathbf{q},\mathbf{v},\dot{\mathbf{v}},t) v^j$ for any antisymmetric tensor C_{ij}. To use it one can define Lagrange's function $L(\mathbf{q},\mathbf{v})$ as solution of partial differential equation [1, 5]

$$\frac{\partial L(\mathbf{q},\mathbf{v})}{\partial v^i} v^i - L(\mathbf{q},\mathbf{v}) = E(\mathbf{q},\mathbf{v}) . \qquad (2)$$

Then Eq. (1) can be rewritten as

$$0 = \left(\frac{\partial^2 L}{\partial v^i \partial v^j} \dot{v}^j + \frac{\partial L}{\partial v^i \partial q^j} v^j - \frac{\partial L}{\partial q^i} \right) v^i . \qquad (3)$$

Then Eq. (3) gives generalized Lagrange equations [5, 6]

$$\frac{d}{dt}\left(\frac{\partial L}{\partial v^i} \right) = \frac{\partial L}{\partial q^i} + C_{ij}(\mathbf{q},\mathbf{v},\dot{\mathbf{v}},t) v^j , \qquad (4)$$

where Cij is an antisymmetric tensor and represents gyroscopic forces.

Examples

If $E(\mathbf{q})$ does not depend on velocities, $L = -E$ is the solution of Eq. (2) and Eq. (4) is changed to

$$-\frac{\partial E}{\partial q^i} = C_{ij}(\mathbf{q},\mathbf{v},t) v^j , \qquad (5)$$

which leads to Hamilton's equations if **C** does not depend on **v**.

This approach can be applied to partial differential equations also. For example, at

$$E = \int_{-\infty}^{\infty} \left(u^3 - \frac{u_x^2}{2} \right) dx , \qquad (6)$$

one gets

$$\frac{\delta E}{\delta u} = 3u^2 + u_{xx} = \int_{-\infty}^{\infty} G(u, x, x', t) u_t(x', t)\, dx' . \qquad (7)$$

For $G = \mathrm{sgn}(x' - x)/2$ it leads to Korteweg - de Vries equation

$$u_t + 6uu_x + u_{xxx} = 0 . \qquad (8)$$

Equations of motion that conserve a given energy $E(\mathbf{q},\mathbf{v})$ were derived in this paper. In general case differential form of gyroscopic forces is not exact and such gyroscopic forces can not be described by additional terms in Lagrangian. The nonuse of variational principle is a remarkable feature of this approach. It allows obtaining more general equations of motion. The alternative axiomatics of the analytical mechanics and the field theory described in this paper is close to the axiomatics of thermodynamics, which is also based on conservation of energy.

References

1. L. D. Landau, and E. M. Lifshitz, *Mechanics*, 3rd edition. Pergamon, Oxford, 1974.
2. H. Goldstein, *Classical mechanics*, 2nd edition. Addison-Wesley, Reading, 1981.
3. A. Sommerfeld, *Mechanics (Lectures on theoretical physics Vol. 1)*, 4th edition. Academic Press, 1964.
4. J. V. José, and E. J. Saletan, *Classical dynamics: a contemporary approach.* Cambridge University Press, 1998.
5. N. A. Vinokurov, *Physics – Uspekhi*, 2014, **57** (6), 593–596.
6. N. A. Vinokurov, arXiv:1505.04786, 2015, https://doi.org/10.48550/arXiv.1505.04786.

Design of a multi-barrel terahertz gyrotron for DNP/NMR spectroscopy

V. E. Zapevalov, A. S. Zuev, O. P. Plankin and **E. S. Semenov**

A.V. Gaponov-Grekhov Institute of Applied Physics of the Russian Academy of Sciences, Nizhny Novgorod, Russia, zapev@ipfran.ru

Introduction

Nowadays, nuclear magnetic resonance (NMR) spectroscopy has become an important research tool in physics, chemistry, biology, medicine, interdisciplinary and for monitoring technological processes [1]. The use of dynamic nuclear polarization (DNP) methods can significantly increase the capabilities of NMR spectrometers in terms of accuracy, reliability and speed of measurements [1]. In large scientific centers, several NMR spectrometers with different frequencies are often used simultaneously, located in the same building, which makes it desirable to have corresponding DNP sources of microwave radiation with different frequencies.

Microwave and terahertz radiation sources with a power of 10–100 W of 263 GHz, 395 GHz, 526 GHz and 594 GHz are required for DNP/NMR spectroscopy with frequencies of 400 MHz, 600 MHz, 800 MHz and 900 MHz (^{1}H each), respectively. Gyrotron is one of the most suitable high-frequency vacuum electronics devices for such purposes. Currently, many gyrotrons with the above frequencies are successfully used in different scientific centers [2]. Most of them operate at low cyclotron harmonics. Unfortunately, a significant disadvantage of the canonical gyrotron during the transition to operation at high cyclotron harmonics is the aggravation of mode competition. In this regard, there is growing interest in non-canonical gyrotrons [3].

Multi-barrel gyrotron concept

Multi-barrel gyrotron (MBG) is one of the attractive non-canonical gyrotrons with improved capabilities for tuning and increasing the operating frequency with additional mode selection [4]. Figure 1 shows the general scheme of a multi-barrel gyrotron.

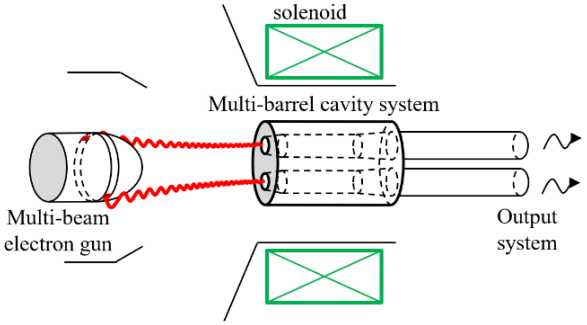

Fig. 1. General scheme of a multi-barrel gyrotron with one cathode-heating unit

The general scheme of a multi-barrel gyrotron includes an adiabatic magnetron injection gun (MIG) forming several helical electron beams (HEB); a cavity system consisting of several barrels (cavities) with axis-encircling beams like in large-orbit gyrotrons [5]; and an energy output system with the transfer of RF power to the output window from each barrel. MBG concept can be used for simultaneous or sequential radiation at frequencies that are multiples of each other in relation to various problems of spectroscopy, diagnostics, and exposure to various objects.

MBG for DNP/NMR spectroscopy

In particular, a multi-barrel gyrotron with simultaneous radiation at frequencies of 263 GHz (n = 2), 395 GHz (n = 3) and 526 GHz (n = 4) at the second, third and fourth cyclotron harmonics is of interest for DNP/NMR spectroscopy [6]. Here n is the cyclotron harmonic number. The gyrotron operates in a single-mode regime in each barrel of the cavity system. Additionally, the possibility of radiation in the fourth barrel of the system at a frequency of 594 GHz at the third cyclotron harmonic was considered.

The calculated output powers were 90, 60 and 40 W with simultaneous radiation at frequencies of 263, 395 and 526 GHz, respectively. The output efficiency is no more than 1%, but it is possible to increase the efficiency using a collector system with single-stage energy recovery. In this way, the efficiency of the gyrotron can be increased fivefold. The maximum output power at 594 GHz in single-frequency regime was about 200 W.

Conclusion

The current of each electron beam in the multi-barrel terahertz gyrotron is significantly limited, which reduces the power level of the output radiation. However, many applications require frequency-tunable terahertz radiation sources with power on the order of 10 W or even less. As research has shown, such a power level is certainly achievable in the devices under consideration. One MBG set up can satisfy the needs of a whole complex of DNP/NMR spectrometers with different frequencies.

Acknowledgements

The work was carried out with the financial support of projects FFUF-2022-0007.

References

1. M. Rosay et al., *Phys. Chem. Chem. Phys*, 2010, **12**, 5850–5860.
2. M. Blank and K. L. Felch, *eMagRes*, 2018, **7**(4), 152–166.
3. V. E. Zapevalov, *Radiophys. Quantum Electron.*, 2018, **61**(4), 272–280.
4. V. E. Zapevalov, A. S. Zuev, and A. N. Kuftin, *Radiophys. Quantum Electron.*, 2020, **63**(2), 97–105.
5. V. L. Bratman, Yu. K. Kalynov, and V. N. Manuilov, *Radiophys. Quantum Electron.*, 2009, **52**(7), 472–481.
6. V. E. Zapevalov, A. S. Zuev, O. P. Plankin, and E. S. Semenov, *Radiophys. Quantum Electron.*, 2023, **66**(1), 1–18.

Experimental studies of operating regimes in planar relativistic surface-wave oscillators with one- and two-dimensional periodic slow-wave structures

V. Yu. Zaslavsky, **A. V. Palitsin**, **Yu. V. Rodin**, **A. V. Gromov**, **M. B. Goykhman**, **D. R. Gulyovsky**, **A. N. Panin** and **N. Yu. Peskov**

A.V. Gaponov-Grekhov Institute of Applied Physics of the Russian Academy of Sciences,
Nizhny Novgorod, Russia, zas-vladislav@ipfran.ru

At present, relativistic Cherenkov surface-wave oscillators (SWO) are promising high-power sources of pulsed microwave radiation. Such sources employ synchronous interaction of a rectilinear electron beam with a decelerated fundamental harmonic of the electromagnetic field in a periodically corrugated waveguide. The amplitude of this harmonic decays with the distance from the corrugation thus forming a surface wave and thereby ensures spatial coherence of radiation in this direction.

However, the advancement of this oscillators class into shorter wavelength ranges at high power levels requires increasing relative size of the interaction space and ensuring mode selection along two transverse coordinates. Under conditions of significant oversize, spatial coherence of radiation can be achieved by using two-dimensional distributed feedback (2D DFB) [1]. Such a feedback mechanism can be implemented by using two-dimensional periodical Bragg structures in which, in addition to conventional longitudinal wave fluxes, there are also transverse ones synchronizing the radiation from large-size relativistic electron beams (REB). In the case of a planar configuration of the SWO, this slow-wave structure (SWS) provides electrodynamic mode selection along all three spatial coordinates [2, 3].

This report is devoted to an experimental study of G – band planar relativistic SWO with 2D DFB implemented using 2D SWS. The project design and oscillator parameters estimations are based on theoretical data obtained through 3D PIC modeling. The SWO were powered by a high-current magnetized REB formed by SINUKI accelerator: accelerating voltage 600–650 kV, operating electron current 1 kA, guiding magnetic field 3T [4]. 2D periodic SWS had a sinusoidal profile of corrugation with depth 0.4 mm and grating period 1.6 mm. In this configuration the nonlinear dynamics are quite simple and a stable excitation of a fundamental mode takes place for system width of $l_x / \lambda \sim 12$. The output power reached ~ 50 MW at a frequency close to 160 GHz.

Experimental investigations of the planar SWO were conducted at the SINUKI accelerator equipped with explosive-emission cathode. An optimized electron-optical system provided the formation of a sheet electron beam with a thickness of about 0.3 mm and a width of about 20 mm with uniform linear current density of 50 A/mm. The total beam current at the input of the device was about 1 kA. To date, proof-of-principle experiments were being carried out to observe generation regimes in the G – band SWO. Fig. 1a presents typical SWO output radiation pulse at an intermediate frequency. The result of radiation frequency heterodyne measurements is presented in Fig. 1b. The data obtained are in good agreement with the result of theoretical predictions.

(a)

(b)

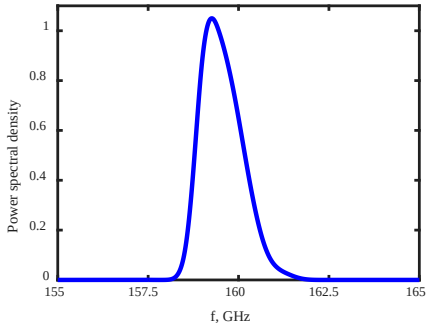

Fig. 1. Results of experimental measurements of the output radiation spectrum of the 160 GHz planar surface wave oscillator. (a) Oscillograms of accelerating voltage (yellow curve) and the output pulse at an intermediate frequency (majenta curve). (b) Power spectral density of output radiation

Acknowledgements

Investigations of SWO with one-dimensional and two-dimensional slow-wave structures were carried out in the frame of the IAP RAS Program No FFUF-2022-0007 and RSF project # 23-72-10094, respectively.

References

1. A. V. Arzhannikov, N. S. Ginzburg, P. V. Kalinin, et al., Phys. Rev. Lett., 2016, 117 (11), 114801.
2. N. S. Ginzburg, A. M. Malkin, A. S. Sergeev, V. Yu. Zaslavsky, Appl. Phys. Lett., 2012, 100 (14), 143510.
3. N. S. Ginzburg, A. M. Malkin, A. S. Sergeev, V. Yu. Zaslavsky, Phys. Plasmas, 2013, 20, 113104.
4. A. V. Palitsin, Yu. V. Rodin, V. Yu. Zaslavsky, et al., IEEE Electron Device Letters, 2023, 44 (2), 317–320.

High-gradient acceleration of electrons by relativistic microwave sources

I. V. Zotova[1], A. E. Fedotov[1], A. A. Vikharev[1], N. S. Ginzburg[1], M. I. Sharypov[2], S. A. Shunaylov[2], V. G. Shpak[2] and **M. I. Yalandin[2]**

[1] A.V. Gaponov-Grekhov Institute of Applied Physics of the Russian Academy of Sciences, Nizhny Novgorod, Russia, zotova@ipfran.ru

[2] Institute of Electrophysics UB RAS, Yekaterinburg, Russia

An increase in the acceleration gradient has traditionally been one of the central problems of accelerator physics. In the currently existing linear electron accelerators powered by L- and S-band klystrons [1], the acceleration gradients do not exceed 100 MV / m (this value is a record, more typical values are 30–50 MV / m). The problem of surpassing the specified level has given rise to a number of new rapidly progressing concepts, including laser-plasma and beam-plasma acceleration, acceleration based on optical-terahertz conversion, etc [2–4]. Nevertheless, research on high-gradient electron acceleration (HGEA) in hollow metallic non-superconducting ("warm") structures remains relevant. Progress in this direction is associated with solving the problem of radio-frequency (rf) breakdown and structure degradation, which is facilitated by the use of higher-frequency, short-pulse radiation with a nanosecond duration.

The indicated requirements stimulated research into the development of laser-controlled switches [5] and compressors [6] of high-power gyrotrons radiation, as a result of which it is expected to obtain 10–20-ns pulses with a power 1–30 MW in the W- and G-bands. At the same time, existing relativistic microwave generators are capable of providing significantly higher short-pulse radiation from the X- to G-bands without the use of additional compression. At present, the most powerful (multi-gigawatt) nanosecond-scale pulses are generated in superradiant backward-wave oscillators (SR BWOs) [7–10]; in more conventional operating regimes of BWOs and surface-wave oscillators, a power level of hundreds of megawatts is reached with pulse durations of up to several tens of nanoseconds. Such sources can be used to test the principles of short-pulse acceleration in various types of metal structures.

The report is devoted to theoretical and experimental studies of high-gradient electron acceleration in fields of short pulses generated by relativistic microwave sources. In particular, this approach was implemented in recent experiments [11], where to demonstrate high-gradient (about 400–500 MV/m) electron acceleration at a full energy gain of ~1 MeV, pumping of a low-Q “pill-box” resonator with a 1-GW /300-ps Ka-band SR pulse was used. The experiment was carried out on a compact (table-top) setup of an original design with two co-axis electron beams formed based on the RADAN accelerator (Fig. 1). An outer tubular beam generated a Cherenkov SR pulse in the backward-wave regime. When moving towards the cathode, this pulse pumped a pill-box resonator, in which the paraxial inner beam was accelerated. Note that the obtained acceleration gradient corresponds to the maximum value demonstrated in a much more cumbersome setup which uses wake-field radiation [12] from pre-formed ultrarelativistic (60 MeV) electron bunches. The experiments also made it possible to determine the limiting breakdown fields on the walls of accelerating structures of 800–100 MV/m, which is important for further C studies.

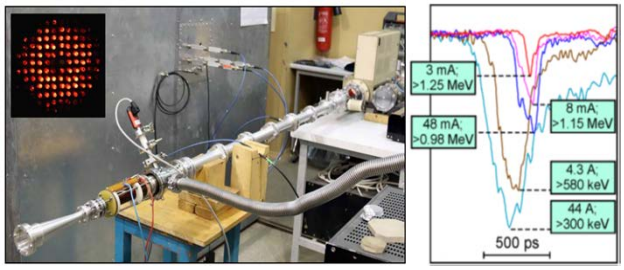

Fig. 1. Experimental setup designed for HGEA by SR pulses (*left*). Current pulses after Al filters with a cutoff energy of up to 1.25 MeV (*right*)

As a further development of these studies, it seems relevant to move into shorter wavelength ranges, as well as to increase the total electron energy. In the latter case, to ensure long-term electron-wave interaction, it is advisable to use traveling wave structures powered by longer pulses (10–20 ns), which can be obtained from relativistic BWOs. The analysis of acceleration possibilities in such systems was carried out on the basis of numerical simulation.

Acknowledgements. The work was supported by RSF under grant No.24-19-00407.

References

1. S. Doebert, et al. (CLIC/CTF3 Collaboration), *Proc. of the XXIV Linear Accelerator Conf. (LINAC08)*, Victoria, BC, Canada, 2008, art. no. 930.
2. E. Esarey, C. Schroeder, and W. Leemans, *Rev. Mod. Phys.*, 2009, **81**, 1229–1285.
3. S. Hooker, *Nat. Photonics*, 2013, **7**, 775–782.
4. E. Nanni, W. Huang, K.-H. Hong, K. Ravi, A. Fallahi, G. Moriena, R. Miller, and F. X. Kärtner, *Nature Comm.*, 2015, **6**, art. no. 8486.
5. M. Othman, J. Picard, S. Schaub, V. Dolgashev, et al., *Appl. Phys. Lett.*, 2020, **117**, art. no. 073502.
6. G. Denisov, A. Palitsin, D. Sobolev, V. Parshin and M. Glyavin, 2023 *Proc. 24th Intern. Vacuum Electronics Conf. (IVEC)*, Chengdu, China, 2023, pp. 1–2.
7. S. Korovin, A. Eltchaninov, V. Rostov, V. Shpak, et al., *Phys. Rev. E*, 2006, **74**, art. no. 016501.
8. V. Rostov, I. Romanchenko, M. Pedos, S. Rukin, et al., Phys. Plasmas, 2016, **23**, art. no. 093103, 2024, 0P12.
9. N. Ginzburg, A. Malkin, A. Sergeev, I. Zheleznov, et al., *Phys. Rev. Lett.*, 2016, **117**, art.no. 204801.
10. N. Ginzburg, V. Zaslavsky, A. Malkin, I. Zotova, et al., *Appl. Phys. Lett.*, 2020, **127**, art. no. 183505.
11. N. Ginzburg, A. Fedotov, S. Kuzikov, K. Sharypov, et al., *Phys. Rev. Accel. Beams*, 2023, **26**, art. no. 060401.
12. W. Tan, S. Antipov, D. Doran, G. Ha, et al., *Phys. Rev. Accel. Beams*, 2022, **25**, 083402.

A new “large-orbit” gyrotron concept

A. S. Zuev, O. P. Plankin, E. S. Semenov and **V. E. Zapevalov**

A.V. Gaponov-Grekhov Institute of Applied Physics of the Russian Academy of Sciences,
Nizhny Novgorod, Russia, andrey.zuev@ipfran.ru

Introduction

At the present time most commercially produced gyrotrons have a traditional design with a magnetron injection gun producing an annular helical electron beam (HEB) [1]. Such an electron-optical system (EOS) has demonstrated high efficiency in all gyrotrons of different frequency ranges, especially in the case of high-power gyrotrons. Currently, there is growing interest in relatively low-power sources in the subterahertz and terahertz ranges, which are in demand in various applications [2]. For most of these applications, radiation power of ten watts is sufficient, which exceeds the capabilities of classical vacuum tubes. Meanwhile, a canonical gyrotron surpasses the required output power and can be considered as a very expensive one. In this regard, there is a demand for the development of new devices of intermediate power levels. This helps to reduce the cost and the dimensions of the set-up, including power supplies, magnetic, control, and cooling systems, etc.

Gyrotron concept

One of the promising sources seems to be a new option, i.e. a “compact gyrotron”. The main idea of this type of gyrodevice to use the advantages of a scheme with an axis-encircling beam, namely, a large-orbit gyrotron (LOG) [3, 4] and to form a HEB by a new version of an adiabatic electron gun. It is proposed to place the emitter near the axis of symmetry of the magnetic system at a certain angle and form the helical beam using crossed electric and magnetic fields. In this case nonadiabatic effects are not used for a HEB formation, unlike previous LOGs [3, 4]. A conventional magnet with a quasi-dipole field distribution (cryo or pulsed) can be used here. But the axial symmetry of the system electrodes is disappeared. Figure 1 shows a scheme of the compact gyrotron with an axis-encircling beam. This electron-optical system is similar to that described in [5] and a simplified version of a multi-barrel gyrotron [6], in which the partial emitter and the corresponding anode are moved towards the center of symmetry of the system.

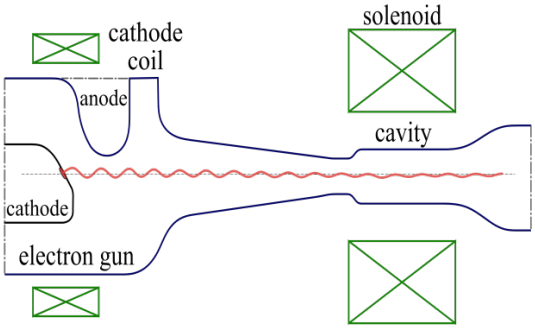

Fig. 1. Scheme of the compact gyrotron with an axis-encircling beam

Further, under the influence of an increasing magnetic field, the electron beam is compressed and enters a quasi-regular cylindrical cavity. The interaction of the electron beam with the RF field of the cavity is carried out like in LOG with the high mode selection. The radiation from the cavity is transported either directly on the operating mode, or converted into a RF field with a required structure and directed through the output window. Additional coils can be used to transport and deposit the electron beam onto the walls of the collector.

395 GHz compact gyrotron

As an example, a compact LOG with radiation frequency of 395 GHz at the second cyclotron harmonic with the operating $TE_{2.5}$ mode was proposed. The cathode emitter was located on the symmetry axis of the magnetic system. Dimensions of the emission section were strongly limited by the required beam dimensions in the interaction region. A triode circuit with an accelerating voltage of 12 kV is considered for additional control of the beam parameters. The calculation of electron trajectories showed the possibility of forming a HEB with a current of 70 mA, a pitch factor of up to 1.4, and a spread of oscillatory velocities at cutoff levels of 0.1 and 0.9 about 30%. According to the preliminary calculations, an output power of 30 W is achievable with an efficiency of 3.6% in such a device.

Conclusion

The concept of LOG makes it possible to form a thin HEB with a high pitch factor and an acceptable spread of oscillatory velocities. The power of gyrotron with the formed HEB is relatively low. Nevertheless, it is quite sufficient for spectroscopic applications of gyrotrons.

Such approach can lead to a significant reduction in the dimensions of the gyrotron set-up due to the use of a “budget” magnetic system with a significantly smaller bore diameter. Similar “compact” magnetic systems are commercially available.

Acknowledgements

The work was carried out with the financial support of projects FFUF-2022-0007.

References

1. A. L. Gol’denberg and M. I. Petelin, *Radiophys. Quantum Electron.*, 1973, **16**(1), 106–111.
2. M. Yu. Glyavin et al., *Phys. Usp.*, 2016, **59**, 595–604.
3. T. Idehara et al., Vacuum, 2005. **77**(4), 539–546.
4. V. L. Bratman, Yu. K. Kalynov, and V. N. Manuilov, *Radiophys. Quantum Electron.*, 2009, **52**(7), 472–481.
5. I. B. Bott, Pat. 1096921 (UK). Radiation Generators. Publ. 29.12.1967.
6. V. E. Zapevalov, A. S. Zuev, and A. N. Kuftin, *Radiophys. Quantum Electron.*, 2020, **63**(2), 97–105.

AUTHOR INDEX

FRONTIERS OF NONLINEAR PHYSICS

VIII INTERNATIONAL CONFERENCE

P R O C E E D I N G S